Copy No._____

Guide for Mechanistic-Empirical Design
OF NEW AND REHABILITATED PAVEMENT STRUCTURES

FINAL DOCUMENT

APPENDIX HH:
FIELD CALIBRATION OF THE THERMAL CRACKING MODEL

NCHRP

Prepared for
National Cooperative Highway Research Program
Transportation Research Board
National Research Council

Submitted by
ARA, Inc., ERES Division
505 West University Avenue
Champaign, Illinois 61820

December 2003

Acknowledgment of Sponsorship

This work was sponsored by the American Association of State Highway and Transportation Officials (AASHTO) in cooperation with the Federal Highway Administration and was conducted in the National Cooperative Highway Research Program which is administered by the Transportation Research Board of the National Research Council.

Disclaimer

Acknowledgements

The research team for NCHRP Project 1-37A: Development of the 2002 Guide for the Design of New and Rehabilitated Pavement Structures consisted of Applied Research Associates, Inc., ERES Consultants Division (ARA-ERES) as the prime contractor with Arizona State University (ASU) as the primary subcontractor. Fugro-BRE, Inc., the University of Maryland, and Advanced Asphalt Technologies, LLC served as subcontractors to either ARA-ERES or ASU along with several independent consultants.

Research into the subject area covered in this Appendix was conducted at ASU as well by consultants to ASU under NCHRP Projects 1-37A as well as 9-19, *Superpave Support and Performance Models Management*. As the principal investigator on NCHRP 9-19 and flexible pavement team leaded on NCHRP 1-37A, Dr. M.W. Witczak lead the entire research effort. He was assisted by Dr. Reynaldo Roque, Dr. Dennis Hiltunen, and Dr. William G. Buttlar in the modification and re-calibration of the Superpave Thermal Cracking model (TCMODEL) developed under the SHRP A005 research contract. Other authors of this Appendix include Drs. Claudia Zapata, W.M. Mirza, Manuel Ayers, and Messrs. Mohammed El-Basyouny and A. Sotil who assisted in the model recalibration effort.

Foreword

The Appendix covers the details of the field calibration of the thermal cracking model that was originally developed under the NCHRP 9-19 research project and recalibrated for the various input hierarchical levels under NCHRP 1-37A. This appendix serves as a supporting reference to PART 3, Chapters 3 and 6.

General Table of Content

Appendix HH

Field Calibration of the Thermal Cracking Model

INTRODUCTION

This Appendix covers the details of the field calibration of the thermal cracking model that was originally developed under the NCHRP 9-19 research project: *Superpave Support and Performance Models Management*. The main purpose of this study, developed by Witczak, Roque, Hiltunen, and Buttlar, was the modification and re-calibration of the Superpave Thermal Cracking model (TCMODEL) developed under the SHRP A005 research contract. The details of the NCHRP 9-19 research results can be found in Annex A.

The re-calibrated model was incorporated into the 2002 Design Guide software based on three different levels of analysis. A general overview of the parameters needed for each level of analysis is presented herein along with the calibration results obtained.

Based on the calibration results of the TCMODEL incorporated into the 2002 Design Guide and given the poor performance of the model for the Level 3 analysis, the ASU research team decided to modify the correlations involved in the process at this level. The new correlations are also presented in the main body of this Appendix.

In addition to a new approach for Level 3 analysis, the results from a study on different calibration factors to the Paris Law are shown in this Appendix. The details of the study can be found in Annex B.

Lastly, a sensitivity analysis was carried out to evaluate the validity of the Level 3 Thermal Cracking model (TCModel) built into the 2002 Design Guide. Details of the analysis can be found in Annex C.

THEORETICAL BACKGROUND

The thermal cracking model in the Design Guide is an enhanced version of the approach originally developed under the SHRP A-005 research contract. A study was completed under the NCHRP 9-19 "Superpave Models" project to facilitate the incorporation of this thermal cracking model (TCMODEL) and related software for use in the Design Guide.

Several major updates have been made to the original TCMODEL and software. These enhancements included the incorporation of an improved analysis technique for converting raw data from the Superpave Indirect Tensile Test (IDT) into fundamental viscoelastic properties of the asphalt mixture, recalibration of the TCMODEL to reflect updated analysis procedures and additional new field data, and the development of comprehensive documentation for the TCMODEL approach.

Thermal Cracking Model

The amount of transverse cracking expected in the pavement system is predicted by relating the crack depth to an amount of cracking (crack frequency) by the following expression:

$$C_f = \beta_1 * N\left(\frac{\log C / h_{ac}}{\sigma}\right) \quad \textbf{(Eq. 1)}$$

where:

C_f	=	Observed amount of thermal cracking.
β_1	=	Regression coefficient determined through field calibration.
$N()$	=	Standard normal distribution evaluated at ().
σ	=	Standard deviation of the log of the depth of cracks in the pavement.
C	=	Crack depth.
h_{ac}	=	Thickness of asphalt layer.

The amount of crack propagation induced by a given thermal cooling cycle is predicted using the Paris law of crack propagation:

$$\Delta C = A\Delta K^n \quad \textbf{(Eq. 2)}$$

where:

ΔC	=	Change in the crack depth due to a cooling cycle.
ΔK	=	Change in the stress intensity factor due to a cooling cycle.
A, n	=	Fracture parameters for the asphalt mixture.

The approach used to evaluate the *A* and *n* parameters is based, in part, upon previous work by Schapery, Molenaar and Lytton. Recalling that the master creep compliance curve can be expressed by the power function to yield:

$$D(\xi) = D_0 + D_1\xi^m \quad \textbf{(Eq. 3)}$$

The *m* value, derived from the compliance curve is used to compute the *n* fracture parameter through the equation:

$$n = 0.8\left(1 + \frac{1}{m}\right) \quad \textbf{(Eq. 4)}$$

Once the *n* value is known, the *A* fracture parameter is computed from the equation:

$$A = 10^{\left(\beta*(4.389 - 2.52*\log(E*\sigma_m*n)\right)} \quad \textbf{(Eq. 5)}$$

where:

E	=	Mixture stiffness.
σ_m	=	Undamaged mixture tensile strength.
β	=	Calibration parameter.

GENERAL OVERVIEW OF CALIBRATION OF THERMAL CRACKING MODEL BY HIERARCHICAL LEVELS

The calibration of the thermal cracking model was accomplished at three hierarchical levels of analysis. Forty two PTI pavement sections were used for the calibration: 22 GPS sections from the LTPP database, 14 sections from the Canadian C-SHRP program, one section from Peoria, IL, and 5 MnROAD cells from the Minnesota DOT. Details and location of the sections are found in the main body of this Appendix.

The calibration of the Paris Law equation was accomplished by using the SHRP and C-SHRP sections.

As shown in Figure A-1, the main inputs required for predicting thermal cracking are the creep compliance and the tensile strength. This is constant at all hierarchical levels. Table A-1 summarizes this data for the forty-two PTI pavement sections included in the analysis.

Level 1 Analysis

The input parameters needed to calibrate the Level 1 analysis of the TC model are:

- Creep compliance data at three different temperatures: -20^{o}C (-4 ^{o}F), -10^{o}C (14 ^{o}F), and 0 ^{o}C (32 ^{o}F) for 1, 2, 5, 10, 20, 50, and 100 second loading time.
- Tensile Strength at –10^{o}C.

The calibration of the Paris Law equation, rendered a β factor equals to 5 for the Level 1 analysis. More details of the model can be found on Part 3, Chapter 3 of the Design Guide. Refer also to Annex B for calibration details and notes.

The reliability of the thermal cracking prediction was evaluated in two different ways: by using the actual historic pavement temperatures during the design period, and by using estimated temperatures based on the Enhanced Integrated Climatic Model (EICM) files. The predicted thermal cracking was compared to the measured thermal cracking and the prediction errors are shown in Figure A-2 and A-3. The average prediction errors were found to be –9.0 ft and 16.2 ft. for the first and second method, respectively. This comparison illustrates the power and the importance of inputting actual historic climatic data for the design period instead of estimated data.

Level 2 Analysis

The input parameters needed to calibrate the Level 2 analysis of the TC model are:

- Creep compliance data at -10^{o}C (14 ^{o}F) for 1, 2, 5, 10, 20, 50, and 100 second loading time.
- Tensile Strength at –10^{o}C.

Similar to the Level 1 analysis, the TCModel was also modified with a β factor (1.5) on the Paris Law, and the predictions were only made on the SHRP and C-SHRP sections.

Predicted thermal cracking values were obtained using the same analyses described for Level 1. The predicted versus measured thermal cracking were compared and the prediction errors are shown in Figure A-4 and A-5. The average prediction errors were found to be 30.1 ft and 49.7 ft. for the first and second approaches, respectively. The difference in errors highlights the importance of having accurate and actual input pavement temperatures.

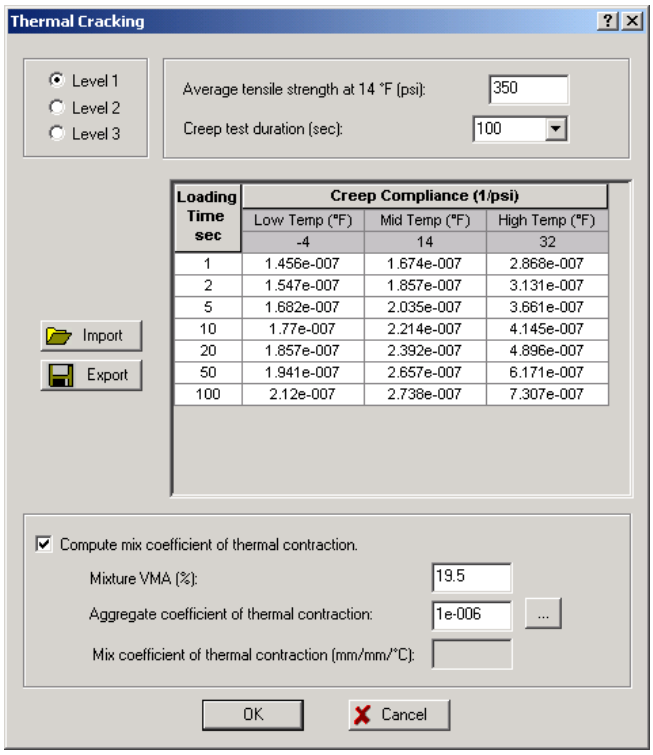

Figure A-1. Input Required by 2002 Design Guide Software to Estimate Thermal Cracking

Table A-1. Creep Compliance and Tensile Strength Data Used in the Calibration of the TC Model

	Mix ID	Peoria IL	404086	041022	322027	201005	161010	161001	311030	491008
	Project ID	PIA	PTI 01-M	PTI 02-M	PTI 06-M	PTI 07-M	PTI 11-M	PTI 12-M	PTI 13-M	PTI 16-M
Tensile Strength (MPa)	High Temp (0 °C)	**4.07**	4.48	3.66	2.40	3.15	3.40	4.39	3.94	3.01
	Int. Temp (-10 °C)	**4.07**	3.78	3.66	2.31	2.95	3.62	4.25	3.10	2.62
	Low Temp (-20 °C)	**4.07**	3.60	3.68	2.02	2.44	3.14	2.93	1.92	2.81
Shift Factors	High Temp	3.25	3.90	3.95	5.75	3.35	3.20	3.65	2.70	5.35
	Int. Temp	2.10	2.70	1.90	5.85	1.55	1.00	2.25	2.50	5.20
Creep Compliance, Low Temp (-20 °C)	1	0.049	0.018	0.023	0.037	0.038	0.030	0.027	0.037	0.031
	2	0.052	0.019	0.023	0.039	0.040	0.032	0.028	0.040	0.032
	5	0.058	0.019	0.024	0.040	0.042	0.035	0.030	0.045	0.033
	10	0.063	0.021	0.025	0.042	0.045	0.037	0.032	0.051	0.034
	20	0.068	0.021	0.026	0.043	0.048	0.039	0.033	0.056	0.035
	50	0.076	0.022	0.027	0.045	0.051	0.041	0.036	0.064	0.038
	100	0.084	0.024	0.029	0.047	0.054	0.045	0.039	0.073	0.037
	200	0.096								
	500	0.111								
	1000	0.122								
Creep Compliance, Int. Temp (-10 °C)	1	0.087	0.026	0.028	0.073	0.050	0.035	0.040	0.087	0.051
	2	0.098	0.029	0.030	0.077	0.053	0.039	0.044	0.100	0.054
	5	0.113	0.032	0.033	0.082	0.057	0.043	0.051	0.123	0.057
	10	0.129	0.035	0.035	0.087	0.058	0.047	0.056	0.146	0.062
	20	0.147	0.038	0.038	0.092	0.066	0.051	0.063	0.170	0.064
	50	0.184	0.041	0.043	0.101	0.069	0.057	0.068	0.217	0.072
	100	0.216	0.044	0.048	0.107	0.073	0.059	0.078	0.266	0.074
	200	0.253								
	500	0.313								
	1000	0.367								
Creep Compliance, High Temp (0 °C)	1	0.124	0.035	0.048	0.056	0.070	0.062	0.060	0.084	0.045
	2	0.149	0.039	0.053	0.063	0.074	0.068	0.070	0.103	0.050
	5	0.190	0.046	0.065	0.074	0.082	0.080	0.086	0.137	0.058
	10	0.228	0.052	0.080	0.086	0.089	0.091	0.102	0.176	0.064
	20	0.275	0.063	0.099	0.090	0.099	0.108	0.121	0.203	0.073
	50	0.368	0.073	0.136	0.111	0.117	0.137	0.157	0.267	0.085
	100	0.458	0.087	0.195	0.127	0.131	0.163	0.192	0.311	0.094
	200	0.586								
	500	0.788								
	1000	1.005								

Table A-1. Continued.

	Mix ID	561007	081047	211034	404088	241634	451008	341011	291010	421597
	Project ID	PTI 17-M	PTI 18-M	PTI 21-M	PTI 22-M	PTI 23-M	PTI 26-M	PTI 27-M	PTI 28-M	PTI 31-M
Tensile Strength (MPa)	High Temp (0 °C)	3.36	2.96	3.65	3.06	3.77	2.94	4.49	1.97	3.02
	Int. Temp (-10 °C)	3.09	2.64	3.35	2.66	2.87	1.63	3.68	1.91	2.80
	Low Temp (-20 °C)	2.46	2.30	2.30	2.40	2.10	2.12	3.13	1.95	2.46
Shift Factors	High Temp	2.55	3.75	4.05	2.35	3.00	3.50	4.00	6.10	4.25
	Int. Temp	1.85	2.55	2.20	1.70	1.65	4.00	2.10	4.35	3.70
Creep Compliance, Low Temp (-20 °C)	1	0.041	0.034	0.028	0.034	0.031	0.042	0.042	0.029	0.035
	2	0.043	0.035	0.028	0.036	0.033	0.045	0.045	0.029	0.036
	5	0.046	0.037	0.030	0.039	0.037	0.048	0.048	0.030	0.039
	10	0.048	0.039	0.031	0.040	0.040	0.051	0.051	0.031	0.040
	20	0.051	0.040	0.032	0.044	0.043	0.053	0.053	0.032	0.041
	50	0.056	0.042	0.035	0.047	0.049	0.056	0.056	0.033	0.043
	100	0.061	0.044	0.036	0.050	0.055	0.057	0.057	0.034	0.045
	200									
	500									
	1000									
Creep Compliance, Int. Temp (-10 °C)	1	0.061	0.046	0.037	0.046	0.048	0.073	0.073	0.047	0.054
	2	0.064	0.049	0.040	0.050	0.054	0.083	0.083	0.050	0.057
	5	0.071	0.054	0.044	0.055	0.062	0.099	0.099	0.055	0.062
	10	0.076	0.058	0.049	0.061	0.070	0.111	0.111	0.060	0.068
	20	0.085	0.063	0.054	0.063	0.079	0.122	0.122	0.066	0.068
	50	0.100	0.071	0.061	0.071	0.097	0.126	0.126	0.074	0.075
	100	0.111	0.078	0.069	0.081	0.112	0.145	0.145	0.084	0.083
	200									
	500									
	1000									
Creep Compliance, High Temp (0 °C)	1	0.064	0.062	0.062	0.047	0.074	0.063	0.063	0.079	0.050
	2	0.073	0.067	0.071	0.056	0.093	0.069	0.069	0.086	0.059
	5	0.091	0.075	0.089	0.070	0.123	0.078	0.078	0.100	0.073
	10	0.106	0.084	0.106	0.079	0.161	0.088	0.088	0.116	0.089
	20	0.132	0.093	0.139	0.101	0.179	0.096	0.096	0.129	0.100
	50	0.164	0.109	0.194	0.107	0.225	0.117	0.117	0.164	0.121
	100	0.221	0.125	0.248	0.125	0.293	0.132	0.132	0.197	0.141
	200									
	500									
	1000									

Table A-1. Continued.

	Mix ID	181028	231026	181037	271087	271028	Cell 16	Cell 17	Cell 26	Cell 27
	Project ID	PTI 32-M	PTI 33-M	PTI 36-M	PTI 37-M	PTI 38-M	Mn\ROAD	Mn\ROAD	Mn\ROAD	Mn\ROAD
Tensile Strength (MPa)	**High Temp (0 °C)**	2.15	4.27	2.34	3.58	2.51	**2.23**	**2.44**	**2.26**	**2.90**
	Int. Temp (-10 °C)	2.05	3.43	2.82	3.04	2.45	**2.23**	**2.44**	**2.26**	**2.90**
	Low Temp (-20 °C)	1.57	2.11	2.47	3.28	2.13	**2.23**	**2.44**	**2.26**	**2.90**
Shift Factors	**High Temp**	3.25	2.15	1.70	3.25	3.35	3.10	2.85	2.40	2.95
	Int. Temp	2.75	1.55	0.90	2.55	2.85	2.50	1.95	1.45	1.85
Creep Compliance, Low Temp (-20 °C)	**1**	0.044	0.036	0.023	0.030	0.027	0.049	0.035	0.059	0.078
	2	0.046	0.039	0.024	0.032	0.029	0.053	0.039	0.066	0.081
	5	0.048	0.045	0.026	0.035	0.032	0.057	0.044	0.077	0.084
	10	0.049	0.050	0.026	0.038	0.034	0.062	0.050	0.088	0.087
	20	0.052	0.055	0.028	0.040	0.037	0.067	0.054	0.101	0.092
	50	0.056	0.063	0.028	0.042	0.040	0.075	0.060	0.119	0.098
	100	0.058	0.072	0.029	0.045	0.043	0.083	0.065	0.136	0.108
	200						0.089	0.079	0.158	0.116
	500						0.094	0.087	0.183	0.125
	1000						0.095	0.098	0.210	0.122
Creep Compliance, Int. Temp (-10 °C)	**1**	0.064	0.057	0.025	0.050	0.058	0.112	0.056	0.110	0.094
	2	0.072	0.067	0.026	0.053	0.053	0.125	0.077	0.123	0.107
	5	0.084	0.084	0.029	0.059	0.060	0.138	0.091	0.144	0.126
	10	0.097	0.103	0.032	0.063	0.063	0.152	0.105	0.165	0.141
	20	0.107	0.128	0.032	0.074	0.076	0.170	0.120	0.191	0.164
	50	0.129	0.175	0.038	0.088	0.086	0.207	0.159	0.233	0.206
	100	0.151	0.231	0.040	0.096	0.099	0.240	0.199	0.267	0.251
	200						0.295	0.227	0.347	0.295
	500						0.370	0.287	0.473	0.392
	1000						0.444	0.354	0.603	0.502
Creep Compliance, High Temp (0 °C)	**1**	0.062	0.067	0.027	0.060	0.059	0.109	0.086	0.112	0.127
	2	0.078	0.091	0.031	0.064	0.063	0.133	0.103	0.142	0.173
	5	0.108	0.134	0.037	0.075	0.071	0.168	0.133	0.220	0.218
	10	0.138	0.184	0.041	0.084	0.076	0.206	0.166	0.310	0.266
	20	0.188	0.245	0.051	0.108	0.087	0.249	0.208	0.414	0.325
	50	0.278	0.356	0.061	0.136	0.106	0.330	0.288	0.619	0.438
	100	0.369	0.485	0.070	0.174	0.117	0.438	0.367	0.859	0.643
	200						0.645	0.482	1.260	0.818
	500						0.940	0.743	1.879	1.192
	1000						1.317	1.072	2.694	1.663

Table A-1. Continued.

	Mix ID	Cell 30	Lamont 1	Lamont 2	Lamont 3	Lamont 4	Lamont 5	Lamont 6	Lamont 7	Sherbrooke A
	Project ID	Mn\ROAD	PTI 31-S	PTI 32-S	PTI 33-S	PTI 34-S	PTI 35-S	PTI 36-S	PTI 37-S	PTI 38-S
Tensile Strength (MPa)	**High Temp (0 °C)**	**2.65**	1.79	2.61	1.63	2.45	1.82	2.05	1.75	2.00
	Int. Temp (-10 °C)	**2.65**	2.38	2.83	3.42	3.20	2.61	3.28	3.29	3.21
	Low Temp (-20 °C)	**2.65**	3.25	3.01	4.00	2.75	3.29	3.02	3.55	3.68
Shift Factors	**High Temp**	2.60	2.20	2.90	2.50	0.90	1.70	1.75	2.05	2.90
	Int. Temp	1.70	2.05	2.55	1.50	0.30	0.95	1.55	1.40	0.95
Creep Compliance, Low Temp (-20 °C)	**1**	0.020	0.057	0.047	0.044	0.057	0.082	0.067	0.058	0.054
	2	0.034	0.060	0.050	0.051	0.061	0.087	0.073	0.062	0.057
	5	0.048	0.064	0.054	0.062	0.067	0.096	0.083	0.070	0.062
	10	0.056	0.067	0.057	0.074	0.074	0.104	0.092	0.079	0.068
	20	0.065	0.073	0.064	0.085	0.077	0.116	0.106	0.087	0.074
	50	0.081	0.081	0.069	0.105	0.088	0.126	0.126	0.105	0.088
	100	0.090	0.086	0.075	0.127	0.100	0.147	0.145	0.124	0.100
	200	0.099								
	500	0.110								
	1000	0.110								
Creep Compliance, Int. Temp (-10 °C)	**1**	0.077	0.090	0.085	0.098	0.053	0.096	0.119	0.087	0.067
	2	0.091	0.096	0.095	0.112	0.060	0.110	0.135	0.102	0.074
	5	0.105	0.108	0.113	0.139	0.070	0.131	0.162	0.132	0.085
	10	0.118	0.114	0.134	0.168	0.084	0.146	0.198	0.173	0.099
	20	0.135	0.142	0.150	0.213	0.090	0.172	0.224	0.207	0.109
	50	0.171	0.162	0.182	0.301	0.126	0.214	0.303	0.323	0.140
	100	0.208	0.190	0.255	0.406	0.134	0.222	0.365	0.406	0.166
	200	0.244								
	500	0.318								
	1000	0.399								
Creep Compliance, High Temp (0 °C)	**1**	0.101	0.081	0.074	0.151	0.056	0.124	0.109	0.102	0.158
	2	0.119	0.093	0.094	0.207	0.072	0.147	0.131	0.144	0.193
	5	0.163	0.112	0.132	0.328	0.101	0.186	0.173	0.228	0.260
	10	0.205	0.131	0.176	0.468	0.125	0.228	0.222	0.324	0.326
	20	0.257	0.158	0.216	0.690	0.180	0.265	0.281	0.477	0.413
	50	0.345	0.194	0.294	1.151	0.226	0.358	0.459	0.732	0.602
	100	0.421	0.225	0.389	1.700	0.307	0.443	0.570	1.134	0.764
	200	0.585								
	500	0.954								
	1000	1.362								

Table A-1. Continued.

	Mix ID	Sherbrooke B	Sherbrooke C	Sherbrooke D	Hearst 1	Hearst 2	Hearst 3
	Project ID	PTI 39-S	PTI 40-S	PTI 41-S	PTI 42-S	PTI 43-S	PTI 44-S
Tensile Strength (MPa)	High Temp (0 °C)	3.00	2.64	2.99	1.35	1.45	1.68
	Int. Temp (-10 °C)	3.07	3.63	3.92	2.52	2.63	2.13
	Low Temp (-20 °C)	3.64	3.66	4.95	3.14	3.15	2.38
Shift Factors	High Temp	2.90	2.10	2.70	1.10	1.95	2.95
	Int. Temp	1.85	0.45	1.40	0.20	0.90	2.05
Creep Compliance, Low Temp (-20 °C)	1	0.026	0.040	0.031	0.074	0.061	0.052
	2	0.027	0.043	0.034	0.079	0.067	0.054
	5	0.030	0.047	0.039	0.088	0.077	0.057
	10	0.032	0.054	0.043	0.100	0.087	0.063
	20	0.035	0.053	0.047	0.114	0.098	0.065
	50	0.039	0.062	0.054	0.139	0.121	0.075
	100	0.041	0.070	0.057	0.171	0.141	0.084
	200						
	500						
	1000						
Creep Compliance, Int. Temp (-10 °C)	1	0.039	0.040	0.046	0.064	0.081	0.087
	2	0.042	0.045	0.052	0.075	0.093	0.097
	5	0.049	0.054	0.063	0.094	0.113	0.115
	10	0.055	0.059	0.077	0.114	0.138	0.135
	20	0.064	0.075	0.089	0.139	0.161	0.155
	50	0.077	0.092	0.113	0.189	0.211	0.203
	100	0.090	0.106	0.147	0.238	0.267	0.250
	200						
	500						
	1000						
Creep Compliance, High Temp (0 °C)	1	0.055	0.084	0.087	0.089	0.131	0.117
	2	0.064	0.104	0.105	0.122	0.167	0.146
	5	0.081	0.137	0.144	0.189	0.232	0.199
	10	0.099	0.176	0.193	0.268	0.317	0.260
	20	0.125	0.206	0.257	0.372	0.373	0.302
	50	0.167	0.279	0.403	0.528	0.560	0.440
	100	0.217	0.326	0.590	0.739	0.745	0.582
	200						
	500						
	1000						

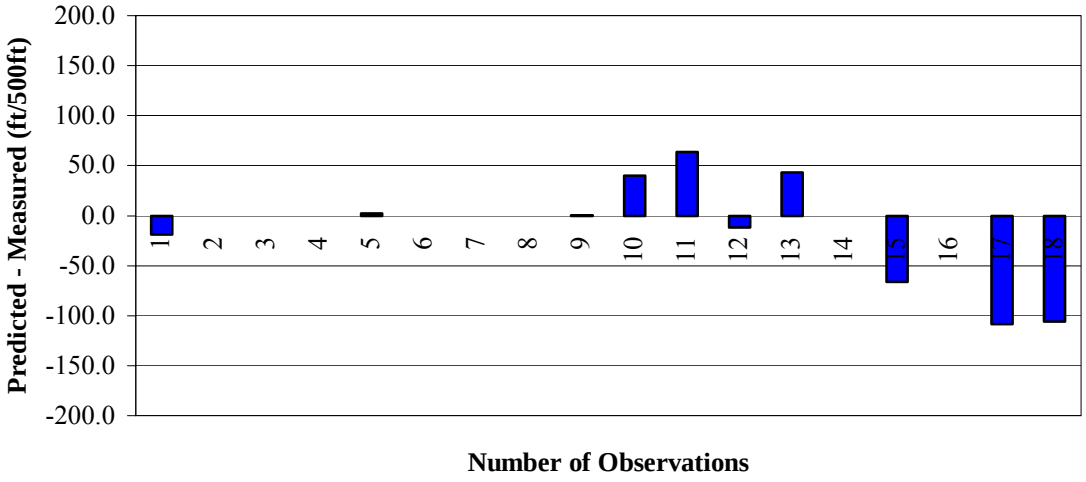

Figure A-2. Level 1 Prediction Errors (Actual Historic Temperature)

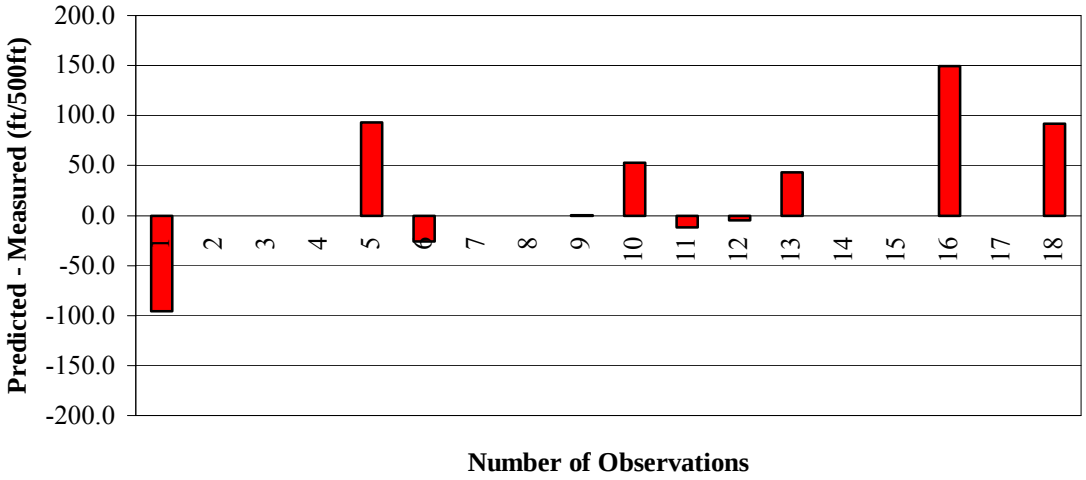

Figure A-3. Level 1 Prediction Errors (Average Temperatures using EICM Files)

Level 3 Analysis

For level 3 analysis, correlations between creep compliance data and the asphalt grade of the pavement were developed based on selected mixtures. For the tensile strength, an average value was used, which came out to be correlated with the asphalt grade as well. Following this approach, the user needed to provide only the grade of the asphalt, and the program would create creep compliance master curves and a value of tensile strength at –10 ^{o}C.

To develop the master curves, the creep compliance data was reduced by means of the shift factors shown in Table A-2. The master curves were then grouped and the average or best-fitted curve was assigned to each asphalt grade group. The master creep

compliance curves and the average assigned to each group are shown in Figures A-6 to A-9.

For the tensile strength, the results of the selected mixtures were grouped by asphalt grade. An average value at –10 ^{o}C was then obtained. Figures A-10 to A-13 show the data used in the analysis.

Based on the empirical creep compliance tensile strength data (shown in Figures A-6 through A-13), default values were estimated as input for the Level 3 of the Design Guide. The summary of the results is presented in Table A-3.

Figures A-14 and A-15 show predicted versus measured values for creep compliance and tensile strength based on the approach suggested for Level 3.

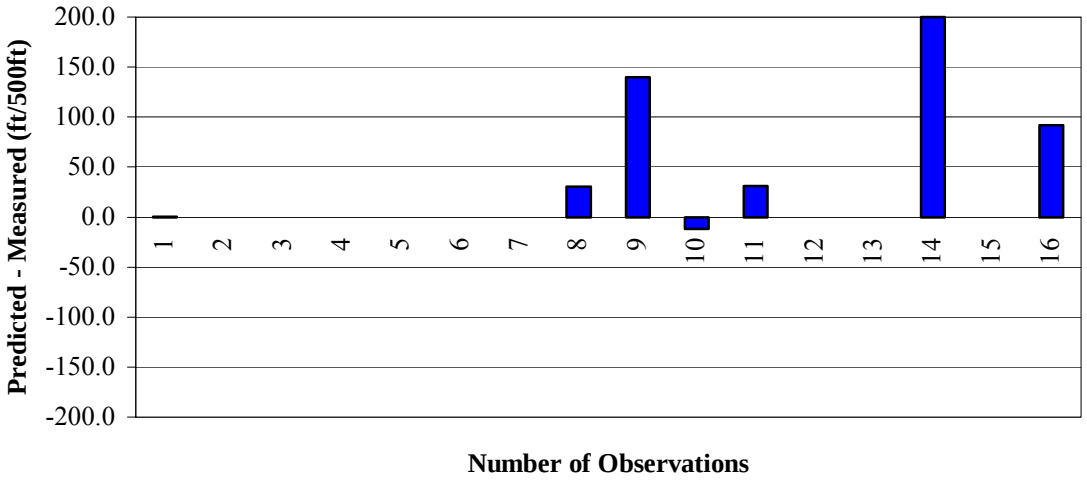

Figure A-4. Level 2 Prediction Errors (Actual Historic Temperature)

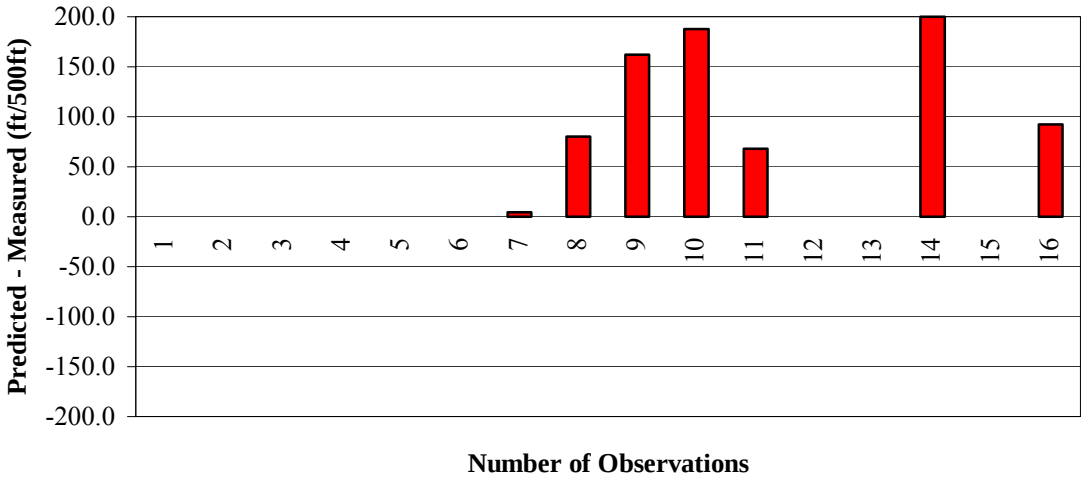

Figure A-5. Level 2 Prediction Errors (Estimated Temperatures using EICM Files)

Table A-2. Shift Factors and Binder Grade for Sections Used in TC Model Calibration

		Pavement Info				Shift Factors	
Mix ID	Project ID	Thickness	Sample Lift	Depth	Binder Grade	High Temp	Int. Temp
Peoria IL	PIA	5.00	Lab	0.00	PG 76-34	3.25	2.10
404086	PTI 01-M	114.30	Binder	50.80	Pen 85-100	3.90	2.70
041022	PTI 02-M	165.10	Surface	12.00	AR-2000	3.95	1.90
322027	PTI 06-M	203.20	Surface	12.00	AC-5	5.75	5.85
201005	PTI 07-M				AC-5	3.35	1.55
161010	PTI 11-M	243.80	Surface	12.00	Pen 60-70	3.20	1.00
161001	PTI 12-M	91.40	Surface	12.00	Pen 85-100	3.65	2.25
311030	PTI 13-M	177.80	Surface	12.00	AC-10	2.70	2.50
491008	PTI 16-M	233.70	Surface	12.00	AC-10	5.35	5.20
561007	PTI 17-M	76.20	Surface	12.00	AC-10	2.55	1.85
081047	PTI 18-M	88.90	Surface	12.00	AC-10	3.75	2.55
211034	PTI 21-M	381.00	Binder	50.00	AC-10	4.05	2.20
404088	PTI 22-M	317.50	Binder	50.00	Pen 85-100	2.35	1.70
241634	PTI 23-M	215.90	Surface	12.00	Pen 85-100	3.00	1.65
451008	PTI 26-M	83.80	Binder	50.00	Pen 85-100	3.50	4.00
341011	PTI 27-M	228.60	Binder	50.00	Pen 85-100	4.00	2.10
291010	PTI 28-M	304.80	Binder	50.00	Pen 60-70	6.10	4.35
421597	PTI 31-M	165.10	Binder	50.00	AC-20	4.25	3.70
181028	PTI 32-M	401.30	Binder	50.00	AC-20	3.25	2.75
231026	PTI 33-M	152.40	Surface	12.00	AC-10	2.15	1.55
181037	PTI 36-M	360.70	Binder	50.00	AC-20	1.70	0.90
271087	PTI 37-M	363.20	Binder	50.00	Pen 120-150	3.25	2.55
271028	PTI 38-M	241.30	Binder	50.00	Unknown	3.35	2.85
Cell 16	Mn\ROAD	196.90	Surface	12.00	AC-20	3.10	2.50
Cell 17	Mn\ROAD	196.90	Surface	12.00	AC-20	2.85	1.95
Cell 26	Mn\ROAD	152.40	Surface	12.00	Pen 120-150	2.40	1.45
Cell 27	Mn\ROAD	76.20	Surface	12.00	Pen 120-150	2.95	1.85
Cell 30	Mn\ROAD	152.40	Surface	12.00	Pen 120-150	2.60	1.70
Lamont 1	PTI 31-S				AC-10	2.20	2.05
Lamont 2	PTI 32-S				Pen 150-200 B	2.90	2.55
Lamont 3	PTI 33-S				AC-2.5	2.50	1.50
Lamont 4	PTI 34-S				AC-10	0.90	0.30
Lamont 5	PTI 35-S				AC-10	1.70	0.95
Lamont 6	PTI 36-S				Pen 150-200 A	1.75	1.55
Lamont 7	PTI 37-S				AC-2.5	2.05	1.40
Sherbrooke A	PTI 38-S				Pen 150-200 A	2.90	0.95
Sherbrooke B	PTI 39-S				AC-10	2.90	1.85
Sherbrooke C	PTI 40-S				AC-10	2.10	0.45
Sherbrooke D	PTI 41-S				Pen 150-200 A	2.70	1.40
Hearst 1	PTI 42-S				AC 2.5	1.10	0.20
Hearst 2	PTI 43-S				Pen 150-200 A	1.95	0.90
Hearst 3	PTI 44-S				Pen 150-200 B	2.95	2.05

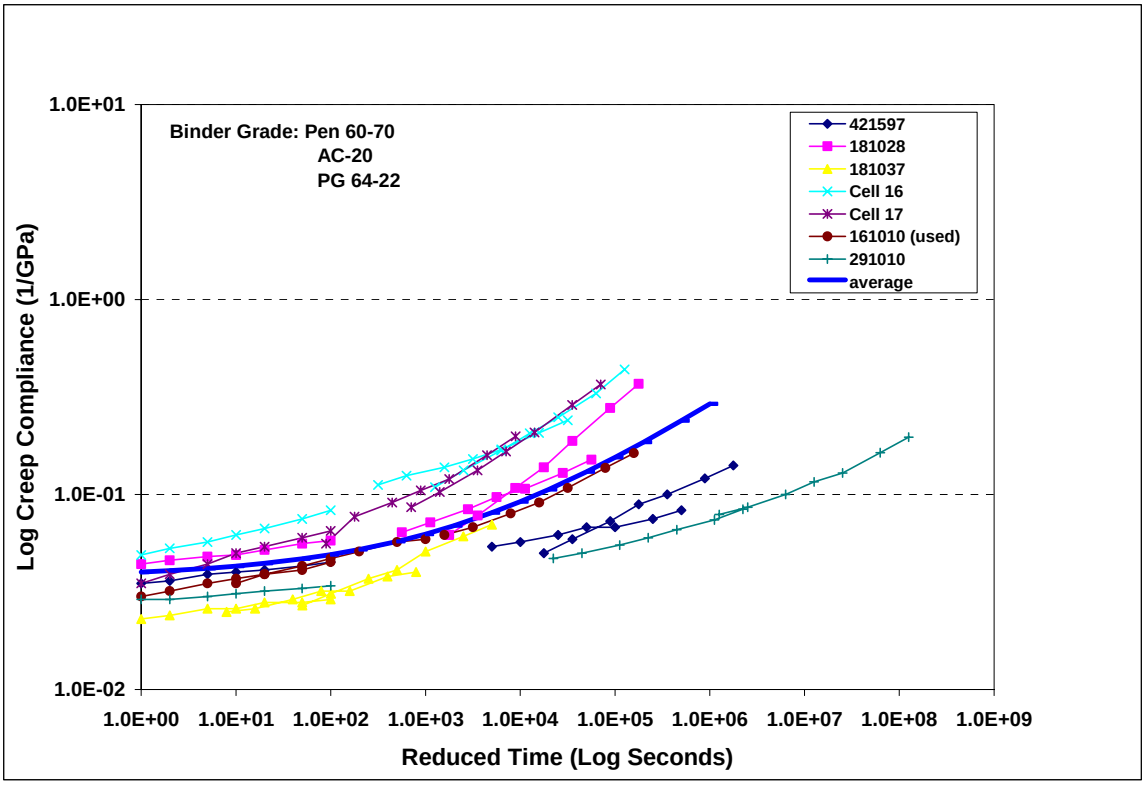

Figure A-6. Master Curves for AC-20, Pen 60-70, and PG 64-22 Binder Grades Mixtures

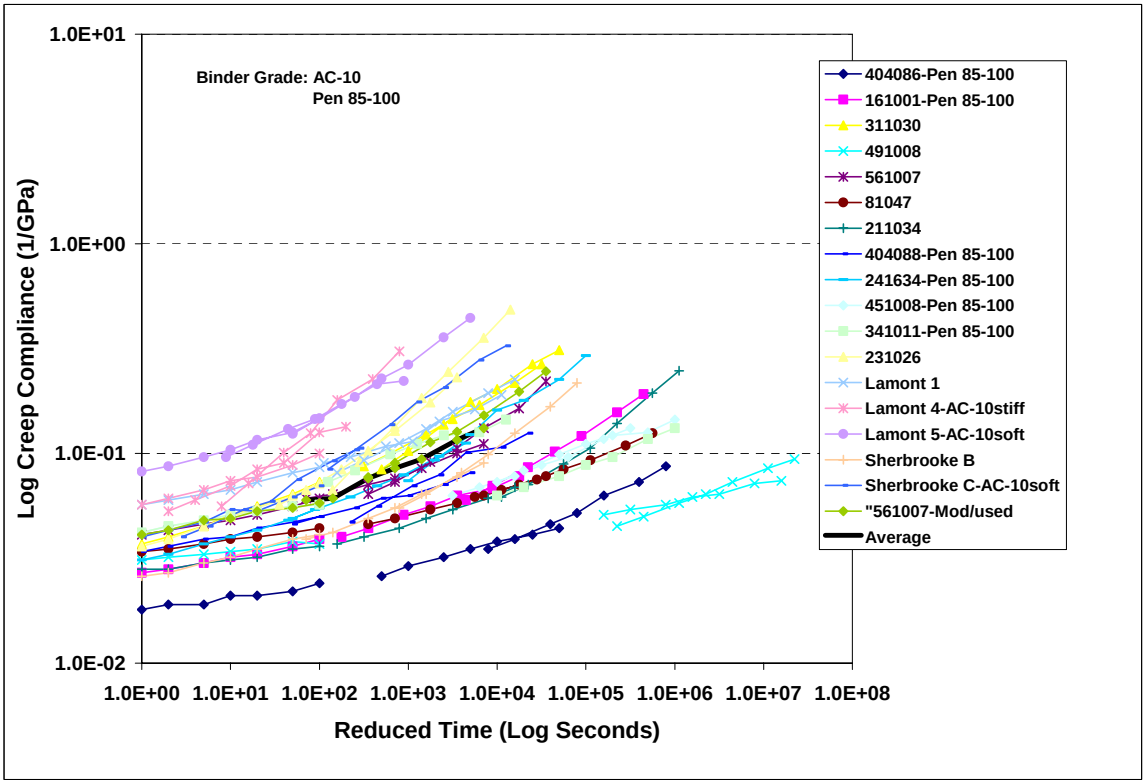

Figure A-7. Master Curves for AC-10 and Pen 85-100 Binder Grades Mixtures

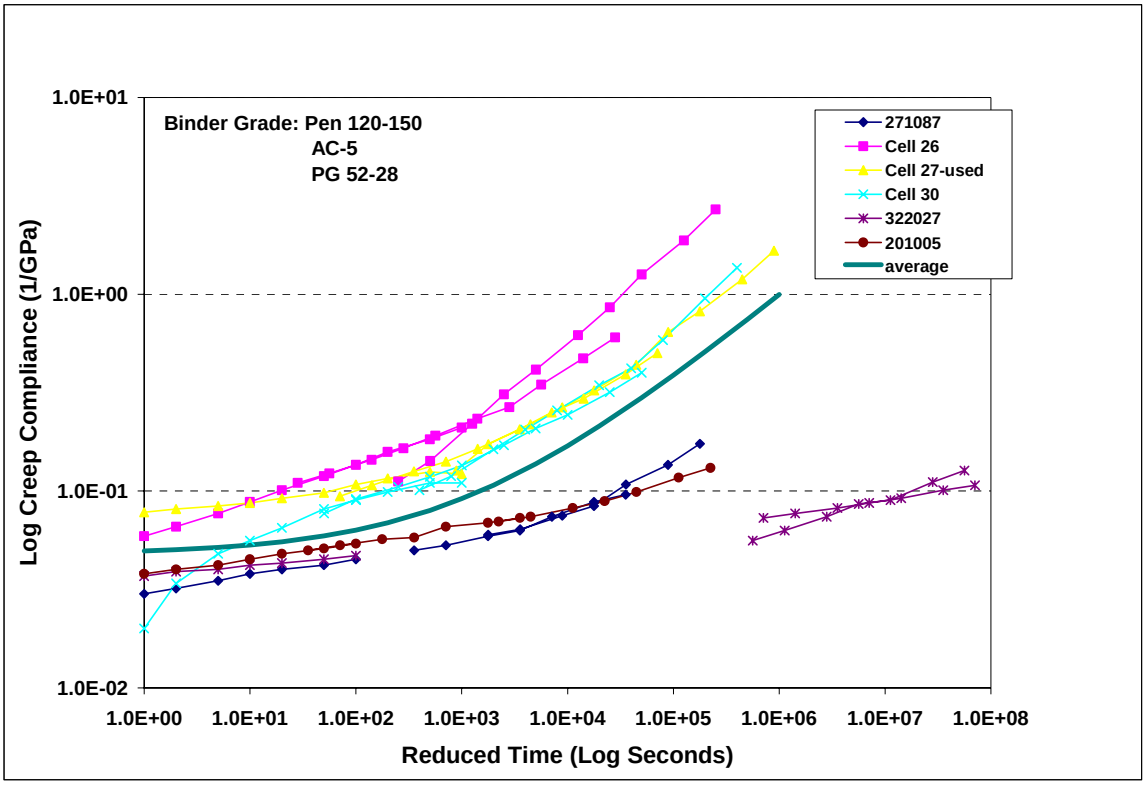

Figure A-8. Master Curves for AC-5, Pen 120-150, and PG 52-28 Binder Grades

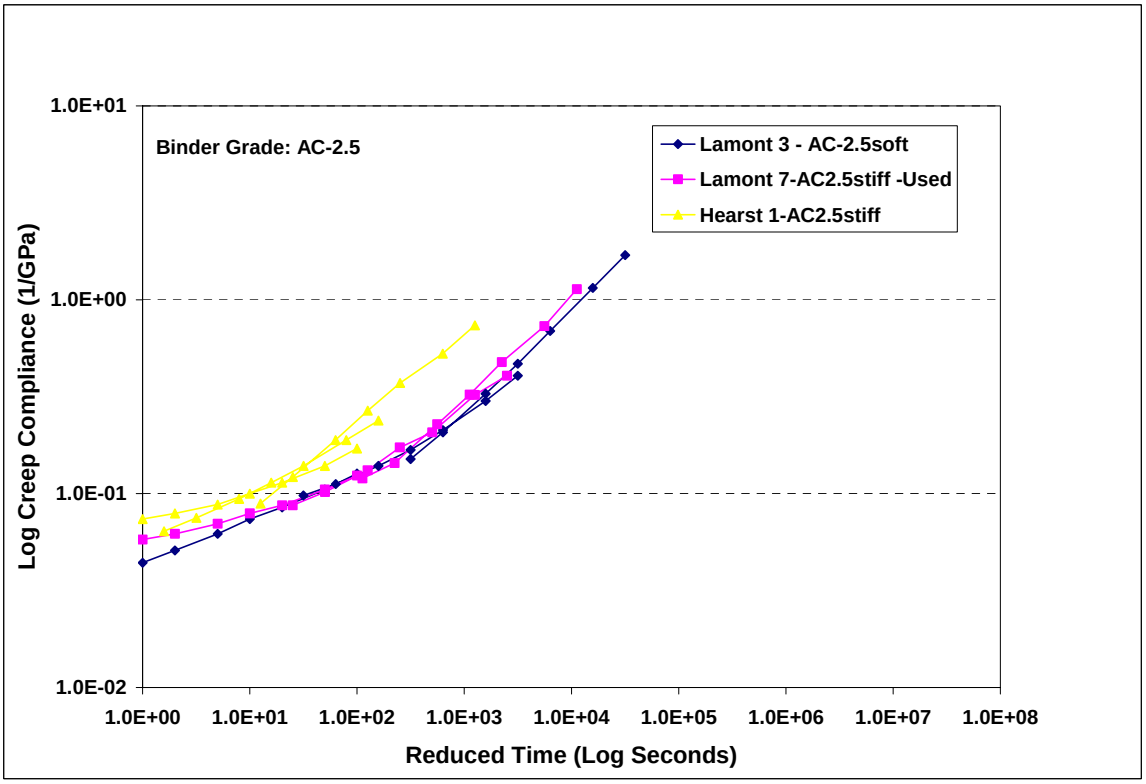

Figure A-9. Master Curves for AC-2.5 Binder Grade Mixtures

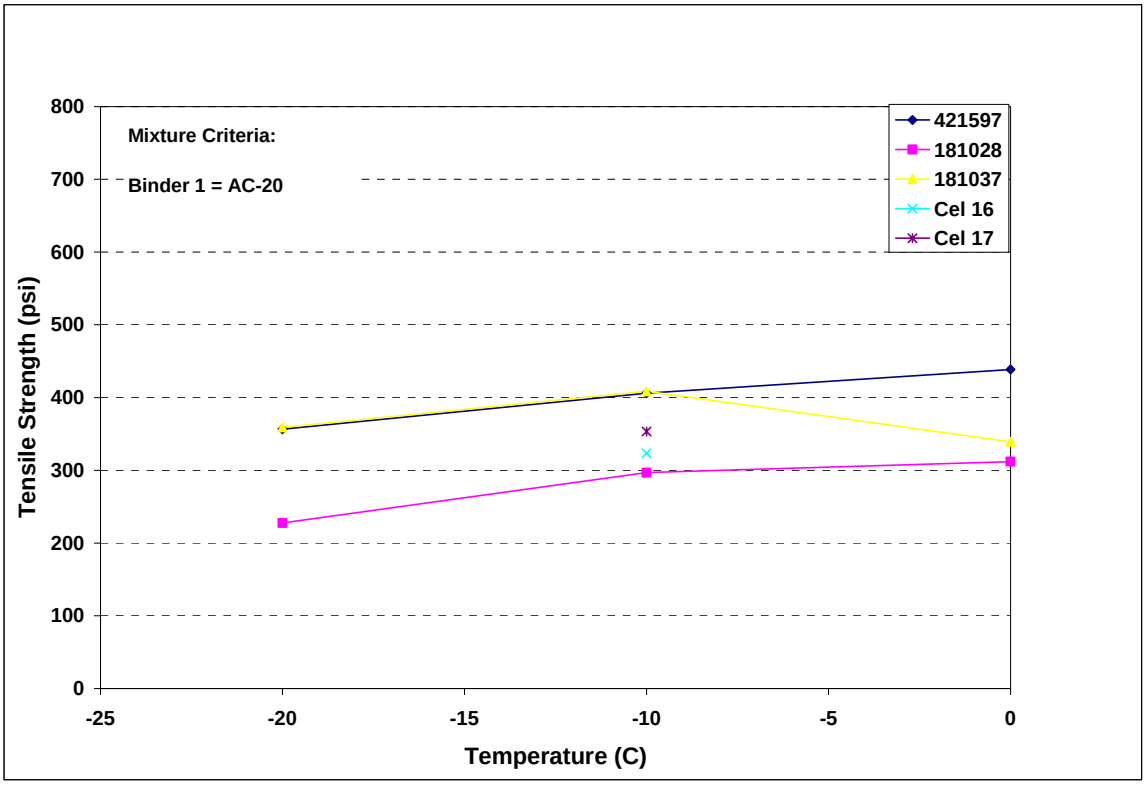

Figure A-10. Tensile Strength Data for AC-20 Grade for Selected Mixtures

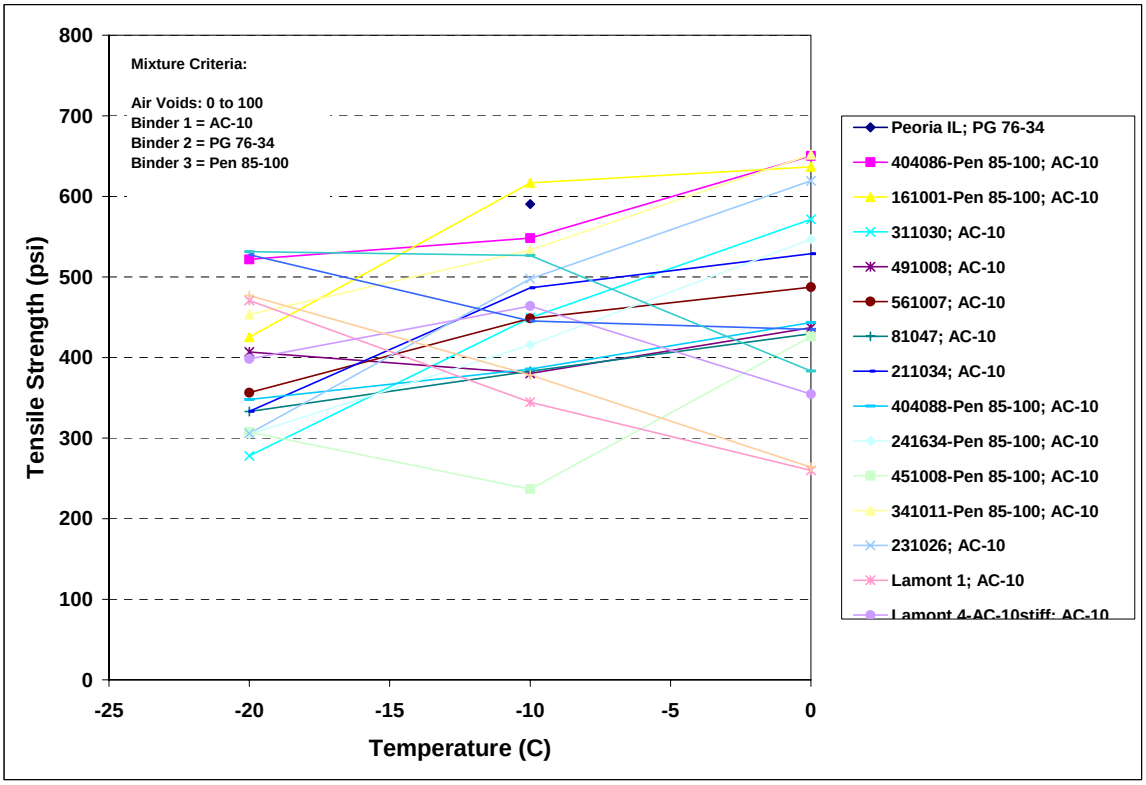

Figure A-11. Tensile Strength Data for AC-10, Pen 85-100, and PG 76-34 Grades for Selected Mixtures

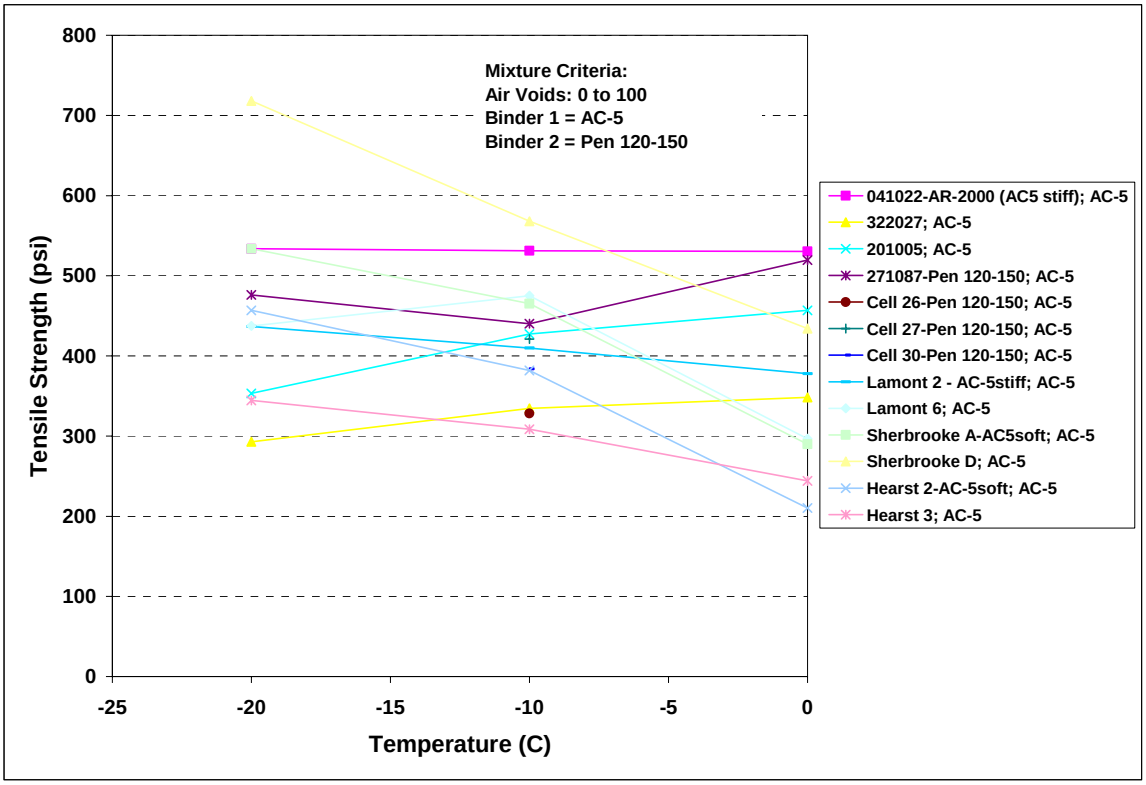

Figure A-12. Tensile Strength Data for AC-5 and Pen 120-150 Binder Grades

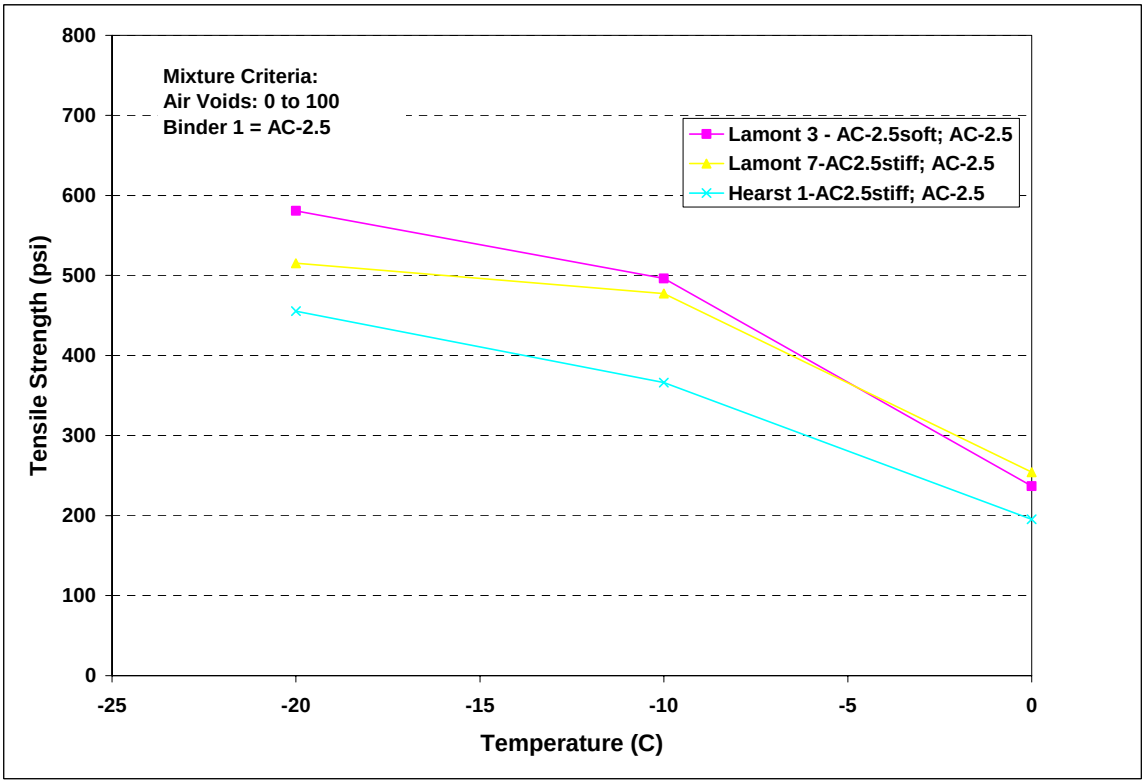

Figure A-13. Tensile Strength Data for AC-2.5 Binder Grade for Selected Mixtures

Table A-3. Creep Compliance and Tensile Strength Default Values Generated for Level 3 Analysis

Binder Grade	Time (sec)	Creep Compliance (1/Gpa)			Tensile Strength at -10 C (psi)
		-20 C	-10 C	0 C	
AC-2.5	1	0.058	0.087	0.120	447
Pen 200-300	2	0.062	0.102	0.144	
PG 46-34	5	0.070	0.132	0.228	
PG 46-40	10	0.079	0.173	0.324	
	20	0.087	0.207	0.477	
	50	0.105	0.323	0.732	
	100	0.124	0.406	1.134	
AC-5	1	0.052	0.087	0.117	421
Pen 120-150	2	0.054	0.097	0.146	
PG 52-28	5	0.057	0.115	0.199	
PG 52-34	10	0.063	0.135	0.260	
	20	0.065	0.155	0.302	
	50	0.075	0.203	0.440	
	100	0.084	0.250	0.582	
AC-10	1	0.041	0.060	0.077	444
Pen 85-100	2	0.043	0.061	0.090	
PG 58-22	5	0.048	0.076	0.113	
PG 58-28	10	0.049	0.085	0.127	
	20	0.053	0.094	0.152	
	50	0.055	0.116	0.197	
	100	0.058	0.132	0.246	
AC-20	1	0.030	0.035	0.062	370
Pen 60-70	2	0.032	0.039	0.068	
PG 64-22	5	0.035	0.043	0.080	
	10	0.037	0.047	0.091	
	20	0.039	0.051	0.108	
	50	0.041	0.057	0.137	
	100	0.045	0.059	0.163	
AC-30	1	0.021	0.024	0.042	350
Pen 40-50	2	0.022	0.027	0.045	
PG 70-16	5	0.024	0.030	0.053	
	10	0.026	0.032	0.060	
	20	0.027	0.035	0.071	
	50	0.028	0.039	0.090	
	100	0.031	0.040	0.106	
PG 64-28	1	0.056	0.075	0.090	511
	2	0.064	0.080	0.105	
	5	0.069	0.090	0.136	
	10	0.075	0.103	0.168	
	20	0.082	0.117	0.212	
	50	0.097	0.139	0.288	
	100	0.104	0.162	0.375	

Table A-3. Continued.

Binder Grade	Time (sec)	Creep Compliance (1/Gpa)			Tensile Strength at -10 C (psi)
		-20 C	-10 C	0 C	
PG 70-34	1	0.063	0.120	0.191	590
	2	0.106	0.148	0.248	
	5	0.124	0.199	0.343	
	10	0.144	0.259	0.459	
	20	0.168	0.332	0.609	
	50	0.214	0.472	0.924	
	100	0.261	0.612	1.276	

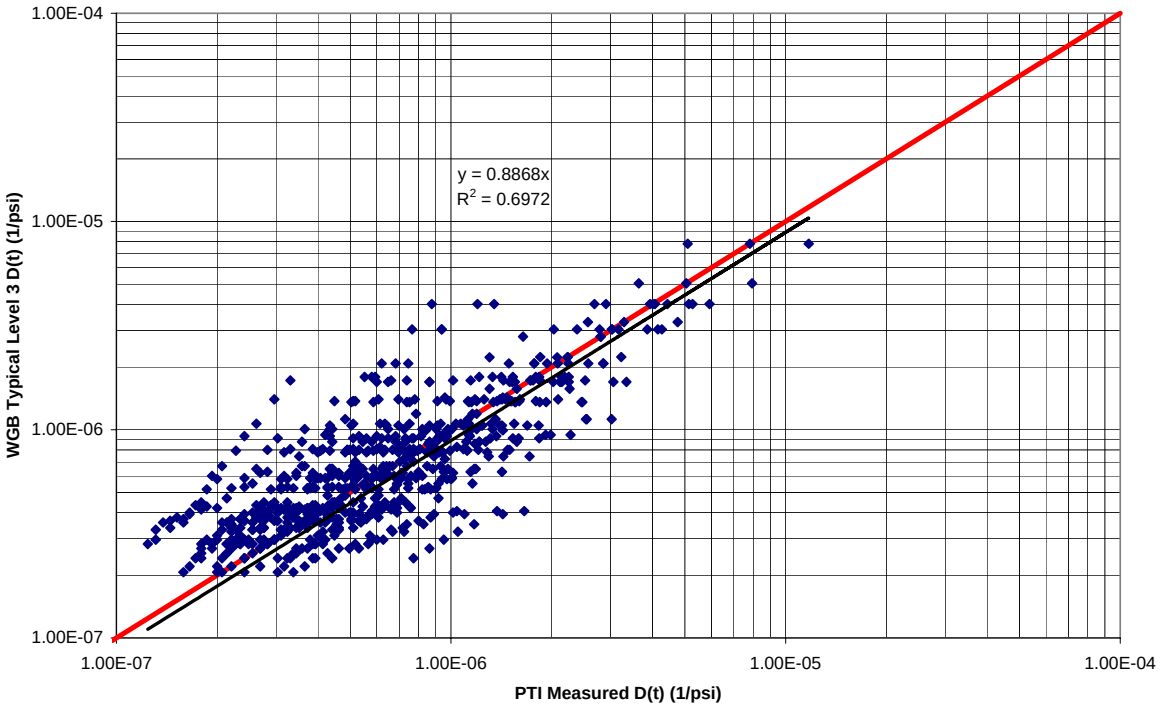

Figure A-14. Measured PTI data set vs. Buttlar's (WGB) Level 3 Typical Creep Compliance Values

The analysis for this level was performed using the LTPP, the SHRP, and the C-SHRP sections mentioned before. The predicted thermal cracking was compared to the observed thermal cracking and the prediction errors are shown in Figure A-16. The average prediction error was found to be 35.3 ft. As expected, the error for Level 3 was higher than the errors found for Levels 1 and 2. A summary of the statistical parameters for the three levels of analysis is shown in Table A-4.

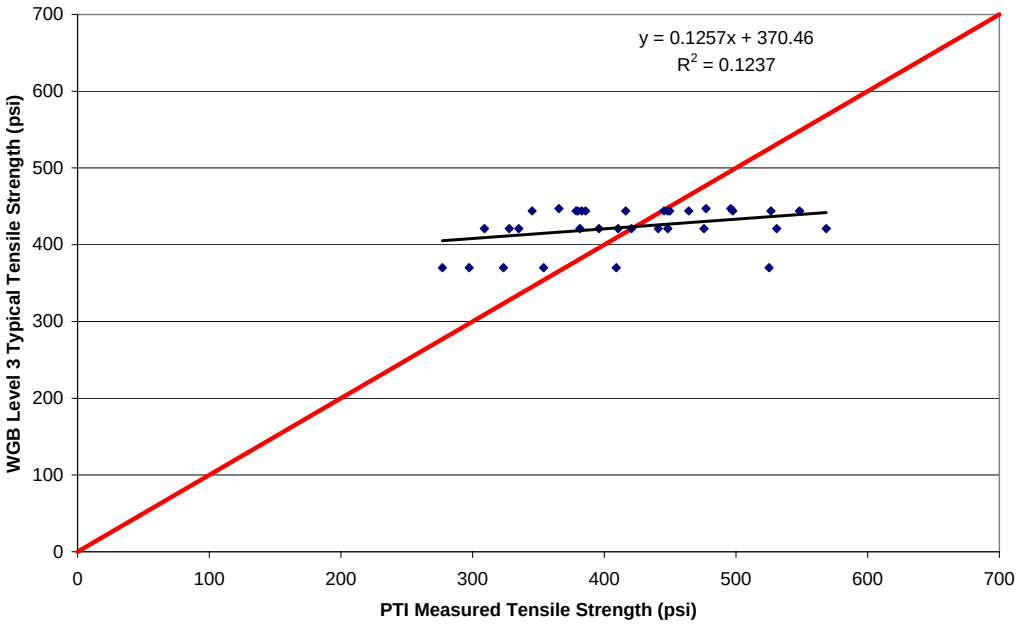

Figure A-15. Buttlar's Level 3 Typical Values for Tensile Strength

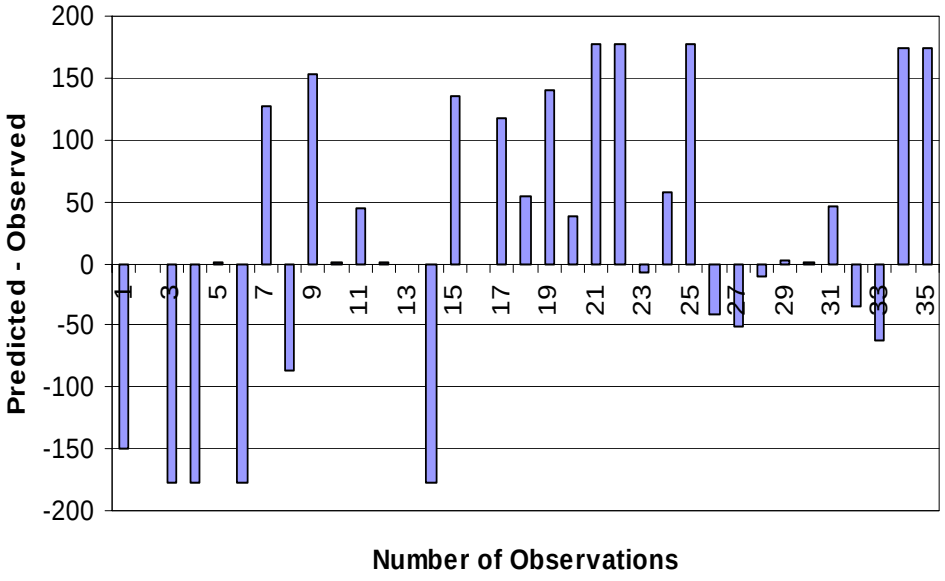

Figure A-16. Level 3 Prediction Errors

Table A-4. Statistics Summary for Calibration of the TC Model

Statistical Parameter	Analysis Level		
	1	2	3
Using actual historic temperature data:			
Average prediction error	-9.0	30.1	35.3
Standard deviation	44.7	60.9	98.4
R^2	0.74	0.25	0.03
Number of sections	35	35	35
Number of observations	35	35	35
Using estimated temperature based on EICM files:			
Average prediction error	16.2	49.7	---

VALIDATION OF THERMAL CRACKING MODEL FOR LEVEL 3 ANALYSIS

Given the poor performance of the thermal cracking distress prediction model for Level 3 analysis ($R^2 = 0.03$), a validation of the model was carried out using 94 sections of the LTPP database. Figure A-17 shows the total measured versus predicted transverse cracking for the selected sections. The total measured value is the weighted average of the low, medium, and high severity transverse cracking reported in the LTPP database, as follows:

$$Total\ Measured\ Cracking = \frac{Low\_Severity + 3\ Medium\_Severity + 5\ High\_Severity}{9} \quad \textbf{(Eq. 6)}$$

As shown in the results depicted in Figure A-17, the thermal cracking predictions values were very low (all of them near zero) compared to the measured total cracking observed in the field. Given the high standard error, the low R^2 and hence, the poor performance when using Level 3 analysis, it was deemed necessary to revised the models.

A FINAL APPROACH TO PREDICT THERMAL CRACKING FOR LEVEL 3 ANALYSIS IN THE DESIGN GUIDE

Revised prediction models for the mix creep compliance and tensile strength using numerical optimization techniques were developed. The new models are based on correlations of the creep compliance and tensile strength data with volumetric and mixture properties.

The creep compliance response at time *t*, can be written as:

$$D(t) = D_1 t^m \quad \textbf{(Eq. 7)}$$

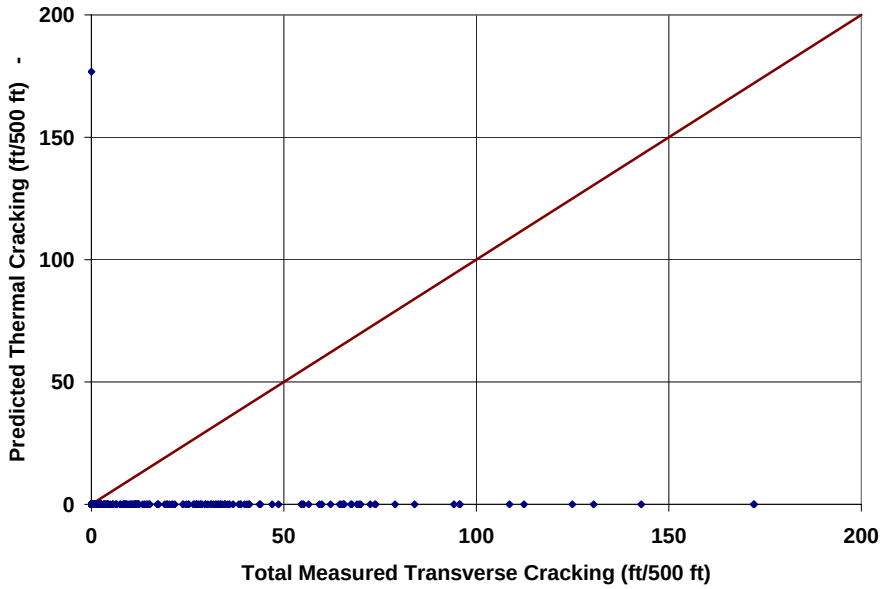

Figure A-17. Level 3 Predicted versus Total Measured Transverse Cracking for 94 LTPP Sections

where D_1 and m are the fracture coefficients obtained from the creep compliance and strength of the mixture; and t, the loading time in seconds.

The creep compliance data used to obtain the fracture coefficients was the same gathered to calibrate the initial model: 22 GPS sections from the LTPP database, 14 sections from the Canadian C-SHRP program, one section from Peoria, IL, and 5 MnROAD cells from the Minnesota DOT. These sections have been referred to as the PTI dataset. The creep compliance data is shown in Table A-1 and Figures A-6 to A-9.

The D_1 and m parameters were found at each temperature available: -20, -10, and 0 ^{o}C. Once the parameters D_1 and m for each selected mixture were found by nonlinear regression analyses, the team proceeded to correlate them against different volumetric and mixture properties, such as air voids, VFA, Penetration, A and VTS parameters, and A_{RTFO} and VTS_{RTFO} values.

The best correlation found for the D_1 fracture parameter was:

$$\log(D_1) = -8.5241 + 0.01306T + 0.7957\log(V_a) + 2.0103\log(VFA) - 1.923\log(A_{RTFO}) \quad \textbf{(Eq. 8)}$$

where: T = Test temperature (^{o}C) (i.e., 0, -10, and –20 ^{o}C)
V_a = Air voids (%)
VFA = Void filled with asphalt (%) = $\dfrac{V_{beff}}{V_{beff} + V_a} \times 100$

A_{RTFO} = Intercept of binder Viscosity-Temperature relationship for the RTFO condition

For the *m* parameter, the best relationship found was:

$$m = 1.1628 - 0.00185T - 0.04596V_a - 0.01126VFA + 0.00247\,Pen_{77} + 0.001683\,Pen_{77}^{0.4605}\,T$$

(Eq. 9)

where: T = Test temperature (^oC) (i.e., 0, -10, and –20 ^oC)
V_a = Air voids (%)
VFA = Void filled with asphalt (%)
Pen_{77} = Penetration at 77 ^oF = $10^{290.5013-\sqrt{81177.288+257.0694*10^{(A+2.72973*VTS)}}}$
A = Intercept of binder Viscosity-Temperature relationship
VTS = Slope of binder Viscosity-Temperature relationship

The outcome of the *m* value was set to a lower limit of 0.01.

The thermal fracture parameters *m* and D_1 were plotted in the creep compliance equation. Figure A-18 shows the measured versus predicted creep compliance. A total of 714 data points were used to obtain the above correlations. With an R^2 of 0.80 and a S_e/S_y of 0.45, the regressions were considered to be acceptable.

The tensile strength at –10 ^oC was also correlated with mixture properties. The best indicators were the air voids, the void filled with asphalt content, the Penetration at 77 ^oF, and the *A* intercept of the binder temperature-viscosity relationship for the RTFO condition. The following correlation was found:

$$S_t = 7416.712 - 114.016V_a - 0.304V_a^2 - 122.592VFA + 0.704VFA^2 + 405.71\log(Pen_{77}) - 2039.296\log(A_{RTFO})$$

(Eq. 10)

where the tensile strength (S_t) is given in psi. A total of 31 data points were used to obtain the above correlation. With an R^2 of 0.62 and a S_e/S_y of 0.68, the correlation was considered to be acceptable. Figures A-19 depicts the measured versus predicted tensile strength. The outcome of the equation was set to a lower limit of 100 psi.

By comparing Figures A-14 and A-18, it is quite evident that the ASU revised models provide better estimates for creep compliance and the error was significantly reduced. From Figure A-15 it is also evident that the typical values suggested initially provide a biased estimate and higher variance for the tensile strength compared to the ASU revised model shown in Figure A-19.

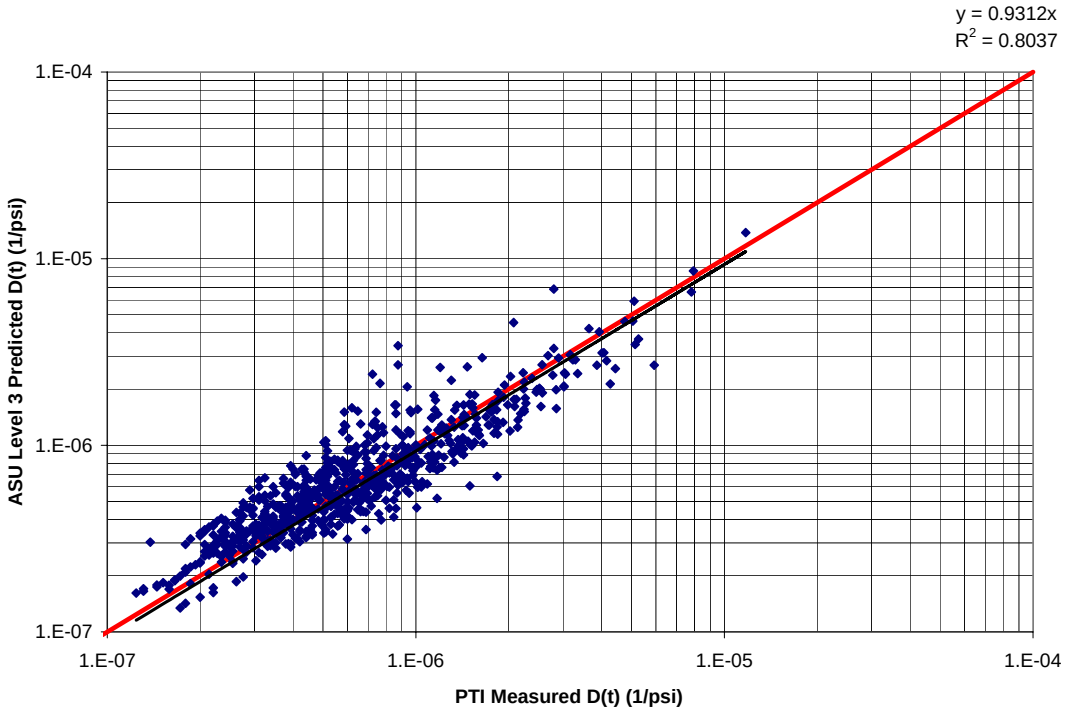

Figure A-18. PTI Measured vs ASU Level 3 Predicted Creep Compliance

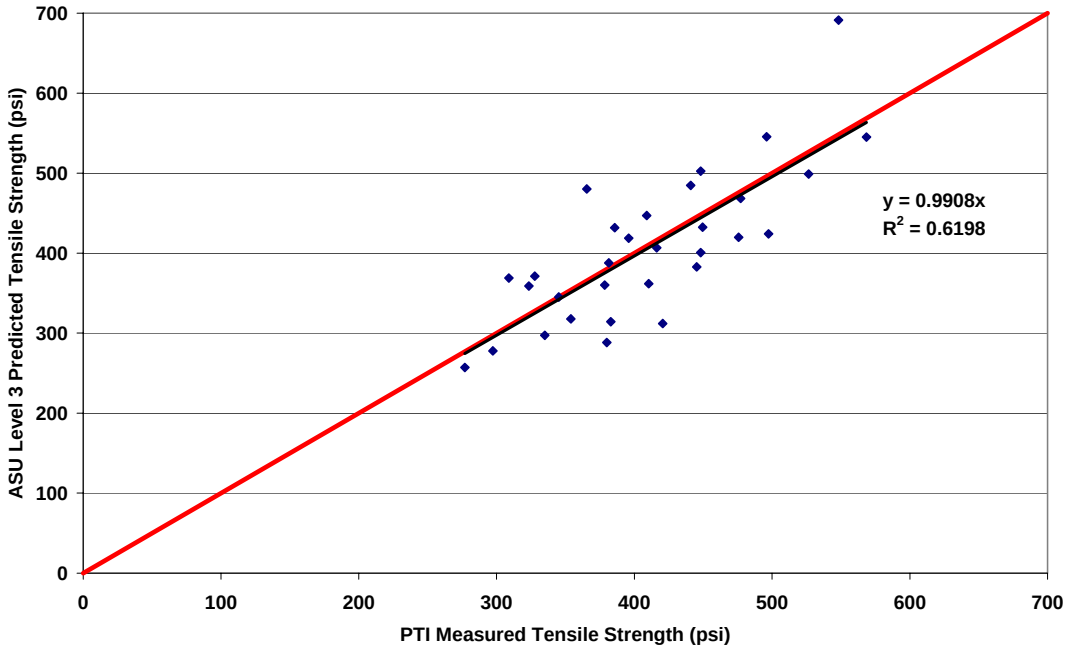

Figure A-19. ASU Level 3 Predicted Tensile Strength at –10 °C

Based on the above correlations, default values for creep compliance and tensile strength for the seven binders used in this analysis were re-calculated. A summary of the results is presented in Table A-5.

Table A-5. Level 3 Creep Compliance and Tensile Strength Data from the Revised Model for Level 3 Analysis

PG Grade	Time (sec)	Creep Compliance (1/psi)			Tensile Strength (psi)
		-20	-10	0	
82-10	1	3.7641E-07	5.08469E-07	6.86855E-07	354.77
	2	4.0378E-07	5.65524E-07	7.92068E-07	
	5	4.4302E-07	6.50888E-07	9.56284E-07	
	10	4.7523E-07	7.23924E-07	1.10277E-06	
	20	5.0977E-07	8.05155E-07	1.27169E-06	
	50	5.5932E-07	9.2669E-07	1.53535E-06	
	100	5.9998E-07	1.03067E-06	1.77053E-06	
76-16	1	3.313E-07	4.47529E-07	6.04535E-07	373.62
	2	3.6223E-07	5.09844E-07	7.17617E-07	
	5	4.0759E-07	6.05731E-07	9.00198E-07	
	10	4.4564E-07	6.90075E-07	1.06859E-06	
	20	4.8724E-07	7.86163E-07	1.26847E-06	
	50	5.4826E-07	9.34018E-07	1.5912E-06	
	100	5.9944E-07	1.06407E-06	1.88885E-06	
70-22	1	3.1396E-07	4.241E-07	5.72886E-07	420.28
	2	3.4383E-07	4.89337E-07	6.96419E-07	
	5	3.8773E-07	5.91225E-07	9.01514E-07	
	10	4.2463E-07	6.82171E-07	1.09591E-06	
	20	4.6504E-07	7.87106E-07	1.33222E-06	
	50	5.2442E-07	9.50994E-07	1.72456E-06	
	100	5.7432E-07	1.09728E-06	2.09644E-06	
64-28	1	3.3816E-07	4.56797E-07	6.17054E-07	422.02
	2	3.686E-07	5.33726E-07	7.72825E-07	
	5	4.1308E-07	6.55652E-07	1.04066E-06	
	10	4.5027E-07	7.66069E-07	1.30337E-06	
	20	4.908E-07	8.95082E-07	1.63239E-06	
	50	5.5003E-07	1.09956E-06	2.19812E-06	
	100	5.9954E-07	1.28473E-06	2.75302E-06	
58-34	1	3.8074E-07	5.14312E-07	6.94746E-07	479.31
	2	4.2726E-07	6.34948E-07	9.43599E-07	
	5	4.9759E-07	8.38901E-07	1.41433E-06	
	10	5.5838E-07	1.03567E-06	1.92094E-06	
	20	6.2661E-07	1.2786E-06	2.609E-06	
	50	7.2975E-07	1.6893E-06	3.91056E-06	
	100	8.1891E-07	2.08554E-06	5.31129E-06	

Table A-5. Continued.

PG Grade	Time (sec)	Creep Compliance (1/psi)			Tensile Strength (psi)
		-20	-10	0	
52-40	1	4.4857E-07	6.05945E-07	8.18528E-07	566.22
	2	5.4677E-07	8.38543E-07	1.286E-06	
	5	7.1033E-07	1.28836E-06	2.33677E-06	
	10	8.6583E-07	1.78291E-06	3.67134E-06	
	20	1.0554E-06	2.4673E-06	5.76811E-06	
	50	1.3711E-06	3.79083E-06	1.04811E-05	
	100	1.6712E-06	5.24598E-06	1.64671E-05	
46-46	1	5.518E-07	7.454E-07	1.007E-06	686.91
	2	8.108E-07	1.296E-06	2.070E-06	
	5	1.348E-06	2.690E-06	5.367E-06	
	10	1.981E-06	4.676E-06	1.103E-05	
	20	2.911E-06	8.126E-06	2.269E-05	
	50	4.841E-06	1.687E-05	5.882E-05	
	100	7.112E-06	2.933E-05	1.209E-04	

Validation of Level 3 Analysis Using the Revised Approach

To further validate the improvements of the thermal cracking predictions where using the latest models for, ASU carried out an analysis comprising two sets of data: 36 LTPP sections that provided information on thermal cracking and the PTI dataset used in the calibration of the models.

Data for 36 LTPP sections (156 observations) was collected and the DG2002 Level 3 analysis was performed using twelve different combinations: three values for the β fracture parameter on the Paris Law: β=1.0, 3.0, and 5.0 (see Eq. 5), and four different ways to determine the measured thermal cracking: Sum of Low, Medium, and High Severity Cracking (3a); Summation of Medium and High (3b); High Values Only (3c); and the use of the Weighted Average of the three severity levels as explained previously (3d). The summary of statistics found for all the combinations is given in Tables A-6, A-7 and A-8.

The errors (predicted – measured thermal cracking) values frequency distributions were plotted associated with each of the combinations mentioned above, and the plots are shown in Figures A-20, A-21, and A-22. Similarly, the plots of predicted versus measured thermal cracking values are shown in Figures A-23, A-24, and A-25.

Table A-6. Statistical Summary for Validation of the TC Model with LTPP Sites
β = 1.0

Statistical Parameter	Analysis Level					
	1	2	3a	3b	3c	3d
Average Prediction Error	NA	NA	-70.64	-2.83	32.42	18.86
Standard Deviation	NA	NA	137.1	103.3	81.92	80.08

Table A-7. Statistical Summary for Validation of the TC Model with LTPP Sites
β = 3.0

Statistical Parameter	Analysis Level					
	1	2	3a	3b	3c	3d
Average Prediction Error	NA	NA	-2.97	64.84	100.1	86.53
Standard Deviation	NA	NA	119.6	101.8	95.14	86.97

Table A-8. Statistical Summary for Validation of the TC Model with LTPP Sites
β = 5.0

Statistical Parameter	Analysis Level					
	1	2	3a	3b	3c	3d
Average Prediction Error	NA	NA	13.20	81.00	116.3	102.7
Standard Deviation	NA	NA	129.7	105.7	94.67	88.80

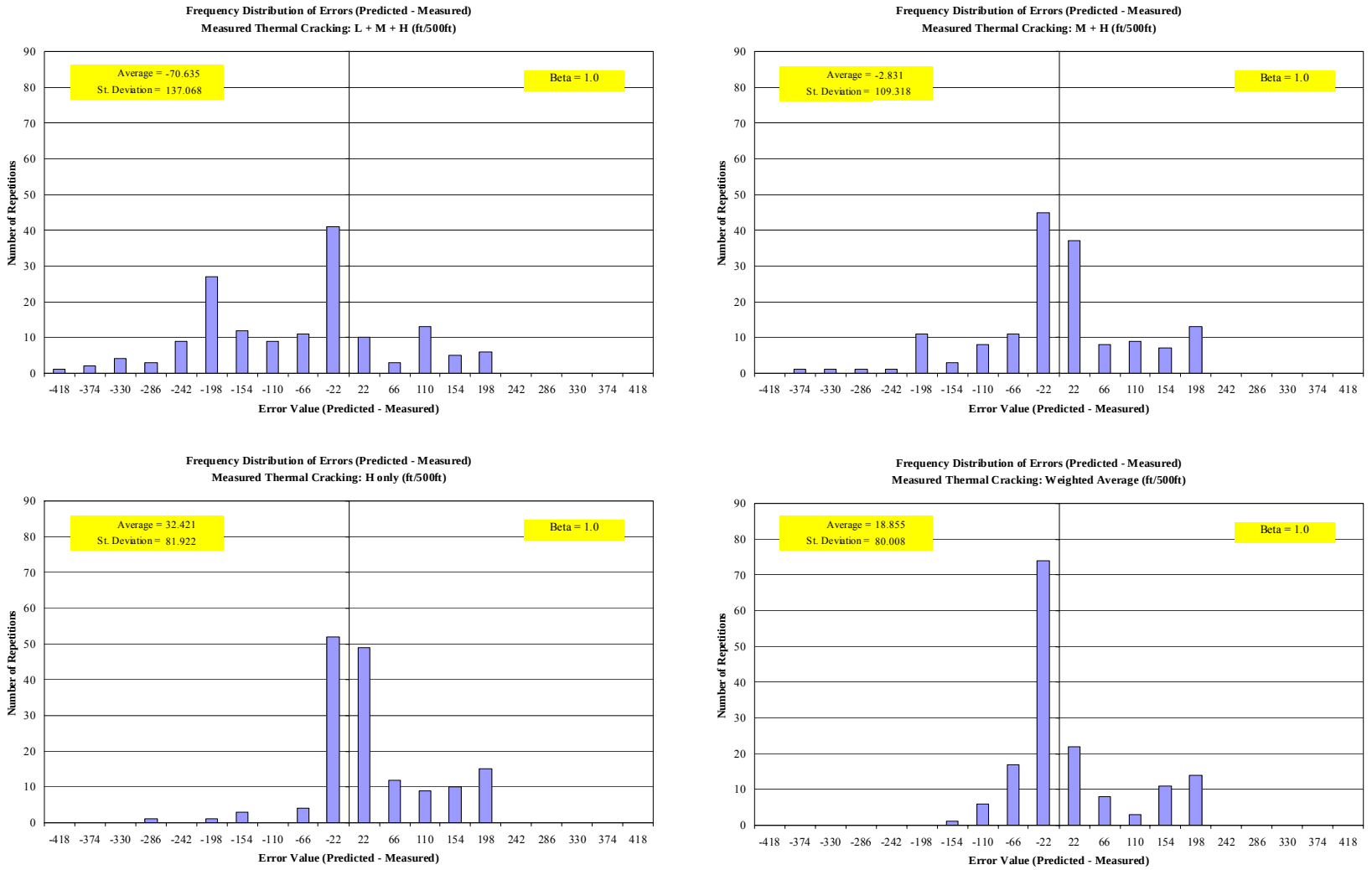

Figure A-20. Summary of Frequency Distribution for Level 3 Analysis with Beta Factor = 1.0

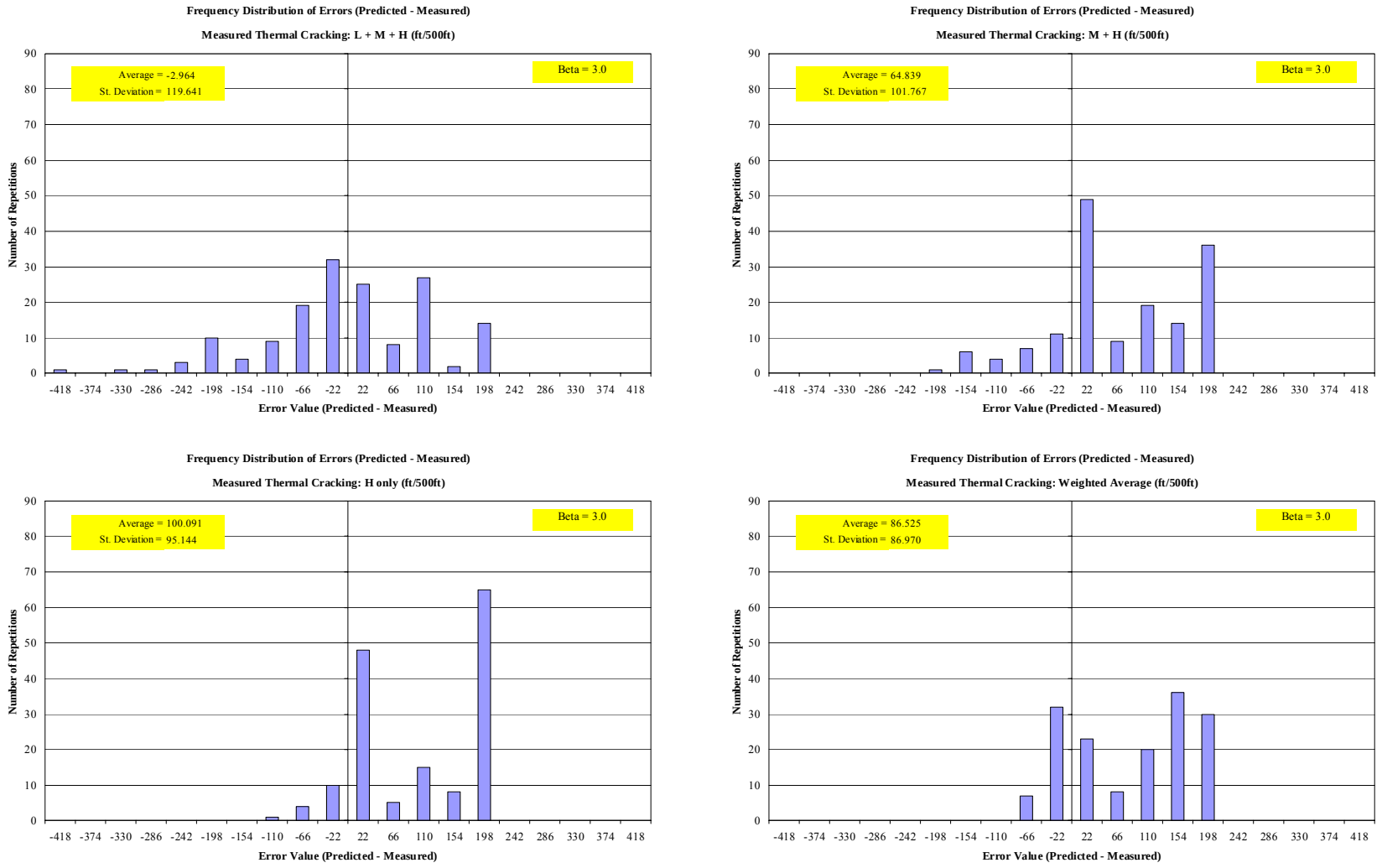

Figure A-21. Summary of Frequency Distribution for Level 3 Analysis with Beta Factor = 3.0

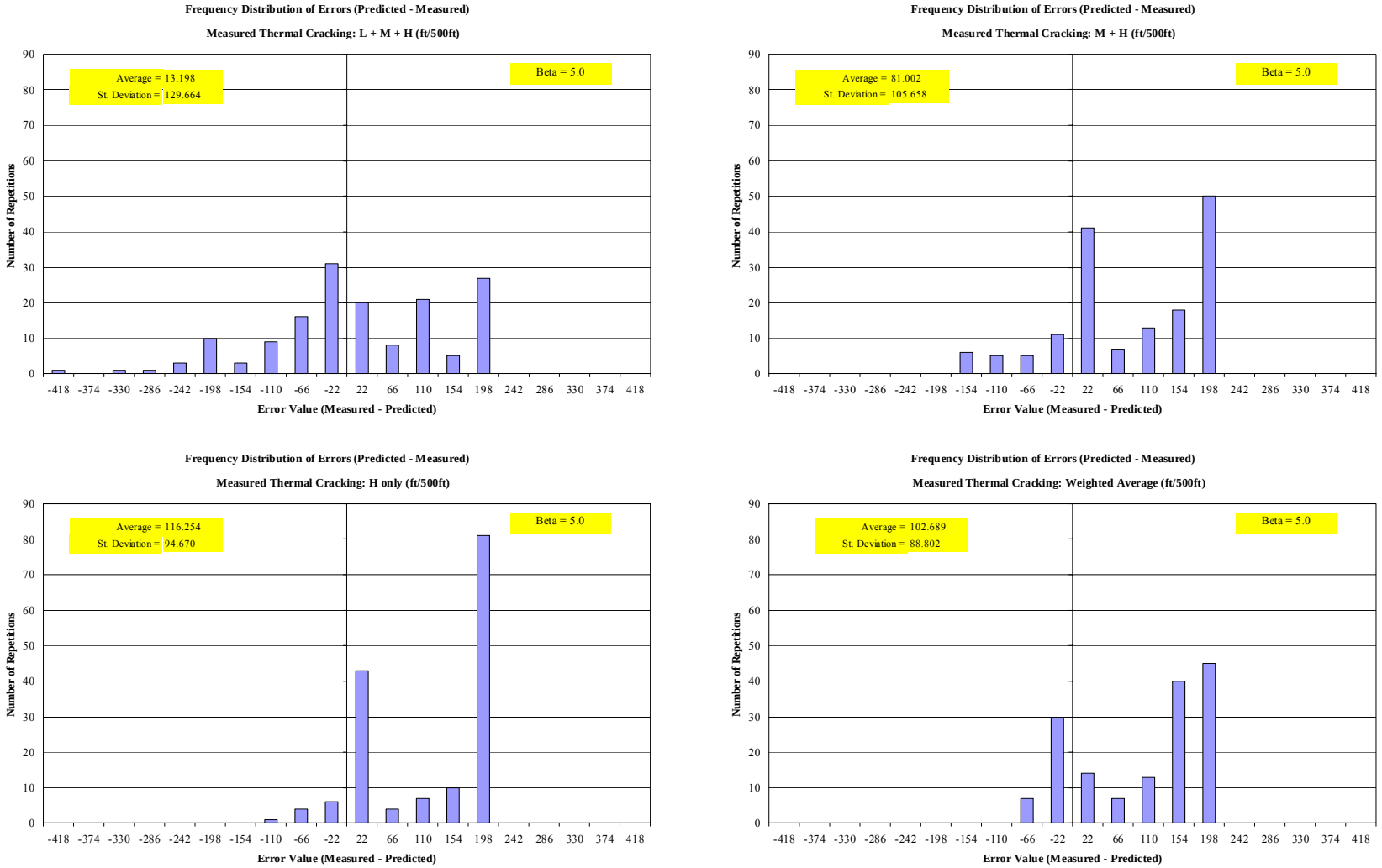

Figure A-22. Summary of Frequency Distribution for Level 3 Analysis with Beta Factor = 5.0

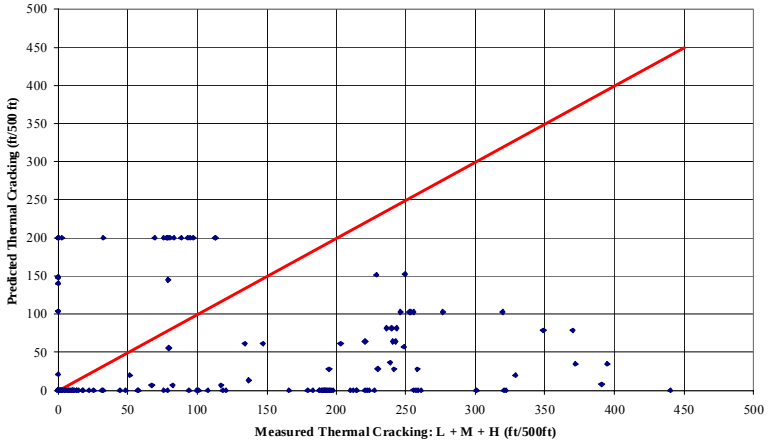

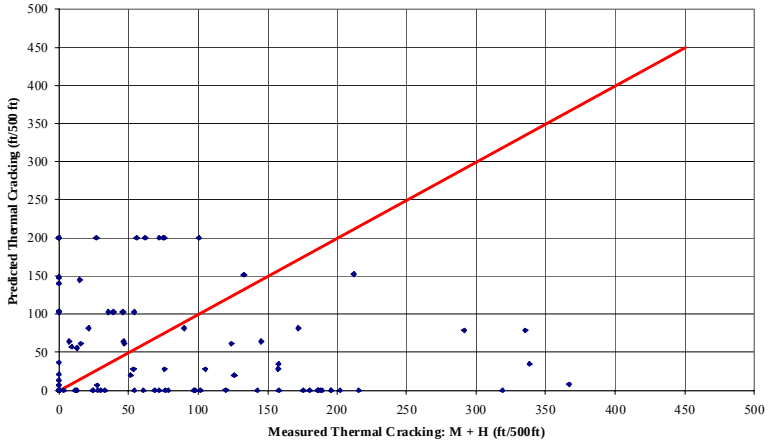

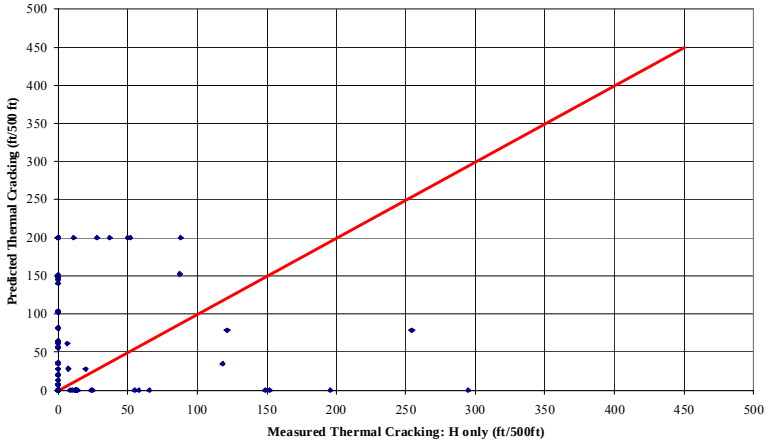

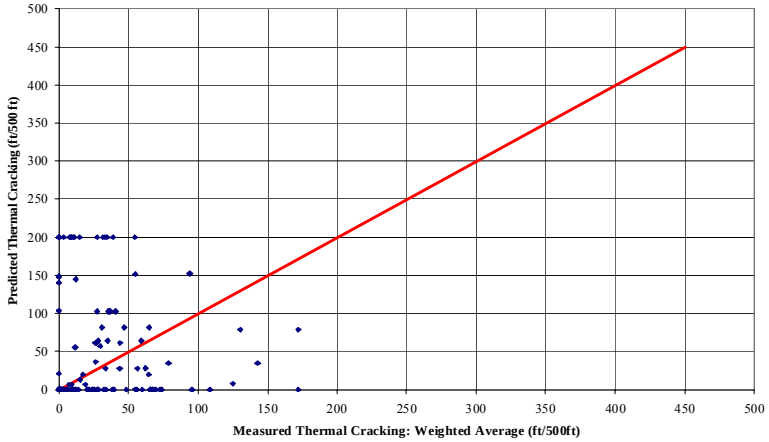

Figure A-23. Summary of Measured versus Predicted Relationships for Level 3 Analysis with Beta Factor = 1.0

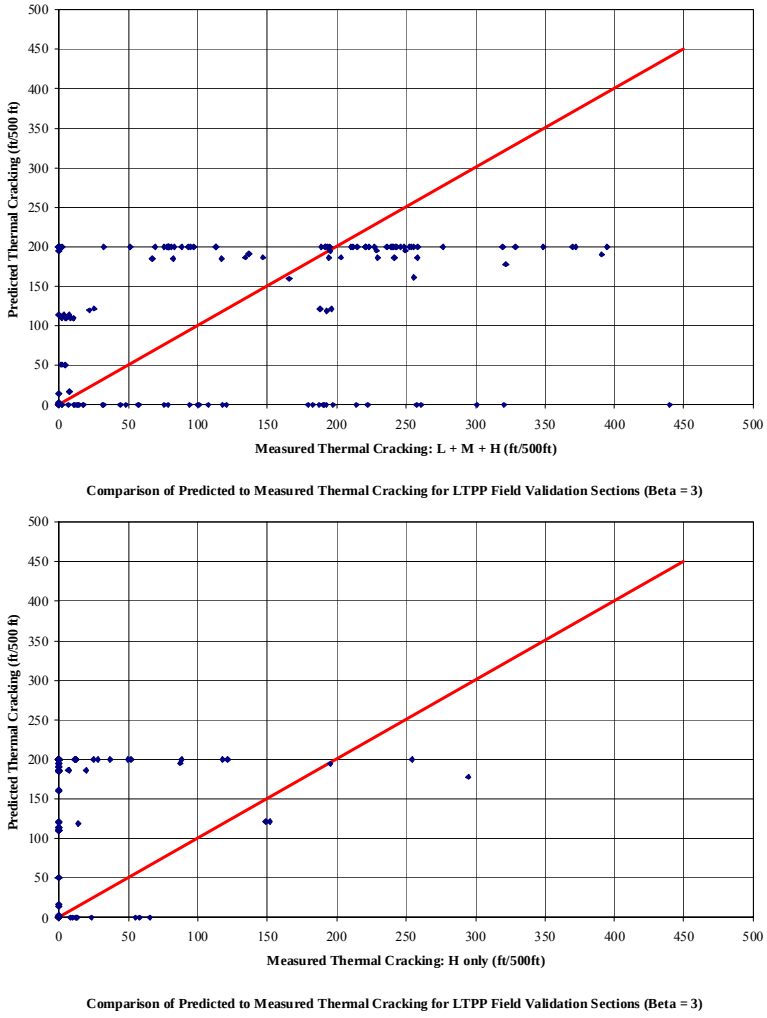

Figure A-24. Summary of Measured versus Predicted Relationships for Level 3 Analysis with Beta Factor = 3.0

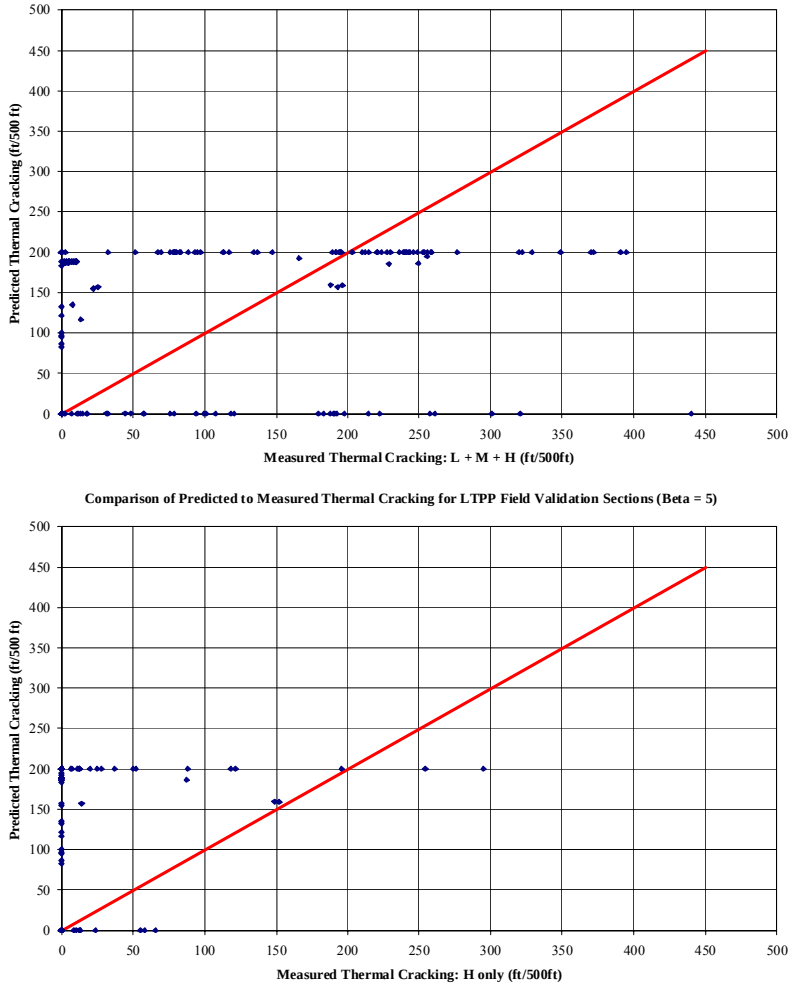

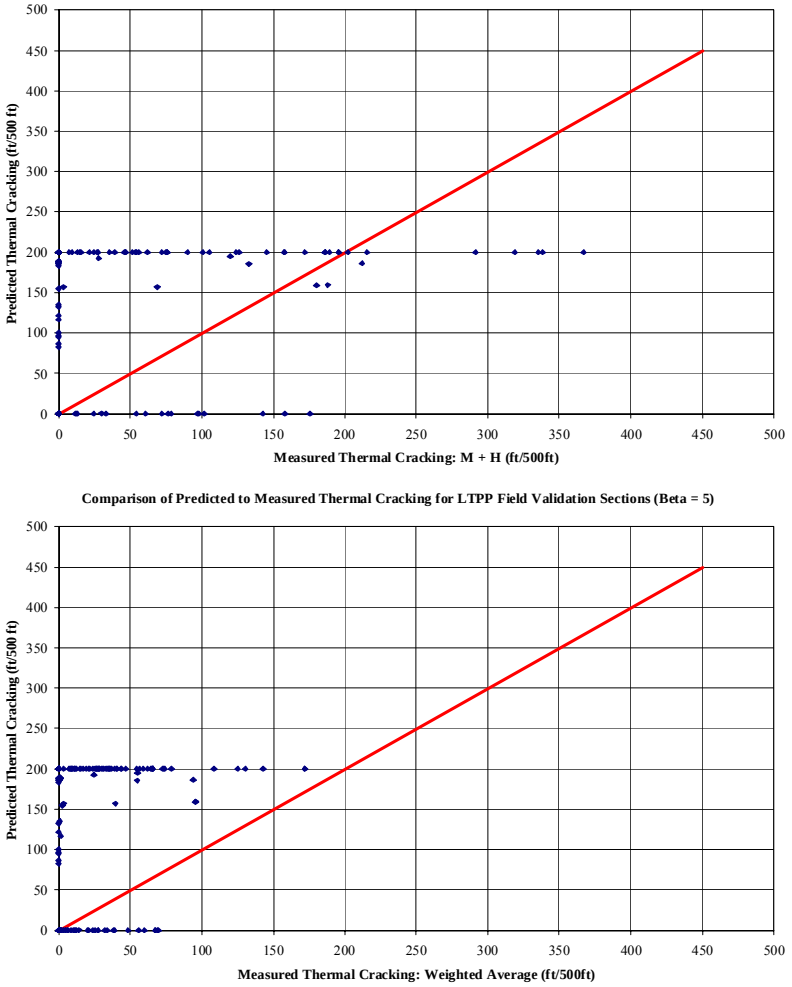

Figure A-25. Summary of Measured versus Predicted Relationships for Level 3 Analysis with Beta Factor = 5.0

Conclusions

The calibration of the thermal cracking models for flexible pavement design was performed for three hierarchical levels of analysis (Levels 1, 2, and 3), being Level 1 the one that involved the greatest amount of measured laboratory data and hence, the one considered to yield the best predictions.

Two cases were considered in the analysis: In the first case, actual pavement temperatures were used to predict thermal cracking. In the second case, the pavement temperatures were estimated based on historical records given by the Enhanced Integrated Climatic model (EICM). Table A-9 summarizes the goodness of the fit, represented by the average standard prediction errors, the standard deviation, and the R^2 for the cases considered.

Table A-9. Statistics Summary for Final Calibration of the TC Model

Statistical Parameter	Analysis Level		
	1	2	3
Using actual historic temperature data:			
Average prediction error	-9.0	30.1	---
Standard deviation	44.7	60.9	---
R^2	0.74	0.25	---
Number of sections	35	35	---
Number of observations	35	35	---
Using estimated temperature based on EICM files:			
Average prediction error	16.2	49.7	86.5
Standard deviation	---	---	87.0
Number of sections	35	35	36
Number of observations	35	35	156

Based on the statistical analysis for the calibration of the model, the following conclusions can be drawn:

1) The average prediction error was found to be lower for Level 1 and higher for Level 3 analysis. The importance of the hierarchical levels approach is one more time emphasized in the calibration of the thermal cracking model. The more measured laboratory data is input into the Design Guide, the better predictions should be expected as shown in the results.

2) For the calibration of Levels 1 and 2 of the thermal cracking model, the average prediction errors were found to be lower in cases where actual historic temperatures were used in the analysis, compared with cases in which estimated temperatures based on the EICM files were utilized. This comparison illustrates the power and highlights the importance of inputting actual historic climatic data for the design period instead of estimated data. Based on these results, it is recommended to use actual historic pavement temperatures from existing climatic files information when considering forensic analysis.

A validation study of the improved level 3 model developed was carried out at ASU. Best estimates and lower variances were found using a Paris law adjustment factor (β) equal to 1.0 (no adjustment) and using the weighted average of the three different severity levels, being the results using β equal to 3.0 quite close. As shown in table A-6, the average and standard error of estimate were lower than that found by the original Level 3 analysis model using the PTI data (compare to Table A-4).

However, a sensitivity analysis performed on the Level 3 Analysis yielded that the model provides the best predictions when a β factor of 3.0 is being used. Therefore, this factor was decided to go with the models developed. The average prediction error and the standard deviation are shown in Table A-9. The details of the sensitivity analysis for Level 3 calibration of the thermal cracking model can be found in Annex C.

ANNEX- A

Modification and Re-calibration of Superpave Thermal Cracking Model

SUPERPAVE SUPPORT AND PERFORMANCE MODELS MANAGEMENT

NCHRP 9-19

PROJECT REPORT

Project Deliverable Task B

MODIFICATION AND RE-CALIBRATION OF SUPERPAVE THERMAL CRACKING MODEL

Superpave Models Team

Dr. M. W. Witczak
Project Principal Investigator

Dr. Reynaldo Roque
Dr. Dennis R. Hiltunen
Dr. William G. Buttlar

DECEMBER 2000

ARIZONA STATE UNIVERSITY

College of Engineering and Applied Sciences
Department of Civil and Environmental Engineering
Tempe, AZ 85287-5306

Acknowledgement

This report was prepared under Task B of the NCHRP 9-19 contract (Superpave Support and Performance Models Management). Dr. Matthew W. Witczak of Arizona State University is the Principal Investigator on this project while Mr. Harold Von Quintus (Fugro/BRE) and Dr. Charles W. Schwartz (University of Maryland) are the Co-principal Investigators.

Dr. Reynaldo Roque, Dr. Dennis Hiltunen and Dr. William Buttlar developed the initial draft report as consultants to Arizona State University and the Project PI for possible eventual implementation into NCHRP 1-37A (Development of the 2002 Guide for the Design of New and Rehabilitated Pavement Structures). Major contributions were made during the review and editing process by the Superpave research team. These comments were subsequently integrated into the final report.

EXECUTIVE SUMMARY

This report describes the work conducted to finalize development of the Thermal Cracking Model (TCMODEL) that was originally developed under the SHRP A005 research contract. The main purpose of this study was to facilitate the incorporation of an updated version of TCMODEL and related software into the complete Superpave software program, which is being assembled as part of the University of Maryland/Arizona State Superpave Models Project.

The updates made to TCMODEL and related software in this project include: 1) incorporation of improved analysis techniques for converting raw data from the Superpave Indirect Tensile Test (IDT) into fundamental properties; 2) recalibration of TCMODEL to reflect updated analysis procedures and to incorporate new field data, and; 3) enhanced documentation for TCMODEL. In addition to the original field specimens and thermal cracking observations from twenty-two SHRP General Pavement Sections (GPS) used in the original calibration of TCMODEL during SHRP, fourteen Canadian SHRP (CSHRP) and five Mn/ROAD sections were also used in the re-calibration of TCMODEL. Although the recalibration included several analysis modifications and nearly twice as many field sections, the newly calibrated model parameters are similar to parameters developed during SHRP research.

The main products resulting from this project include: 1) an updated software suite, including modules for IDT data reduction and thermal cracking predictions, and; 2) a final report, which includes technical background on data analysis and model calibration, along with documentation for the new software suite. The Superpave Models Team will utilize these products in the development of revised Superpave performance prediction software, which serves as a supplement to Superpave volumetric mixture design procedures.

Table of Contents

List of Figures

List of Tables

Chapter 1

Introduction

1.1. Background

This report describes the work conducted to finalize development of the Thermal Cracking Model (TCMODEL) that was originally developed under the SHRP A-005 research contract and subsequently incorporated into the Superpave software developed under the SHRP A-001 research contract. The main purpose of this study was to facilitate the incorporation of an updated version of TCMODEL and related software into the complete Superpave software program, which is being assembled as part of the University of Maryland/Arizona State Superpave Support and Performance Models Management Project (NCHRP 9-19).

The updates made to TCMODEL and related software in this project include:

1. Incorporation of improved analysis techniques for converting raw data from the Superpave Indirect Tensile Test (IDT) into fundamental properties

2. Recalibration of TCMODEL to reflect updated analysis procedures and to incorporate new field data from Canadian SHRP (CSHRP) and Mn/ROAD projects

3. Enhanced documentation for the use of TCMODEL to make thermal cracking performance predictions

1.2. Project Tasks

This project involved the following five tasks:

- Task 1: Review and Correct Existing Model as Needed
- Task 2: Finalize and Incorporate New Data Reduction Software
- Task 3: Debug and Evaluate the Revised Model
- Task 4: Calibration of Revised Model
- Task 5: Documentation and Incorporation into Superpave software

Details of the work performed as part of these tasks is described in the following sections.

1.2.1. Task 1: Review and Make Necessary Corrections to Existing Model

This work involved a detailed review of the existing computer code for the thermal cracking model to investigate the cause of the problems that were cited in the evaluation conducted by the Superpave Models Team. Some examples of problems cited include: incorrect temperature conversions, unusually low thermal stress predictions in some instances, and incorrect properties determined from indirect tensile test data. The source of all problems were identified and corrected accordingly.

1.2.2. Task 2: Finalize and Incorporate New Data Reduction Software

Work performed subsequent to SHRP has led to the following findings:

- The method used to generate the master creep compliance curve within the thermal cracking model incorporated into the existing Superpave software can lead to significant errors in thermal cracking performance predictions

- The trimmed mean approach used in the existing Superpave software to reduce indirect tensile test data may in some instances include erroneous measurements (e.g. non-responsive gages) in the computation of creep compliance and strength

These findings indicated that the data reduction software used to determine properties and to generate the master creep compliance curve within the existing Superpave model needed to be modified. Therefore, the work involved in this task was as follows:

- Determine modifications necessary to make the new data reduction software compatible with the existing thermal cracking model

- Make necessary modifications

- Incorporate the modified data reduction software into the existing thermal cracking model

As part of work conducted subsequent to the SHRP program, two computer programs had been developed to address the problems described above. The computer program MASTER was developed to automatically generate master creep compliance curves (and m-value) from either 100- or 1000-second creep compliance data obtained from the Superpave indirect tensile test (IDT) and without the need for binder data. The model has been shown to be accurate and robust. Furthermore, work with this system has shown that master curves produced with 100-second creep test data are essentially equivalent to master curves produced with 1000-second data.

The second program is a modified version of the data reduction program developed to determine creep compliance and strength using data from the Superpave IDT. This program

provides strategic output that allows the user to evaluate the validity of the test data used to determine creep compliance and strength. The program then allows the user to modify the data reduction process to assure that erroneous data are not included in the determination of material properties. Significant experience with the new system has shown that the need to modify data reduction is always evident, such that data reduction can be accomplished systematically with relatively little opportunity for subjective decisions on the part of the user.

Both of these computer programs were incorporated into the existing thermal cracking model. It should be noted that the format in which the Superpave IDT data are required for input to the new data reduction software is different than the format for the data reduction software in the existing Superpave model. It is recommended that the new format be used and, therefore, required of Superpave users in the future.

1.2.3. Task 3: Debug and Evaluate the Revised Model

This task involved performing model runs to identify and solve any problems that existed with the revised model. Superpave IDT test data and pavement temperature data obtained from investigations conducted for the Canadian Strategic Highway Research Program (C-SHRP) was used for this purpose. These data have been fully evaluated and are known to be reliable.

1.2.4. Task 4: Calibrate the Model

It is seldom possible to develop a model for a complex, macro-scale physical phenomenon that predicts actual behavior perfectly. Statistical methods are often employed to generate and/or modify model parameters that allow a model to match as closely as possible actual observed behavior.

In this task, the revised thermal cracking model was recalibrated to update the model parameters. Three data sets were employed for model recalibration: the 23 SHRP GPS pavement sections used for the original calibration, 14 pavement sections evaluated by the authors for C-SHRP, and 5 test cells from the Minnesota Department of Transportation Road Research Program (Mn/ROAD). Data for each of the pavement sections was then reconstituted for input to the revised model. This data was used to predict thermal cracking performance for each of the 41 sections. Finally, nonlinear regression was performed to determine the model parameters. The techniques used in the original model calibration effort were once again followed, as documented in the SHRP A-357 report (Lytton et al. [1993]).

1.2.5. Task 5: Documentation and Technical Assistance

The objectives of this task were two-fold. First, details concerning the newly recalibrated thermal cracking model were compiled, as presented in this report, which includes the following documentation:

- Technical features of the thermal cracking model
- Recalibration details, as described in task 4

- Information for inclusion in a user's manual, to be subsequently developed by the Superpave Models team.

Second, this task provided technical services to the Superpave Models team for integration of the revised thermal cracking model into a Window-based computer program.

1.3. Research Products

The following two products resulted from this project:

1. **A Revised And Calibrated Model -** The revised model predicts thermal cracking performance of pavements using pavement temperature data and test results from the Superpave IDT creep and strength test. The model was provided in the form of a FORTRAN-based computer code, which involved a modification of the existing code within the Superpave software. The modifications include recent improvements to IDT data reduction, an expanded set of field performance data for model calibration, and recalibrated model coefficients.

2. **Final Report -** The remainder of this report describes the technical features of the thermal cracking model and provides documentation that can be incorporated into a user's manual. The report also describes calibration activities that were conducted, and the new calibration coefficients for TCMODEL.

1.4. Organization of This Report

The organization of the remainder of this report is as follows:

- Chapter 3 describes routine data analysis procedures, including the conversion of raw IDT creep test data into creep compliance and the conversion of IDT strength test data into mixture tensile strength. The latter portion of Chapter 3 describes data analysis procedures that have been modified since the initial calibration of TCMODEL. These modifications include construction of the creep compliance master curve, and interactive user input screens, which allow user-defined modifications to the standard trimmed mean approach for data reduction. The screens also allow the user to manually input Poisson's ratio of the mixture, in the event that alternate measures of this parameter are desired for input.

- Chapter 4 documents the activities involved in preparing IDT data from the 41 mixtures used in the recalibration effort, the steps involved in the recalibration of TCMODEL, and the results of the recalibration.

- Chapter 5 provides a summary of the recalibration effort reported herein and recommendations for future enhancements to TCMODEL.

Detailed appendices are included as part of this report, which document the fundamental properties obtained with the Superpave IDT, along with other model inputs and outputs that were generated as part of this project.

Chapter 2

A Mechanics-Based Prediction Model for Thermal Cracking of Asphaltic Concrete Pavements

2.1 Introduction

The purpose of this chapter is to describe the mechanics-based thermal cracking performance model (TCMODEL) developed as part of the SHRP A-005 contract, which will be used in the AASHTO 2002 design guide. TCMODEL predicts the amount (or frequency) of thermal cracking that will develop in a pavement as a function of time. Inputs to the model include: the fundamental properties (master creep compliance curve and failure limits as a function of temperature) obtained from the Superpave IDT (AASHTO TP9-94 [1996]), pavement structure, and site-specific weather data. The measured material properties can be used in the model to determine whether or not a particular mixture will meet specific thermal cracking performance requirements. Thus, this system provides the basis for development of a true performance-based mixture specification for thermal cracking.

2.2 The Thermal Cracking Mechanism

As described by Haas et al. (1987), Roque, Hiltunen, and Stoffels (1993), and others, the primary mechanism leading to thermal cracking is shown in Figure 2.1. Contraction strains induced by cooling lead to thermal tensile stress development in the restrained surface layer. Thermal stress development is greatest in the longitudinal direction of the pavement because there is more restraint in that direction. Also, thermal stresses are greatest at the surface of the pavement because pavement temperature is lowest at the surface. Depending upon the magnitude of these stresses and the asphalt mixture's resistance to fracture (crack propagation), transverse cracks may develop at different points along the length of the pavement.

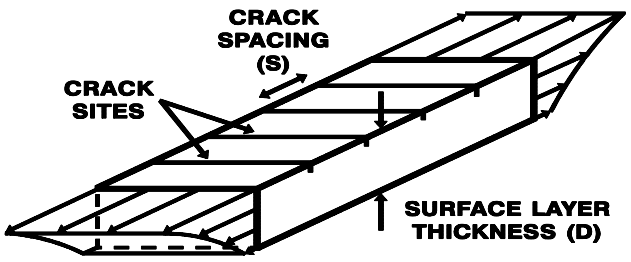

Figure 2.1. Schematic of Physical Model of Pavement Section

For very severe cooling cycles (very low temperatures and/or very fast cooling rates) transverse thermal cracks may develop at specific locations within the pavement under one or very few cooling cycles. This is generally referred to as low temperature cracking. Additional cracks will develop at different locations as the pavement is exposed to subsequent cooling cycles.

For milder cooling conditions, cracks may advance and develop at a slower rate, such that it may take several cooling cycles for cracks to propagate completely through the surface layer. This is generally referred to as thermal fatigue cracking. As for low temperature cracking, cracks will develop faster at some locations within the pavement than at others.

Note that the mechanism of failure is the same for low temperature cracking as for thermal fatigue cracking; the only difference is in the rate at which cracking occurs. Thus, one may refer to both phenomena as thermal cracking.

2.3 Previous Models

At the start of the SHRP A-005 project, there were no existing models to predict thermal cracking performance (amount of cracking versus time) using fundamental, low-temperature mixture properties. Empirical models have been developed (Fromm and Phang [1972]; Haas et al. [1987]) to predict the number of cracks or crack spacing, but these models do not include time as a variable, and they are primarily based upon asphalt cement properties rather than mixture properties. Other existing models predicted a mixture's cracking potential (COLD, Finn et al. [1986]; CRACK3, Roque and Ruth [1990]), but did not predict thermal cracking performance in terms of amount of cracking versus time. A model called THERM, developed by Lytton, Shanmugham, and Garrett [1983] provides thermal cracking predictions as a function of time, but relies on estimated mixture properties rather than mixture properties directly measured at low temperatures. Therefore, the SHRP A-005 program undertook the development of a new thermal cracking model that predicted thermal cracking performance (amount of cracking versus time) using mixture properties measured from the IDT, along with site-specific environmental and structural information. The resulting thermal cracking model was called TCMODEL, which includes the following features:

- Mixture characterization that includes the measured time and temperature dependent behavior of the mixture.
- Pavement temperatures that are computed on an hourly basis throughout the life of the pavement.
- Thermal stress predictions that account for time-dependent relaxation and nonlinear cooling rates.
- Stress predictions as a function of depth.
- Amount of cracking versus time using a mechanics-based approach.

A detailed description of the model and its development is presented in the following sections.

2.4 Physical Model

The physical representation of the actual pavement structure assumed in TCMODEL is shown in Figures 2.1 and 2.2. In Figure 2.1 an asphaltic concrete surface layer of thickness D is shown to be subjected to a tensile stress distribution with depth. The stresses develop due to contraction of the asphaltic concrete material during cooling. The stresses are not uniform with depth because of a thermal gradient, i.e., the pavement temperatures vary with depth. It is assumed that within the surface layer there are potential crack sites uniformly spaced at a distance S. At each of these crack sites the induced thermal stresses can potentially cause a crack to propagate through the surface layer (Figure 2.2), at which time it is assumed that a transverse crack will be visible on the pavement surface. It is assumed that each of these cracks can propagate at different rates due to spatial variation of the relevant material properties within the surface layer.

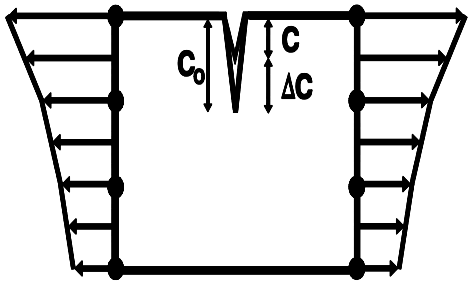

Figure 2.2. Schematic of Crack Depth Fracture Model

The thermal cracking model consists of two main components:

1) A mechanics-based model that calculates the downward progression of a vertical crack at a single crack site having average material properties.

2) A probabilistic model that calculates the global amount of thermal cracking visible on the pavement surface from the current average crack depth and the assumed distribution of crack depths within the surface layer.

2.5 Model Components

Flow diagrams of the thermal cracking model are shown in Figures 2.3 and 2.4. Figure 2.3 illustrates the interrelationships between the five major components of the model. These five components are the:

- Inputs module
- Superpave Indirect tensile test (IDT) and IDT transformation model
- Environmental effects model (Integrated Climactic Model)
- Pavement response model

- Pavement distress model

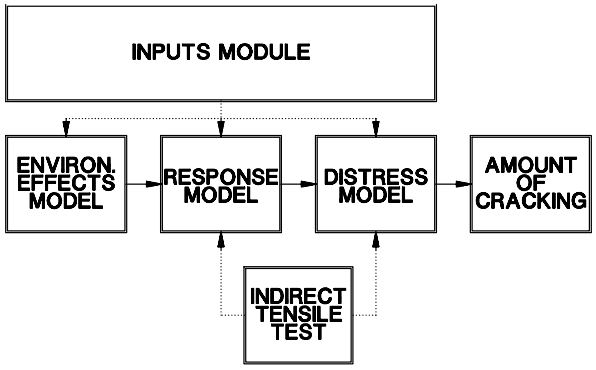

Figure 2.3. Major Components of the Thermal Cracking Model

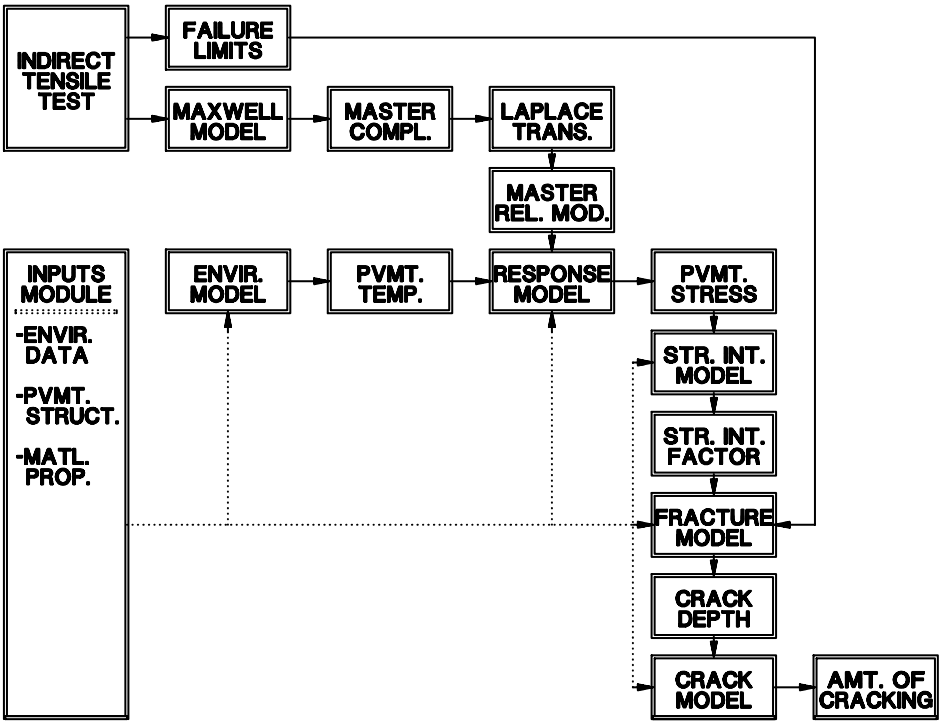

Figure 2.4. Detailed Schematic of the Thermal Cracking Model

Figure 2.4 provides more detailed information for each of the model components, which are individually described in the following sections.

2.5.1 Inputs Module

The input data includes pavement structure information, pavement material properties, and site-specific environmental data. A detailed inventory of the specific inputs in each of these three categories is as follows:

- Pavement structure
  - Layer types: asphaltic concrete, stabilized base, or AASHTO classification for unbound granular materials and soils
  - Layer thicknesses
- Pavement material properties (Note: the properties described below are used primarily for pavement temperature predictions; the properties required for pavement response calculations come from the indirect tensile test at low temperatures (IDT) described in the next section)
  - Coefficient of thermal contraction of asphaltic concrete
  - Unit weight, thermal conductivity, heat capacity, surface emissivity factor, surface short-wave absorptivity, and maximum allowable convection coefficient of asphaltic concrete
  - Constant deep-ground temperature, freezing temperature of soil, and lower and upper limits of freezing range of soil
- Environmental data
  - Minimum and maximum daily air temperatures
  - Times of day when minimum and maximum air temperatures occur
  - Latitude of site
  - Average monthly wind velocity
  - Average monthly sunshine

The linear coefficient of thermal contraction for the asphalt mixture is computed using the following relationship, which is a modified version of the relationship proposed by Jones, Darter, and Littlefield (1968):

$$B_{MIX} = \frac{VMA * B_{AC} + V_{AGG} * B_{AGG}}{3 * V_{TOTAL}} \quad \textbf{(2.1)}$$

where: B_{MIX} = linear coefficient of thermal contraction of the asphalt mixture (1/°C)

B_{AC} = volumetric coefficient of thermal contraction of the asphalt cement in the solid state (1/°C)
B_{AGG} = volumetric coefficient of thermal contraction of the aggregate (1/°C)
VMA = percent volume of voids in the mineral aggregate (equals percent volume of air voids plus percent volume of asphalt cement minus percent volume of absorbed asphalt cement)
V_{AGG} = percent volume of aggregate in the mixture
V_{TOTAL} = 100 percent

Given that coefficients of thermal contractions of asphalt cement and aggregate are not measured as part of routine mixture design, an average value of volumetric coefficient of thermal contraction of 3.45×10^{-4}/°C is recommended for all asphalt binders. A sensitivity analysis revealed that the thermal coefficient for a typical mixture varied by a maximum of five percent when the contraction coefficient of the binder was varied by the range reported for the SHRP MRL binders. The variation resulting from most of the asphalts was even less. Similarly, the thermal contraction coefficient of a typical mixture was found to be insensitive to typical variations in reported contraction coefficients for a particular type of aggregate. One reason for this is that the coefficient of thermal contraction for a typical aggregate is about two orders of magnitude less that the contraction coefficient of asphalt cement. Therefore, it is adequate to use published values of contraction coefficients for the type of aggregate being used. VMA and V_{AGG} of the mixture can be obtained from tests routinely performed as part of the mixture design process.

Contraction coefficients determined from this relationship appear to be reasonably accurate. Coefficients determined for four mixtures produced from SHRP MRL materials, agreed well with measured values reported by most researchers in the literature, and resulted in reasonably accurate predictions of thermal stresses and fracture temperatures measured in the thermal stress restrained specimen test (TSRST) (Lytton et al. [1993]).

2.5.2 Use of Superpave IDT in TCMODEL

If one considers the primary mechanism of thermal cracking shown in Figure 2.1 (thermal stress development and crack propagation), the primary material properties controlling this mechanism are the viscoelastic properties, which control thermal stress development, and the fracture properties, which control the rate of crack development. These are the properties that are measured and controlled by the Superpave IDT (Figure 2.5). The following section provides a description of the material models assumed in the data analysis performed on IDT test data, and a description of the IDT transformation model, which converts test results to a form appropriate for the pavement response model.

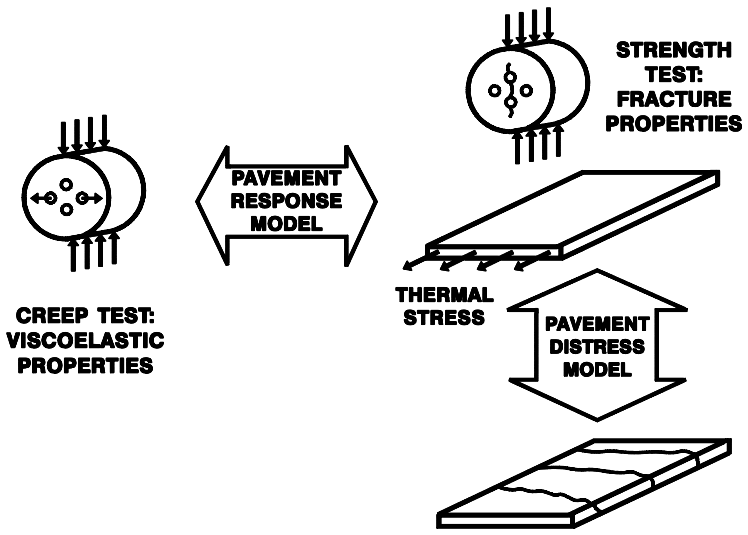

Figure 2.5. Materials Characterization with the IDT

2.5.2.1 Viscoelastic Properties

The viscoelastic properties of the asphaltic concrete mixture control the level of stress development during cooling. More specifically, the time- and temperature-dependent relaxation modulus of the mixture is the property needed to compute thermal stresses in the pavement according to the following constitutive equation:

$$\sigma(\xi) = \int_0^{\xi} E(\xi - \xi') \frac{d\varepsilon}{d\xi'} d\xi' \qquad \textbf{(2.2)}$$

where:

	$\sigma(\xi)$	=	stress at reduced time ξ
	$E(\xi-\xi')$	=	relaxation modulus at reduced time $\xi-\xi'$
	ε	=	strain at reduced time ξ (= $\alpha(T(\xi') - T_0)$)
	α	=	linear coefficient of thermal contraction
	$T(\xi')$	=	pavement temperature at reduced time ξ'
	T_0	=	pavement temperature when $\sigma = 0$
	ξ'	=	variable of integration

This constitutive equation is described in detail in the Pavement Response Model section below.

A generalized Maxwell model was selected to represent the viscoelastic properties of the asphaltic concrete mixture in relaxation. A schematic representation of the model is shown in Figure 2.6.

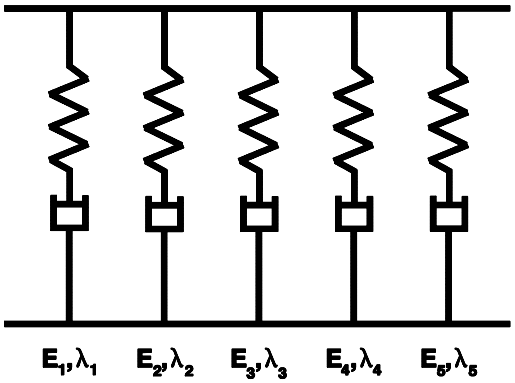

Figure 2.6. Generalized Maxwell Model for Relaxation Modulus

Mathematically, the relaxation modulus for a generalized Maxwell model can be expressed according to the following Prony series:

$$E(\xi) = \sum_{i=1}^{N+1} E_i e^{-\xi/\lambda_i} \quad \textbf{(2.3)}$$

where: $E(\xi)$ = relaxation modulus at reduced time ξ
E_i, λ_i = Prony series parameters for master relaxation modulus curve (spring constants or moduli and relaxation times for the Maxwell elements)

This function describes the relaxation modulus as a function of time at a single temperature, which is generally known as the reference temperature. The function defined at the reference temperature is called the master relaxation modulus curve. Relaxation moduli at other temperatures are determined by using the method of reduced variables (time-temperature superposition), which assumes that the mixture behaves as a thermorheologically simple material. Relaxation moduli at other temperatures are determined by replacing real time (i.e., time corresponding to the temperature of interest) with reduced time (i.e., time corresponding to the temperature at which the relaxation modulus is defined) according to the following equation:

$$\xi = \frac{t}{a_T} \quad \textbf{(2.4)}$$

where:

ξ = reduced time
t = real time
a_T = temperature shift factor

The relaxation modulus function is obtained by transforming the following time-dependent creep compliance function, which is determined by performing creep tests at multiple temperatures:

$$D(\xi) = D(\infty) - \sum_{i=1}^{N} D_i e^{-\xi/\tau_i} + \frac{\xi}{\eta_v} \quad \textbf{(2.5)}$$

or

$$D(\xi) = D(0) + \sum_{i=1}^{N} D_i\left(1 - e^{-\xi/\tau_i}\right) + \frac{\xi}{\eta_v} \qquad \textbf{(2.6)}$$

where:

$$D(\infty) = D(0) + \sum_{i=1}^{N} D_i \qquad \textbf{(2.7)}$$

and:

$D(\xi)$	=	creep compliance at reduced time ξ
ξ	=	reduced time $= t/a_T$
a_T	=	temperature shift factor
$D(\infty), D(0), D_i, \tau_i, \eta_v$	=	Prony series parameters

Prony series parameters and shift factors are obtained by performing creep compliance tests at multiple temperatures and mathematically shifting data from different temperatures to establish one smooth, continuous curve. This process is illustrated conceptually in Figure 2.7. The resulting curve is called the master creep compliance curve. Details on how compliance curves are obtained at individual temperatures from indirect tensile creep tests are presented in Roque and Buttlar (1992) and Buttlar and Roque (1994). Additional details on how individual compliance curves are shifted to obtain the master curve are presented in the IDT Transformation Model section below. Details on the transformation of the master creep compliance curve to obtain the master relaxation modulus curve are also included in the IDT Transformation Model section.

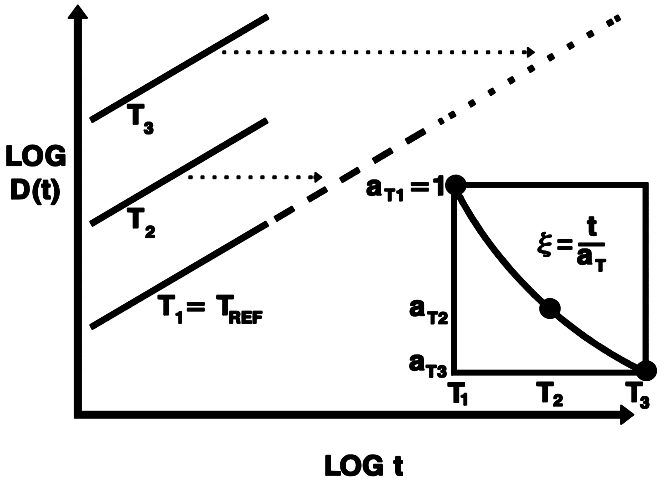

Figure 2.7. Development of the Master Creep Compliance Curve (MCCC)

2.5.2.2 Fracture Properties

The amount of crack propagation induced by a given thermal cooling cycle can be predicted using the Paris law of crack propagation:

$$\Delta C = A\Delta K^n \quad \textbf{(2.8)}$$

where:

ΔC	=	change in the crack depth due to a cooling cycle
ΔK	=	change in the stress intensity factor due to a cooling cycle
A,n	=	fracture parameters for the asphalt mixture

As explained in the Crack Depth (Fracture) Model section below, the change in crack depth (ΔC) is computed and accumulated on a daily basis to determine the total crack depth as a function of time. The crack depth is related to the total amount of cracking by way of a crack depth distribution function. The idea is that material variability along the length of the pavement section will result in different crack depths, even for the same exposure conditions. The crack depth distribution governs how much cracking is observed in a particular section having a specific crack depth computed on the basis of average material properties.

Thus, the material properties that directly influence the amount of cracking that will develop in a pavement subjected to specified levels of thermal stress are the fracture parameters *A* and *n*. Since it is not practical to perform fracture tests for mixture specification purposes, fracture parameters *A* and *n* must be determined on the basis of material properties measured as part of the specification tests, along with theoretical or experimental relationships between measured properties and fracture parameters *A* and *n*. Schapery's theory of crack propagation in nonlinear viscoelastic materials (Schapery [1973]) indicates that the fracture parameters *A* and *n* are theoretically related to:

- The slope of the linear portion of the log compliance-log time master curve determined from creep tests (*m*)
- The undamaged strength of the material
- The fracture energy density of the material determined experimentally by monitoring the energy release through crack propagation

Figure 2.8 shows how the *m*-value is obtained by fitting a power model through the master creep compliance curve obtained from the IDT (see IDT Transformation Model section below for further details). The undamaged strength is obtained by performing a strength test at a fairly rapid constant rate of deformation (0.5 in/min). This rate was selected such that as little damage as possible would be induced prior to failure, suggesting that the strength being measured is in fact, an undamaged strength.

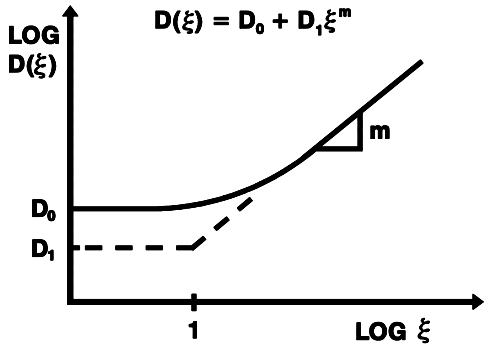

Figure 2.8. Power Model for Master Creep Compliance Curve

However, determination of the fracture energy density would require additional and fairly complex testing, which could not be incorporated into a mixture specification scenario. Fortunately, experimental results indicate that fairly reasonable estimates of *A* and *n* can be obtained from the *m*-value and the strength of the material. Experiments by Molenaar (1984) led to the following relationship:

$$\log A = 4.389 - 2.52 * \log(E * \sigma_m * n) \qquad \textbf{(2.9)}$$

where: E = mixture stiffness
σ_m = mixture strength

Molenaar measured all material properties to develop this relationship. Experiments conducted by Lytton, Shanmugham, and Garrett (1983) led to the following relationships:

$$\log A = -\frac{n + 0.69}{0.511} \qquad \textbf{(2.10)}$$

and

$$n = 0.8 * (1 + \frac{1}{m}) \qquad \textbf{(2.11)}$$

Both researchers found *A* was related to *n*, and Lytton found that *n* was related to *m*. Both of these findings agree with Schapery's theoretical development for nonlinear viscoelastic materials, where Schapery proved that both *A* and *n* are related to *m*, but *A* is also a function of the fracture energy density of the material. Molenaar's equation apparently indicates that the material strength and stiffness are suitable surrogates for the fracture energy density in determining the parameter *A*. Lytton's work appears to indicate that *A* may depend only upon *m*.

Molenaar's form of equation to determine *A* was selected for use, since it seems reasonable that the material's resistance to fracture should depend on the failure limit as well as its stiffness.

Lytton's relationship was selected to determine *n*. Both the *m*-value and strength for use in these relationships are determined from the indirect tensile creep and failure test developed by the PTI research team.

Since the meaning of mixture stiffness included in Molenaar's relationship is unclear, particularly when considering variable temperature conditions during thermal stress development, it was decided that this value should be determined as a calibration coefficient as part of the field calibration efforts (see Model Calibration section below). The following equation was determined after field calibration:

$$\log A = 4.389 - 2.52 * \log(k * \sigma_m * n) \qquad \textbf{(2.12)}$$

where: k = coefficient determined through field calibration = 10,000
σ_m = undamaged mixture strength

This equation is used to determine the fracture parameter *A*. The parameter *n* is determined as a function of *m*, using the equation developed by Lytton, Shanmugham, and Garrett (1983) and presented above. Therefore, the two measured properties used to obtain the fracture parameters are:

- The *m*-value, which is the slope of the linear portion of the log compliance-log time relationship determined from creep tests

- The undamaged strength of the mixture

2.5.2.3 Superpave Indirect Tensile Test at Low Temperatures (IDT)

The IDT was developed at Penn State as part of the SHRP A-005 research contract. The test was designed to obtain the viscoelastic properties needed to predict thermal stress development and the fracture properties needed to predict rate of crack development. A new measurement and analysis system that allows accurate determination of asphalt concrete properties from the indirect tensile test was also developed as part of this work (Roque and Buttlar [1992], Buttlar and Roque [1994]). The IDT is conducted on asphaltic concrete specimens in two phases:

- Short-term creep tests (100 seconds) at multiple temperatures are used to determine the viscoelastic properties.

- A tensile strength test is used along with the viscoelastic properties to determine the fracture properties of the mixture.

A detailed description of the IDT and associated data reduction procedures are given in Chapter 3.

The use of fracture mechanics to evaluate failure requires the use of the undamaged tensile strength of the asphalt mixture. The average tensile strength at -10 °C was selected to represent the undamaged tensile strength of the asphalt mixture at all temperatures for the following reasons:

- It is well known that asphalt mixture strength increases with decreasing temperature until a maximum value is reached at a specific temperature, below which the

strength decreases with decreasing temperature. The temperature at which the strength peaks varies from mixture to mixture. The strength reduction at lower temperatures is probably a result of internal damage caused by stresses induced by differential contraction between aggregate and binder. Therefore, strengths measured below the temperature where the strength peaks were considered to be damaged strengths, which are not compatible with the theory being used to predict failure.

- For all of the mixtures evaluated as part of the SHRP A-005 study, the peak strength always occurred at temperatures lower than -10 °C. Based on this information, the strength measured at -10 °C may generally be considered to be a conservative estimate of the undamaged tensile strength of the mixture at temperatures less than or equal to -10 °C.

- Tensile strengths at temperatures higher than -10 °C were not directly input to the model because of time constraints associated with completing the work. Given that in most cases, significant thermal stress levels are not induced until temperatures approach -10 °C, this may have little influence on the model predictions. However, this effect was not evaluated.

2.5.2.4 IDT Transformation Model

The purpose of the IDT transformation model is to determine the master relaxation modulus curve from the creep compliance measurements. The relaxation modulus is a direct input into the pavement response model described below. The transformation from the creep compliance test results to the master relaxation modulus curve is accomplished in two steps. First, the master creep compliance curve is generated from the creep compliance test results at different temperatures. A generalized Voight-Kelvin model is used to represent the master creep compliance curve. Second, the master relaxation modulus curve is determined from the master creep compliance curve via the hereditary integral.

The generalized Voight-Kelvin model was chosen to represent the master creep compliance curve for three primary reasons:

- Experience has shown that this functional form fits the measured data extremely well.

- This model greatly simplifies the transformation of the master creep compliance curve to the master relaxation modulus curve (described in the next section).

- This model greatly simplifies the solution of the viscoelastic constitutive model used to calculate pavement stresses (described in Pavement Response Model section below).

Within the thermal cracking model, the shift factor-temperature relationship is modeled as piecewise linear between shift factors determined at the specified test temperatures, assuming a

semi-log relationship between the natural logarithm of the shift factors versus arithmetic temperature. In other words, shift factors at arbitrary temperatures are determined by linearly interpolating, assuming a semi-log relationship, between the shift factors determined from the regression. Linear extrapolation, assuming a semi-log relationship, is performed to obtain shift factors at temperatures outside the range of measurements.

The second step in the regression routine is to fit a second functional form to the master creep compliance information. This second functional form is the following power model:

$$D(\xi) = D_0 + D_1 \xi^m \quad \textbf{(2.13)}$$

where $D(\xi)$ and ξ are as defined previously, and D_0, D_1, and m are the coefficients of the functional form (Figure 2.8). The primary purpose for fitting this functional form is to determine the parameter m. This parameter is essentially the slope of the linear portion of the master creep compliance curve on a log-log plot. As previously discussed, it has been found to be an important parameter in distinguishing between the thermal cracking performance of different materials, and is a direct input into the crack depth (fracture) model described below.

Master Relaxation Modulus Curve

As previously described, the viscoelastic constitutive equation used in the pavement response model requires that the time and temperature dependent relaxation modulus of the material be known. It is common to formulate the constitutive equation in terms of relaxation modulus when the stress response to a known strain input is desired, which is the case here. However, it is also accepted and understood that creep tests on viscoelastic materials are typically easier to conduct and the results are more reliable than relaxation test results. Therefore, an indirect tensile creep test was developed for measuring the viscoelastic properties.

The viscoelastic property determined from a creep test is known as the creep compliance. The creep compliance is simply the time dependent strain divided by the constant stress. However, the property required for the stress predictions is the relaxation modulus, as discussed above. Sometimes the relaxation modulus is approximated as simply the inverse of the creep compliance. However, this is not correct. The inverse of the creep compliance is the creep modulus (or creep stiffness), and not the relaxation modulus. Although under some conditions (e.g., low temperatures and short loading times with hard materials) the two moduli are approximately equal, this is generally not the case. Since the creep compliance and the true relaxation modulus are related, it is relatively simple to determine the true relaxation modulus, rather than approximate it. As previously discussed, the calculations are particularly easy if a generalized Voight-Kelvin model is used to represent the master creep compliance curve.

For a viscoelastic material, the relationship between creep compliance and relaxation modulus is given by the hereditary integral:

$$\int_0^{\infty} D(t - \tau) \frac{dE(\tau)}{d\tau} d\tau = 1 \quad \textbf{(2.14)}$$

Taking the Laplace transformation of each side results in:

$$L[D(t)] * L[E(t)] = \frac{1}{s^2} \qquad \textbf{(2.15)}$$

where:

$L[D(t)]$	=	the Laplace transformation of the creep compliance, $D(t)$
$L[E(t)]$	=	the Laplace transformation of the relaxation modulus, $E(t)$
s	=	the Laplace parameter
t	=	time (or reduced time, ξ)

A computer program has been developed to solve this equation for the master relaxation modulus, $E(\xi)$, given the master creep compliance, $D(\xi)$. The program essentially performs the following steps:

1. Computes the Laplace transformation of the master creep compliance curve, $L[D(\xi)]$, where $D(\xi)$ is defined by the Prony series described in Equation 2.5
2. Multiplies $L[D(\xi)]$ by s^2
3. Computes the reciprocal of $s^2 * L[D(\xi)]$, which is $L[E(\xi)]$
4. Computes $E(\xi)$, which is the inverse Laplace transformation of the step 3 result. $E(\xi)$ will then have the Prony series functional form given in Equation 2.3.

The master relaxation modulus curve determined from the master creep compliance curve for PTI Section 38 is shown in Figure 2.9.

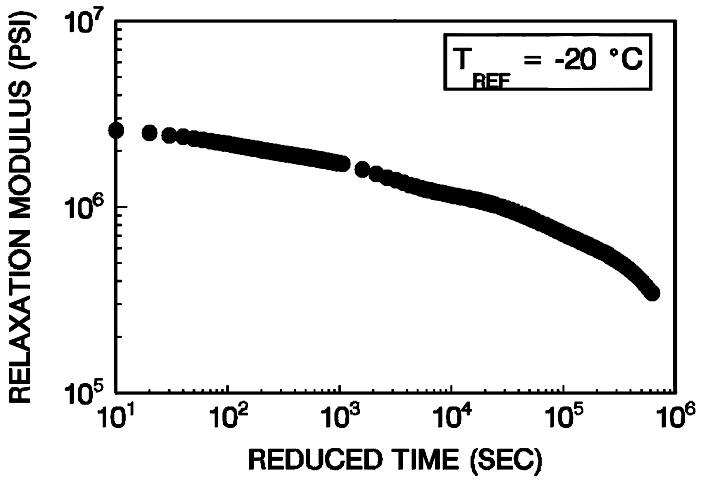

Figure 2.9. Master Relaxation Modulus Curve for PTI Section 38

The transformation program has been independently verified by comparing the results to those produced by *Mathematica*, which is a software system for doing mathematics by computer and is able to perform Laplace transformations. An example from these comparisons is shown in table 2.1 for PTI section 38. As observed, the Prony series parameters from the two independent determinations are virtually identical.

Table 2.1 Master Relaxation Modulus Prony Series Parameters for PTI Section 38

Method	Moduli (psi)					Relaxation Times (sec)				
	E_1	E_2	E_3	E_4	E_5	λ_1	λ_2	λ_3	λ_4	λ_5
TCModel	200788	481712	746006	510000	756131	24.5578	117.270	2097.13	44221.3	792186.
Mathematica	200788	481712	746007	509999	756131	24.5578	117.270	2097.14	44221.4	792186.

Also, comparisons made between the relaxation modulus computed as described and the creep modulus have shown that they in fact are not equivalent, and thus it would not be accurate to approximate the relaxation modulus with the creep modulus. In all cases compared the differences were not dramatic; however, in all cases differences did exist.

In summary, the following procedure is followed in determining the master relaxation modulus function from IDT test results:

1. Perform 100-second creep tests at multiple temperatures and reduce the data (i.e., determine creep compliance versus time) following the IDT procedures described in Chapter 3.

2. Determine the master creep compliance curve and the temperature shift factors from the 100-second creep compliance curves at multiple temperatures. Fit both the generalized Voight-Kelvin and power model functions to the master creep compliance curve.

3. Determine the master relaxation modulus curve from the master creep compliance curve via the hereditary integral. The temperature shift factors for the master relaxation modulus curve are as determined for the creep compliance data, i.e., the same shift factors are applicable to both the creep and relaxation data.

2.5.3 Environmental Effects Model

The environmental effects model is used to predict the temperature conditions within the pavement system using environmental data and material properties. The model is based upon the program developed at the Texas Transportation Institute for the Federal Highway Administration (Lytton, et al. [1989]). The following points are relevant:

- The input/output capabilities of the environmental effects model were modified to suit the needs of the thermal cracking model.

- The model uses the minimum and maximum daily air temperatures recorded at site-specific weather stations as input.

- The model predicts pavement temperatures with depth and outputs every hour.

- The model predictions have compared favorably with measured pavement temperatures (Lytton et al. [1993]).

2.5.4 Pavement Response Model

The pavement response model predicts the stresses within the pavement system using the material properties and pavement structure information, and the pavement temperature predictions from the environmental effects model. The following points are relevant:

- The model is based upon a one-dimensional constitutive equation; an approximate means has been developed to model the two-dimensional stress distribution within the asphalt layer.

- The model uses the predicted pavement temperatures from the environmental effects model.

- The model uses the master relaxation modulus curve determined from the indirect tensile test at low temperatures (IDT).

- Predictions made with the pavement response model have compared favorably with stresses and fracture temperatures measured by the thermal stress restrained specimen test (TSRST) (Lytton et al. [1993]).

The model developed for thermal stress predictions within the asphalt layer is based upon the following one-dimensional constitutive equation, which is Boltzmann's Superposition Principle (Figure 2.10) for linear viscoelastic materials:

$$\sigma(\xi) = \int_0^{\xi} E(\xi - \xi') \frac{d\varepsilon}{d\xi'} d\xi' \qquad \textbf{(2.16)}$$

where:

	$\sigma(\xi)$	=	stress at reduced time ξ
	$E(\xi-\xi')$	=	relaxation modulus at reduced time $\xi-\xi'$
	ε	=	strain at reduced time ξ (= $\alpha(T(\xi') - T_0)$)
	α	=	linear coefficient of thermal contraction
	$T(\xi')$	=	pavement temperature at reduced time ξ'
	T_0	=	pavement temperature when $\sigma = 0$
	ξ'	=	variable of integration

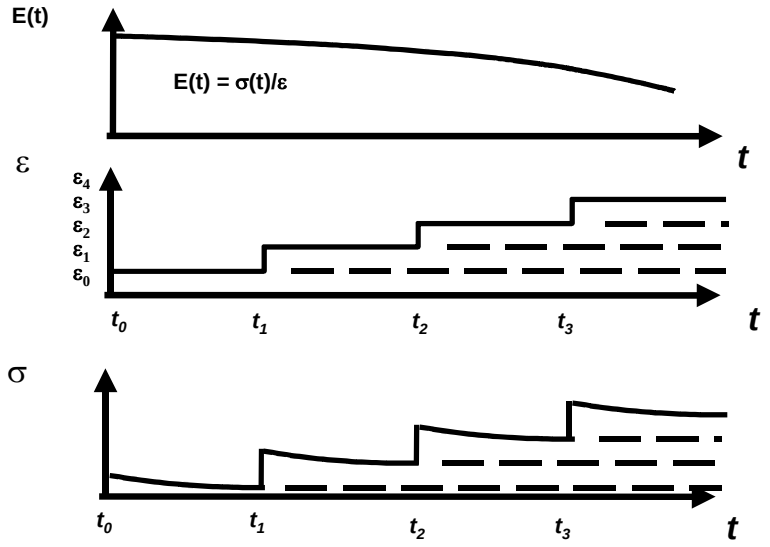

Figure 2.10. Schematic of Boltzmann's Superposition Principle for Linear Viscoelastic Materials

The equation essentially models the asphalt layer as a uniaxial rod that is fixed at each end. The constitutive equation is initially written in terms of reduced time, ξ, because time-temperature superposition is being used to represent the creep compliance and relaxation modulus curves. The use of time-temperature superposition means that the asphalt mixture is modeled as a thermorheologically simple material. With a change of variables, the equation is written in terms of real time, t, as follows:

$$\sigma(t) = \int_0^t E[\xi(t) - \xi'(t)] \frac{d\varepsilon}{d't} d't \qquad \textbf{(2.17)}$$

Using the Prony series representation of $E(\xi)$ (Equation 2.3), the following finite difference solution to the above equation has been developed (Soules, et al. [1987]):

$$\sigma(t) = \sum_{i=1}^{N+1} \sigma_i(t) \qquad \textbf{(2.18)}$$

where:

$$\sigma_i(t) = e^{-\Delta\xi/\lambda_i} \sigma_i(t - \Delta t) + \Delta\varepsilon\, E_i \frac{\lambda_i}{\Delta\xi}\left(1 - e^{-\Delta\xi/\lambda_i}\right) \qquad \textbf{(2.19)}$$

$\Delta\varepsilon$ and $\Delta\xi$ are the changes in strain and reduced time, respectively, over time t-Δt to t, and all other variables are as previously defined.

It should be noted that the use of a one-dimensional constitutive model was necessitated by the fact that stress predictions must be made at small time intervals over analysis periods of many years using a personal computer. Obviously, the stresses vary with depth due to a temperature gradient within the layer. Previous thermal cracking models have based their stress predictions solely on the pavement temperature at the surface, and have assumed that these stresses exist throughout the layer. In fact, the stresses reduce with increased depth, and thus such assumptions overpredict the amount of damage within the pavement for a given temperature cycle. In lieu of using a more accurate two- or three-dimensional model, an approximate means has been developed to approximate this stress distribution using the one-dimensional model.

The pavement response model performs the following sequence of computations:

- Temperatures are predicted at multiple depths (nodes) within the asphaltic concrete layer using the environmental effects model. The nodes are located at 2-inch intervals.
- Temperature-induced strains are computed at each of the nodes.
- The one-dimensional model presented earlier is used to predict stresses at each node, thus establishing an approximate stress distribution with depth.

An example of these computations is presented in Figures 2.11 through 2.16 for PTI test section 38, which is a 9.5-inch thick pavement located in Frazee, MN. The computations are for a very cold 48-hour period. Figures 2.11 and 2.12 show temperature as a function of time and depth, respectively, while Figures 2.13 and 2.14 show strains as a function of time and depth. The thermal stresses corresponding to these changes in temperature and strain are presented in Figure 2.15 as a function of time and in Figure 2.16 as function of depth.

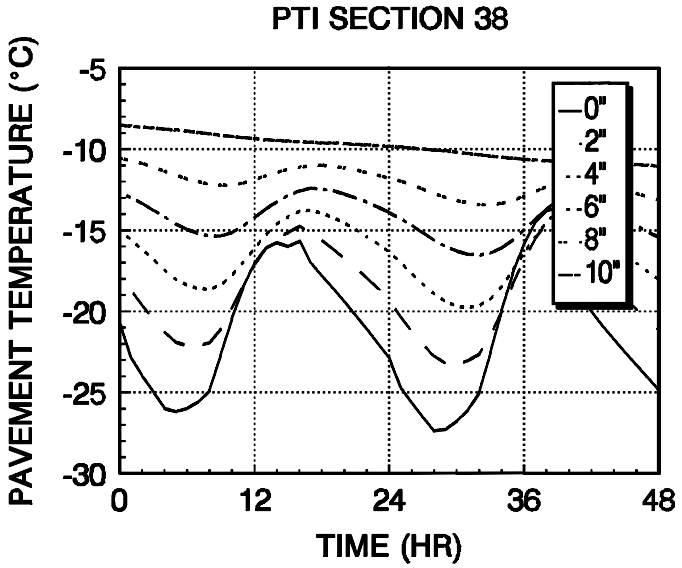

Figure 2.11. Typical Pavement Temperature versus Time for PTI Section 38

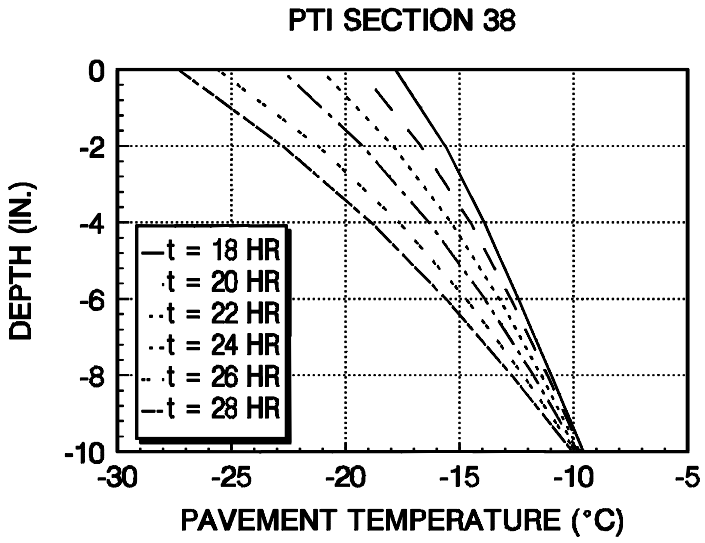

Figure 2.12. Typical Pavement Temperature versus Depth for PTI Section 38

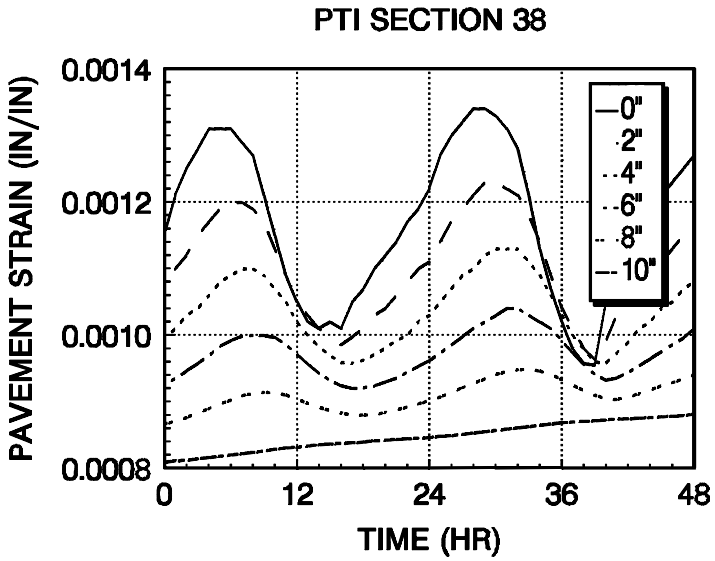

Figure 2.13. Typical Pavement Strain versus Time for PTI Section 38

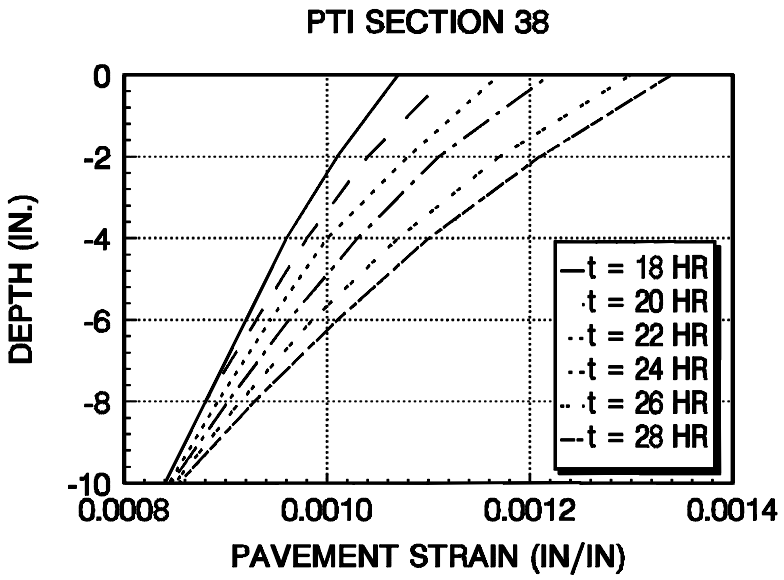

Figure 2.14. Typical Pavement Strain versus Depth for PTI Section 38

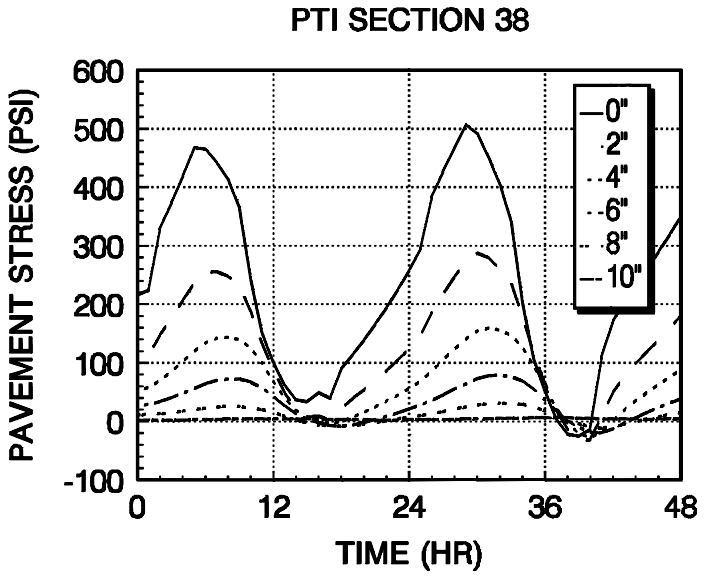

Figure 2.15. Typical Pavement Stress versus Time for PTI Section 38

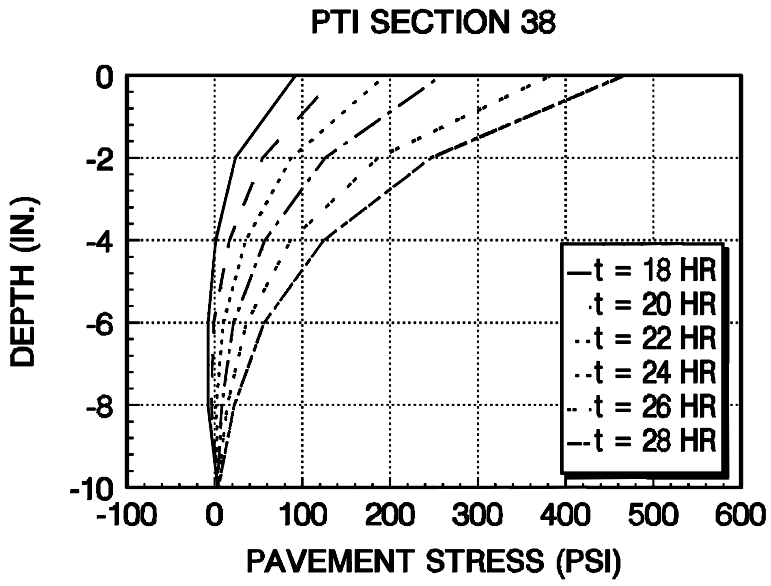

Figure 2.16. Typical Pavement Stress versus Depth for PTI Section 38

The predicted stress distribution is used as input to the crack depth (fracture) model. The fracture model uses the stress at the current location of the crack tip to calculate the crack advancement.

2.5.5 Pavement Distress Model

The pavement distress model consists of three primary parts: the stress intensity factor model, the crack depth (fracture) model, and the crack amount model. The stress intensity factor model predicts the stress at the tip of a local vertical crack using the far-field stress computed by the pavement response model and the pavement structure and material properties. Based upon the stress at the tip of the crack, the crack depth (fracture) model predicts the amount of crack propagation due to the imposed stress. Finally, the crack amount model predicts the number (or frequency) of thermal cracks per unit length of pavement from the depth of the local vertical crack and the probabilistic crack distribution model.

2.5.5.1 Stress Intensity Factor Model

The stress intensity factor model (CRACKTIP) is a two-dimensional finite element (FEM) program that models a single vertical crack in the asphaltic concrete layer via a crack tip element. The CRACKTIP program was developed at the Texas Transportation Institute (Chang, Lytton, and Carpenter [1976]). Suitable finite element meshes were identified and side-by-side comparisons of the CRACKTIP finite element program with the ANSYS program and with standard handbook solutions were performed in order to verify the accuracy of the CRACKTIP program for use in the thermal cracking model.

It was determined that computer run times would be excessive if the CRACKTIP finite element model were to be incorporated directly into the thermal cracking model. Therefore, an investigation was conducted to determine if a simplified equation could be developed to predict the results of the CRACKTIP program. The approach was to presolve the CRACKTIP program for a broad range of conditions and determine whether a simple relationship could be developed to obtain a reasonable estimate of the stress intensity factors predicted by the model. The following regression equation was determined to provide reasonably accurate estimates of stress intensity factors:

$$K = \sigma(0.45 + 1.99\, C_o^{0.56}) \qquad \textbf{(2.20)}$$

where: K = stress intensity factor
σ = far-field stress from pavement response model at depth of crack tip
C_o = current crack length

The regression equation is used in the thermal cracking model in lieu of the CRACKTIP program.

2.5.5.2 Crack Depth (Fracture) Model

The Paris Law for crack propagation is used to predict the change in depth of a local crack subjected to a given cooling cycle:

$$\Delta C = A\Delta K^n \qquad \textbf{(2.21)}$$

where: ΔC = change in the crack depth due to a cooling cycle
ΔK = change in the stress intensity factor due to a cooling cycle
A,n = fracture parameters for the asphalt mixture

The change in crack depth (ΔC) is computed and accumulated on a daily basis to determine the total crack depth as a function of time. In order to perform these computations, the asphalt concrete layer is subdivided into four sublayers as shown in Figure 2.17. On any given cooling cycle, the crack is never allowed to propagate any further than one sublayer. Thus, for a given cooling cycle one of two things can occur:

- The crack can propagate some finite distance less than the distance between the crack tip and the bottom of the sublayer within which the crack tip is located.

- If the crack is predicted to propagate below the sublayer within which the crack tip is located, or if the induced stress is greater than the strength of the mixture, then the crack is assumed to propagate to the bottom of the sublayer within which it is located.

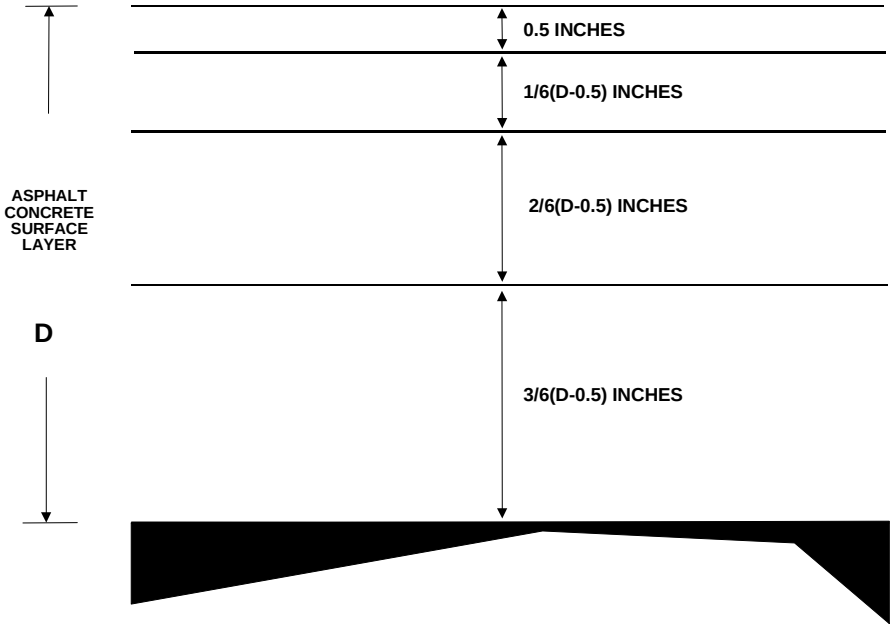

Figure 2.17. Sublayer Model for Asphaltic Concrete Surface Layer

Although not strictly correct, this procedure was developed to reduce the effects of unrealistic predictions in crack depth that occur when very high stress intensity factors exist near the surface. Although the stresses and stress intensity factors are high near the surface, they may be significantly lower with depth, such that propagation would not proceed as fast as predicted. The next day's cooling cycle would determine if in fact the induced stresses would propagate the crack further. Therefore, in severe environments a crack could propagate completely through the surface layer in as little as four days. This would imply that the pavement would be severely cracked after four days. In fact, a finite amount of cracking would have developed in previous days.

The computed crack depth as a function of time is shown for PTI section 38 (described earlier) in Figure 2.18. As explained in the next section, the crack depth is related to the total amount of cracking by way of a crack depth distribution function. The idea is that material variability along the length of the pavement section will result in different crack depths, even for the same exposure conditions. The crack depth distribution governs how much cracking is observed in a particular section having a specific crack depth computed on the basis of average material properties.

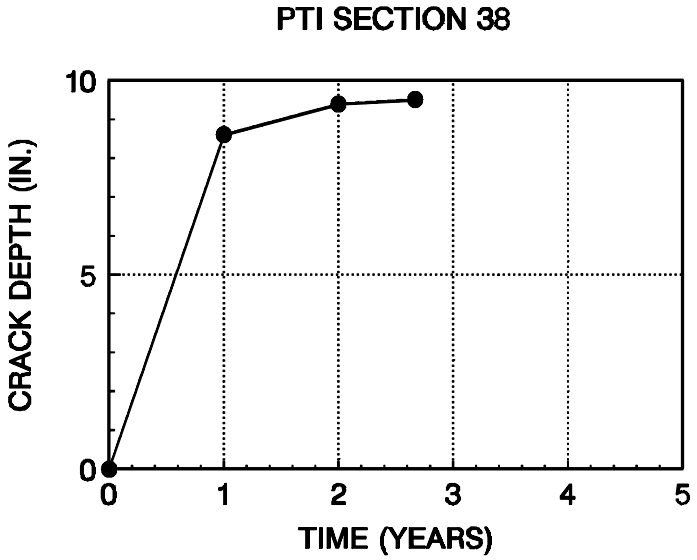

Figure 2.18. Crack Depth versus Time for PTI Section 38

2.5.5.3 Crack Amount Model

In order to predict the amount of cracking per unit length of pavement section from the average crack depth and the distribution of crack depths within the section, the following assumptions were made:

- Within a given pavement section there is a maximum number of thermal cracks that can occur and these cracks are uniformly spaced throughout the section (or conversely, there exists a minimum crack spacing beyond which no further cracks will develop). This assumption appears rational because, below a certain crack spacing, insufficient friction exists to develop the stresses required to advance another crack. Initially, each of these potential cracks starts out as a very small local vertical crack (or flaw, fissure, etc.) at the surface of the asphaltic concrete layer.

- A crack is not counted (or observed) as a crack until the local vertical crack propagates through the entire depth of the asphaltic concrete surface layer. In other words, no contribution is made to the amount of global thermal cracking until the local vertical crack breaks through the surface layer.

- For a given pavement section at a given point in time, each of the local vertical cracks defined above has potentially propagated a different amount through the surface layer because of the fact that the material properties of the pavement vary spatially throughout the section. This spatial distribution of crack depths is assumed to be normally distributed. The mean of the distribution is assumed to be equal to the crack depth computed from the mechanistic model described above using the material properties measured in the laboratory. The variance of the distribution is unknown, and was included in the model as a coefficient to be estimated during the

calibration efforts. The variance was assumed to be constant across all pavement sections.

Based upon the above assumptions, the model shown in Figure 2.19 was developed between the amount of cracking for the pavement section and the proportion of the maximum number of vertical cracks that have actually broken through the surface layer. Essentially, the amount of cracking is a function of the probability that the crack depth is equal to or greater than the thickness of the surface layer. As shown in the Figure, this probability is determined by assuming that the logarithm of the depth of cracks in the pavement is normally distributed with mean equal to log C_o (the crack depth predicted by the model), and a variance of σ^2. The amount of cracking is computed as follows:

$$AC = \beta_1 * P\,(\log C > \log D) \qquad \textbf{(2.22)}$$

or,

$$AC = \beta_1 * N\left(\frac{\log C/D}{\sigma}\right) \qquad \textbf{(2.23)}$$

where:

	AC	=	observed amount of thermal cracking
	β_1	=	regression coefficient determined through field calibration
	P ()	=	probability that () is true
	N ()	=	standard normal distribution evaluated at ()
	σ	=	standard deviation of the log of the depth of cracks in the pavement
	C	=	crack depth
	D	=	thickness of surface layer

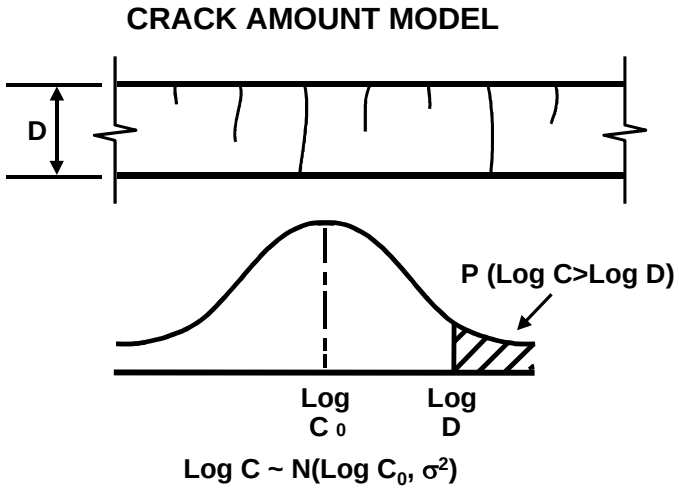

Figure 2.19. Crack Amount Model: Crack Depth Distribution

This particular model, which is based on the logarithm of *C* and *D*, was selected for the following reasons:

- As seen in the equations presented above, use of the logarithm form implies that the amount of cracking is proportional to the ratio of *C*/*D*, which has the effect of normalizing the effect of surface layer thickness.

- The use of log C_o also implies that the variance of the crack depth increases as the crack depth increases. This appeared to be a rational effect.

Results of the field calibration indicated that $\beta_1 = 353.5$ and $\sigma = 0.769$ (see Model Calibration section below).

The predicted amount of cracking versus time for PTI section 38 is shown in Figure 2.20. The severe environment (Frazee, MN) combined with the relatively stiff asphalt mixture in this section resulted in very severe cracking after the first winter.

It should be noted that this model does not predict any more than 50% of the total possible amount of cracking that can develop in the pavement. This corresponds to the instant when the average crack depth is equal to the thickness of the surface layer, which implies that 50% of all

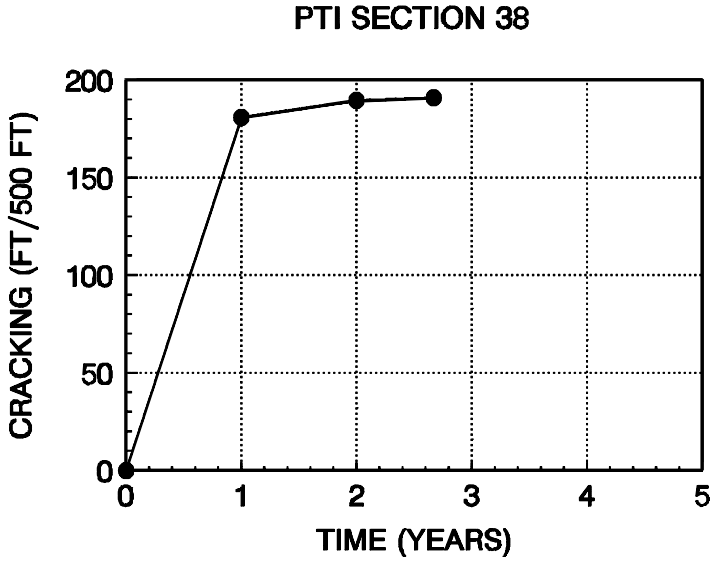

Figure 2.20. Amount of Cracking versus Time for PTI Section 38

cracks in the pavement are deeper than the thickness of the surface layer (i.e., cracking has developed according to the definition set forth above) and 50% of the cracks have not penetrated through the surface layer (i.e., cracking has not developed). Based on field observations and calibrations conducted as part of this investigation, a maximum amount of cracking of 400 ft of

cracking per 500 ft of pavement, which corresponds to a crack frequency of 1 crack per 15 ft of pavement, was selected as the maximum amount of thermal cracking that would typically develop in a pavement. Thus, the model predicts a maximum amount of cracking of about 200 ft per 500 ft of pavement (i.e., 1 crack per 30 ft). Therefore, when the model predicts 200 ft of cracking after five years of service, the proper interpretation is that the pavement can be expected to have at least 200 ft of cracking after five years. Given that a pavement with a crack every 30 ft is generally considered severely cracked, the predictions made by the model were considered to be sufficient for proper evaluation of performance.

Documented cases of pavements cracking at spacings less than 15 ft exist. Deme and Young (1987) reported crack spacings as small as 8 ± 6.5 ft on sand subgrade sections that were designed for early failure. Deme and Young (1987) have also observed that additional transverse cracks have developed in the traffic lane between full-width transverse cracks, but they attribute the occurrence of these cracks to the combined effects of traffic loads and temperature. The present model only considers thermal effects, and, as noted earlier, it is questionable whether sufficient friction would exist to develop the stresses required to advance another crack when the cracked sections are less than 15 ft long. Further, many pavement engineers would consider crack spacings smaller than 15 ft unacceptable. It would not be rational to design a pavement for crack spacings smaller than 15 ft. Thus, a minimum crack spacing of 15 ft was chosen for the initial version of the new thermal cracking model.

Chapter 3

Analysis of IDT Creep and Strength Data

This chapter summarizes the standard analyses conducted to convert Superpave IDT raw data into creep compliance, Poisson's ratio, and tensile strength, and documents the procedures and algorithms developed to generate the required master curve models for TCMODEL. A basic flowchart describing the analysis steps required to convert raw data from the Superpave IDT to the proper fundamental properties required by TCMODEL is given in Figure 3.1. The data reduction procedures that have remained unchanged since the initial calibration of TCMODEL are documented first, in section 3.1 and 3.2. Sections 3.3 and 3.4 present recent improvements in the analysis of IDT data. All of the data used in the recalibration of TCMODEL, as described later in this report, have been analyzed using these improved analysis techniques.

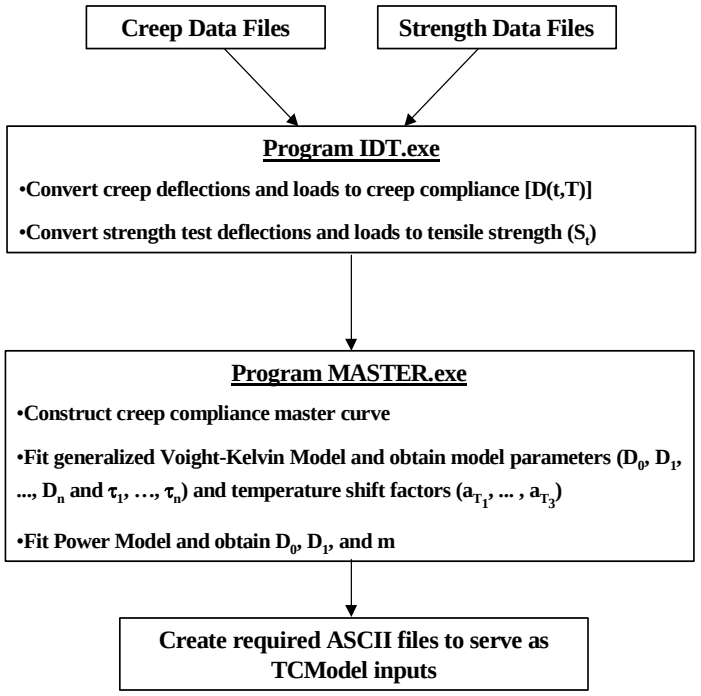

Figure 3.1. Data Reduction Flowchart

3.1 IDT Test Protocols and Determining Creep Compliance

A measurement and analysis system was developed by Roque and Buttlar (1992) to obtain accurate, fundamental mixture properties at low temperatures using a new device, called the Superpave Indirect Tensile Tester (IDT) (Figure 3.2). Finite element analyses of diametrally

loaded cylindrical specimens have indicated that properties cannot be accurately determined from measurements obtained on the perimeter of the specimen. Stress concentrations near loading heads do not allow for the accurate determination of Poisson's ratio, which is required for accurate interpretation of the deformation response. This and other problems were overcome by obtaining vertical and horizontal measurements in the center of flat faces of cylindrical specimens (Figure 3.2).

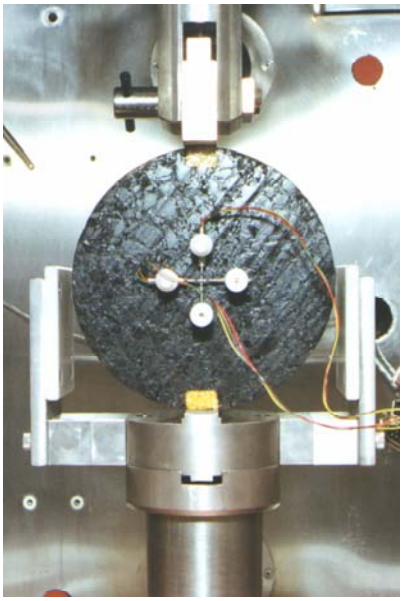

Figure 3.2. Superpave Indirect Tensile Test Device

This measurement system is an extension of the system developed by Anderson and Hussain [Hussain (1990)]. Other advantages of this system include the following: 1) measurement errors caused by specimen rotation are reduced or eliminated; 2) stresses are nearly uniform in the measurement zone.

It was determined that analyses of stresses and deformations within the specimen are needed to accurately interpret deflections obtained from the test. Finite element analyses showed that deformations and stresses on flat faces of cylindrical specimens are dependent upon specimen thickness and Poisson's ratio. Roque and Buttlar (1992) developed a set of correction factors to perform a pseudo-three-dimensional analysis based upon conventional, two-dimensional plane-stress solutions. The following sections detail the development of current IDT testing and analysis protocols, which are specified in AASHTO TP-9 (1996).

3.1.1 Developments in Testing Methods

Strain Limits Established to Keep Specimens in the Linear Range

The analysis system presented later in this study is valid only for specimens tested at temperatures and loading times where the material exhibits linear elastic or linear viscoelastic behavior. Experience has shown that specimens tested at 0^{o} C and lower generally exhibit linear behavior for tests up to 1000 seconds in duration if creep loads are kept low enough. It was

found that choosing loads which limit horizontal tensile strains to 500 microstrains or less helps to keep asphalt mixture behavior safely within the linear range. An operator should stop a test immediately if strains are found to be in violation of these limits. Specimens should be allowed to recover for a minimum of three minutes before reloading at a different level.

Specimen Conditioning Recommendations

Observing consistent specimen conditioning techniques, as with any test method, will lead to more accurate and repeatable results. The most critical specimen conditioning concerns for this test have been identified as temperature, humidity, and preloading or seating loads. Specimens should be cooled at test temperature for three to twelve hours before testing. The minimum recommended cooling time of three hours was determined by embedding thermocouples in the middle of Marshall-sized test specimens and cooling them from room temperature (20^{o} C) to very low test temperatures (-25^{o} C). The maximum recommended cooling time was established to avoid the effects of low temperature physical hardening, a phenomenon observed by Bahia (*3*) in asphalt cements. However, the effects of this phenomenon on the properties of asphalt mixtures are not thoroughly understood at this time.

Tests have clearly shown that variation in moisture within specimens may have a dramatic effect on low temperature mixture compliance. Thus, humidity conditioning of specimens is highly recommended. A humidity conditioning procedure that has been used successfully at Penn State University requires storing specimens at 30 percent relative humidity and 20^{o} C for a minimum of three days prior to testing to ensure uniform and consistent moisture content.

Test Chamber Temperature Tolerance

Because asphalt concrete properties are highly temperature-dependent, careful control of test chamber temperatures is required to obtain accurate material properties. A test chamber temperature set point accuracy of +/- 0.5^{o} C is practical and generally acceptable. However, because low temperature measurements on asphalt concrete are extremely small, large temperature fluctuations within this range during testing can lead to significant drift in deflection measurements. Thus, it is recommended that once a test is initiated (where the actual temperature is within +/- 0.5^{o} C of the target temperature), temperature should be held within +/- 0.2^{o} C of set point during the entire test.

3.1.2 Developments In Analysis Procedures

Review of Existing Analysis Procedures

A brief review of the measurement and analysis system as presented by Roque and Buttlar (1992) will aid in the understanding of newer analysis methods. A finite element study of diametrally-loaded cylindrical specimens showed that measurements obtained with the new system needed to be corrected to account for three-dimensional effects. Bulging of specimens (Figure 3.3a) was found to affect both horizontal and vertical measurements. Bulging correction factors dependent upon Poisson's ratio and specimen geometry were developed to account for this phenomenon. In addition, three-dimensional stress states were found to differ dramatically

from those predicted by conventional two-dimensional plane-stress theory (Figure 3.3b). Stress correction factors, also dependent upon Poisson's ratio and specimen geometry, were presented in tabular form. Finally, it was found that horizontal and vertical deformations measured over finite gage lengths were related to point strains at the center of the flat face by a constant. After two-dimensional stresses and strains were corrected to account for three-dimensional effects, creep compliance was obtained by applying Hooke's law. Because several correction factors were functions of Poisson's ratio, which is not known a priori, the original analysis scheme involved a somewhat tedious iterative solution scheme.

The following sections present a simple set of equations, which can be used to directly obtain creep compliance, Poisson's ratio, and other quantities of interest. These equations were obtained by pre-solving the iterative analysis scheme and fitting simple functions through the results.

Creep Compliance

Tensile creep compliance, D(t), is usually the primary quantity to be obtained from the creep test. Poisson's ratio is indirectly very important because it strongly influences the three-dimensional behavior of the specimen and thus plays an important role in the calculation of creep compliance. Poisson's ratio, by definition, is a function of X/Y, where:

X/Y = Absolute value of the ratio of measured horizontal deflection (x-direction) to measured vertical deflection (y-direction), where the x, y, and z axes are defined on Figure 3.3b.

The absolute value is taken for convenience to avoid the negative ratio that occurs since x and y deflections are always of opposite sign (tensile deflections versus compressive deflections). Thus, creep compliance adjusted for three-dimensional effects can be expressed as a function of X/Y. A method for calculating a representative X/Y from the creep test will be presented later.

Creep compliance for the biaxial stress state that exists on the specimen face ($\sigma_z=0$), is obtained through Hooke's law:

$$D(t) = \frac{\varepsilon_x}{\sigma_x - \nu \sigma_y} \qquad \textbf{(3.2)}$$

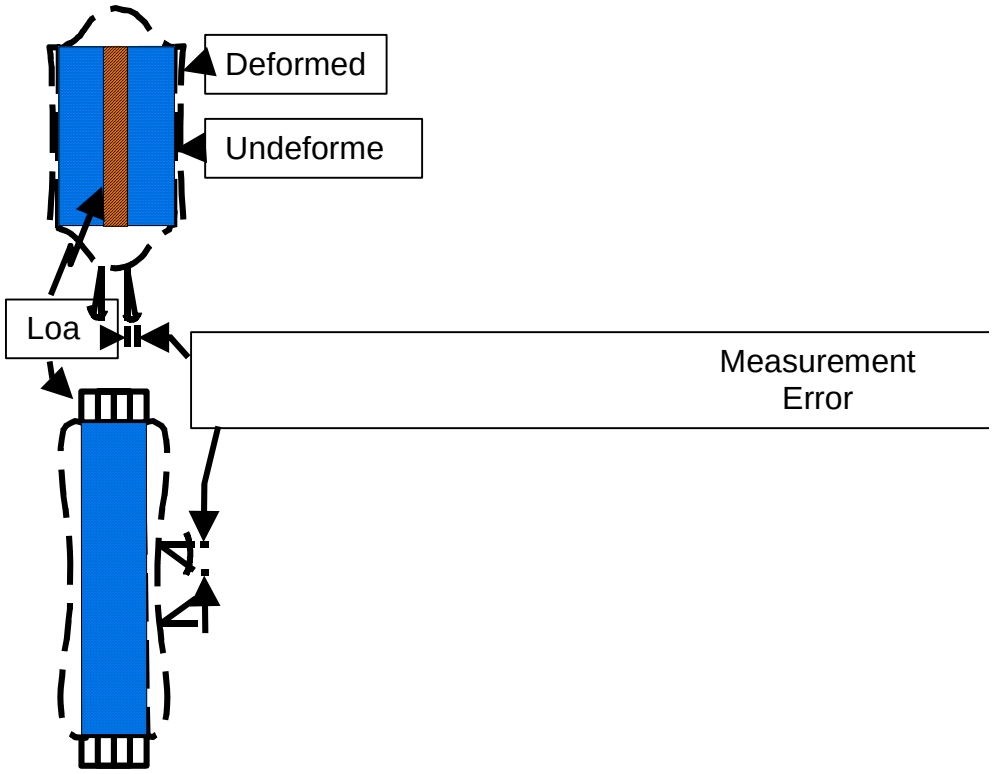

Figure 3.3a. Specimen Bulging

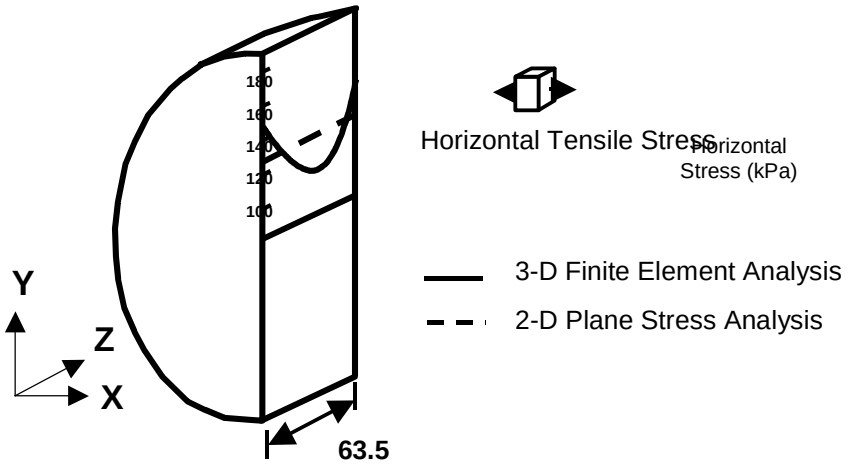

Figure 3.3b. Horizontal Stress Distribution: 2-D Versus 3-D

Figure 3.3. Three-Dimensional Phenomena in Indirect Tension Specimens

Substituting correction factors to account for three-dimensional effects (*1*):

$$D(t) = \frac{\frac{H_M(t)}{GL} * 1.071 * C_{BX}}{\frac{2P}{\pi t D}(C_{SX} + 3\nu C_{SY})} \quad \textbf{(3.3)}$$

Where,

ε_x = Horizontal strain
σ_x = Horizontal stress
σ_y = Vertical stress
ν = Poisson's ratio
$H_M(t)$ = Measured horizontal deflection at time t
GL = Gage length (=25.4 mm for 101.6 mm dia., =38.1 mm for 152.4 mm dia.)
C_{BX} = Horizontal bulging correction factor
P = Creep load
C_{SX} = Horizontal stress correction factor
C_{SY} = Vertical stress correction factor

t, D = As defined before

Rearranging equation 3.3, we obtain equations 3.4 and 3.5:

$$D(t) = \frac{H_m(t) * D * t}{P * GL} * (C_{CMPL}) \quad \textbf{(3.4)}$$

$$C_{CMPL} = \frac{1.071 * \pi * C_{BX}}{2(C_{SX} + 3\nu C_{SY})} \quad \textbf{(3.5)}$$

Where,
C_{CMPL} is a non-dimensional creep compliance factor that was found to vary linearly with $(X/Y)^{-1}$, as shown in Figure 3.4. This relationship is given by equation 3.6:

$$C_{CMPL} = 0.6354\left(\frac{X}{Y}\right)^{-1} - 0.332 \quad \textbf{(3.6)}$$

This factor is restricted to the following limits (equations 3.7 and 3.8):

$$0.20 \le \frac{t}{D} \le 0.65 \quad \textbf{(3.7)}$$

$$[0.704 - 0.213(\frac{t}{D})] \leq C_{CMPL} \leq [1.566 - 0.195(\frac{t}{D})] \quad \textbf{(3.8)}$$

The above limits define the horizontal portions of the data on Figure 3.4. These limits are a direct consequence of the limits imposed on Poisson's ratio, as described below.

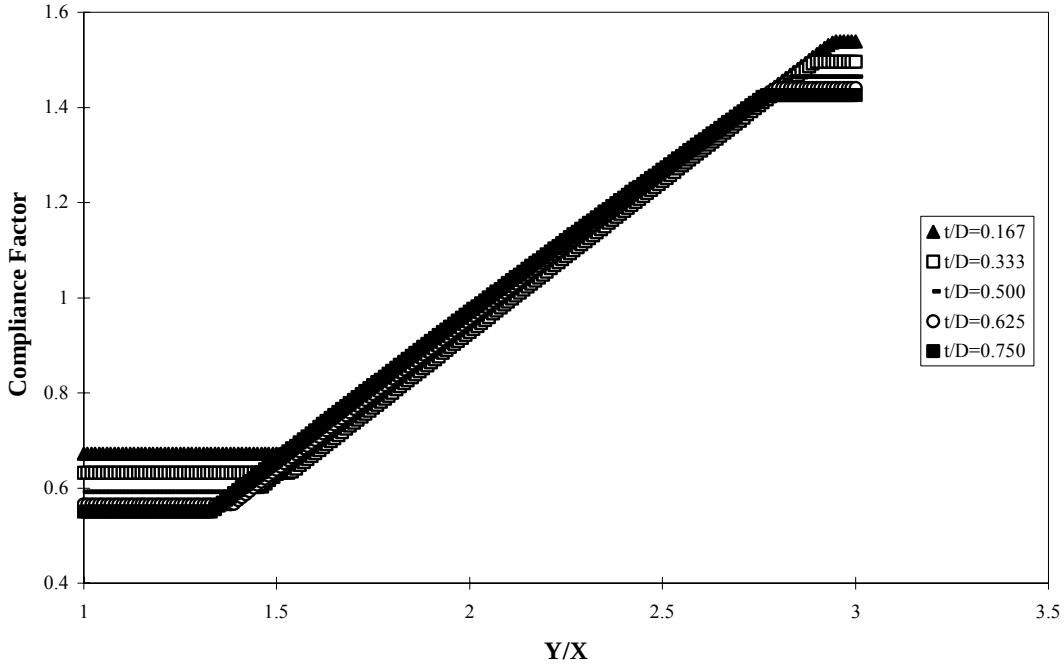

Figure 3.4. Compliance Factor versus $(X/Y)^{-1}$ and t/D

Poisson's Ratio

The calculation of creep compliance presented in the previous section had Poisson's ratio inherently built into the solution via the $(X/Y)^{-1}$ term and did not require the direct solution of Poisson's ratio. However, if a measure of Poisson's ratio of the mixture is desired, it can be easily computed. Poisson's ratio was determined to be related to X/Y and specimen aspect ratio (t/D) through a family of curves (Figure 3.5).

The curves were fit with a single function (equation 3.9) using linear regression and least squares estimators:

$$\nu = -0.10 + 1.480(\frac{X}{Y})^2 - 0.778(\frac{t}{D})^2(\frac{X}{Y})^2 \quad \textbf{(3.9)}$$

Where,

$$0.05 \le \nu \le 0.50 \qquad \textbf{(3.10)}$$

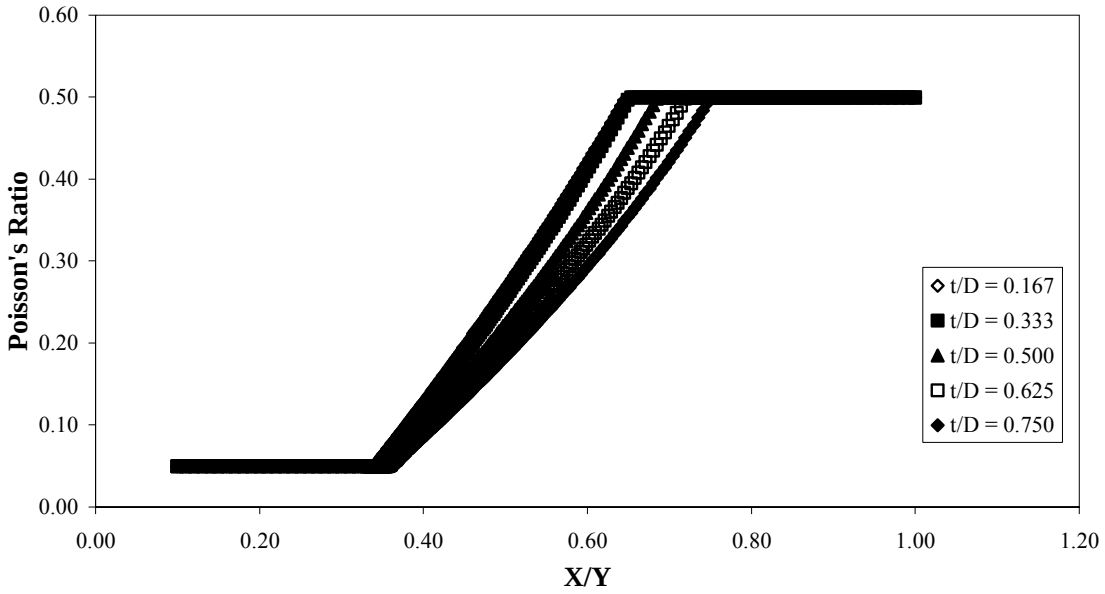

Figure 3.5. Poisson's Ratio versus X/Y and t/D

Here, the regression variables reflect the quadratic form of the relation between X/Y and Poisson's ratio and account for the effect of t/D on the relation.

As described by the limits above (equation 3.10), Poisson's ratio is restricted between 0.05 and 0.50. These limits were imposed to prohibit unrealistic values of Poisson's ratio from entering into other computations. The upper limit of 0.50 was selected to coincide with the upper bound of Poisson's ratio for elastic materials. Although the lower bound of 0.05 is seldom approached, it was instituted to help keep compliance factors within reasonable limits for unrealistic X/Y values. An analysis method aimed at using replication to arrive at a more statistically stable estimate of Poisson's ratio is presented later in this section.

Other Quantities

Other quantities that may be useful in other pavement response or prediction models are presented in the following equations. The maximum tensile stress, corrected to account for three-dimensional effects, can be obtained by (equations 3.11 and 3.12):

where,

$$\sigma_X = \frac{2 * P}{\pi * t * D}(C_{SX}) \qquad \textbf{(3.11)}$$

$$C_{SX} = 0.948 - 0.01114(t/D) - 0.2693(\nu) + 1.436(t/D)(\nu) \quad \textbf{(3.12)}$$

The maximum compressive stress, also corrected for three-dimensional effects is:

$$\sigma_Y = -\frac{6 * P}{\pi * t * D}(C_{SY}) \quad \textbf{(3.13)}$$

where,

$$C_{SY} = 0.901 + 0.138(\nu) + 0.287(t/D) - 0.251(\nu)(t/D) - 0.264(t/D)^2 \quad \textbf{(3.14)}$$

Finally, maximum tensile strain, corrected for specimen bulging and conversion to point strain, is obtained by (equations 3.15 and 3.16):

$$\varepsilon_X = \frac{H_M}{GL} * 1.072 * C_{BX} \quad \textbf{(3.15)}$$

where,

$$C_{BX} = 1.03 - 0.189(t/D) - 0.081(\nu) + 0.089(t/D)^2 \quad \textbf{(3.16)}$$

3.1.3 Obtaining Reliable Measures of Poisson's Ratio and Creep Compliance

Accurate measures of Poisson's ratio are necessary to obtain reasonable values of creep compliance (Roque and Buttlar [1992]). However, because of the variability in asphalt mixtures, unreliable measures of Poisson's ratio may be obtained when using measurements from a single face. Several approaches based upon using replication to arrive at more reliable values were considered. Of all methods considered, the most reliable results were obtained by taking a trimmed mean of deflections measured on replicate specimens and calculating a single Poisson's ratio and creep compliance for the mixture.

The trimmed mean involves ranking observations numerically, "trimming" the highest and lowest values, and averaging the remaining observations. By using the trimmed mean technique to obtain average horizontal and vertical strains for the mixture, a single, representative Poisson's ratio is determined for the mixture based upon measured deflections

from all the replicate specimens.

Because replicate specimens may have different thicknesses, creep loads, and possibly diameters, deflections must be normalized so that they can be properly ranked and trimmed. The first step is to find the average thickness, diameter, and creep load of the specimens (equations 3.17-3.19), where the summation on i varies from 1 to the n number of specimens.

$$t_{AVG} = \frac{\sum t_i}{n} \quad \textbf{(3.17)}$$

$$D_{AVG} = \frac{\sum D_i}{n} \quad \textbf{(3.18)}$$

$$P_{AVG} = \frac{\sum P_i}{n} \quad \textbf{(3.19)}$$

Where,

n = Number of specimens

Each of the i^{th} horizontal and vertical deflection arrays are then multiplied by the following normalization factor (equation 3.20) to obtain normalized deflections (equations 3.21 and 3.22):

$$C_{NORM_i} = \left(\frac{t_i}{t_{avg}}\right) * \left(\frac{D_i}{D_{avg}}\right) * \left(\frac{P_{avg}}{P_i}\right) \quad \textbf{(3.20)}$$

$$V(t)_{NORM_i} = V_M(t)_i * C_{NORM_i} \quad \textbf{(3.21)}$$

$$H(t)_{NORM_i} = H_M(t)_i * C_{NORM_i} \quad \textbf{(3.22)}$$

The trimmed mean of the normalized deflection arrays are then obtained by ranking each of the horizontal and vertical arrays according to their normalized deflection values in a window around the middle of the test. For example, consider a 100 second creep test with three replicates and horizontal and vertical measurements taken on both sides of each specimen (Figure 3.6). Because the data arrays contain measurements taken every 10 seconds and some small level of noise is present in the data, a "noise-insensitive" approximation of the normalized deflection at t=50 seconds is obtained by averaging the 9 values in a window between t=46 and t=54 seconds. These "mid-test" averages of the 6 horizontal and 6 vertical deflection arrays are then ranked numerically to identify the middle 4 horizontal and middle 4 vertical deformation arrays (the trimmed mean discards the upper and lower observations) to be used in subsequent steps.

The horizontal and vertical deflection arrays remaining after trimming are averaged to obtain the trimmed mean deflection arrays (equations 3.23 and 3.24), where the summation on j varies from 1 to the 2n-2 sorted deflection arrays.

$$H(t)_{TRIM} = \frac{\sum H(t)_{NORM_j}}{2n-2} \qquad \textbf{(3.23)}$$

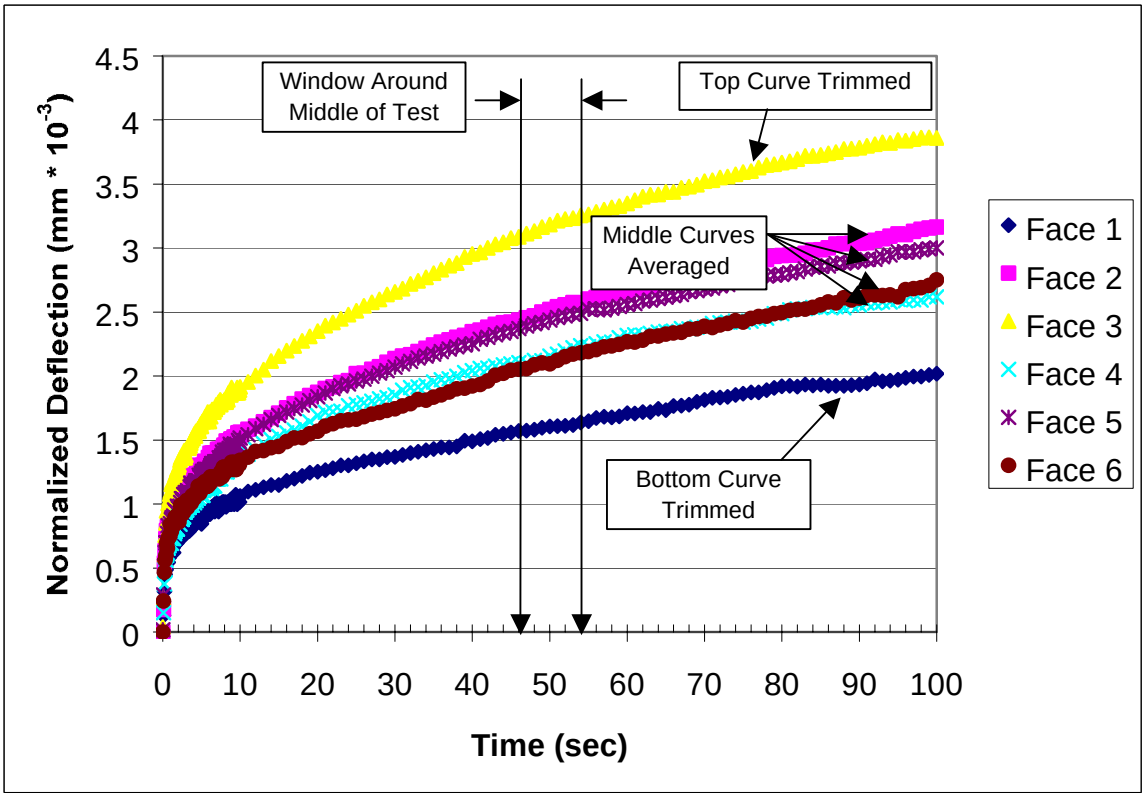

Figure 3.6. Trimmed Mean Approach for Obtaining $H(t)_{avg}$ and $V(t)_{avg}$

$$V(t)_{TRIM} = \frac{\sum V(t)_{NORM_j}}{2n-2} \qquad \textbf{(3.24)}$$

The scalar quantity, $(X/Y)_{TRIM}$, is then calculated for the entire test (equation 3.25), where the summation is taken over all elements in the array.

$$\left(\frac{X}{Y}\right)_{TRIM} = \frac{\sum H(t)_{TRIM}}{\sum V(t)_{TRIM}} \qquad \textbf{(3.25)}$$

The remainder of the analysis can be performed using equations 3.1 through 3.17, after making the following substitutions:

$t = t_{AVG}$
$D = D_{AVG}$
$P = P_{AVG}$
$X/Y = (X/Y)_{TRIM}$
$H_M(t) = H(t)_{TRIM}$

3.2 Obtaining Mixture Tensile Strength from IDT Measurements

Tensile strength is an important property that is commonly used to evaluate effects of moisture, and to determine the fracture resistance of asphaltic mixtures. A method has been developed to accurately determine tensile strength from indirect tensile test results (Buttlar et al., 1996). Data reduction and analysis procedures have been developed to identify the instant of fracture during strength testing, as well as the stress at the location of fracture (i.e. the true tensile strength). Test data showed that mixture tensile strength determined using conventional (plane stress) analysis methods is an over-prediction of the true tensile strength of the mixture. More importantly, the level of over-prediction was found to vary between mixtures, an effect that may result in misleading interpretations of the relative strength between two mixtures. In addition, the fracture propagation model used in TCMODEL relies on an estimate of undamaged tensile strength of the mixture at low temperatures as one of its input parameters (Lytton et al., 1993). This can generally be accomplished by conducting a tensile strength test at a high rate of loading on an undamaged specimen. The procedures presented in the following sections outline the development of a method to determine a fundamental measure of mixture tensile strength from specimens tested in the Superpave IDT.

ASTM Standard Test Method D 4867-92, the NCHRP Asphalt-Aggregate Mixture Analysis System (AAMAS: Von Quintus, Hughes, and Sherocman, 1992), and Superpave Levels II and III procedures for mixture design and evaluation (Lytton et al., 1993), all make use of tensile strength determined from indirect tensile testing to evaluate moisture, fatigue, and thermal cracking performance of asphalt concrete. Conventionally, plane stress analysis has been used to determine tensile strength from indirect tensile test results. However, analytical work by Roque and Buttlar (1992), Heinicke and Vinson (1988), and others has clearly indicated that the stress state within indirect tensile specimens is far from being plane stress. Strictly speaking, plane stress conditions apply only for very thin disks, whereas asphalt mixture specimen thickness is generally 50 mm or greater. Therefore, tensile strengths computed using conventional analysis methods may be significantly in error.

3.2.1 Development of Tensile Failure in Diametrally Loaded Specimens

Figure 3.7 shows a diametrally loaded Marshall-sized specimen (102 mm diameter, 63 mm thick), and the tensile stress distribution along its axis of symmetry computed using two analytical methods: 1) three-dimensional finite element analysis, and 2) two-dimensional or plane stress analysis. For plane stress analysis, the tensile stress is obviously constant along the axis of symmetry, whereas the three-dimensional analysis shows that tensile stresses actually vary along this axis and reach a maximum at the edge of the specimen. This clearly indicates that tensile failure in diametrally loaded specimens initiates at the edges of the specimen at a load level that is lower than that required to break the entire specimen in half. Therefore, the tensile strength of the asphalt mixture is exceeded at the edges of the specimen well before the maximum load required to break the entire specimen is reached.

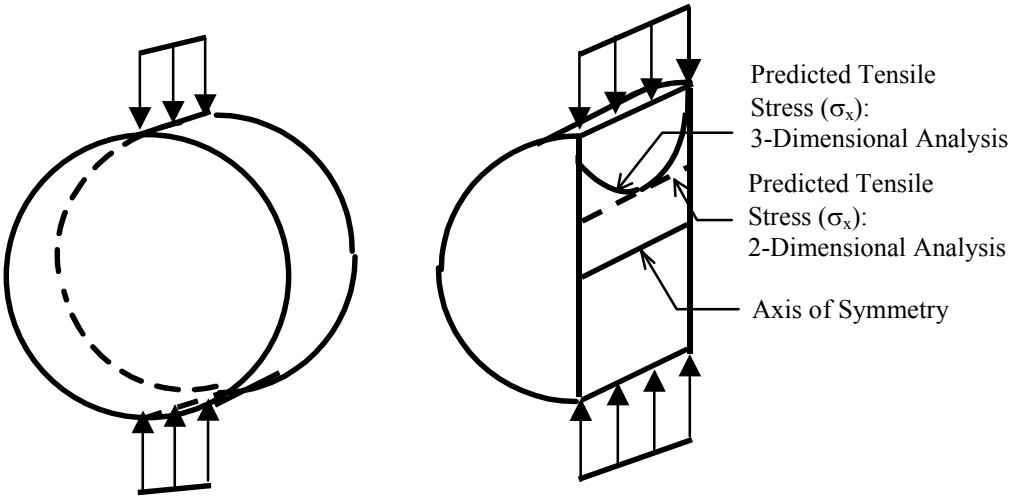

(a) Diametrally Loaded Specimen

(b) Tensile Stress Distributions Along Axis of Symmetry

Figure 3.7. Tensile Stresses in Diametrally-Loaded Specimens

Figure 3.8a shows the progression of failure of a cylindrical specimen subjected to diametral loading. As long as the load is such that the tensile stresses at all points within the specimen are lower than the tensile strength of the asphalt mixture, the specimen remains undamaged ($P < P_{fail}$). The load level will eventually reach the point where the tensile stresses at the edges of the specimen equal (or slightly exceed) the tensile strength of the mixture ($P = P_{fail}$), and the specimen will begin to fracture at the edges. Additional load ($P > P_{fail}$) will then cause the stresses in the central portion of the specimen to exceed the tensile strength of the mixture until the specimen finally breaks in two ($P = P_{max}$). Figure 3.8b illustrates failure as assumed to occur if plane stress conditions held true. Since tensile stresses are assumed to be uniform across the entire specimen, the specimen is assumed to remain undamaged until the maximum load is applied to the specimen ($P = P_{fail} = P_{max}$). Therefore, tensile strengths computed using plane stress analysis should generally over-predict the true tensile strength of asphalt mixtures.

From an experimental point of view, one can then determine the true tensile strength of the asphalt mixture by determining the stress level at the edge of the specimen at the instant when the specimen begins to fail (i.e. at load $P = P_{fail}$ in Figure 3.8a). However, in order to do this, one must be able to accomplish the following: 1) the measurement system used must be able to detect the instant when fracture develops at the edges of the specimen; and 2) the measurement and analysis system must be able to compute stresses that occur at the edge of a three-dimensional specimen.

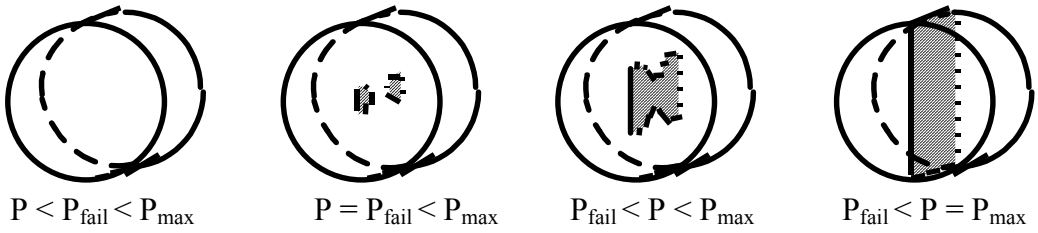

(a) Using Finite Thickness Analysis (3-Dimensional)

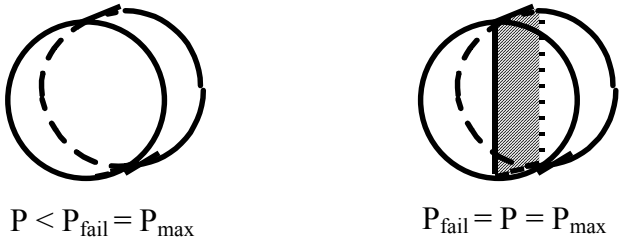

(b) Using Plane Stress Analysis (2-Dimensional)

Figure 3.8. Progression of Failure of Specimen Subjected to Diametral Load

The latter problem has been solved by Roque and Buttlar (1992) and Buttlar and Roque (1994), who presented equations to determine stresses, strains, Poisson's ratio, and modulus from tests performed on diametrally loaded specimens of finite thicknesses (plane stress assumes the specimen thickness to be infinitesimally small). The system developed by Roque and Buttlar requires the use of the measurement system shown in Figure 3.9, which is the system developed for use with the Superpave IDT (indirect tensile test). Since, as shown in Figure 3.9, this measurement system measures deformations in the immediate vicinity of maximum tensile stress, it was also found to be suitable to identify the instant when fracture develops at the edges of the specimen. The specific procedure developed to accomplish this is explained in the following section.

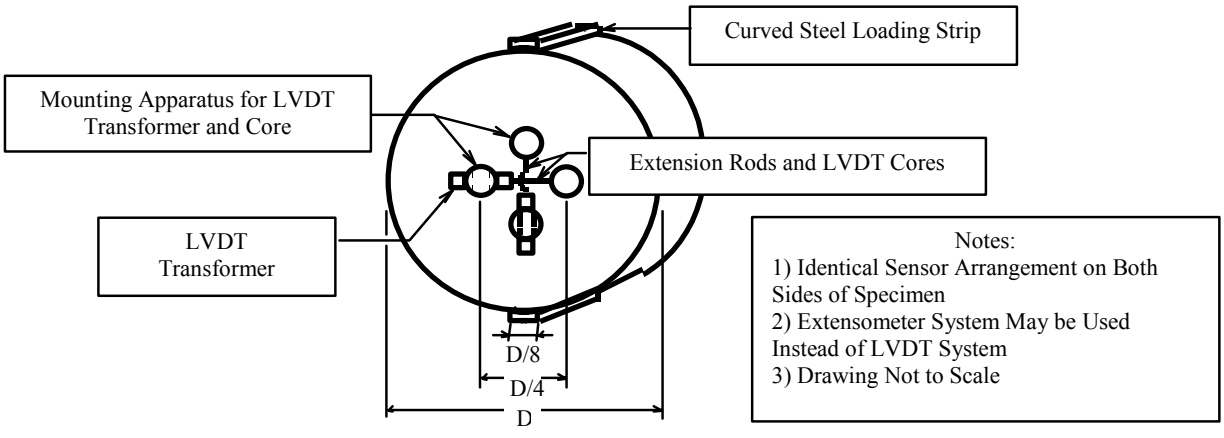

Figure 3.9. IDT Surface-Mounted Measurement System

3.2.2 Detecting the Instant of Fracture During Strength Tests

At the instant when cracking initiates at the edges of diametrally loaded specimens (Figure 3.8a, $P = P_{fail}$), one would expect to see an increase in the rate of horizontal deformation in the vicinity of the crack because the specimen has been weakened at that location and the effective stiffness of the mixture has been reduced. This increase should be detected by the horizontal LVDTs on the measurement system shown in Figure 3.9. Therefore, one should be able to identify the instant of fracture by analyzing the rate of deformation of the horizontal LVDTs during strength tests.

Figure 3.10 shows typical results from indirect tensile strength tests performed on asphalt mixtures using the measurement system shown in Figure 3.9. The specific results shown in the Figure were for a test conducted at a constant rate of ram displacement of 12.5 mm/min on a 150-mm diameter, 50-mm thick dense-graded asphalt concrete specimen at 0 C. Figure 3.10a shows that the rate of loading was roughly constant from initial loading through breaking of the specimen. Figure 3.10b shows that the increase in vertical deformations was also fairly constant and that vertical deformations were greater than horizontal deformations. Both of these observations were as expected, since vertical deformation is directly proportional to load and vertical stresses are higher than horizontal stresses at the location of measurement.

Figure 3.10b also shows that there was a significant increase in the rate of horizontal deformation on one side of the specimen well before the maximum load (i.e. the load required to break the specimen in half) was reached. This indicated that failure had occurred first at the location where the rate of deformation increased, and then additional load contributed to failure of the entire specimen. Generally, the rate of increase, and consequently, initial failure, was observed on one side of the specimen only (although in some cases, the rate of both horizontal deformations increased concurrently). This was also expected, since in practice, the load will generally be higher on one side of the specimen than the other (i.e. the load is not perfectly distributed by the loading head or the specimen is skewed), and the fracture resistance of the asphalt mixture will vary from location to location within the specimen. Therefore, even if the stress states were identical on both sides of the specimen, one side of the specimen can generally be expected to fail before the other.

Figure 3.10c shows the method that was developed to identify the instant of failure consistently from deformation measurements. As shown in Figure 3.10b, the change in rate of horizontal deformation occurs somewhat gradually over a period of time, so it is generally difficult to consistently identify the time at which a significant change in rate of deformation occurred. However, it was determined that one could consistently identify the change in horizontal response by plotting the difference between the vertical and the horizontal measurements (Y-X in Figure 3.10c). Theoretically, the vertical and horizontal stresses and deformations increase proportionately with load, which indicates that the difference between vertical and horizontal deformations should increase at a constant rate as long as the specimen is undamaged. However, once tensile failure develops, the rate of horizontal deformation will increase relative to the rate of vertical deformation and the difference between the vertical and horizontal deformations will reach a maximum.

This effect is illustrated in Figure 3.10c, where the instant of failure is identified as the time when the difference between the vertical and horizontal deformations reaches a peak, or $(Y\text{-}X)_{peak}$. If both sets of vertical and horizontal gages reach a peak, the instant of failure is taken as the time when the first peak is reached. Other methods of identifying the instant of failure, such a drawing tangents through the deformation- time plot or attempting to define the rate of change of the slope of the deformation-time plot, were also attempted, but these were found to be more difficult and less consistent than the method shown in Figure 3.10c.

Once the instant of failure is defined, the tensile strength of the asphalt mixture is determined by computing the stress corresponding to the load at the instant of failure using the following equation developed by Buttlar and Roque (1994):

$$TS = \frac{2\,P_{fail}\,C_{SX}}{\pi\,D\,t} \tag{3.26}$$

where:

$$C_{SX} = 0.948 - 0.01114\left(\frac{t}{D}\right) - 0.2693(\upsilon) + 1.436\left(\frac{t}{D}\right)(\upsilon) \tag{3.27}$$

$$\upsilon = -0.10 + 1.480\left(\frac{X'}{Y'}\right)^2 - 0.778\left(\frac{t}{D}\right)^2\left(\frac{X'}{Y'}\right)^2 \tag{3.28}$$

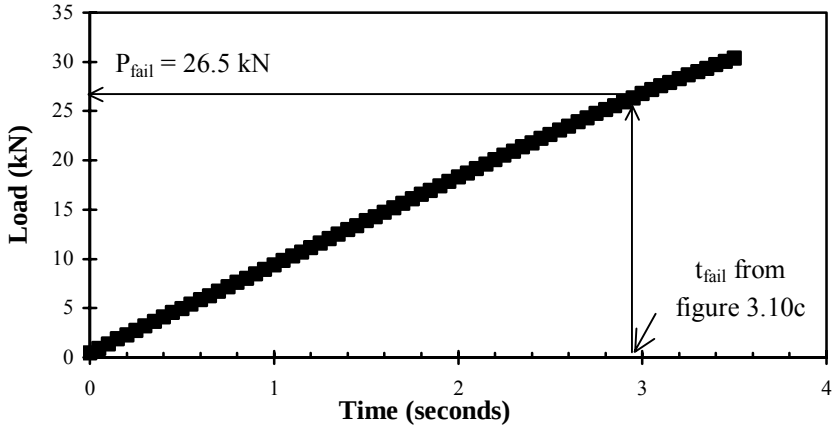

(a) Load versus Time

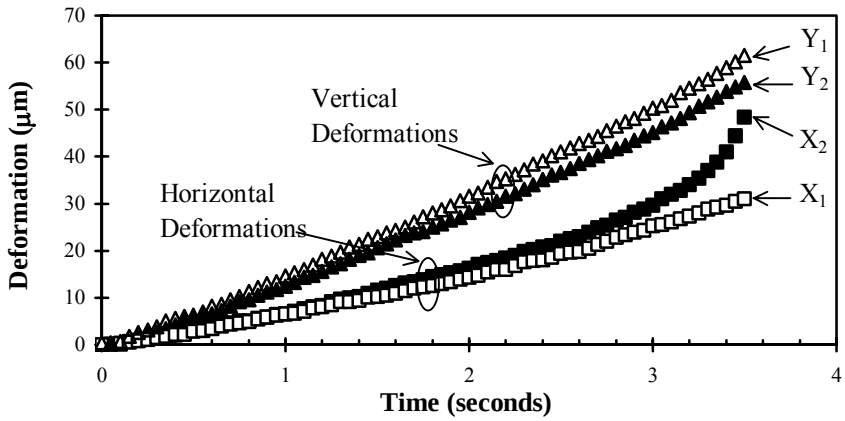

(b) Deformation versus Time

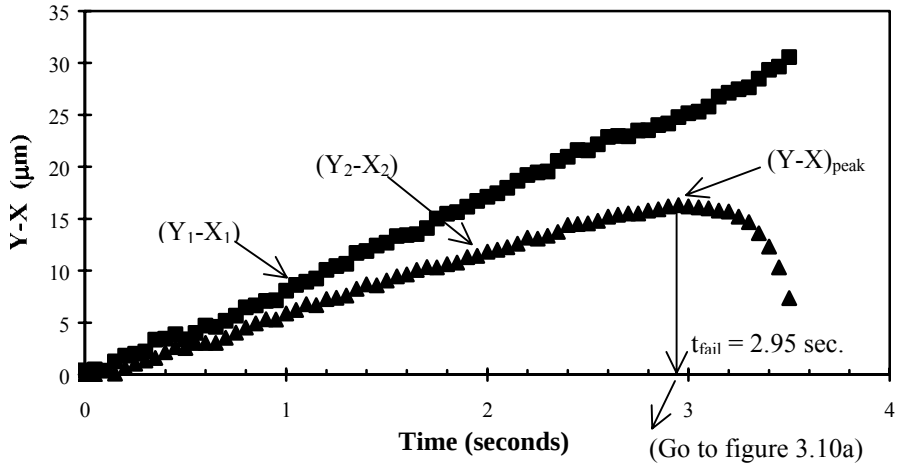

(b) (Y-X) versus Time

Figure 3.10. IDT Strength Test Results

and where:

TS = True tensile strength
P_{fail} = Indirect tensile load when cracking initiates (Figure 3.10a)
t = Specimen thickness
D = Specimen diameter
ν = Poisson's ratio
X' and Y' = Trimmed mean deformations determined at $P_{fail}/2$, horizontal and vertical

The trimmed mean values of X' and Y' to compute Poisson's ratio should be determined using the approach described by Buttlar and Roque (1994). Briefly, the approach requires three replicate strength tests, which result in six sets of vertical (Y) deformations and six sets of horizontal (X) deformations. Deformations for each of the three replicate tests are obtained at a

load level corresponding to $P_{fail}/2$. Deformations obtained from the three specimens are then normalized to account for differences in load and specimen dimensions according to the procedure described by Buttlar and Roque (1994). The normalized deformations are then ranked, the largest and smallest values are deleted (trimmed), and an average deformation is determined from the four remaining deformations. Thus, the trimmed mean vertical deformation (Y') and trimmed mean horizontal deformation (X') is obtained and used to compute one Poisson's ratio that is used in the computation of tensile strength of all three specimens.

3.2.3 Summary of IDT Strength Analysis

The following points can be drawn regarding tensile strength determination from IDT strength test data:

- Tensile failure in diametrally-loaded specimens occurs well before the maximum load required to split the specimen
- The measurement system used in the SHRP Indirect Tensile Test (IDT) is suitable to identify the instant of failure during strength tests
- Tensile strengths computed using conventional plane stress analysis of diametrally loaded specimens generally over-predict the true tensile strength of asphalt mixtures
- More importantly, tensile strengths computed using conventional plane stress analysis might result in misleading interpretations of the relative strengths between two mixtures
- The tensile strength at first failure, or “true tensile strength,” is an appropriate tensile strength parameter for thermal crack prediction using TCMODEL

3.3 Recent Developments in Superpave IDT Data Analysis

This section documents the changes made in the analysis of Superpave IDT data that have occurred since the original calibration of TCMODEL in 1992. There were three significant changes, as follows:

- A method was developed to utilize 100-second creep compliance data sets, which lead to more accurate creep compliance master curves. The method involves extrapolating log compliance-log time curves, by fitting a second order polynomial function to the log-log data at each test temperature. The method corrects inaccuracies noted in the procedure originally proposed in SHRP, as reported by Buttlar and Roque (1996).

- The improved procedures summarized above necessitated the development of automated master curve fitting procedures. A Fortran program called "Master.exe" was developed to meet this need.

- A study conducted by Roque et al. [1997] concluded that a menu system should be added to the software that converts raw IDT data to fundamental properties. The menu system allows the user to run a "standard analysis" or to manually select several analysis options, including a manual trimmed mean of horizontal and/or vertical deflection curves, and manually-input Poisson's ration values.

Thus, a two-fold benefit for recalibrating TCMODEL is now evident: 1) the three aforementioned analysis changes will be incorporated in future IDT analysis software; thus, TCMODEL should be recalibrated to reflect these changes, and; 2) the number of test sections available to calibrate TCMODEL has significantly improved since the first calibration (previously 22 sections, now 41 available). The following sections describe the three main analysis changes listed above.

3.3.1 New Extrapolation Procedure for 100-Second Creep Data

One of the main components of the Superpave mixture design and analysis system, originally developed under the Strategic Highway Research Program (SHRP), is a mechanics-based thermal cracking performance prediction model (TCMODEL). Thermal stresses are predicted by TCMODEL based upon a viscoelastic characterization of the asphalt mixture at low temperatures. The sophisticated viscoelastic stress analysis performed carefully tracks the stress history of the mixture, and consequently, mixture properties must be known at very long loading times. The time-temperature superposition principle has been employed to allow the required properties to be obtained from creep tests of relatively short duration. However, the techniques originally used in Superpave to construct the creep compliance master curve have been found to be problematic (Buttlar and Roque, 1996a). New analysis techniques are presented which were found to produce accurate performance predictions with as little as 100 seconds of creep testing and without the need for supplementary binder data.

A key challenge faced by the research team involved the development of measurement and analysis techniques to provide the creep compliance master curve (CCMC) and shift factor-

temperature relationship (log a_T versus T) required by TCMODEL (figure 3.10). The formation of the CCMC can be understood by considering a graphical manipulation (horizontal shifting) of creep compliance curves measured at different temperatures, as illustrated in figure 3.10. The horizontal distances by which the individual curves are shifted to form a smooth, continuous master curve, are quantitatively known as the temperature shift factors. The master curve is created at one of the temperatures used in testing, and the temperature shift factors are used to obtain compliances at other temperatures.

The benefit of the CCMC and shift factor-temperature relationship is that a complete viscoelastic characterization of an asphalt mixture at low temperatures can be obtained with short duration creep test data. The resulting characterization allow accurate interpolation of test data between test temperatures and the ability to predict creep response at loading times several orders of magnitude larger than those used in the actual creep tests. This is important, since TCMODEL keeps tract of the stress history of the pavement for many hours at a time, in order to allow complete relaxation of stresses induced in previous time intervals to occur. Since it would be impractical to conduct creep tests for such long time intervals, the CCMC method is a powerful and necessary tool for thermal cracking analysis using TCMODEL.

The key to obtaining accurate shift factors is to have sufficient overlap (figure 3.10b) between creep compliance curves at adjacent temperatures. Without sufficient overlap, there is no definite way to determine the proper horizontal shifting distance for a given compliance curve. Furthermore, without sufficient overlap, a gapped master curve would result, which could lead to computational problems with the rheological material modeling algorithm used in TCMODEL.

3.3.1.1 Difficulties Associated With Master Curve Modeling at Low Temperatures

The technique presented in the preceding section for relating the time- and temperature-dependent response of a viscoelastic material is known as the time-temperature superposition principle, and is applicable to a class of materials that are said to be thermorheologically simple. Major strides were made in the research conducted under SHRP to apply this principle to asphalt mixtures at low temperatures (Lytton et al. [1993]), but not without serious challenges. When creep compliance curves (log creep compliance versus log time) and temperature shift factors follow simple, predictable patterns (figure 3.10), it is a straightforward process to determine the minimum amount of creep testing required to provide overlap between creep compliance curves for construction of the CCMC. However, it has been found that creep compliance curves for asphalt mixtures at low temperatures are often irregularly spaced and unpredictable (Buttlar, 1996), as shown in figure 3.11.

In some cases, creep tests of over 100,000 seconds (>1 day) would be required to provide overlap in compliance curves at adjacent temperatures (0, -10, and -20 C, in the case of Superpave). Often, however, overlap between creep compliance curves at adjacent temperatures is achieved with as little as 100 seconds. Thus, the use of excessively long creep tests to provide overlap for master curve construction is not only impractical, but is unnecessary in most cases.

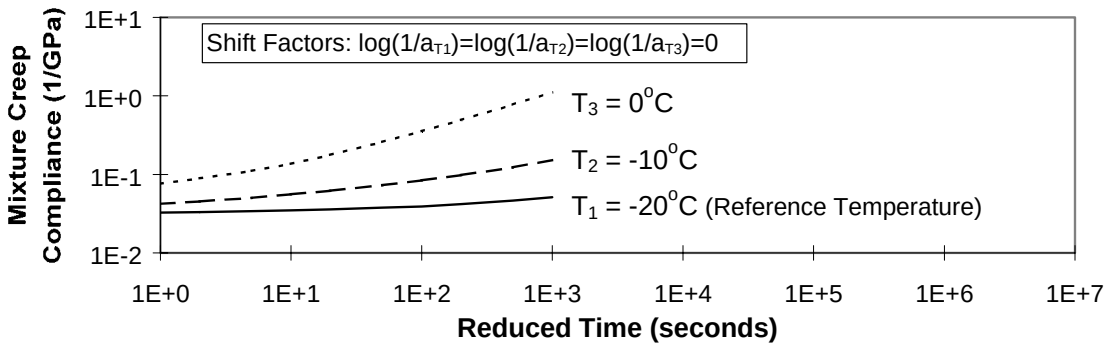

Figure 3.10a. Unshifted Creep Compliance Data

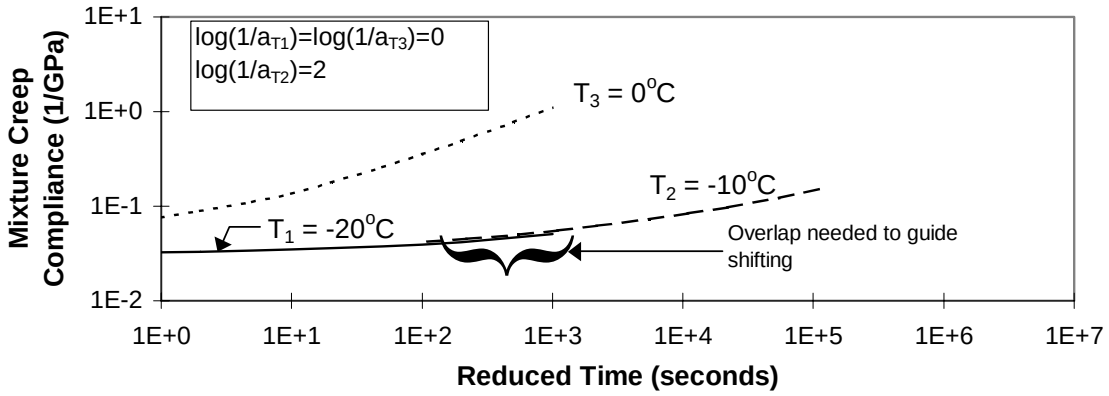

Figure 3.10b. Shifted Creep Compliance Data at -10 C

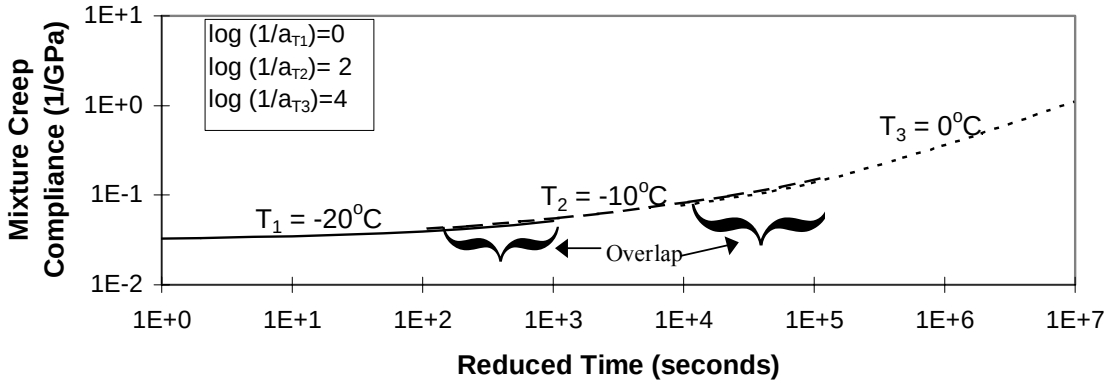

Figure 3.10c. Completed Master Creep Compliance Curve

Figure 3.10. Idealized Creep Compliance Master Curve Formation

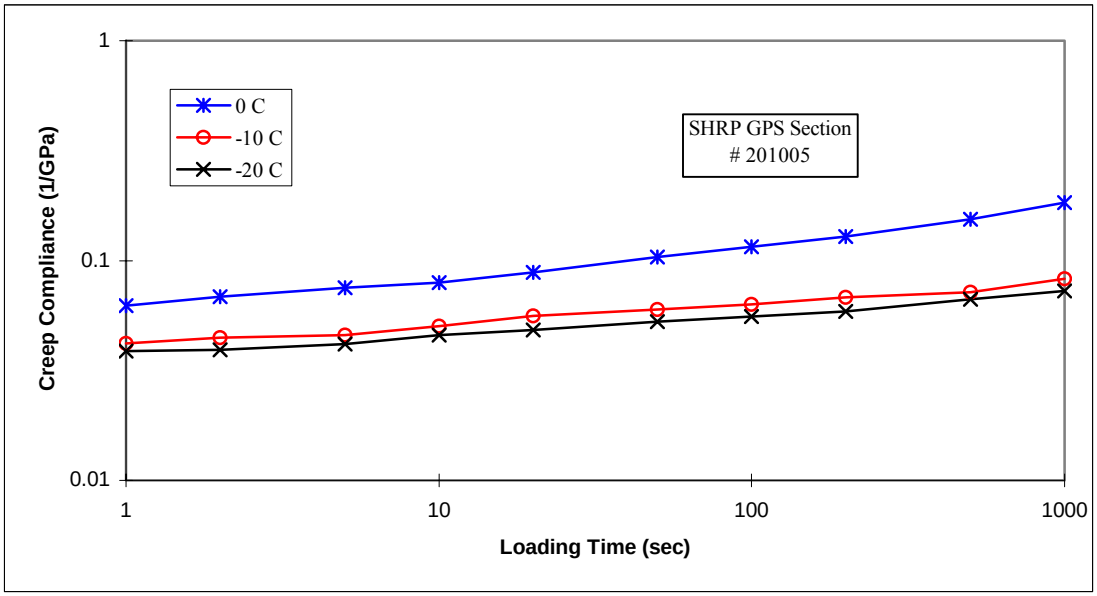

Figure 3.11. Uneven Compliance Curve Spacing for Field-Aged Mixture

The approach taken in Superpave to address this dilemma was to perform 100-second creep tests and to extrapolate mixture compliances to provide the required overlap. Buttlar (1996) and Buttlar and Roque (1996a) recently revisited this data extrapolation procedure, which is shown in figure 3.12.

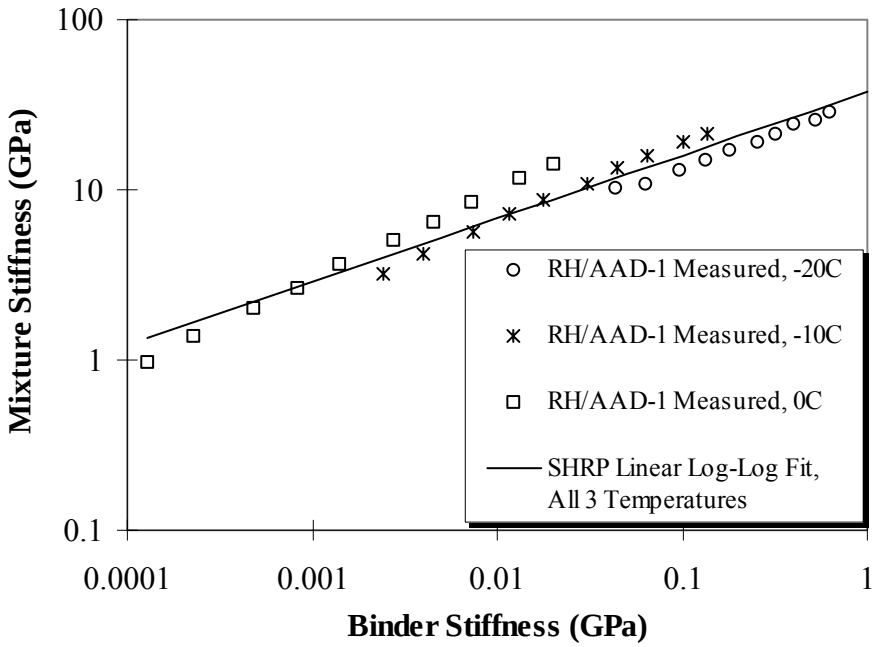

Figure 3.12. Single-Function Linear Log-Log Binder to Mixture Stiffness Relationship Currently Used in Superpave

Gaps between mixture creep compliances measured at adjacent temperatures are essentially bridged by fitting a linear log-log model through the data points on the log of mixture stiffness-log of binder stiffness plot. However, several undesirable consequences arise when using this method, namely:

1) The mixture master curve formed as a result of relating mixture stiffness to binder stiffnesses exhibits shape similarity to the binder master curve, even though the magnitudes are quite different;

2) Mixture shift factors obtained with the original Superpave scheme are found to be identical to the shift factors of the corresponding binder data used, because of the master curve shape similarity, usually resulting in mixture shift factors which are predicted to be too large, and;

3) Errors in shift factors combined with other modeling inaccuracies associated with the single-function, linear log-log binder-to-mixture stiffness relationship usually lead to the over prediction of mixture stiffness in critical regions of the master curve. The modeling inaccuracies also typically result in the under prediction of 'm,' which is an important parameter used in the fracture mechanics model contained within TCMODEL. Both of these effects result in the over prediction of cracking severity.

3.3.1.2 Current State-of-the-Art

Buttlar (1996) developed a nonlinear log-log, multiple-function binder-to-mixture stiffness model (figure 3.13) which was found to accurately predict thermal cracking performance with 100-second mixture creep tests. However, it was recommended that the complicated calibrated micromechanical relationship used to form the nonlinear log-log relationship in the study be reevaluated to determine if a simpler function could be used (Buttlar and Roque [1996a]). Furthermore, the results of the study suggested the possibility of directly extrapolating log creep compliance log time curves (figure 3.14) to provide overlap between compliance curves, thus eliminating the need for binder data.

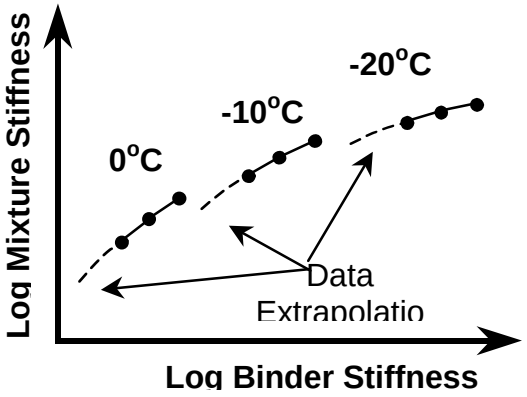

Figure 3.13. Illustration of Nonlinear Log-Log Binder to Mixture Stiffness Extrapolation

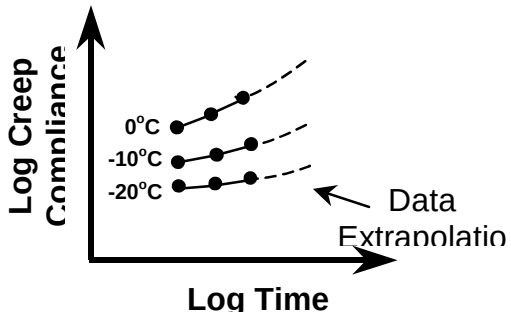

Figure 3.14. Illustration of Log Compliance-Log Time Extrapolation

The following sections describe the analyses conducted by Buttlar and Roque (1997) to validate the use of 100-second creep test data and log-compliance-log-time data extrapolation technique. The objectives of the analyses were: 1) To evaluate new methods for constructing mixture master creep compliance curves, including a method which does not require binder bending beam rheometer (BBR) stiffnesses, and; 2) To determine the minimum creep test duration that could be used in conjunction with the new techniques without sacrificing accuracy of thermal cracking performance predictions.

Five mixtures were selected for analysis, which were felt to represent the most challenging types of creep measurements typically encountered with respect to the development of mixture master compliance curves (Table 3.1). Field-aged mixtures were predominantly used in the study by Buttlar and Roque (1997) because it can be challenging to develop master curves for these mixes and, thus, it was felt that they would help differentiate between the different master curve modeling techniques studied. Mixes 3 and 4 exhibit highly uneven spacing of compliance curves at evenly spaced temperature intervals. This is thought to be indicative of microdamage in the asphalt mastic, caused by excessive differential thermal contraction between asphalt and aggregate during cooling (Buttlar et al. [1996]).

Table 3.1 Description of Mixtures Selected for Analysis

Mix #	Description	Master Curve Characteristic
1	Field Mix: SHRP GPS 041022	Very High Stiffness
2	Field Mix: CSHRP Sherbrooke Section C	Very Low Stiffness
3	Field Mix: SHRP GPS 341011	Uneven Spacing of Compliance Curves (Damage)
4	Field Mix: SHRP GPS 201005	Uneven Spacing of Compliance Curves (Damage)
5	Lab Compacted Mix w/ Modified Binder: PG 76-22	Mixture with Modified Binder

Although the Superpave IDT is typically used to conduct 100-second mixture creep tests, the Buttlar and Roque (1997) study utilized creep tests run for a duration of 1000 seconds, so that appropriate comparisons could be drawn between longer and shorter test durations. In their studuy, creep tests were performed at 0, -10, and -20C. Immediately after each creep test, a strength test involving the application of a 51-mm per minute failure rate was performed. Binder bending beam rheometer (BBR) tests were performed at -15C (-18C for the CSHRP mixture). Binder stiffnesses were determined at loading times of 15, 30, 60, 120, and 240 seconds.

3.3.1.3 Analysis Methods

The effects of various master curve modeling techniques on thermal cracking performance prediction was studied by considering a series of analysis methods, as given in table 3.2. The key parameters evaluated were creep test duration and data extrapolation technique.

The goal of the analyses conducted was to investigate test protocols and analysis procedures aimed at minimizing creep test duration, while maintaining accurate thermal cracking performance predictions. Thus, the accuracy of TCMODEL itself is not under investigation herein. Interested readers can refer to Roque, Hiltunen, and Stoffels (1993) and Roque et al. (1994) for detailed descriptions of TCMODEL validation efforts. In general, these studies have indicated that TCMODEL provides very realistic thermal cracking performance predictions for pavements throughout the United States and Canada.

Table 3.2 Description of Analysis Methods Used to Prepare Master Curve Data

Analysis Method	Duration of Creep Test Data	Data Modeling or Extrapolation Scheme
0	1000 sec	Control Method, No Extrapolation
1	100 sec	Multiple Function, D vs. t^1, Polynomial
2	100 sec	Multiple Function, B/M^2, Polynomial
3	100 sec	Single Function, B/M, Linear Log-Log
4	10 sec	Multiple Function, D vs. T, Polynomial
5	10 sec	Multiple Function, B/M, Polynomial

[1]Log creep compliance versus log time extrapolation
[2]Log binder versus log mixture stiffness extrapolation

The steps used in the analysis of IDT test results to obtain thermal cracking performance predictions were:

1) Convert raw data collected in the IDT creep and strength tests to creep compliances and tensile strengths according to procedures described by Buttlar and Roque (1994), and Buttlar et al. (1996).

2) Filter creep compliances to generate an approximate logarithmic spacing. Loading times selected were: 1, 2, 5, and 10 seconds for analyses based upon 10 seconds of creep data; 1,

2, 5, 10, 20, 50, and 100 seconds for analyses based upon 100 seconds of creep data; and 1, 2, 5, 10, 20, 50, 100, 200, 500, and 1000 seconds for analyses based upon 1000 seconds of creep data.

3) Extend 10- and 100-second creep compliance curves to 1000 seconds using each of the two selected extrapolation techniques, as described below.

Binder-to-Mixture Stiffness Extrapolations. This technique involves fitting a function to relate the log of mixture stiffness to the log of binder stiffness, as illustrated in figure 3.13, and then extrapolating the fitted function to provide overlap between creep compliances at adjacent temperatures. A second order polynomial was selected, as given by equation 3.29:

$$logS_M = a(logS_B)^2 + b(logS_B) + c \qquad \textbf{(3.29)}$$

where:

S_M = Mixture stiffness modulus (1/creep compliance)
S_B = Binder stiffness modulus
a, b, c = Least squares regression coefficients

Binder stiffnesses were estimated at temperatures and loading times corresponding to those selected for mixture data by constructing a binder master stiffness curve, based upon bending beam stiffnesses. A hyperbolic model developed by Christensen (1992) was used, as given by equation 3.30:

$$S_B = 3G_g\left[1+\left(\frac{t_r}{t_0}\right)^{\frac{\log 2}{R}}\right]^{\frac{R}{\log 2}} \qquad \textbf{(3.30)}$$

where:

t_r = Reduced time = $t\left(\frac{a_T}{a_{Tref}}\right)$
t = Loading time
T = Evaluation temperature
T_{ref} = Reference temperature
^oK = $^oC + 273$
G_g = Glassy modulus, taken as 1 GPa
R, t_0 = Determined from regression

and:

$$\log\left(\frac{a_T}{a_{Tref}}\right) = 13{,}589\left[\frac{1}{T} - \frac{1}{T_{ref}}\right] \qquad \textbf{(3.31)}$$

Equation 3.31 is called the Ahrennius function and is used to approximate relative changes in binder shift factors with changes in temperature. Although the Ahrennius function is generally only accurate below the glass transition temperature of asphalt binders, Buttlar (1996) showed that this relation was suitable for the estimation of binder stiffnesses at 0, -10 and -20C for the purpose of generating binder-to-mixture stiffness relationships. A broad range of binders were considered, from field-aged mixtures and from laboratory compacted mixtures.

The second-order polynomial function selected (equation 3.29) has the advantages of being readily fit to measured data with linear regression and, more importantly, that the fitted parameter 'a' can be used to screen data to verify that it follows expected trends. Buttlar and Roque (1996a) have shown experimentally and through micromechanical analyses that the log mixture stiffness-log binder stiffness relationship should plot as concave downward, which concurs with previous experimental findings (Huekelom and Klomp [1964], and Bonnaure et al. [1977]). Thus, the 'a'-term in equation 3.29 is expected to be negative.

Log Creep Compliance-Log Time Extrapolations. The recommended approach for extending mixture creep compliances measured at low temperatures to longer loading times is given by equation 3.32:

$$logD(t) = A(logt)^2 + B(logt) + C \qquad \textbf{(3.32)}$$

where:

D(t) = Mixture creep compliance
T = Loading time
A, B, C = Least squares regression coefficients

Since the log D(t)-log t relationship plots concave upward, as shown in figure 3.14, the quadratic term 'a' is expected to be positive.

4) Construct CCMC's by shifting compliance curves at individual temperatures. In doing so, temperature shift factors are obtained. Data were shifted relative to a reference temperature of -20C (figure 3.10).

5) Fit the CCMC's with a generalized Voight-Kelvin model, given by equation 3.33:

$$D(t) = D_0 + \sum_{j=1}^{4} D_j (1 - e^{\xi/\tau_j}) + \frac{\xi}{\eta_v} \qquad \textbf{(3.33)}$$

where:

ξ = Reduced time = t_i/a_{Ti}
t_i = Loading time
a_{Ti} = Temperature shift factors
T_1, T_2, T_3 = Test temperatures (-20, -10, and 0C)
τ_j= Retardation times
D_0, D_j = Compliance coefficients or Prony Series Parameters

Buttlar (1996) found that the fitting of equation 3.33 to the CCMC using least squares regression was most robust when the retardation times, τ_j, were evenly spaced across the master curve in the log of reduced time domain. Given the selection of a reference temperature of -20 C, the breadth of the master curve in the reduced time domain is related to the shift factor at 0 C, or a_{T3}. A scheme was developed to automate the selection of evenly spaced retardation times, as follows:

$$\log \tau_1 = 0.33\left(\log \frac{1}{a_{T3}} + 2\right) \qquad \textbf{(3.34a)}$$

$$\log \tau_2 = 0.55\left(\log \frac{1}{a_{T3}} + 2\right) \qquad \textbf{(3.34b)}$$

$$\log \tau_3 = 0.75\left(\log \frac{1}{a_{T3}} + 2\right) \qquad \textbf{(3.34c)}$$

$$\log \tau_4 = \left(\log \frac{1}{a_{T3}} + 2\right) \qquad \textbf{(3.34d)}$$

The advantage of pre-solving for the retardation times, τ_j, using equations 3.34a-3.34d is that linear regression may be used to fit the Prony series (equation 3.33) to the CCMC. If the τ_j parameters were left as unknowns, then nonlinear regression would be required, which is considerably more tedious and unnecessary.

6) Fit the CCMC with a power model, given by equation 3.35, to obtain m (see also Figure 2.8):

$$D(t) = D_0 + D_1 \xi^m \quad \textbf{(3.35)}$$

Equation 3.35 was fitted to all master curves such that the sum of squared errors (SSE) was minimized with respect to the differences between the log of fitted and log of measured creep compliances. Originally, equation 3.35 was fit such that the sum of squared errors (SSE) was minimized with respect to differences in arithmetic quantities. However, it was found that this caused the regression to be heavily weighted towards fitting compliances at longer reduced loading times, which can be up to two orders or magnitude larger than those at very short reduced loading times for the temperatures and loading times used in this study.

7) Develop techniques for generating specific cracking levels for relative performance comparisons. The primary goal of the analyses conducted was to study the relative differences in predicted thermal cracking between a control case involving 1000-second creep testing and the surrogate methods examined in this study, which involve the use of shorter loading times (10 and 100 seconds) and various data extension techniques. Since only relative differences in performance were sought, this allowed some freedom in choosing certain input parameters for the thermal cracking model. Specifically, the thermal coefficient of contraction and asphalt concrete layer thickness were defined as being constant for all mixtures considered, at $2.4 \times 10^{-5}/^{o}C$ and 150mm, respectively, as opposed to using site-specific information.

The selection of temperature files to be used to predict and compare relative thermal cracking of the various analysis methods considered was carried out with the goal of avoiding performance extremes; i.e., to avoid such severe climatic conditions that all methods would be found to predict terminal cracking in the first year, and conversely, to avoid such mild conditions that all methods would be found to predict zero cracking throughout the entire analysis period (30 years).

This was done by generating a series of temperature files of varying severity from two 'seed' temperature files. By modifying these two temperature files with across the board temperature increases or decreases to all temperature data points, a series of temperature files were created, ranging from very mild to very harsh conditions. This approach was developed to alter only the magnitudes of temperature cycles, while leaving the cooling rates intact.

The CCMC corresponding to the control case for each mixture considered was then submitted to TCMODEL using temperature files of increasing severity (5C increments), until a predefined level of cracking severity was achieved. Terminal cracking was arbitrarily set at 190 meters of thermal cracking per 500 lane meters. Temperature adjustments were selected so as to produce terminal cracking in the control case in a window of 12 to 25 years of pavement age, if possible. A summary describing the 'seed' temperature files and temperature adjustments used is described in table 3.3.

Table 3.3. Summary of Temperature Data Used in Thermal Cracking Analysis

Mix	Seed Temperature File	Adjustment (^{o}C)
1	Washington, DC, 1981	-10
2	Fargo, ND, 1981	-25
3	Washington, DC, 1981	-15
4	Washington, DC, 1981	+8
5	Washington, DC, 1981	-15

The temperature files used contain hourly pavement temperatures at multiple depths and were generated from minimum/maximum daily air temperatures using the FHWA Integrated Model of the Environmental Effects on Pavements (Lytton et al. [1993]), which is contained within the Superpave software, for a period of one year. The same temperature file was used for each year of thermal cracking analysis for a given mixture. The techniques described provide a relatively simple way to distinguish between predicted cracking caused by relatively minor differences in the master curve, shift factors, and the m-parameter. The only disadvantage of the method is that the differences in thermal cracking predicted are somewhat arbitrary and were found to be fairly sensitive to minor changes in mixture rheological parameters. Thus, the method is viewed as a conservative tool for evaluating candidate material modeling techniques, as only the very best methods will produce favorable results.

Run TCMODEL for the remaining analysis methods (1-5) using the temperature files selected in step 7.

3.3.1.4 Results

The results of the thermal cracking performance prediction comparisons are presented in figure 3.15, and summarized in table 3.4. The 100-second log creep compliance-log time extrapolation (method 1) yielded predictions similar to the control method (0), with no prediction varying by more than 5 years. Considering the conservative nature of the analysis techniques used, this method was found to predict performance quite closely to the control case. A typical master curve and fitted Prony series is presented in Figure 3.16, for the control case. Figure 3.17 presents the predicted amount of thermal cracking versus time from TCMODEL, for mixture #1.

Tables 3.5a, 3.5b, and 3.5c contain values for the m-parameter and shift factors obtained from generating master curves for each mixture and analysis method. Shift factors and m-values for analysis methods 1 and 2 were generally very close to those of the control case, with the exception that the binder-to-mixture stiffness extrapolation method was found to consistently yield slightly high m-values.

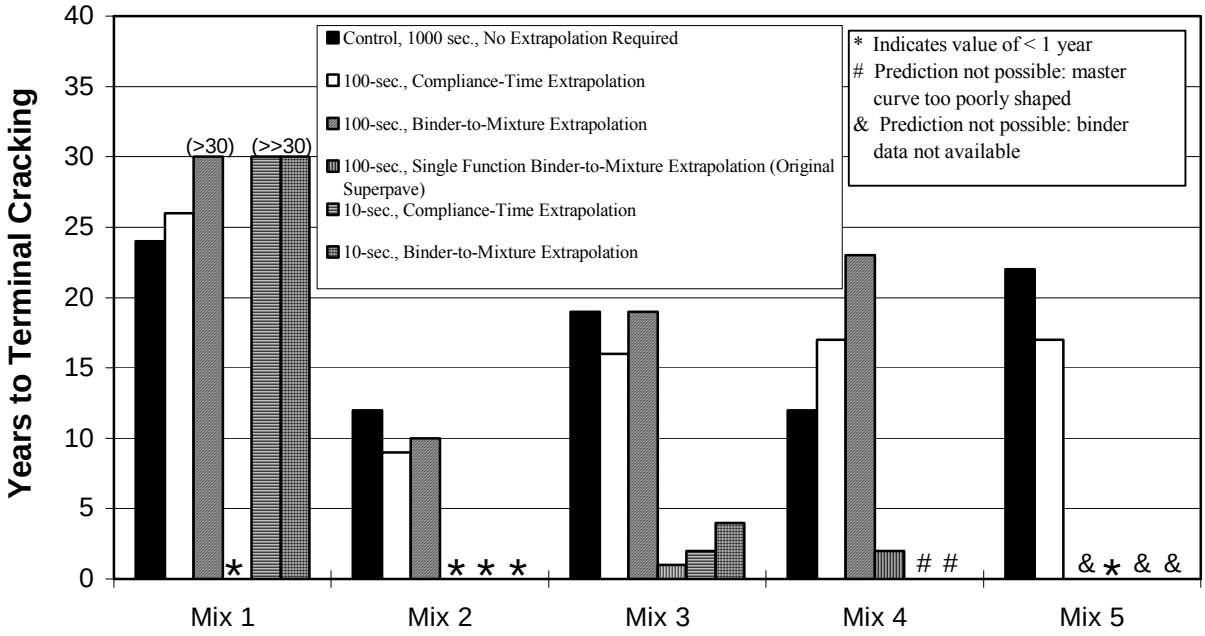

Figure 3.15. Thermal Cracking Prediction Comparison for the Six Analysis Methods

Table 3.4. Summary of Thermal Cracking Performance Predictions

Method	Duration of Creep Test Data	Data Modeling Scheme	Prediction Quality Relative to Control
1	100 sec.	Mult. Function, D vs t	Good
2	100 sec.	Mult. Function, B/M	Fair
3	100 sec.	Single Function, B/M	Poor
4	10 sec.	Mult. Function, D vs t	Poor
5	10 sec.	Mult. Function, B/M	Poor

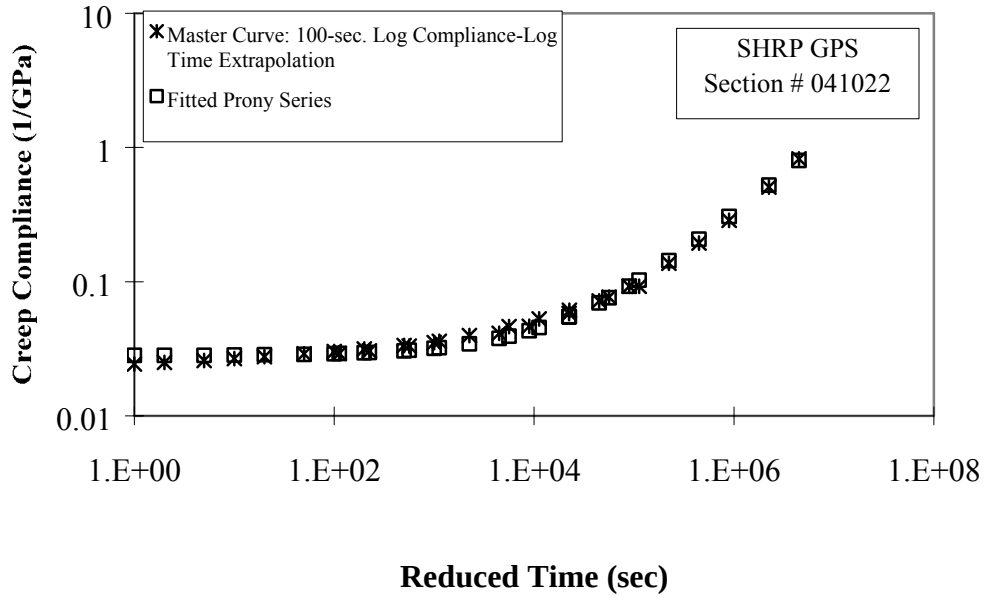

Figure 3.16. Typical Creep Compliance Master Curve and Fitted Prony Series

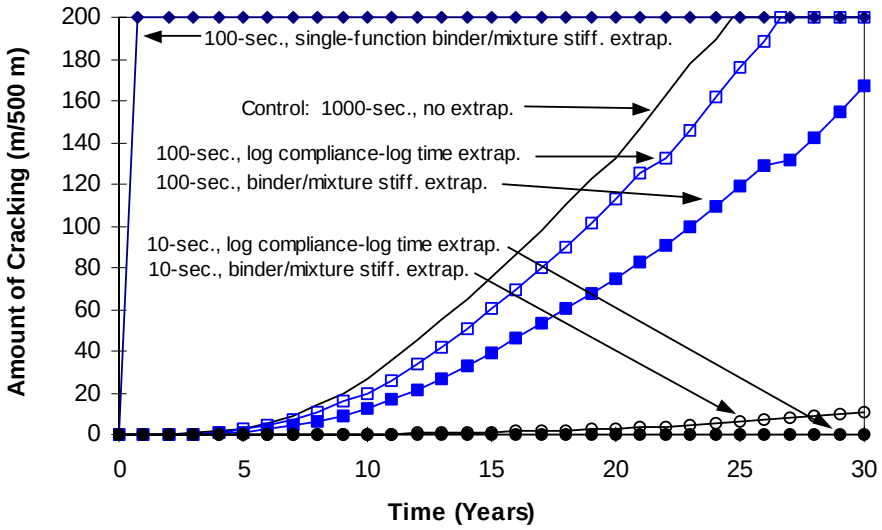

Figure 3.17. Thermal Cracking Predictions for SHRP GPS Section 041022

Table 3.5a. Summary of m-values

	Analysis Method†					
Mix	**0**	**1**	**2**	**3**	**4**	**5**
1	0.605	0.635	0.670	0.175	0.620	0.705
2	0.510	0.545	0.555	0.300	0.625	0.645
3	0.485	0.520	0.535	0.230	0.345	0.385
4	0.220	0.230	0.240	0.165	#	#
5	0.375	0.365	#	#	#	#

Table 3.5b. Log of Temperature Shift Factors at -10^{o}C

	Analysis Method†					
Mix	**0**	**1**	**2**	**3**	**4**	**5**
1	2.20	2.05	2.05	2.04	2.25	1.95
2	0.85	0.90	0.90	2.04	1.00	0.90
3	2.20	2.35	2.20	2.04	2.55	2.30
4	0.50	0.50	0.50	2.04	#	#
5	1.30	1.45	#	#	#	#

Table 3.5c. Log of Temperature Shift Factors at 0^{o}C

	Analysis Method†					
Mix	**0**	**1**	**2**	**3**	**4**	**5**
1	3.70	3.65	3.60	3.93	3.10	2.65
2	2.10	2.25	2.25	3.93	1.75	1.50
3	3.65	3.95	3.80	3.93	4.55	4.15
4	2.50	2.35	2.35	3.93	#	#
5	2.25	2.40	#	#	#	#

†Method 0 = Control, 1000 sec., No Extrapolation Required
Method 1 = 100-sec., Compliance-Time Extrapolation
Method 2 = 100-sec., Binder-to-Mixture Extrapolation
Method 3 = 100-sec., Single Function Binder-to-Mixture Extrapolation (Original Superpave)
Method 4 = 10-sec., Compliance-Time Extrapolation
Method 5 = 10-sec., Binder-to-Mixture Extrapolation
#Indicates that prediction was not possible

The single-function (linear log-log), 100-second binder-to-mixture stiffness extrapolation method (#3), originally developed for Superpave, was observed to produce poor thermal cracking predictions (figure 3.15). This is consistent with the finding of Buttlar (1996), and Buttlar and Roque (1996a) who showed that the single-function procedure typically led to a gross under prediction of number of years to terminal cracking.

Master curve modeling techniques 4 and 5, involving the extrapolation of 10-second creep compliance curves, were also found to produce poor results. Unlike 100-second creep data, 10 seconds was clearly found to be an insufficient amount of data, often leading to erratic

extrapolations. In some cases the extrapolations produced creep compliances curves that were uncharacteristically flat, and in other cases, those that were uncharacteristically curved. This made construction of the CCMC impossible in several cases as noted in figure 3.15.

3.3.1.5 Summary of 100-Second Data Procedures

The study by Buttlar and Roque (1997) investigated analysis methods geared towards improving the techniques used in the thermal cracking portion of the Superpave mixture design and analysis system. The methods were developed in an effort to improve the accuracy of predictions made using the thermal cracking software in Superpave and to determine the minimum creep test duration needed to produce accurate results.

Based upon the findings of this research, it was concluded that:

1) The creep compliance master curve (CCMC) for asphalt mixtures at low temperatures can be adequately constructed using creep compliance curves that are 100 seconds in duration, for test temperatures of 0, -10 and -20C.
2) Binder data is not needed to extend mixture creep compliances to longer loading times for construction of the CCMC.

3.4 Development of Program MASTER

Central to the mechanics-based thermal cracking model used in Superpave is the prediction of thermally-induced stresses based upon a master curve and shift factor concept. The original version of Superpave had procedures for automated construction of the mixture creep compliance master curve from measured mixture properties. However, recent studies have indicated the need for several new modeling techniques, the development of which has resulted in the need for substantially more sophisticated procedures for automated construction of the master curve.

This section details the development of a computer program called MASTER, which automates master curve construction using built-in logic capabilities designed to handle the wide variety of measured responses encountered in practice. MASTER was found to closely agree with manually determined shift factors for thirty-six field mixtures investigated. The program was also found to be extremely robust, producing rational shift factors even when used to analyze complicated, thermally-damaged materials.

The greatest challenge in fully automating TCMODEL for Superpave involved the construction of the creep compliance master curve and shift factor-temperature relationship (log a_T versus T) required by TCMODEL (Figure 3.18). The master curve and shift factors are used to obtain a complete viscoelastic characterization of an asphalt mixture at low temperatures with creep data of relatively short duration. Analyses conducted by Buttlar and Roque (1997) have determined that the most suitable creep testing protocol for the Superpave IDT (Figure 3.1) is to perform 100-second creep tests at each of three test temperatures. However, regardless of the creep test duration, it is sometimes necessary to extrapolate mixture compliances to longer loading times to provide the required overlap for accurate determination of shift factors (Figure 3.18).

As described in Section 3.1, the original extrapolation technique used in Superpave led to errors in shift factors, and consequently, a new procedure was developed. The new procedure involved extrapolating log creep compliance-log time data using a second-order polynomial function to provide the necessary overlap between compliance curves at adjacent temperatures, and visually shifting the data to obtain temperature shift factors. However, visually shifting data, even when performed by a trained engineer is cumbersome and results are subjective. It was therefore concluded that automated procedures should be developed for the new techniques to be suitable for the Superpave system, which prompted the work conducted in this study.

The goal was to create a fully automated, robust program that could handle the many different types of compliance curves encountered in practice, including those associated with specimens thermally damaged upon cooling to very low temperatures (Buttlar and Roque [1996], Kim and El Hussain [1995]).

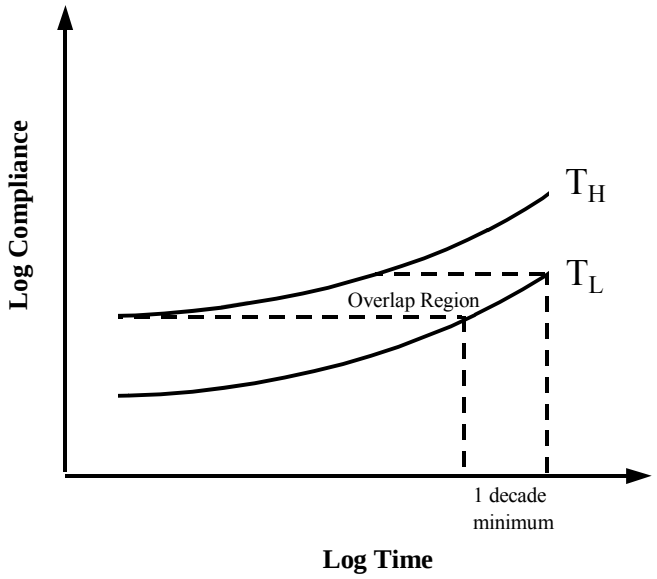

Figure 3.18. Overlap Region for Shifting Creep Compliance Curves

3.4.1 Description Of Computer Program Master

The general steps taken by the computer program MASTER to obtain the master curve parameters are:

- Read compliance data from data files
- Fit second degree polynomial to log compliance-log time data at each temperature
- Obtain temperature shift factors for each temperature using fitted compliance-time data
- Discretize fitted compliance-reduced time curves to ten data points per temperature, using an even spacing in the log time domain
- Fit specific rheological models to the discretized master curve data to satisfy TCMODEL formatting requirements for input, and store parameters in a data file

The details and development of these steps are given in the following sections.

3.4.2 Fitting Creep Compliance-Time Data

The master curve is constructed by shifting creep compliance curves on a log compliance-log time plot (Figure 3.18). Therefore, it is necessary for MASTER to convert the compliance-time data to log compliance-log time data before fitting the data. The log compliance-log time data are fit with a second-degree polynomial function for each of the three test temperatures. The resulting fitted compliance curves are used in all subsequent procedures. There are two primary reasons for utilizing fitted data at this stage of the analysis: 1) any noise present in the test data is smoothed out with the simple polynomial function, and; 2) the use of a function to describe the compliance-time data for each test temperature facilitates interpolation and/or extrapolation of creep compliances, which is sometimes required to shift the compliance data.

The log compliance-log time data are first fit with a linear function to check whether the slope of the line is positive or negative:

$$log\,[D(t)] = m\,log\,(t) + b \qquad \textbf{(3.36)}$$

where:

$D(t)$ = Creep compliance at time t

t = Time

m = Slope of the line

b = Log [$D(t)$] axis intercept

If m is less than zero the slope is negative, indicating a decrease in creep compliance with time, and the program will terminate because it is not rational for compliance to decrease with time. If the slope is positive (i.e., m > 0), the program will fit a second-degree polynomial to the data and check whether the relationship is concave upward:

$$log\,[D(t)] = A\,[log\,(t)]^2 + B\,[log\,(t)] + C \qquad \textbf{(3.37)}$$

where:

A, B, C = Polynomial coefficients

A check is then made to see if A is greater than zero, verifying that the relationship is concave upward. If it is not, this indicates that the creep compliance will eventually decrease with time, and the linear function (equation 3.36) is used to represent the log compliance-log time relationship.

3.4.3 Shifting Fitted Creep Compliance-Time Data

Obtaining accurate temperature shift factors is the key to developing accurate master curves. Therefore, the most important part of the program MASTER was the development of a reliable method to obtain the shift factors. MASTER uses the time-temperature superposition principle in order to obtain the temperature shift factor for each fitted creep compliance data curve (Figure 3.18). The temperature shift factors are defined as follows:

a_{T1} = 1 = Shift factor for the lowest (reference) temperature

a_{T2} = Shift factor for the intermediate temperature

a_{T3} = Shift factor for the highest temperature

It is convenient to report shift factors in terms of log $(1/a_{Ti})$ because this quantity corresponds to the number of decades the compliance curve is shifted along the log time axis.

A subroutine was developed in MASTER to shift a single compliance curve to an adjacent compliance curve at a lower temperature. For illustrative purposes the following convention will be used:

T_L curve = Compliance curve at the lower temperature

T_H curve = Compliance curve at the higher temperature

A certain amount of overlap is required to accurately shift the T_H curve to align with the T_L curve. Sufficient overlap was defined as the portion of overlap on the T_H curve having an interval of time on the log time axis equal to at least 1 decade (Figure 3.18). There are four different cases of possible orientations of the two compliance curves that can occur, which affect the procedures used to determine the overlapping region. The following sections describe these four cases and the logic coded into MASTER to identify each case.

Case 1

This is the general case where the T_H curve is above the T_L curve as shown in Figures 3.19a and 3.19b. The following steps were used to define points on each compliance curve as shown in each figure:

1. Define 'A' as the point on the T_H curve at the initial loading time t_A of 1 second.
2. Define 'B' as the point on the T_L curve having the same compliance as point A and a loading time equal to t_B.
4. Check for sufficient overlap based on 1 decade relative to the T_L curve. This is done by determining the difference between the log of time t_B and the log of the final loading time t_C (100 seconds for Superpave) to determine whether or not this difference exceeds 1.0: log (t_C) - log $(t_B) \leq 1$ (sufficient overlap)

Sufficient overlap (Figure 3.19a)

4. Define ‘C’ as the point on the T_L curve at the final loading time t_C.
5. Define ‘D’ as the point on the T_H curve having the same compliance as point C.

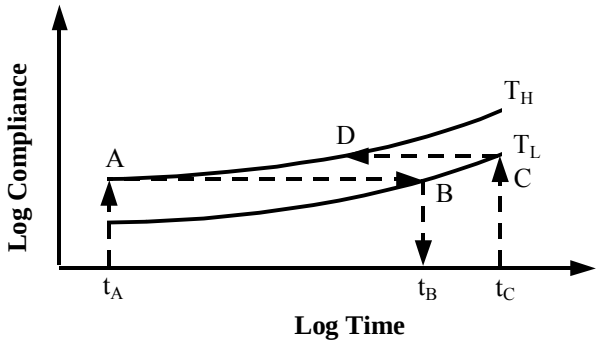

Figure 3.19a. Sufficient Overlap

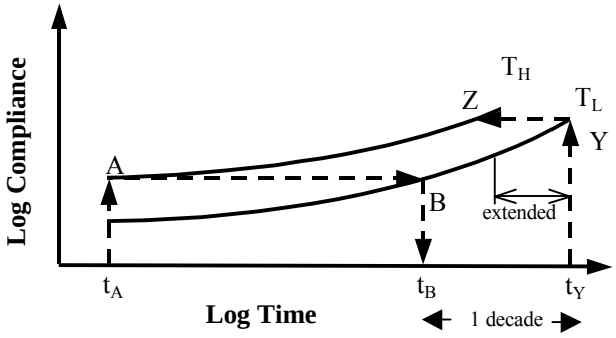

Figure 3.19b. Insufficient Overlap

Figure 3.19. Compliance Curves, “Case 1” Overlap

Insufficient overlap (Figure 3.19b)

4. Define 'Y’ as the point on the T_L curve at the time t_Y where:

   $$\log (t_Y) = \log (t_B) + 1$$

   The polynomial fit of the log compliance-log time plot is used to extend the T_L curve past the final loading time t_C to create the minimum overlap.

5. Define ‘Z’ as the point on the T_H curve having the same compliance as point Y.

If there is sufficient overlap, points A, B, C, and D define the overlap region. If there is insufficient overlap, points A, B, Y, and Z define the overlap region. While most compliance curves encountered in practice fall under case 1, on rare occasions other cases are encountered. In order for MASTER to be robust, it was necessary to develop routines to handle the other possible compliance curve arrangements, as described by cases 2 through 4.

Case 2

Case 2 is shown in Figure 3.20. In this case the T_L curve starts below the T_H curve but then crosses it. When the compliance curves cross in this manner, it was determined that there would be enough overlap to accurately perform the shifting without any extension of the data. The following steps were used to define the points of overlap:

1. Define 'A' as the point on the T_H curve at the initial loading time of 1 second.
2. Define 'B' as the point on the T_L curve having the same compliance as point A.
3. Define 'C' as the point on the T_H curve at the final loading time.
4. Define 'D' as the point on the T_L curve having the same compliance as point C.

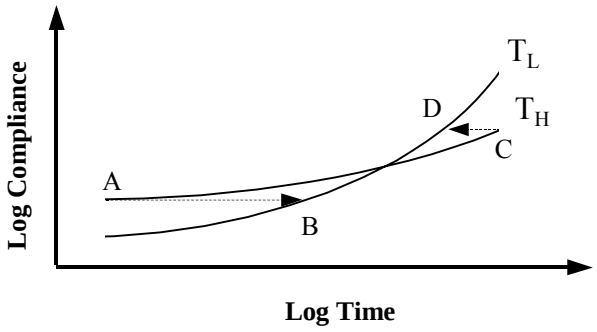

Figure 3.20. Compliance Curves, "Case 2" Overlap

Case 3

Case 3 is similar to case 2 with the exception that the T_H curve starts below the T_L curve. Again, since the curves cross, sufficient overlap exists without extension of either curve. The four points A, B, C, and D used to define the overlap are found by:

1. Define 'A' as the point on the T_L curve at the initial loading time of 1 second.
2. Define 'B' as the point on the T_H curve having the same compliance as point A.
3. Define 'C' as the point on the T_L curve at the final loading time.
4. Define 'D' as the point on the T_H curve having the same compliance as point C.

Case 4

Figures 3.21a and 3.21b show the last possibility of compliance curve orientation. This is a very rare case where the T_H curve is completely below the T_L curve. This case can occur at low temperatures when severe microdamage results in a damaged asphaltic matrix (Buttlar and Roque [*6*]), causing a net increase in mixture creep compliance (decrease in 'stiffness'). The following steps were used to define points on each compliance curve as shown in Figures 3.21a and 3.21b:

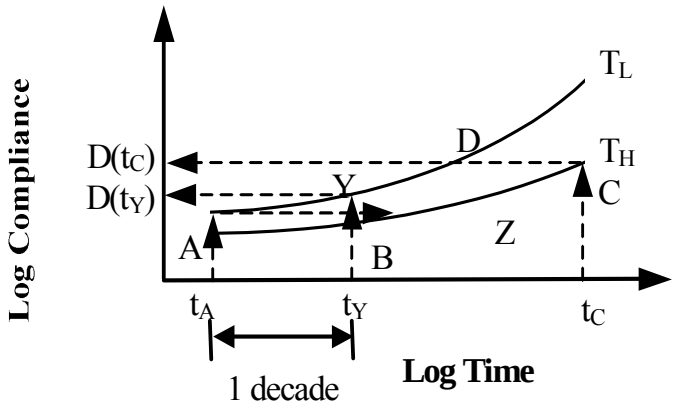

Figure 3.21a. Sufficient Overlap

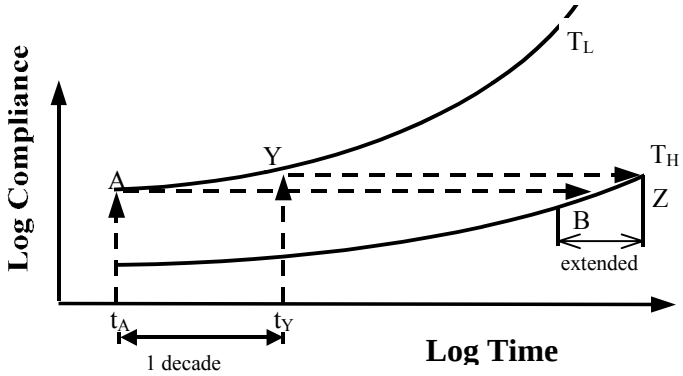

Figure 3.21b. Insufficient Overlap

Figure 3.21. Compliance Curves, "Case 4" Overlap

1. Define 'A' as the point on the T_L curve at the initial loading time of 1 second.
2. Define 'B' as the point on the T_H curve having the same compliance as point A.
3. Define time t_Y as 1 decade higher than the initial loading time t_A :

   $$\log (t_Y) = \log (t_A) + 1$$

4. Check for sufficient overlap based on 1 decade relative to the T_L curve. This is done by using the compliance at time t_Y on the T_L curve and the compliance at the final loading time t_C on the T_H curve and the equation:

$$D(t_C)_{TH} \geq D(t_Y)_{TL} \text{ (sufficient overlap)}$$

Sufficient overlap (Figure 3.21a)

5. Define 'C' as the point on the T_H curve at the final loading time t_C.
6. Define 'D' as the point on the T_L curve having the same compliance as point C.

Insufficient overlap (Figure 3.21b)

5. Define 'Y' as the point on the T_L curve at the time t_Y.
6. Define 'Z' as the point on the T_H curve having the same compliance as point Y. This extends the T_H curve past the final loading time t_C to create the minimum overlap.

If there is sufficient overlap, points A, B, C, and D define the overlap region. If there is insufficient overlap, points A, B, Y, and Z define the overlap region.

Least Squares Shifting

MASTER shifts compliance curves to obtain shift factors by minimizing the horizontal distance (error sum of squares, or SSE) on the log time axis between the overlapping portions of the two compliance curves previously defined. Figure 3.22 illustrates the procedure that would be used for a "case 1" overlap. MASTER searches to find the shift factor that minimizes the SSE of the points D1 through D5, as follows:

$$SSE = \sum_{i=1}^{5} \left[XE2(i) - \left(XE1(i) + log\left(\frac{1}{a_T} \right) \right) \right]^2 \quad \textbf{(3.38)}$$

where all quantities are as defined on Figure 3.22.

The minimum value of the SSE is stored and used later in the program to evaluate the quality of the master curves.

Checking for a "Double Kink" Master Curve

Sometimes adjacent compliance curves are nonparallel, and when shifted, can form a "kink" in the master curve. When the compliance curve at the middle temperature is nonparallel to the adjacent curves, a "double kink" is formed in the master curve as shown in Figure 3.23a. It was decided that if the compliance curves at the lower and upper temperature were fairly parallel, then more reliance should be placed on these two curves to determine the shift factors rather than the intermediate temperature curve. Therefore, a better method of constructing the

$$D1 = \log [D(t_C)_{T_L}] = \log [D(t_D)_{T_H}]$$

$$D5 = \log [D(t_A)_{T_L}] = \log [D(t_B)_{T_H}]$$

$$D2 = D1 + 0.25 (D5 - D1)$$

$$D3 = D1 + 0.50 (D5 - D1)$$

$$D4 = D1 + 0.75 (D5 - D1)$$

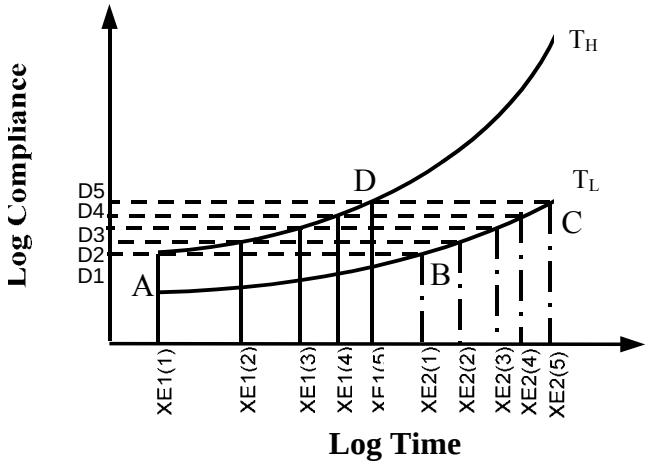

Figure 3.22. Error Sum of Squares Evaluation Locations

master curve would be to first shift the compliance curve at the upper temperature to line up with the compliance curve at the lower temperature to form one curve as shown in Figure 3.23b. The compliance curve at the middle temperature is then shifted to line up with newly formed curve. This method would produce a master curve that represented a stiffer asphalt mixture than that produced by shifting compliance curves at adjacent temperatures as shown in Figure 3.23a. A greater amount of thermal cracking will be predicted with a stiffer mixture and thus a more conservative evaluation of asphalt mixture performance will be obtained using the approach shown in Figure 3.23b.

MASTER incorporates this logic by checking for the double kink in the master curve, and then (if necessary) re-shifting the compliance curves to form an improved master curve. Upon visual inspection of master curves and comparisons of the error sum of squares (SSE) of their overlapping section, a method of identifying the "double kink" case was developed. It was determined that an SSE value of 0.1 constituted a significant "kink."

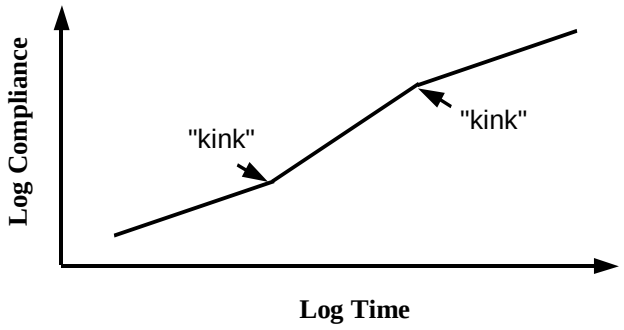

Figure 3.23a. The "Double Kink" Master Curve

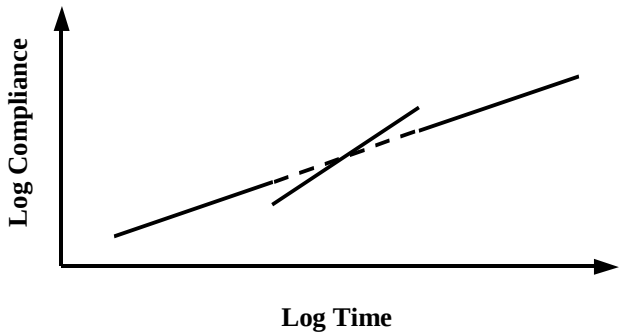

Figure 3.23b. Improved Shifting Method

Figure 3.23. The "Double Kink" Master Curve and Improved Shifting Method

The general steps that MASTER performs to handle the "double kink" master curve are outlined in Figure 3.24. MASTER first checks for a "double kink" by evaluating the SSE values:

$$SSE_1 \geq 0.1 \quad \text{and} \quad SSE_2 \geq 0.1 \quad \text{(double kink)}$$

where:

SSE_1 = Error sum of squares between the overlapping portions of the shifted compliance curves at the lowest and intermediate temperatures

SSE_2 = Error sum of squares between the overlapping portions of the shifted compliance curves at the intermediate and highest temperatures

If there is no "double kink" (either SSE < 0.1) then the temperature shift factors values previously obtained are kept. If a "double kink" is found then MASTER will shift the compliance curve at the highest temperature to line up with the compliance curve at the lowest temperature

and a corresponding shift factor and SSE value are obtained. Master compares SSE values to evaluate the alternative shifting method:

$$SSE_3 \leq SSE_1 \quad \text{and} \quad SSE_3 \leq SSE_2 \quad \text{(improved shifting)}$$

where:

SSE_3 = Error sum of squares between the overlapping portions of the shifted compliance curves at the lowest and highest temperatures

If shifting was not improved, then the shift factor values previously obtained are kept.

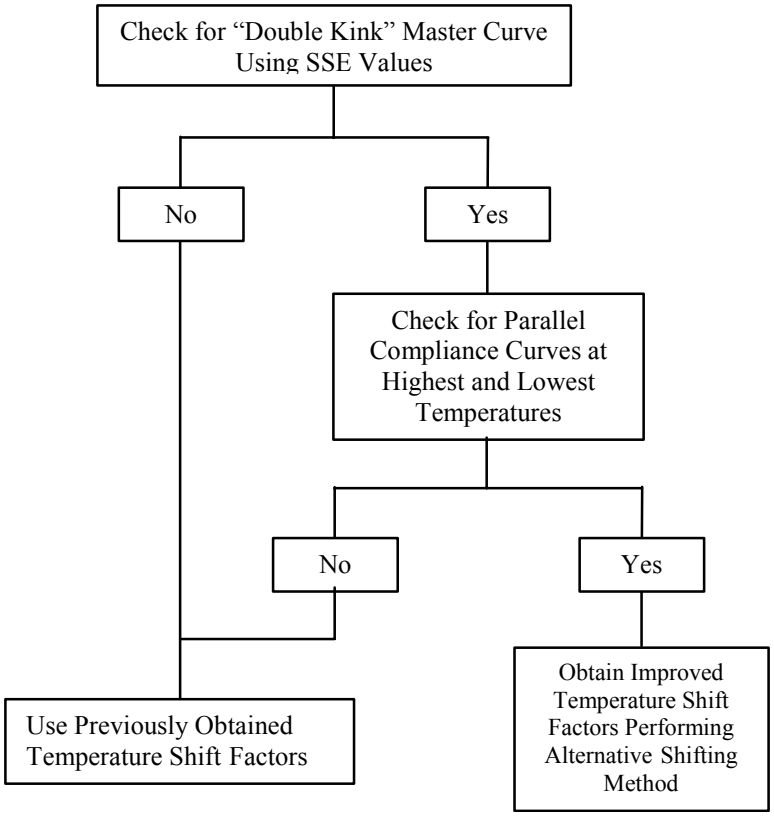

Figure 3.24. General Steps to Handle "Double Kink" Master Curve

3.4.4 Evaluation Of Master

Analyses were conducted to verify that the newly developed program produced rational shift factors for the broad range of materials considered in this study. Thus, shift factors were first obtained manually, by visually shifting creep compliance curves at different temperatures to a pre-selected reference temperature (-20 C), to form a single master curve. The program MASTER was then executed and the shift factors obtained from MASTER were compared to visual shifts. Since differences in shift factors are not related to performance in a simple manner,

additional comparisons were made by taking master curve information generated manually and by MASTER and using the information along with TCMODEL to predict thermal cracking performance. This permitted the differences in shift factors obtained with the two methods to be compared on the basis of predicted performance.

3.4.4.1 Subjectivity of Visually Shifting Compliance Curves

Analyses have been conducted to establish typical variability in shift factors for master curves constructed by different engineers (Roque et al. [*8*]). This measure of variability is useful in qualifying differences between visual and computer generated shift factors, given that the control case (visual shifts) has a degree of inherent subjectivity. In their study, two analysts were given identical compliance curve data, but arrived at shift factors (log $[1/a_T]$) that varied by about 20% on average. Two occurrences were cited as causing difficulties in performing visual shifts and therefore leading to subjective results: 1) having very little or no overlap between adjacent compliance curves, and; 2) having overlapping portions of adjacent compliance curves that are nonparallel or "kinked." Therefore, one cannot obtain "exact" temperature shift factors. Thus, it might be argued that the shift factors determined by an automated routine are superior to those determined by hand shifting because subjective error is eliminated through standardized routines. The comparisons presented in the following section are intended primarily to show that MASTER provides reasonable shift factors that are comparable to those obtained by hand shifting.

3.4.4.2 Comparison of Shift Factors: MASTER Versus Visual

Figure 3.25 shows that shift factors determined by MASTER compared favorably with shift factors determined by visually shifting the data. The "visual" shift factors were actually determined with the aid of a scientific spreadsheet. The spreadsheet was developed to graphically display the creep compliance curves, which the user could easily shift by typing in the desired shift factor in a designated cell. Using a trial-and-error process, reasonable shift factors could normally be determined in about five minutes.

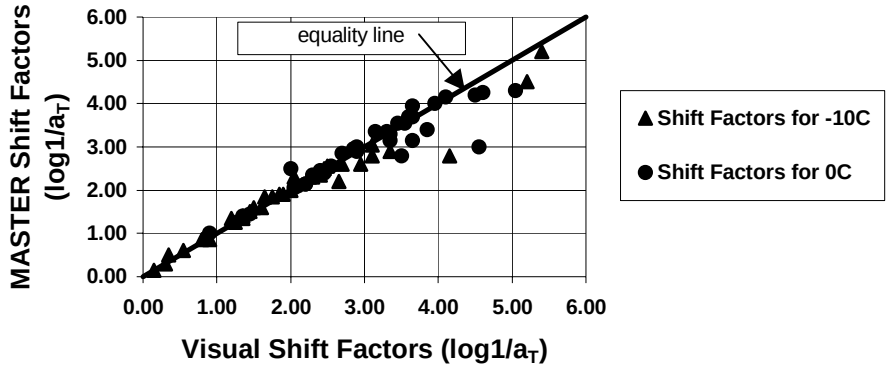

Figure 3.25. Equality Plot Comparing Shift Factors Produced by MASTER to Visually Based Shift Factors

3.4.4.3 Comparison of Thermal Cracking Performance: MASTER Versus Visual

TCMODEL computes thermal cracking performance in terms of amount of transverse cracking, in meters, per 500 meters of linear pavement length as a function of pavement age. In this evaluation, the number of years required to reach a specified terminal cracking level was chosen as the performance criterion. TCMODEL halts execution at a cracking level of 190 m of thermal cracking per 500 m of linear distance. For convenience, this cracking level was used as the terminal cracking level for the performance evaluations conducted in this study.

Experience has shown that care must be taken to arrive at meaningful comparisons that are based upon relative thermal cracking predictions. Consider the analysis at hand, where compliance data from a number of field sections has been measured and temperature files are available. A dilemma arises because if the actual weather files are used in performance predictions, it would only be possible to compare the visual and automated master curve generation procedures in cases where intermediate cracking levels were observed in the field. Cases where zero or very little cracking occurred over a long period of time or where severe cracking occurred very rapidly would not permit useful comparisons of relative thermal cracking performance to be made. On the other hand, one could arbitrarily choose weather files such that an intermediate cracking level was obtained, which would give good resolution in making relative thermal cracking comparisons. A detailed procedure to select appropriate temperature files has been reported by Buttlar and Roque (1997). The procedure involves sequentially running TCMODEL using environments of increasing severity until intermediate cracking levels are obtained. The only disadvantage to this method is that TCMODEL appears to be very sensitive to small differences in master curve parameters, including shift factors, when this procedure is used. Thus, predicted differences in performance should be viewed as fairly conservative.

Figure 3.26 shows that the predictions made using MASTER compared very favorably with those based on visually determined shift factors.

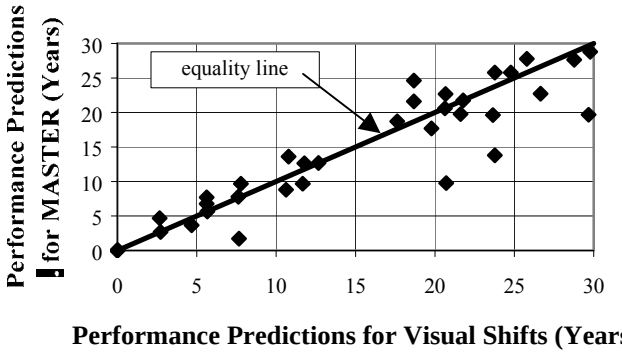

Figure 3.26. Equality Plot Comparing Performance Predictions: MASTER Versus Visually-Shifted Master Curves

Several of the predictions plotted significantly away from the unity line; however, the performance of the program MASTER appears to be very reasonable given: 1) the conservative nature of the analyses conducted, as described above, and; 2) that some of the deviation from the unity line is due to the subjectivity of determining shift factors visually. Thus, MASTER not only produces results that are comparable to those associated with visual shifting, but also saves time, avoids bias, and eliminates the need for training users to become proficient in constructing master curves.

Three of the asphalt mixtures that produced the largest difference in performance predictions between master curves constructed by MASTER and master curves constructed visually were examined closer to confirm that MASTER produced rational shift factors. Figure 3.27 clearly indicates that MASTER provided reasonable shifts for these mixtures.

3.4.5 Conclusions Regarding MASTER.exe

1) The program MASTER was found to closely agree with manual master curve constructions when evaluated against thirty-six field-aged mixtures. The program was also found to be extremely robust, producing rational shift factors even when posed with complicated, thermally-damaged materials.

2) It can be argued that MASTER is in fact a superior method of constructing master curves as compared to visually based constructions made by a trained engineer. MASTER uses standardized routines, which produce consistent shift factors for the creep compliance master curve.

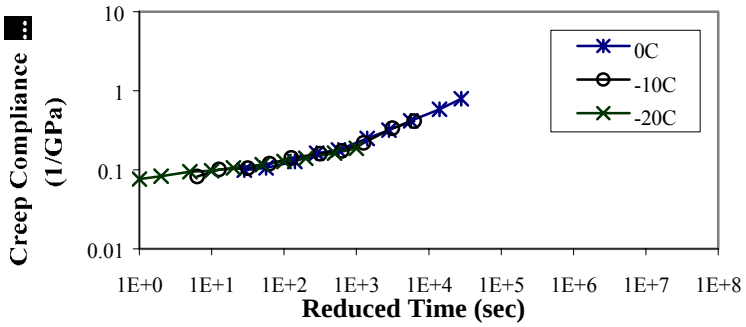

Figure 3.27a. Shifted Compliance Curves for CSHRP/PTI Section 35

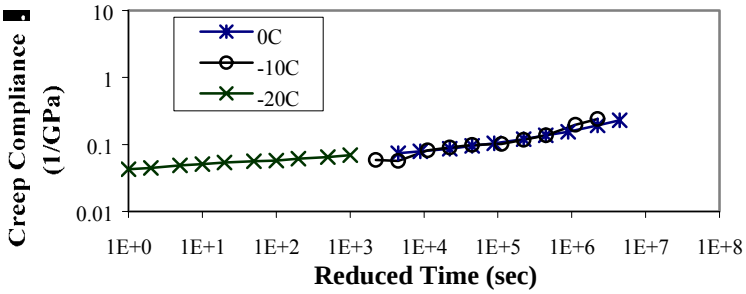

Figure 3.27b. Shifted Creep Compliance Curves for SHRP GPS/PTI Section 26

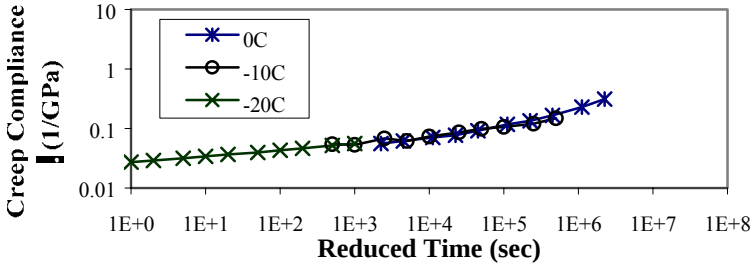

Figure 3.27c. Shifted Creep Compliance Curves for SHRP GPS/PTS Section 38

Figure 3.27. Master Curve Constructions Produced by MASTER

Chapter 4

Material Inputs for TCModel Recalibration

This chapter summarizes the steps involved in recalibrating TCMODEL to selected field sites, utilizing creep and strength data from the Superpave IDT and corresponding field performance data. As explained in the previous chapter, modifications to data analysis procedures for the IDT have necessitated a recalibration of TCMODEL. Furthermore, the number and breadth of field sections available for TCMODEL calibration since the original calibration in 1992 has nearly doubled. To be consistent with current Superpave IDT protocols (AASHTO TP9-94 [1996]), the 1000-second creep data form the original 22 GPS sections were truncated to create 100-second data files. It should be noted that there are still some areas for future research, which, once completed and incorporated, would serve to further strengthen the accuracy and breadth of TCMODEL. These items are discussed at the end of this chapter.

4.1 Model Recalibration Procedures

As explained in the previous chapter, the modifications to IDT data reduction procedures did not include changes to the analysis of strength data. However, the modifications did change the analysis of creep compliance data. Based upon these program updates, creep data from all GPS sections used in the original calibration of TCMODEL had to be re-analyzed, which involved the following steps:

- Original 1000-second creep data files were trimmed down to 100-second creep data files.
- The 100-second creep data was then analyzed using the updated IDT.exe program, using the default trimmed mean option (high and low values were eliminated). Manual face selection was employed when required.
- The master curve generation program (MASTER.exe) was then executed.

4.1.1 Summary of Field Sections used During Recalibration

Prior to reporting the results of these analysis steps, it is necessary to summarize the field sections used in this study. Included in this study are twenty-two GPS sections (SHRP general pavement sections), fourteen Canadian SHRP sections, and five Mn/ROAD sections, as summarized in Tables 4.1 through Table 4.3, respectively.

4.1.2 Data Trimming

With 100-second creep data files created, IDT.exe was utilized to process the data based upon the default settings of the program, which trims the high and low defection values of each section. The results of this analysis were carefully examined to assure that the program was selecting the most appropriate faces for trimming. This selection process was based upon a visual survey of each section's raw deflection plot.

Table 4.1. GPS Sections Utilized in the Recalibration of TCMODEL

SHRP ID	PTI[1] Code	Location	AC Thickness (in.)
404086	01-M	Chickasaw, OK	8.5
041022	02-M	Hackberry, AZ	--
322027	06-M	Oasis, NV	9.25
201005	07-M	Ottawa, KS	13.0
161010	11-M	Idaho Falls, ID	10.75
161001	12-M	Coeur D'Alene, ID	3.5
311030	13-M	Edison, NE	7.5
491008	16-M	Marysvale, UT	9.25
561007	17-M	Cody, WY	3.5
081047	18-M	Rangley, CO	4.0
211034	21-M	Glasgow, KY	14.25
404088	22-M	Ponca City, OK	12.5
241634	23-M	Berlin, MD	3.5
451008	26-M	Salem, SC	4.75
341011	27-M	Trenton, NJ	9.25
291010	28-M	Waynesville, MO	13.0
421597	31-M	Lawrenceville, PA	6.25
181028	32-M	Huntington, IN	15.0
231026	33-M	Farmington, ME	6.25
181037	36-M	Boonville, IN	14.0
271087	37-M	Farmington, MN	16.0
271028	38-M	Frazee, MN	9.5

[1]PTI = Pennsylvania Transportation Institute

Table 4.2. C-SHRP Sections Utilized in the Recalibration of TCMODEL

C-SHRP ID	PTI Code	Location	AC Thickness (in.)
Lamont 1	31-S	Lamont, Alberta	4.0
Lamont 2	32-S	Lamont, Alberta	4.0
Lamont 3	33-S	Lamont, Alberta	4.0
Lamont 4	34-S	Lamont, Alberta	4.0
Lamont 5	35-S	Lamont, Alberta	4.0
Lamont 6	36-S	Lamont, Alberta	4.0
Lamont 7	37-S	Lamont, Alberta	4.0
Sherbrooke A	38-S	Sherbrooke, Quebec	4.75
Sherbrooke B	39-S	Sherbrooke, Quebec	4.75
Sherbrooke C	40-S	Sherbrooke, Quebec	4.75
Sherbrooke D	41-S	Sherbrooke, Quebec	4.75
Hearst 1	42-S	Hearst, Ontario	2.0
Hearst 2	43-S	Hearst, Ontario	2.0
Hearst 3	44-S	Hearst, Ontario	2.0

Table 4.3. Mn/ROAD Sections Utilized in the Recalibration of TCMODEL

Section ID	Traffic Volume	Location	AC Thickness (in.)
Cell 16	High/ I-94	Ostego, Minnesota	7.75
Cell 17	High/ I-94	Ostego, Minnesota	7.75
Cell 26	Low/ Closed Loop	Ostego, Minnesota	6.0
Cell 27	Low/ Closed Loop	Ostego, Minnesota	3.0
Cell 30	Low/ Closed Loop	Ostego, Minnesota	5.0

Table 4.4 summarizes the manual data trimming employed on the 41 sections considered in the recalibration project. The table also specifies at which temperature the trimming of the data was preformed and for which face (face X – horizontal face, face Y – vertical face). Of the 246 sets of data examined (41 sections x 3 temperatures x 2 [X and Y measurements]), manual data trimming was required in 38 instances, or about 15% of the time. However, recent experience with the IDT has suggested that a much lower incidence of manual data trimming is required for IDT analyses on laboratory-compacted mixtures. This is a reflection of the recent advances in IDT surface-mounted sensor technology, coupled with the consistency of laboratory-compacted specimens relative to field cores, which are used in the calibration process per necessity.

Once data trimming was finalized, MASTER was then executed to acquire creep compliance and Poisson's ratio data for all sections. These results are summarized in Appendix A. As mentioned previously, it was not necessary to reanalyze strength data for this project. Tensile strength results are summarized in Appendix B.

The creep compliance and tensile strength data was then utilized by the MASTER program to acquire master creep compliance curves, as displayed in Appendix C. Furthermore, the shift factor and power law parameters acquired from the execution of MASTER are summarized in Appendix D.

Table 4.4. Summary of Data Trimming Procedures

Section ID	Face Selection					
	-20 C		-10 C		0 C	
	Face X	Face Y	Face X	Face Y	Face X	Face Y
404086				M		
041022					M	M
322027					M	
201005			M	M		
161010						
161001		M				
311030					M	
491008		M	M			
561007						
081047						M
211034						M
404088				M	M	
241634						
451008						
341011						
291010			M		M	
421597						
181028						
231026						
181037						
271087						
271028						
Lamont 1						M
Lamont 2			M		M	
Lamont 3						
Lamont 4					M	
Lamont 5			M			
Lamont 6			M	M	M	M
Lamont 7		M				
Sherbrooke A					M	
Sherbrooke B		M				
Sherbrooke C						
Sherbrooke D	M	M			M	M
Hearst 1						
Hearst 2						M
Hearst 3		M				
Cell 16		M				
Cell 17	M					
Cell 26					M	
Cell 27						
Cell 30		M				

The data contained in all four appendices are summarized in Table 4.5, below.

Table 4.5. Summary of Data Included in Appendices

Appendix A	• Creep compliance at 1, 2, 5, 10, 20, 50, and 100 second loading time and 0, -10, and -20 C • Poisson's ratio at 0, -10, and -20 C
Appendix B	• Tensile strength at 0, -10, and -20 C, 3 replicates
Appendix C	• Creep compliance master curves
Appendix D	• Shift factors at 0 and -10 C • Voight-Kelvin model (up to 10 parameters), representing master creep compliance curve • Power model parameters (D_0, D_1, and m-value)

4.2 Recalibration Results: Initial Trial

Nonlinear regression analyses were performed to determine twelve different values of β_1 and σ (one for each fracture parameter *k*) for the following model:

$$AC = \beta_1 * N\left(\frac{\log C/D}{\sigma}\right) \qquad (5.24)$$

where:

AC	=	observed amount of thermal cracking
β_1	=	regression coefficient determined through field calibration
$N()$	=	standard normal distribution evaluated at ()
σ	=	standard deviation of the log of the depth of cracks in the pavement
C	=	crack depth
D	=	thickness of surface layer

In essence, twelve models were obtained, each with its own *k*, β_1, σ, and R^2. The model with the highest R^2 had the following parameters:

- k = 8000
- β_1 = 332.7
- σ = 0.148
- R^2 = 0.476

Another way to evaluate the goodness of fit of the model is to directly compare the predicted to the observed amount of cracking by categorizing the predicted and observed levels of cracking as follows:

- Zero cracking: 0 to 25 ft of cracking per 500-ft section (< 1 crack per 250 ft)
- Low cracking: 25 to 75 ft of cracking per 500-ft section (from 1 crack per 250 ft to 1 crack per 85 ft)
- Medium cracking: 75 to 150 ft of cracking per 500-ft section (from 1 crack per 85 ft to 1 crack per 40 ft)
- High cracking: greater than 150 ft of cracking per 500-ft section (> 1 crack per 40 ft)

The results of this comparison using predicted cracking determined with the model parameters presented above is presented in Figure 4.1. The results may be summarized as follows:

- Eleven of thirteen high cracking sections were predicted to be high cracking sections.
- Five of six intermediate cracking sections were predicted to be intermediate cracking to high cracking sections.
- Two of the two low cracking sections were predicted to be zero or low cracking.
- Of the twenty zero cracking sections, thirteen were predicted to be zero cracking, two were predicted to be low cracking, one was predicted to be medium cracking, and four were predicted to be high cracking sections.

		OBSERVED CRACKING			
		ZERO	LOW	MED	HIGH
PREDICTED CRACKING	ZERO	13	2	1	4
	LOW	1	1		
	MED	1		1	4
	HIGH	2			11

Figure 4.1. Observed versus Predicted Cracking (Initial Calibration)

When viewed in this manner, the correlation between predicted and measured cracking appeared fairly strong. As shown in Figure 4.1, only eight predictions were off the diagonal by two or more cells. Of the other 33 predictions, 26 were on the diagonal (meaning excellent prediction), and 7 were just one cell off the diagonal (implying a fairly good prediction). So the correspondence between predicted and observed cracking was excellent or good for 33 of the 41 test sections. However, the off diagonal predictions clearly had a very strong influence on R^2, which was relatively low (0.476).

Therefore, data and inputs for the test sections corresponding to the off-diagonal predictions in Figure 4.1 were carefully reviewed for quality and accuracy to determine whether problems in the data may have caused some error in prediction. PTI sections 21, 22, 31, 34S, 36, and 44S were reviewed:

- Sections 21, 22, 34S, and 36 were found to have suspicious 100-second master curves. The original 1000-second master curves developed from measurements during the SHRP and C-SHRP projects produced thermal cracking model predictions consistent with observed performance. For this recalibration effort, 100-second compliance curves were interpolated from the original 1000-second data. These 100-second data were then analyzed with the new data interpretation software to produce mixture master curves. The performance predictions made with these new master curves are inconsistent with both observed performance and with the predictions made using the original master curves.

- Section 31 was found to have a master creep compliance curve drastically different than the compliance master curves of any of the other mixtures tested. The variation in shift factors with temperature for this mixture was far greater than for the other mixtures. The implication is that even small errors in estimating pavement temperatures during the life of the pavement could lead to very serious errors in predicted cracking for these mixtures. This section was eliminated from the original calibration of the model during SHRP.

- Section 44S appears to be an anomaly. Several performance predictors, including St. Anne, predicted fracture temperatures, and both the original and recalibrated Superpave thermal cracking models, suggest that the section should experience significant thermal cracking. Yet, no cracking was reportedly observed after three winters.

4.3 Results of Second Calibration

Because of the problems with the data from the six test sections cited above, these test sections were not included in a second calibration of the model. Once again, nonlinear regressions were performed to determine twelve different values of β_1 and σ (one for each fracture parameter k). It was determined that the model with the highest R^2 had the following parameters:

- k = 10,000
- β_1 = 353.5
- σ = 0.769
- R^2 = 0.88

These parameters were used to generate the comparison between predicted and observed thermal cracking presented in Figure 4.2 and Tables 4.6 through 4.8. As shown in the tables and figure, the correspondence between predicted and observed cracking was excellent or good for the remaining 35 test sections.

		OBSERVED CRACKING			
		ZERO	LOW	MED	HIGH
PREDICTED CRACKING	ZERO	16			
	LOW	2			
	MED			2	4
	HIGH				11

Figure 4.2. Observed versus Predicted Cracking (Final Calibration)

Table 4.6. Thermal Cracking Performance Data for C-SHRP Sections

C-SHRP ID	PTI Code	Location	Observed Cracking (ft/500 ft)	Predicted Cracking (ft/500 ft)
Lamont 1	31-S	Lamont, Alberta	109.7	177
Lamont 2	32-S	Lamont, Alberta	≥200	177
Lamont 3	33-S	Lamont, Alberta	0	0
Lamont 4	34-S	Lamont, Alberta	≥200	NA
Lamont 5	35-S	Lamont, Alberta	23.8	0
Lamont 6	36-S	Lamont, Alberta	0	1
Lamont 7	37-S	Lamont, Alberta	0	0
Sherbrooke A	38-S	Sherbrooke, Quebec	0	0
Sherbrooke B	39-S	Sherbrooke, Quebec	0	4
Sherbrooke C	40-S	Sherbrooke, Quebec	0	0
Sherbrooke D	41-S	Sherbrooke, Quebec	0	0
Hearst 1	42-S	Hearst, Ontario	0	0
Hearst 2	43-S	Hearst, Ontario	0	0
Hearst 3	44-S	Hearst, Ontario	0	NA

Table 4.7. Thermal Cracking Performance Data for GPS Sections

SHRP ID	PTI Code	Location	Observed Cracking (ft/500 ft)	Predicted Cracking (ft/500 ft)
404086	01-M	Chickasaw, OK	96	75
041022	02-M	Hackberry, AZ	0	11
322027	06-M	Oasis, NV	≥200	177
201005	07-M	Ottawa, KS	≥200	177
161010	11-M	Idaho Falls, ID	≥200	176
161001	12-M	Coeur D'Alene, ID	0	13
311030	13-M	Edison, NE	36	8
491008	16-M	Marysvale, UT	≥200	174
561007	17-M	Cody, WY	≥200	177
081047	18-M	Rangley, CO	≥200	177
211034	21-M	Glasgow, KY	0	NA
404088	22-M	Ponca City, OK	96	NA
241634	23-M	Berlin, MD	0	0
451008	26-M	Salem, SC	96	177
341011	27-M	Trenton, NJ	36	0
291010	28-M	Waynesville, MO	120	177
421597	31-M	Lawrenceville, PA	24	NA
181028	32-M	Huntington, IN	12	5
231026	33-M	Farmington, ME	12	0
181037	36-M	Boonville, IN	≥200	NA
271087	37-M	Farmington, MN	132	177
271028	38-M	Frazee, MN	≥200	177

Table 4.8. Thermal Cracking Performance Data for Mn/ROAD Sections

Section ID	Location	Observed Cracking (ft/500 ft)	Predicted Cracking (ft/500 ft)
Cell 16	Ostego, MN	≥200	177
Cell 17	Ostego, MN	≥200	177
Cell 26	Ostego, MN	0	14
Cell 27	Ostego, MN	≥200	177
Cell 30	Ostego, MN	108	130

4.4 Summary of TCMODEL Recalibration

Results of the recalibration effort clearly indicate that mixture properties measured from the Superpave IDT are strongly correlated to thermal cracking performance in the field. Therefore, the Superpave thermal cracking prediction system, including the Superpave IDT and the performance-based thermal cracking model (TCMODEL) appears to adequately represent and account for the most significant factors that influence thermal cracking of pavements in the field. The thermal cracking model parameters, determined in the final calibration, are recommended for thermal cracking performance prediction. Extreme care should be exercised when evaluating thermal cracking performance of mixtures exhibiting extreme variations in shift factors with temperatures, because even small errors in estimating air or pavement temperatures may result in significant errors in predicted thermal cracking. A conservative approach with these materials would be to use temperature data that are slightly colder than those of the site being investigated.

4.5 Future Research Areas

Although this report summarizes improvements to TCMODEL that should result in more accurate, more reliable thermal cracking predictions, there are still portions of TCMODEL that could be improved in the future that were not addressed in this work. One area worthy of study is the effect of mixture aging in the field on thermal cracking development. TCMODEL does not directly account for mixture aging with time; however, the model assumes that the very top of the pavement (the top 2.54 mm or 0.1") has numerous "starter crack" locations. The assumption that starter cracks are present allows the use of a single crack propagation law (Paris law for stable crack growth), which eliminates the need for a crack initiation model. The presence of starter cracks partially eliminates the importance of having a mixture aging model included as part of the thermal cracking model, since the pavement aging gradient is most severe at the very surface of the pavement. In addition, the fact that TCMODEL is calibrated to field performance also indirectly accounts for the effects of mixture aging in the field. In the future, TCMODEL can be improved once a better understanding of the effects of mixture aging on fracture behavior is obtained.

A second area where TCMODEL can be improved in the future which is also related to fracture, is in the utilization of tensile strength data. Currently, TCMODEL utilizes mixture tensile strength at a single test temperature of -10 C, and then develops fracture parameters by taking this value as an estimate of the undamaged tensile strength of the mixture, as described in chapter 2, along with a slope parameter from the master compliance curve (m-value). In the future, TCMODEL can be improved once a better understanding of mixture fracture behavior is obtained, and when improved fracture models are available. A third area where TCMODEL can be improved in the future is in the response model. Currently a pseudo two-dimensional pavement response model is used, which accounts only for temperature-induced stresses and strains. Recent work has indicated that traffic loads applied during critical cooling events can increase tensile stresses by more than fifty percent (Waldhoff, Buttlar and Kim [2000]). Although TCMODEL is calibrated to field performance and therefore indirectly accounts for average traffic effects, as three-dimensional finite element modeling becomes more computationally efficient, an improved response model should be incorporated into TCMODEL.

Chapter 5

Conclusions and Recommendations

This report described the work conducted to finalize development of the Thermal Cracking Model (TCMODEL) that was originally developed under the SHRP A-005 research contract. The main purpose of this study was to facilitate the incorporation of an updated version of TCMODEL and related software into the complete Superpave software program, which is being assembled as part of the University of Maryland/Arizona State Superpave Support and Performance Models Management Project (NCHRP 9-19).

The updates made to TCMODEL and related software in this project included: 1) incorporation of improved analysis techniques for converting raw data from the Superpave Indirect Tensile Test (IDT) into fundamental properties; 2) recalibration of TCMODEL to reflect updated analysis procedures and to incorporate new field data, and; 3) enhanced documentation for TCMODEL. In addition to the original field specimens and thermal cracking observations from twenty-two SHRP General Pavement Sections (GPS) used in the original calibration of TCMODEL during SHRP, fourteen Canadian SHRP (CSHRP) and five Mn/ROAD sections were also used in the re-calibration of TCMODEL. Although the recalibration included several analysis modifications and nearly twice as many field sections, the newly calibrated model parameters are similar to parameters developed during SHRP research.

Results of the calibration effort clearly indicate that mixture properties measured from the Superpave IDT are strongly correlated to thermal cracking performance in the field. Therefore, the Superpave thermal cracking prediction system, including the Superpave IDT and the performance-based thermal cracking model (TCMODEL) appears to adequately represent and account for the most significant factors that influence thermal cracking of pavements in the field.

The thermal cracking model parameters, determined in the final calibration, are recommended for thermal cracking performance prediction. Extreme care should be exercised when evaluating thermal cracking performance of mixtures exhibiting extreme variations in shift factors with temperatures, because even small errors in estimating air or pavement temperatures may result in significant errors in predicted thermal cracking. A conservative approach with these materials would be to use temperature data that are slightly colder than the temperatures for the site being investigated.

TCMODEL appears to adequately represent and account for the most significant factors that influence thermal cracking of pavements in the field. The mechanics basis of the model allows the pavement engineer to directly account for:

- The measured time- and temperature-dependent behavior of the mixture.
- Pavement thickness.

- Detailed environmental conditions (e.g., pavement temperatures) throughout the life of the pavement.

Additional research is recommended in the following areas:

- A procedure for using TCMODEL predictions in the design asphaltic paving mixtures at various levels of design reliability.

- Improved crack propagation models

- Incorporation of a mixture aging model into TCMODEL prediction

- Incorporation of a three-dimensional finite element response model into TCMODEL, which will allow traffic effects on thermal cracking development to be more directly accounted for.

REFERENCES

AASHTO TP-9, American Association of State Highway and Transportation Officials, Provisional Standards, Washington, D.C., Third Edition, pp. 292-303, June 1996.

Bahia, H., *Low Temperature Isothermal Physical Hardening of Asphalt Cements*. Ph.D. Thesis, The Pennsylvania State University, University Park, PA, 1991.

Bonnaure, F., Gest, G., Gravois, A., and P. Uge, "A New Method of Predicting the Stiffness of Asphalt Paving Mixtures," *Journal of the Association of Asphalt Paving Technologists*, Vol. 46, pp. 64-100, 1977.

Buttlar, W. G., *Relationships Between Asphalt Binder and Mixture Stiffnesses at Low Temperatures for the Control of Thermal Cracking Performance Prediction*. Ph.D. Dissertation, The Pennsylvania State University, University Park, PA, 1996.

Buttlar, W.G. and R. Roque, "Development and Evaluation of the Strategic Highway Research Program Measurement and Analysis System for Indirect Tensile Testing at Low Temperatures," *Transportation Research Record No. 1454*, Transportation Research Board, Washington, D.C., pp. 163-171, 1994.

Buttlar, W.G., and R. Roque, "Evaluation of Empirical and Theoretical Models to Determine Asphalt Mixture Stiffnesses at Low Temperatures," *Journal of the Association of Asphalt Paving Technologists*, Vol. 65, 1996.

Buttlar, W.G., Roque, R., and N. Kim "Accurate Asphalt Mixture Tensile Strength," *Accepted for Presentation at the American Society of Civil Engineers Fourth Materials Conference*, Washington D.C., November 1996.

Buttlar, W.G., and R. Roque, "Effect of Asphalt Mixture Master Compliance Modeling Technique on Thermal Cracking Pavement Performance," *Proceedings of the 8th International Conference on Asphalt Pavements*, International Society for Asphalt Pavements, Seattle, Washington, Vol. 2, pp. 1659-1669, 1997.

Buttlar, W. G., Roque, R., and B. Reid, "An Automated Procedure for Generation of the Creep Compliance Master Curve for Asphalt Mixtures," Transportation Research Record, No. 1630, National Research Council, National Academy Press, Washington, D. C., pp. 28-36, 1998.

Chang, H. S., Lytton, R. L., and S.H. Carpenter, "Prediction of Thermal Reflection Cracking in West Texas," *Research Report No. TTI-2-8-73-18-3*, Texas Transportation Institute, Texas A&M University, College Station, Texas, March 1996.

Christensen, D.W., *Mechanical Modeling of the Linear Viscoelastic Behavior of Asphalt Cements,* Ph.D. Dissertation, The Pennsylvania State University, University Park, PA, 1992.

Deme, I. J. and F.D. Young, "Ste. Anne Test Road Revisited Twenty Years Later," *Proceedings of the Canadian Technical Asphalt Association*, Vol. XXXI, 1987.

Finn, F., Saraf, C. L., Kulkarni, R., Nair, K., Smith, W., and A. Abdullah, "Development of Pavement Structural Subsystems," *NCHRP Report 291*, Transportation Research Board, Washington, D. C., December, 59 pp, 1986.

Heinicke, J.J. and T.S. Vinson, "Effect of Test Condition Parameters on IRM," *Journal of Transportation Engineering*, ASCE, Vol. 114, No. 2, pp. 153-172, 1988.

Heukelom, W. and A. J. G. Klomp, "Road Design and Dynamic Loading," *Journal of the Association of Asphalt Paving Technologists*, Ann Arbor, Michigan, Vol. 33, pp. 92-123, 1964.

Hussain, S. R., *Evaluation of Low Temperature and Pavement Deformation Characteristics of Some Polymer Modified Asphalts.* Master of Science Thesis, Department of Civil Engineering, University of Alberta, Spring, 1990.

Jones, G. M., Darter, M. I., and G. Littlefield, "Thermal Expansion-Contraction of Asphaltic Concrete," *Proceedings of the Association of Asphalt Paving Technologists*, Vol. 37, pp. 56-97, 1968.

Kim, K. W. and H. M. El Hussein, "Effect of Differential Thermal Contraction on Fracture Toughness of Asphalt Materials at Low Temperatures," *Journal of the Association of Asphalt Paving Technologists*, Vol. 64, pp. 474-499, 1995.

Lytton, R. L., Pufahl, D. E., Michalak, C. H., Liang, H. S., and B. J. Dempsey, "An Integrated Model of the Climatic Effects on Pavements," *Report No. FHWA-RD-90-033*, Federal Highway Administration, Washington, D. C., November 1989.

Lytton, R.L., Roque, R., Uzan, J., Hiltunen, D.R., Fernando, E., and S.M. Stoffels, "Performance Models and Validation of Test Results," *Strategic Highway Research Program Report A-357*, Project A-005, Washington, D.C., 1993.

Lytton, R. L., Shanmugham, U., and B. D. Garrett, "Design of Asphalt Pavements for Thermal Fatigue Cracking, *Research Report No. FHWA/TX-83/06+284-4*, Texas Transportation Institute, Texas A&M University, College Station, Texas, January 1983.

Molenaar, A.A.A., "Fatigue and Reflection Cracking Due to Traffic Loads," *Proceedings of the Association of Asphalt Paving Technologists*, Vol. 53, pp. 440-474, 1984.

Neter, J., Wasserman, W., and M. H. Kutner, *Applied Linear Statistical Models: Regression, Analysis of Variance, and Experimental Designs*, Third Edition, Richard D. Irwin, Inc., Homewood, Illinois, 1990.

Roque, R. and W.G. Buttlar, "Development of a Measurement and Analysis System to Accurately Determine Asphalt Concrete Properties Using the Indirect Tensile Test," *Journal of the Association of Asphalt Paving Technologists*, Vol. 61, pp. 304-332, 1992.

Roque, R. and B. E. Ruth, "Mechanisms and Modeling of Surface Cracking in Asphalt Pavements," *Journal of the Association of Asphalt Paving Technologists*, Vol. 59, pp. 396-421, 1990.

Roque, R., Buttlar, W. G., Ruth, B. E., Tia, M., Dickison, S. W., and B. Reid, "Evaluation of the SHRP Indirect Tension Tester to Mitigate Cracking in Asphalt Concrete Pavements and Overlays," Draft Final Report to Florida Department of Transportation, University of Florida Engineering and Industrial Experiment Station, Gainesville, FL, 1997.

Roque, R., Hiltunen, D. R., Romero, P., and W. G. Buttlar, "Canadian SHRP Investigation to Evaluate Asphalt Mixture and Binder Criteria to Predict and Control Thermal Cracking," Draft Report to CSHRP, June 1994.

Roque, R., Hiltunen, D. R., and S. M. Stoffels, "Field Validation of SHRP Asphalt Binder and Mixture Specification Tests to Control Thermal Cracking Through Performance Modeling," *Journal of the Association of Asphalt Paving Technologists*, Vol. 62, 1993.

Schapery, R. A., "A Theory of Crack Growth in Viscoelastic Media," *ONR Contract No. N00014-68-A-0308-003, Technical Report No. 2, MM 2764-73-1*, Mechanics and Materials Research Center, Texas A&M University, College Station, Texas, March 1973.

Soules, T. F., Busbey, R. F., Rekhson, S. M., Markovsky, A., and M. A. Burke, "Finite-Element Calculation of Stresses in Glass Parts Undergoing Viscous Relaxation," *Journal of the American Ceramic Society*, Vol. 70, No. 2, pp. 90-95, 1987.

Von Quintus, H.L., Hughes, C. S., and J.A. Sherocman, "NCHRP Asphalt-Aggregate Mixture Analysis System Procedure," *Transportation Research Record No. 1353*, Transportation Research Board, Washington, D.C., pp. 90-99, 1992.

Waldhoff, A.S., Buttlar, W.G., and J. Kim "Evaluation of Thermal Cracking at Mn/ROAD Using the Superpave IDT, *Proceeding of the Canadian Technical Asphalt Association*, 45th Annual Conference, Winnipeg, Manitoba, Polyscience Publications, Inc., Laval, Quebec, Canada, pp. 228-259, 2000.

Appendix A

Superpave IDT Results:
Creep Compliance and Poisson's Ratio

Table A.1.a. Creep Compliance and Poisson's Ratio Data Results: SHRP General Pavement Study Mixtures

Parameter	Temperature (°C)	Time	404086	041022	322027	201005
Creep Compliance (1/GPa)	-20	1	0.018	0.023	0.037	0.038
		2	0.019	0.023	0.039	0.040
		5	0.019	0.024	0.040	0.042
		10	0.021	0.025	0.042	0.045
		20	0.021	0.026	0.043	0.048
		50	0.022	0.027	0.045	0.051
		100	0.024	0.029	0.047	0.054
	-10	1	0.026	0.028	0.073	0.050
		2	0.029	0.030	0.077	0.053
		5	0.032	0.033	0.082	0.057
		10	0.035	0.035	0.087	0.058
		20	0.038	0.038	0.092	0.066
		50	0.041	0.043	0.101	0.069
		100	0.044	0.048	0.107	0.073
	0	1	0.035	0.048	0.056	0.070
		2	0.039	0.053	0.063	0.074
		5	0.046	0.065	0.074	0.082
		10	0.052	0.080	0.086	0.089
		20	0.063	0.099	0.09	0.099
		50	0.073	0.136	0.111	0.117
		100	0.087	0.195	0.127	0.131
Poisson's Ratio	-20		0.33	0.42	0.37	0.38
	-10		0.50	0.50	0.23	0.35
	0		0.50	0.50	0.50	0.32

Table A.1.b Creep Compliance and Poisson's Ratio Data Results: SHRP General Pavement Study Mixtures

Parameter	Temperature (°C)	Time	161010	161001	311030	491008
Creep Compliance (1/GPa)	-20	1	0.030	0.027	0.037	0.031
		2	0.032	0.028	0.040	0.032
		5	0.035	0.030	0.045	0.033
		10	0.037	0.032	0.051	0.034
		20	0.039	0.033	0.056	0.035
		50	0.041	0.036	0.064	0.038
		100	0.045	0.039	0.073	0.037
	-10	1	0.035	0.040	0.087	0.051
		2	0.039	0.044	0.100	0.054
		5	0.043	0.051	0.123	0.057
		10	0.047	0.056	0.146	0.062
		20	0.051	0.063	0.170	0.064
		50	0.057	0.068	0.217	0.072
		100	0.059	0.078	0.266	0.074
	0	1	0.062	0.060	0.084	0.045
		2	0.068	0.070	0.103	0.050
		5	0.080	0.086	0.137	0.058
		10	0.091	0.102	0.176	0.064
		20	0.108	0.121	0.203	0.073
		50	0.137	0.157	0.267	0.085
		100	0.163	0.192	0.311	0.094
Poisson's Ratio	-20		0.42	0.42	0.47	0.50
	-10		0.50	0.50	0.46	0.36
	0		0.41	0.50	0.25	0.42

Table A.1.c. Creep Compliance and Poisson's Ratio Data Results: SHRP General Pavement Study Mixtures

Parameter	Temperature (°C)	Time	561007	081047	211034	404088
Creep Compliance (1/GPa)	-20	1	0.041	0.034	0.028	0.034
		2	0.043	0.035	0.028	0.036
		5	0.046	0.037	0.030	0.039
		10	0.048	0.039	0.031	0.040
		20	0.051	0.040	0.032	0.044
		50	0.056	0.042	0.035	0.047
		100	0.061	0.044	0.036	0.050
	-10	1	0.061	0.046	0.037	0.046
		2	0.064	0.049	0.040	0.050
		5	0.071	0.054	0.044	0.055
		10	0.076	0.058	0.049	0.061
		20	0.085	0.063	0.054	0.063
		50	0.100	0.071	0.061	0.071
		100	0.111	0.078	0.069	0.081
	0	1	0.064	0.062	0.062	0.047
		2	0.073	0.067	0.071	0.056
		5	0.091	0.075	0.089	0.070
		10	0.106	0.084	0.106	0.079
		20	0.132	0.093	0.139	0.101
		50	0.164	0.109	0.194	0.107
		100	0.221	0.125	0.248	0.125
Poisson's Ratio	-20		0.37	0.50	0.50	0.47
	-10		0.31	0.50	0.50	0.50
	0		0.50	0.50	0.50	0.50

Table A.1.d. Creep Compliance and Poisson's Ratio Data Results: SHRP General Pavement Study Mixtures

Parameter	Temperature (°C)	Time	241634	451008	341011	291010
Creep Compliance (1/GPa)	-20	1	0.031	0.042	0.026	0.029
		2	0.033	0.045	0.028	0.029
		5	0.037	0.048	0.030	0.030
		10	0.040	0.051	0.032	0.031
		20	0.043	0.053	0.034	0.032
		50	0.049	0.056	0.037	0.033
		100	0.055	0.057	0.038	0.034
	-10	1	0.048	0.073	0.038	0.047
		2	0.054	0.083	0.042	0.050
		5	0.062	0.099	0.048	0.055
		10	0.070	0.111	0.055	0.060
		20	0.079	0.122	0.062	0.066
		50	0.097	0.126	0.076	0.074
		100	0.112	0.145	0.087	0.084
	0	1	0.074	0.063	0.077	0.079
		2	0.093	0.069	0.097	0.086
		5	0.123	0.078	0.133	0.100
		10	0.161	0.088	0.168	0.116
		20	0.179	0.096	0.216	0.129
		50	0.225	0.117	0.313	0.164
		100	0.293	0.132	0.416	0.197
Poisson's Ratio	-20		0.50	0.29	0.43	0.50
	-10		0.50	0.26	0.40	0.39
	0		0.50	0.29	0.24	0.26

Table A.1.e. Creep Compliance and Poisson's Ratio Data Results: SHRP General Pavement Study Mixtures

Parameter	Temperature (°C)	Time	421597	181028	231026	181037
Creep Compliance (1/GPa)	-20	1	0.035	0.044	0.036	0.023
		2	0.036	0.046	0.039	0.024
		5	0.039	0.048	0.045	0.026
		10	0.040	0.049	0.050	0.026
		20	0.041	0.052	0.055	0.028
		50	0.043	0.056	0.063	0.028
		100	0.045	0.058	0.072	0.029
	-10	1	0.054	0.064	0.057	0.025
		2	0.057	0.072	0.067	0.026
		5	0.062	0.084	0.084	0.029
		10	0.068	0.097	0.103	0.032
		20	0.068	0.107	0.128	0.032
		50	0.075	0.129	0.175	0.038
		100	0.083	0.151	0.231	0.040
	0	1	0.050	0.062	0.067	0.027
		2	0.059	0.078	0.091	0.031
		5	0.073	0.108	0.134	0.037
		10	0.089	0.138	0.184	0.041
		20	0.100	0.188	0.245	0.051
		50	0.121	0.278	0.356	0.061
		100	0.141	0.369	0.485	0.070
Poisson's Ratio	-20		0.22	0.24	0.28	0.45
	-10		0.25	0.22	0.38	0.50
	0		0.37	0.36	0.50	0.32

Table A.1.f. Creep Compliance and Poisson's Ratio Data Results: SHRP General Pavement Study Mixtures

Parameter	Temperature (°C)	Time	271087	271028
Creep Compliance (1/GPa)	-20	1	0.030	0.027
		2	0.032	0.029
		5	0.035	0.032
		10	0.038	0.034
		20	0.040	0.037
		50	0.042	0.040
		100	0.045	0.043
	-10	1	0.050	0.058
		2	0.053	0.053
		5	0.059	0.060
		10	0.063	0.063
		20	0.074	0.076
		50	0.088	0.086
		100	0.096	0.099
	0	1	0.060	0.059
		2	0.064	0.063
		5	0.075	0.071
		10	0.084	0.076
		20	0.108	0.087
		50	0.136	0.106
		100	0.174	0.117
Poisson's Ratio	-20		0.50	0.50
	-10		0.42	0.38
	0		0.50	0.50

Table A.2.a. Creep Compliance and Poisson's Ratio Results: Canadian SHRP Mixtures

Parameter	Temperature (°C)	Time	Lamont 1	Lamont 2	Lamont 3	Lamont 4
Creep Compliance (1/GPa)	-20	1	0.057	0.047	0.044	0.057
		2	0.060	0.050	0.051	0.061
		5	0.064	0.054	0.062	0.067
		10	0.067	0.057	0.074	0.074
		20	0.073	0.064	0.085	0.077
		50	0.081	0.069	0.105	0.088
		100	0.086	0.075	0.127	0.100
	-10	1	0.090	0.085	0.098	0.053
		2	0.096	0.095	0.112	0.060
		5	0.108	0.113	0.139	0.070
		10	0.114	0.134	0.168	0.084
		20	0.142	0.150	0.213	0.090
		50	0.162	0.182	0.301	0.126
		100	0.190	0.255	0.406	0.134
	0	1	0.081	0.074	0.151	0.056
		2	0.093	0.094	0.207	0.072
		5	0.112	0.132	0.328	0.101
		10	0.131	0.176	0.468	0.125
		20	0.158	0.216	0.690	0.180
		50	0.194	0.294	1.151	0.226
		100	0.225	0.389	1.700	0.307
Poisson's Ratio	-20		0.38	0.50	0.10	0.50
	-10		0.30	0.50	0.50	0.50
	0		0.50	0.49	0.41	0.50

Table A.2.b. Creep Compliance and Poisson's Ratio Results: Canadian SHRP Mixtures

Parameter	Temperature (°C)	Time	Lamont 5	Lamont 6	Lamont 7	Sherbrooke A
Creep Compliance (1/GPa)	-20	1	0.082	0.067	0.058	0.054
		2	0.087	0.073	0.062	0.057
		5	0.096	0.083	0.070	0.062
		10	0.104	0.092	0.079	0.068
		20	0.116	0.106	0.087	0.074
		50	0.126	0.126	0.105	0.088
		100	0.147	0.145	0.124	0.100
	-10	1	0.096	0.119	0.087	0.067
		2	0.110	0.135	0.102	0.074
		5	0.131	0.162	0.132	0.085
		10	0.146	0.198	0.173	0.099
		20	0.172	0.224	0.207	0.109
		50	0.214	0.303	0.323	0.140
		100	0.222	0.365	0.406	0.166
	0	1	0.124	0.109	0.102	0.158
		2	0.147	0.131	0.144	0.193
		5	0.186	0.173	0.228	0.260
		10	0.228	0.222	0.324	0.326
		20	0.265	0.281	0.477	0.413
		50	0.358	0.459	0.732	0.602
		100	0.443	0.570	1.134	0.764
Poisson's Ratio	-20		0.46	0.50	0.50	0.50
	-10		0.29	0.50	0.26	0.50
	0		0.46	0.50	0.50	0.33

Table A.2.c. Creep Compliance and Poisson's Ratio Results: Canadian SHRP Mixtures

Parameter	Temperature (°C)	Time	Sherbrooke B	Sherbrooke C	Sherbrooke D	Hearst 1
Creep Compliance (1/GPa)	-20	1	0.026	0.040	0.031	0.074
		2	0.027	0.043	0.034	0.079
		5	0.030	0.047	0.039	0.088
		10	0.032	0.054	0.043	0.100
		20	0.035	0.053	0.047	0.114
		50	0.039	0.062	0.054	0.139
		100	0.041	0.070	0.057	0.171
	-10	1	0.039	0.040	0.046	0.064
		2	0.042	0.045	0.052	0.075
		5	0.049	0.054	0.063	0.094
		10	0.055	0.059	0.077	0.114
		20	0.064	0.075	0.089	0.139
		50	0.077	0.092	0.113	0.189
		100	0.090	0.106	0.147	0.238
	0	1	0.055	0.084	0.087	0.089
		2	0.064	0.104	0.105	0.122
		5	0.081	0.137	0.144	0.189
		10	0.099	0.176	0.193	0.268
		20	0.125	0.206	0.257	0.372
		50	0.167	0.279	0.403	0.528
		100	0.217	0.326	0.590	0.739
Poisson's Ratio	-20		0.50	0.50	0.50	0.23
	-10		0.50	0.47	0.50	0.50
	0		0.40	0.50	0.50	0.50

Table A.2.d. Creep Compliance and Poisson's Ratio Results: Canadian SHRP Mixtures

Parameter	Temperature (°C)	Time	Hearst 2	Hearst 3
Creep Compliance (1/GPa)	-20	1	0.061	0.052
		2	0.067	0.054
		5	0.077	0.057
		10	0.087	0.063
		20	0.098	0.065
		50	0.121	0.075
		100	0.141	0.084
	-10	1	0.081	0.087
		2	0.093	0.097
		5	0.113	0.115
		10	0.138	0.135
		20	0.161	0.155
		50	0.211	0.203
		100	0.267	0.250
	0	1	0.131	0.117
		2	0.167	0.146
		5	0.232	0.199
		10	0.317	0.260
		20	0.373	0.302
		50	0.560	0.440
		100	0.745	0.582
Poisson's Ratio	-20		0.50	0.50
	-10		0.50	0.46
	0		0.50	0.50

Table A.3. Creep Compliance and Poisson's Ratio Results: Mn/ROAD Mixtures

Parameter	Temperature (°C)	Time	Cell 16	Cell 17	Cell 26	Cell 27	Cell 30
Creep Compliance (1/GPa)	-20	1	0.049	0.035	0.059	0.078	0.020
		2	0.053	0.039	0.066	0.081	0.034
		5	0.057	0.044	0.077	0.084	0.048
		10	0.062	0.050	0.088	0.087	0.056
		20	0.067	0.054	0.101	0.092	0.065
		50	0.075	0.060	0.119	0.098	0.081
		100	0.083	0.065	0.136	0.108	0.090
		200	0.089	0.079	0.158	0.116	0.099
		500	0.094	0.087	0.183	0.125	0.110
		1000	0.095	0.098	0.210	0.122	0.110
	-10	1	0.112	0.056	0.110	0.094	0.077
		2	0.125	0.077	0.123	0.107	0.091
		5	0.138	0.091	0.144	0.126	0.105
		10	0.152	0.105	0.165	0.141	0.118
		20	0.170	0.120	0.191	0.164	0.135
		50	0.207	0.159	0.233	0.206	0.171
		100	0.240	0.199	0.267	0.251	0.208
		200	0.295	0.227	0.347	0.295	0.244
		500	0.370	0.287	0.473	0.392	0.318
		1000	0.444	0.354	0.603	0.502	0.399
	0	1	0.109	0.086	0.112	0.127	0.101
		2	0.133	0.103	0.142	0.173	0.119
		5	0.168	0.133	0.220	0.218	0.163
		10	0.206	0.166	0.310	0.266	0.205
		20	0.249	0.208	0.414	0.325	0.257
		50	0.330	0.288	0.619	0.438	0.345
		100	0.438	0.367	0.859	0.643	0.421
		200	0.645	0.482	1.260	0.818	0.585
		500	0.940	0.743	1.879	1.192	0.954
		1000	1.317	1.072	2.694	1.663	1.362
Poisson's Ratio	-20		0.20	0.20	0.25	0.20	0.21
	-10		0.18	0.28	0.23	0.17	0.25
	0		0.25	0.35	0.14	0.22	0.23

Appendix B

Superpave IDT Results:
Tensile Strength

Table B.1.a. Tensile Strength Results: SHRP General Pavement Study Mixtures

	Temperature (°C)	Replicate	404086	041022	322027	201005
Tensile Strength (MPa)	-20	1	4.00	3.35	1.92	3.48
		2	4.69	4.07	2.46	2.66
		3	4.76	3.56	2.82	3.30
		Average	**4.48**	**3.66**	**2.40**	**3.15**
	-10	1	3.53	4.06	2.73	2.97
		2	3.35	3.70	2.41	2.98
		3	4.46	3.23	1.79	2.88
		Average	**3.78**	**3.66**	**2.31**	**2.95**
	0	1	2.92	4.01	1.53	2.15
		2	4.08	3.38	2.63	2.58
		3	3.79	3.65	1.90	2.58
		Average	**3.60**	**3.68**	**2.02**	**2.44**

Table B.1.b. Tensile Strength Results: SHRP General Pavement Study Mixtures

	Temperature (°C)	Replicate	161010	161001	311030	491008
Tensile Strength (MPa)	-20	1	2.85	5.09	3.82	3.61
		2	3.77	3.75	3.83	2.62
		3	3.57	4.32	4.17	2.81
		Average	**3.40**	**4.39**	**3.94**	**3.01**
	-10	1	3.49	4.08	2.92	2.87
		2	3.72	4.54	3.28	2.20
		3	3.64	4.14	3.09	2.80
		Average	**3.62**	**4.25**	**3.10**	**2.62**
	0	1	3.36	2.82	1.84	2.90
		2	2.92	3.10	1.86	2.22
		3	3.15	2.88	2.04	3.29
		Average	**3.14**	**2.93**	**1.92**	**2.81**

Table B.1.c. Tensile Strength Results: SHRP General Pavement Study Mixtures

	Temperature (°C)	Replicate	561007	081047	211034	404088
Tensile Strength (MPa)	-20	1	3.78	3.04	3.59	1.84
		2	3.10	2.70	3.94	2.88
		3	3.20	3.14	3.42	4.45
		Average	**3.36**	**2.96**	**3.65**	**3.06**
	-10	1	3.36	2.56	2.85	3.32
		2	3.55	2.49	3.84	2.19
		3	2.37	2.87	3.37	2.46
		Average	**3.09**	**2.64**	**3.35**	**2.66**
	0	1	2.58	2.22	2.11	2.49
		2	2.46	2.46	2.50	2.28
		3	2.33	2.22	2.29	2.42
		Average	**2.46**	**2.30**	**2.30**	**2.40**

Table B.1.d. Tensile Strength Results: SHRP General Pavement Study Mixtures

	Temperature (°C)	Replicate	241634	451008	341011	291010
Tensile Strength (MPa)	-20	1	3.92	3.09	4.56	2.19
		2	3.54	2.94	4.51	1.65
		3	3.86	2.78	4.42	2.07
		Average	**3.77**	**2.94**	**4.49**	**1.97**
	-10	1	2.82	1.70	3.51	2.07
		2	2.51	1.26	3.25	2.00
		3	3.27	1.94	4.27	1.65
		Average	**2.87**	**1.63**	**3.68**	**1.91**
	0	1	2.20	1.83	2.91	1.18
		2	2.02	2.14	3.36	1.95
		3	2.09	2.39	3.11	2.71
		Average	**2.10**	**2.12**	**3.13**	**1.95**

Table B.1.e. Tensile Strength Results: SHRP General Pavement Study Mixtures

	Temperature (°C)	Replicate	421597	181028	231026	181037
Tensile Strength (MPa)	-20	1	2.66	2.07	4.55	2.54
		2	3.60	2.23	4.15	2.38
		3	2.81	2.16	4.11	2.10
		Average	**3.02**	**2.15**	**4.27**	**2.34**
	-10	1	2.56	2.01	3.23	2.44
		2	3.29	2.04	3.83	3.01
		3	2.55	2.08	3.24	3.00
		Average	**2.80**	**2.05**	**3.43**	**2.82**
	0	1	2.00	1.18	2.88	2.58
		2	2.68	1.40	1.74	2.67
		3	2.69	2.13	1.71	2.17
		Average	**2.46**	**1.57**	**2.11**	**2.47**

Table B.1.f. Tensile Strength Results: SHRP General Pavement Study Mixtures

	Temperature (°C)	Replicate	271087	271028
Tensile Strength (MPa)	-20	1	3.85	2.42
		2	2.98	2.70
		3	3.92	2.41
		Average	**3.58**	**2.51**
	-10	1	3.78	2.40
		2	2.72	2.37
		3	2.60	2.57
		Average	**3.04**	**2.45**
	0	1	3.26	2.35
		2	3.13	1.98
		3	3.46	2.06
		Average	**3.28**	**2.13**

Table B.2.a. Tensile Strength Results: Canadian SHRP Mixtures

	Temperature (°C)	Replicate	Lamont 1	Lamont 2	Lamont 3	Lamont 4
Tensile Strength (MPa)	-20	1	3.33	3.08	4.17	2.51
		2	3.89	3.03	3.96	2.67
		3	2.51	2.93	3.88	3.06
		Average	**3.25**	**3.01**	**4.00**	**2.75**
	-10	1	2.97	2.07	3.40	3.41
		2	1.78	3.15	3.31	3.26
		3	0.00	3.25	3.56	2.93
		Average	**2.38**	**2.83**	**3.42**	**3.20**
	0	1	1.58	2.37	1.60	2.42
		2	1.19	2.79	1.84	2.36
		3	2.61	2.66	1.45	2.55
		Average	**1.79**	**2.61**	**1.63**	**2.45**

Table B.2.b. Tensile Strength Results: Canadian SHRP Mixtures

	Temperature (°C)	Replicate	Lamont 5	Lamont 6	Lamont 7	Sherbrooke A
Tensile Strength (MPa)	-20	1	3.21	3.51	3.54	4.25
		2	3.77	3.21	3.80	3.51
		3	2.89	2.33	3.32	3.28
		Average	**3.29**	**3.02**	**3.55**	**3.68**
	-10	1	2.74	3.50	3.19	3.27
		2	2.75	2.85	3.11	3.14
		3	2.34	3.47	3.58	2.87
		Average	**2.61**	**3.28**	**3.29**	***3.09***
	0	1	1.73	2.33	1.51	1.88
		2	1.58	2.09	1.79	2.11
		3	2.15	1.72	1.96	2.01
		Average	**1.82**	**2.05**	**1.75**	**2.00**

Table B.2.c. Tensile Strength Results: Canadian SHRP Mixtures

	Temperature (°C)	Replicate	Sherbrooke B	Sherbrooke C	Sherbrooke D	Hearst 1
Tensile Strength (MPa)	-20	1	4.00	3.23	5.21	3.12
		2	3.46	3.67	5.11	3.29
		3	3.44	4.09	4.53	3.00
		Average	**3.64**	**3.66**	**4.95**	**3.14**
	-10	1	3.74	3.39	4.20	2.11
		2	2.58	3.57	3.97	2.48
		3	2.89	3.93	3.58	2.98
		Average	**3.07**	**3.63**	**3.92**	**2.52**
	0	1	3.42	2.52	2.90	1.57
		2	2.81	2.72	2.96	1.34
		3	2.77	2.69	3.12	1.13
		Average	**3.00**	**2.64**	**2.99**	**1.35**

Table B.2.d. Tensile Strength Results: Canadian SHRP Mixtures

	Temperature (°C)	Replicate	Hearst 2	Hearst 3
Tensile Strength (MPa)	-20	1	3.06	2.74
		2	3.21	2.49
		3	3.18	1.89
		Average	**3.15**	**2.38**
	-10	1	2.52	2.29
		2	2.54	1.92
		3	2.83	2.17
		Average	**2.63**	**2.13**
	0	1	1.63	1.73
		2	1.25	1.65
		3	1.47	1.67
		Average	**1.45**	**1.68**

Table B.3. Tensile Strength Results: Mn/ROAD Mixtures

	Temperature (°C)	Replicate	Cell 16	Cell 17	Cell 26	Cell 27	Cell 30
Tensile Strength (MPa)	-10	1	2.19	3.01	2.52	2.96	2.93
		2	2.34	2.09	1.97	2.97	2.48
		3	2.16	2.21	2.30	2.78	2.78
		Average	**2.23**	**2.44**	**2.26**	**2.90**	**2.73**

Appendix C

Creep Compliance Master Curve

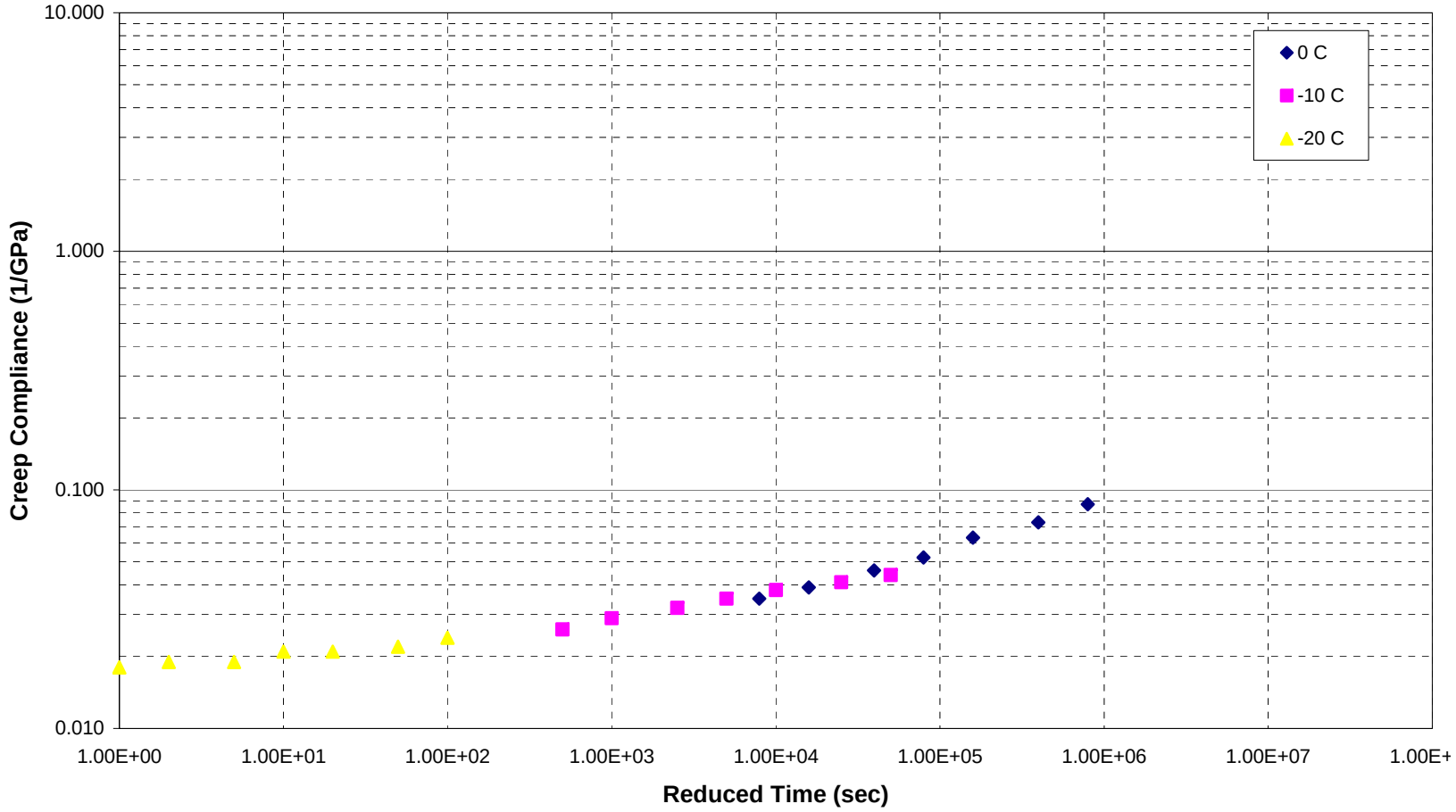

Figure C - 1. Creep Compliance Master Curve - SHRP 404086

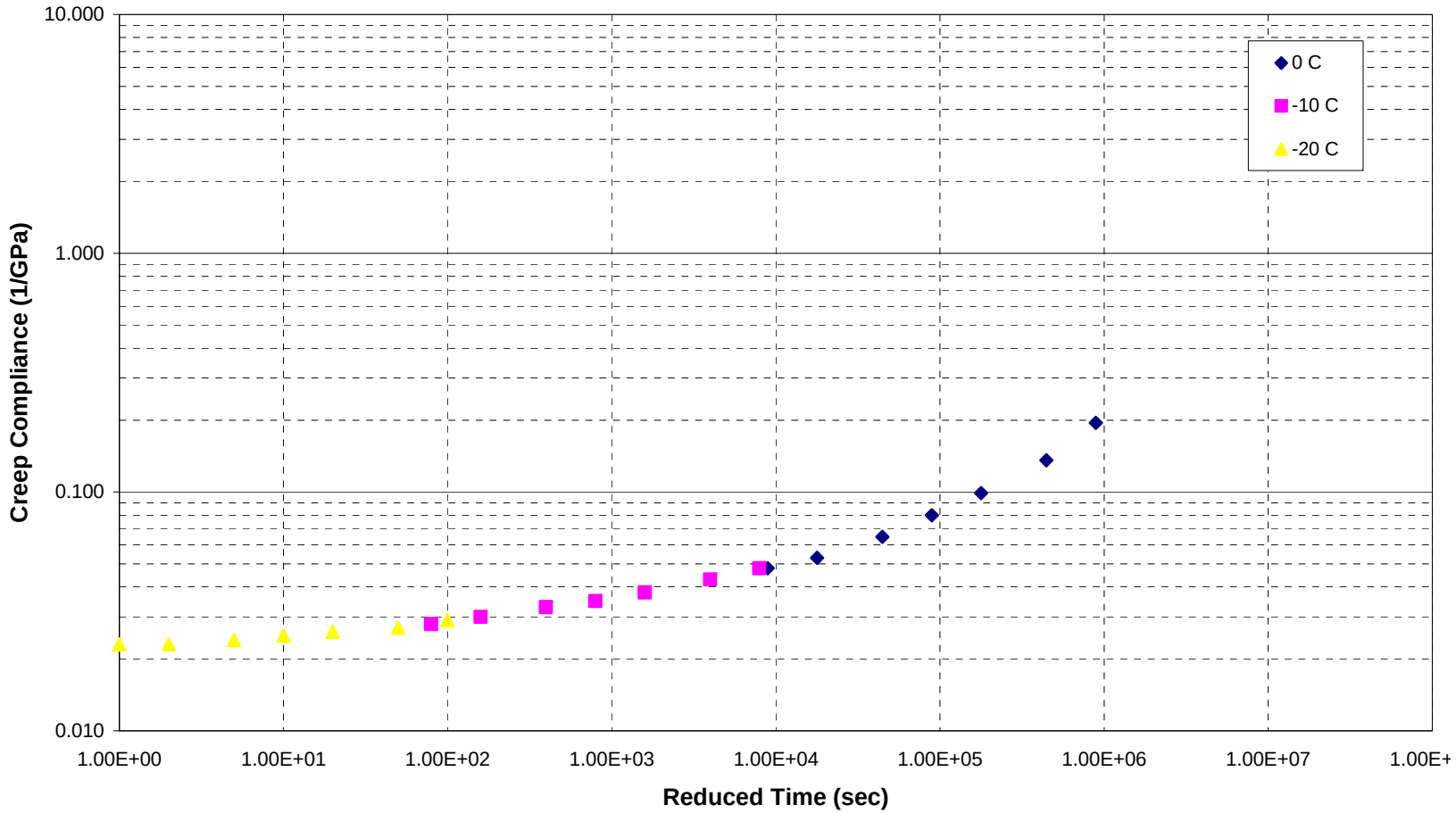

Figure C - 2. Creep Compliance Master Curve - SHRP 041022

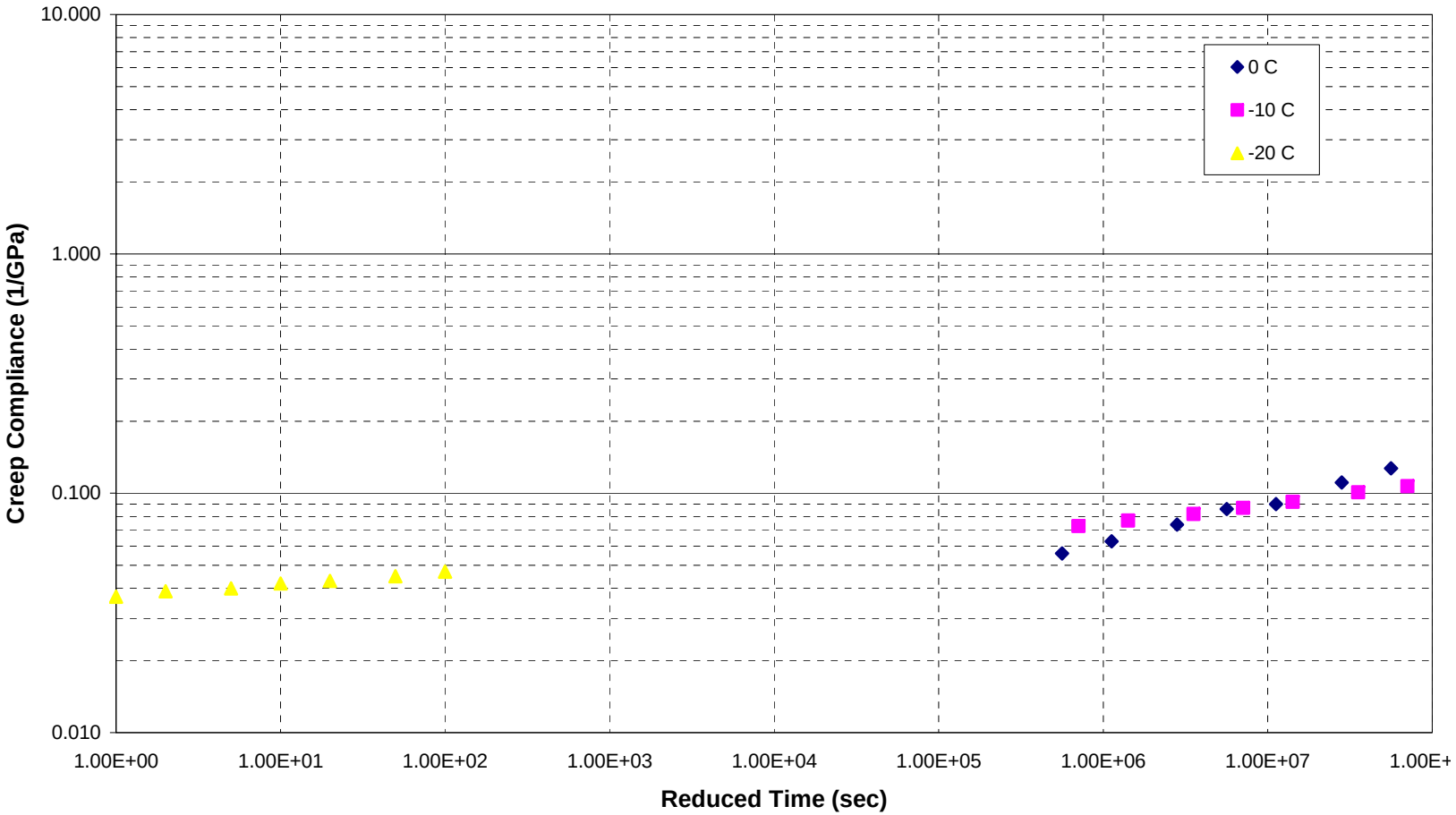

Figure C - 3. Creep Compliance Master Curve - SHRP 322027

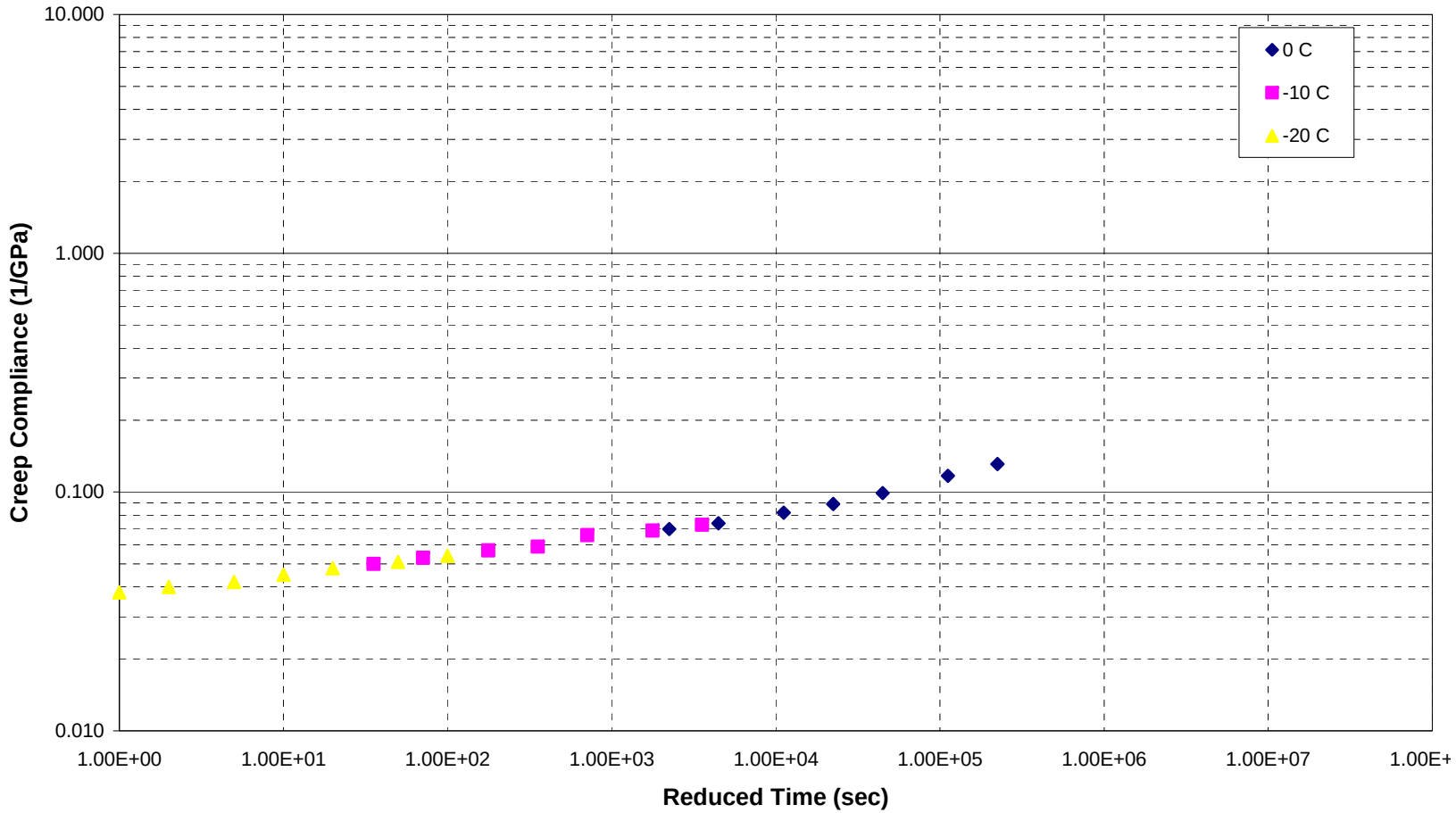

Figure C - 4. Creep Compliance Master Curve - SHRP 201005

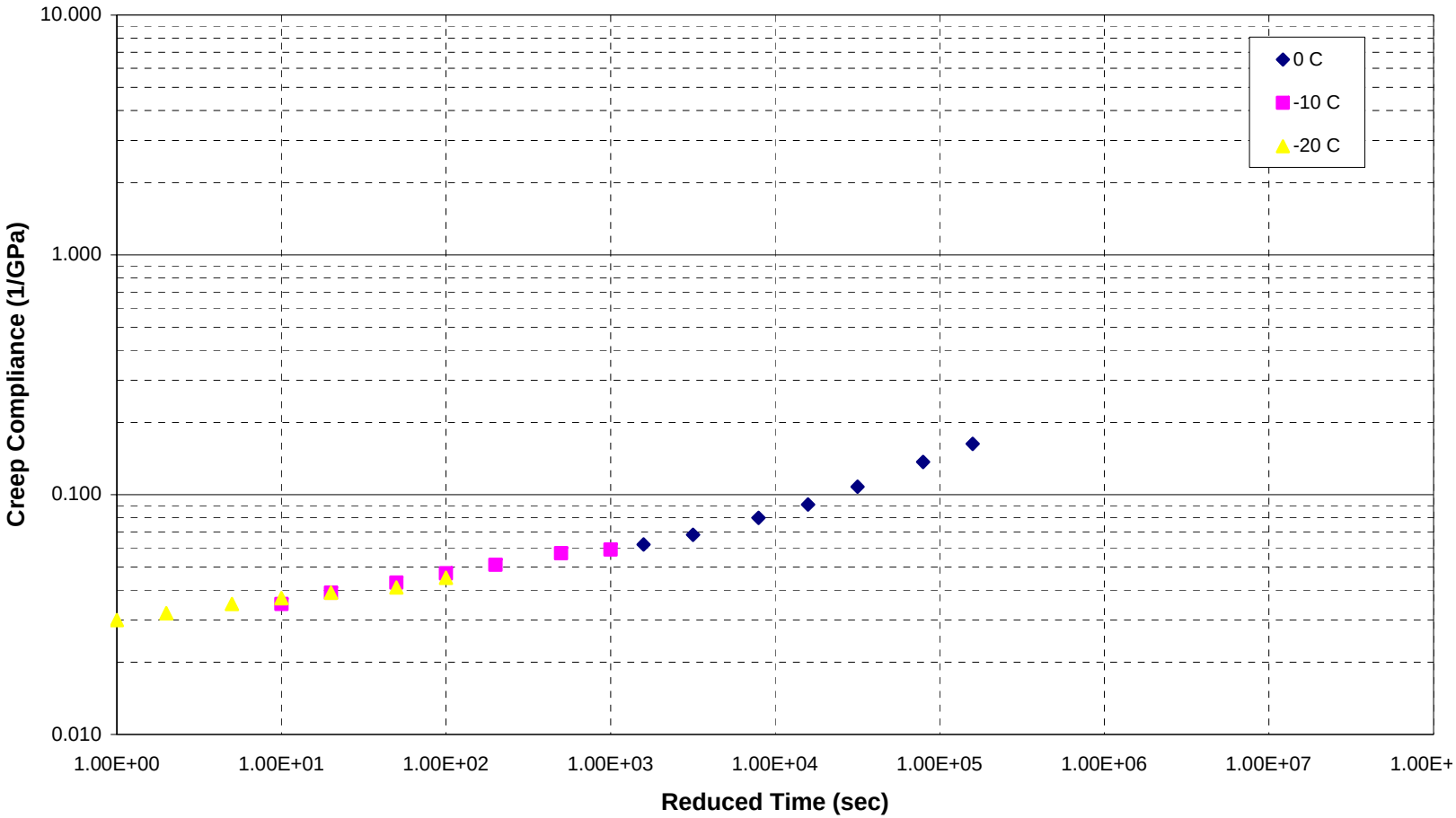

Figure C - 5. Creep Compliance Master Curve - SHRP 161010

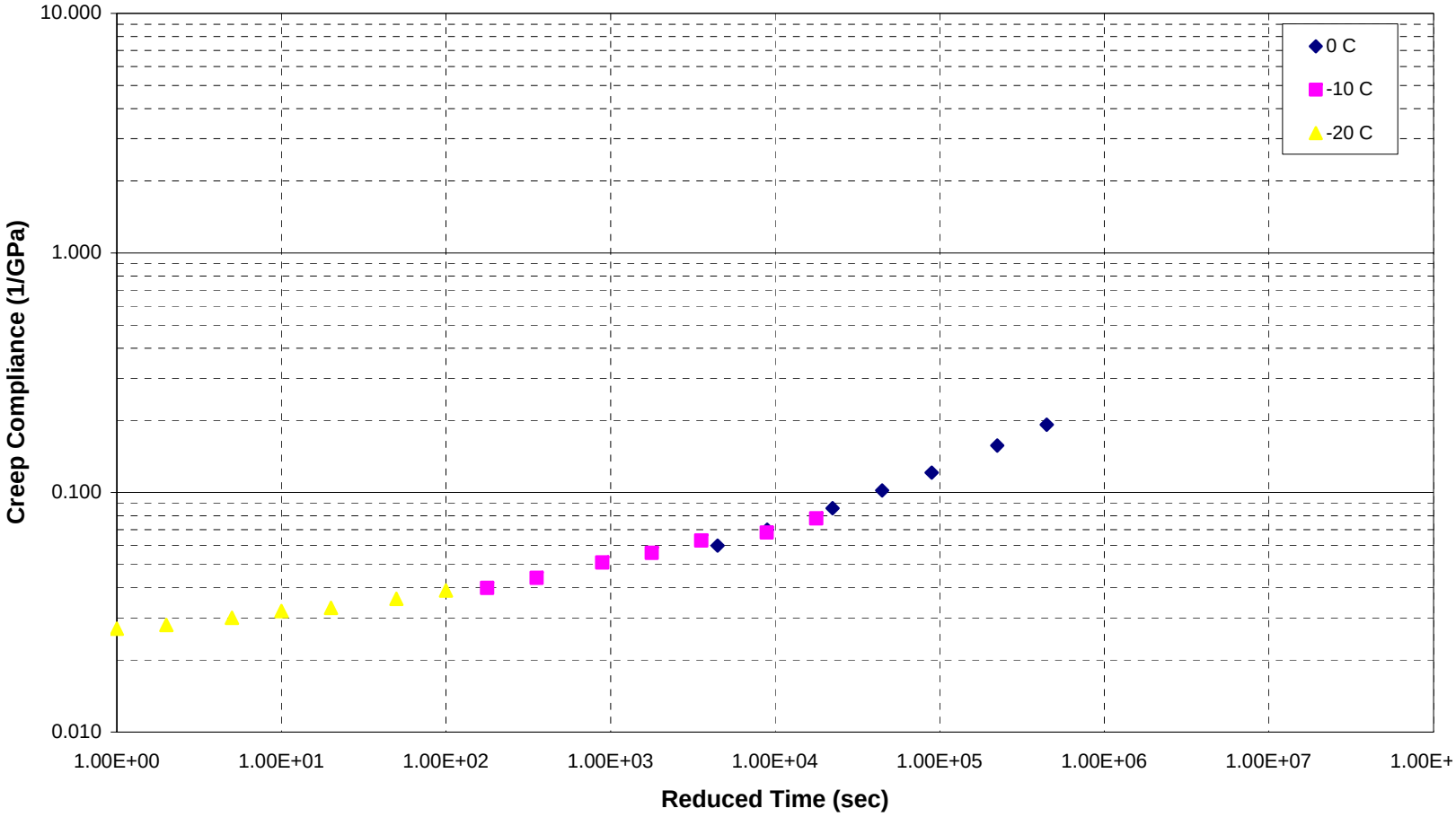

Figure C - 6. Creep Compliance Master Curve - SHRP 161001

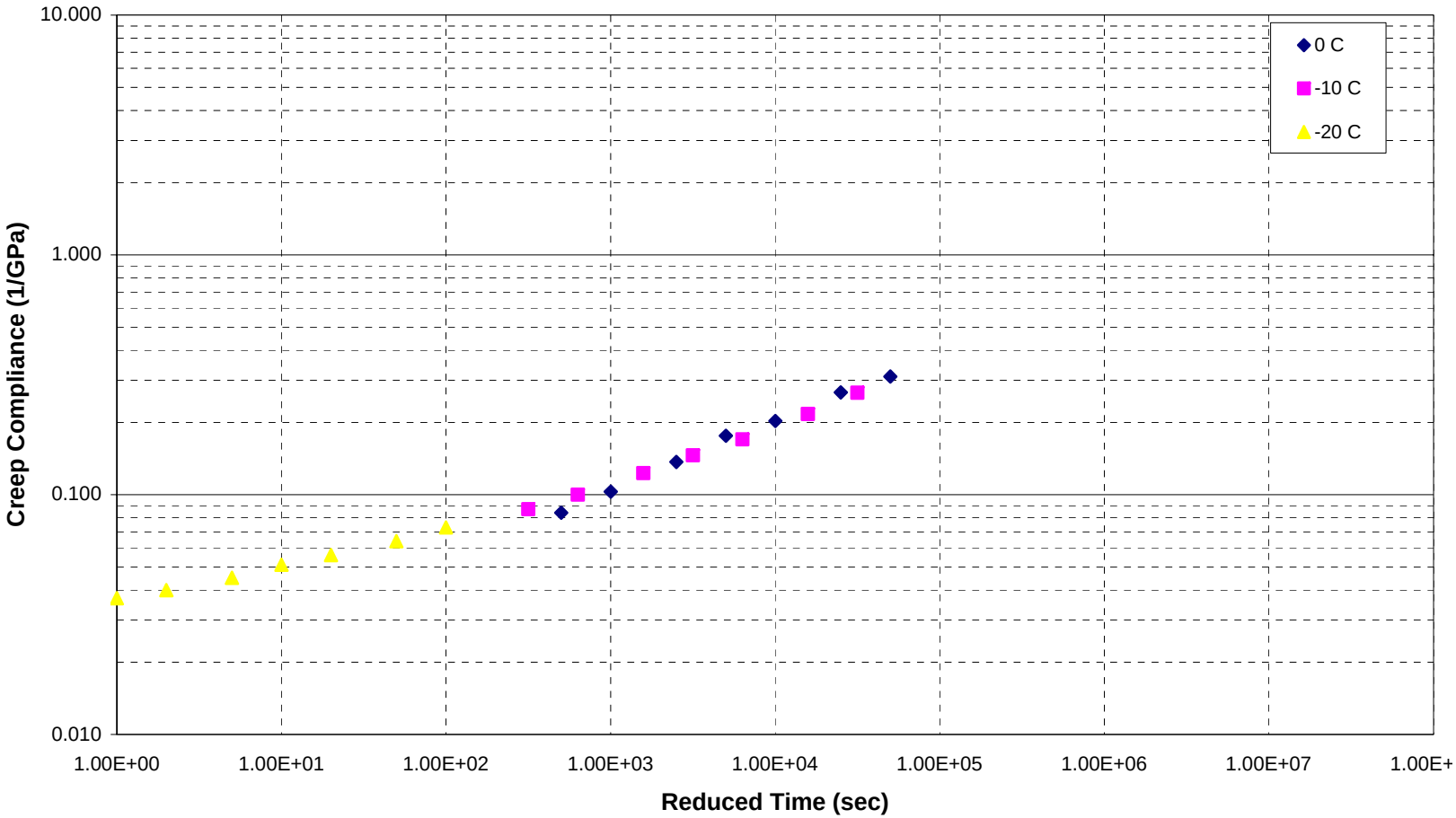

Figure C - 7. Creep Compliance Master Curve - SHRP 311030

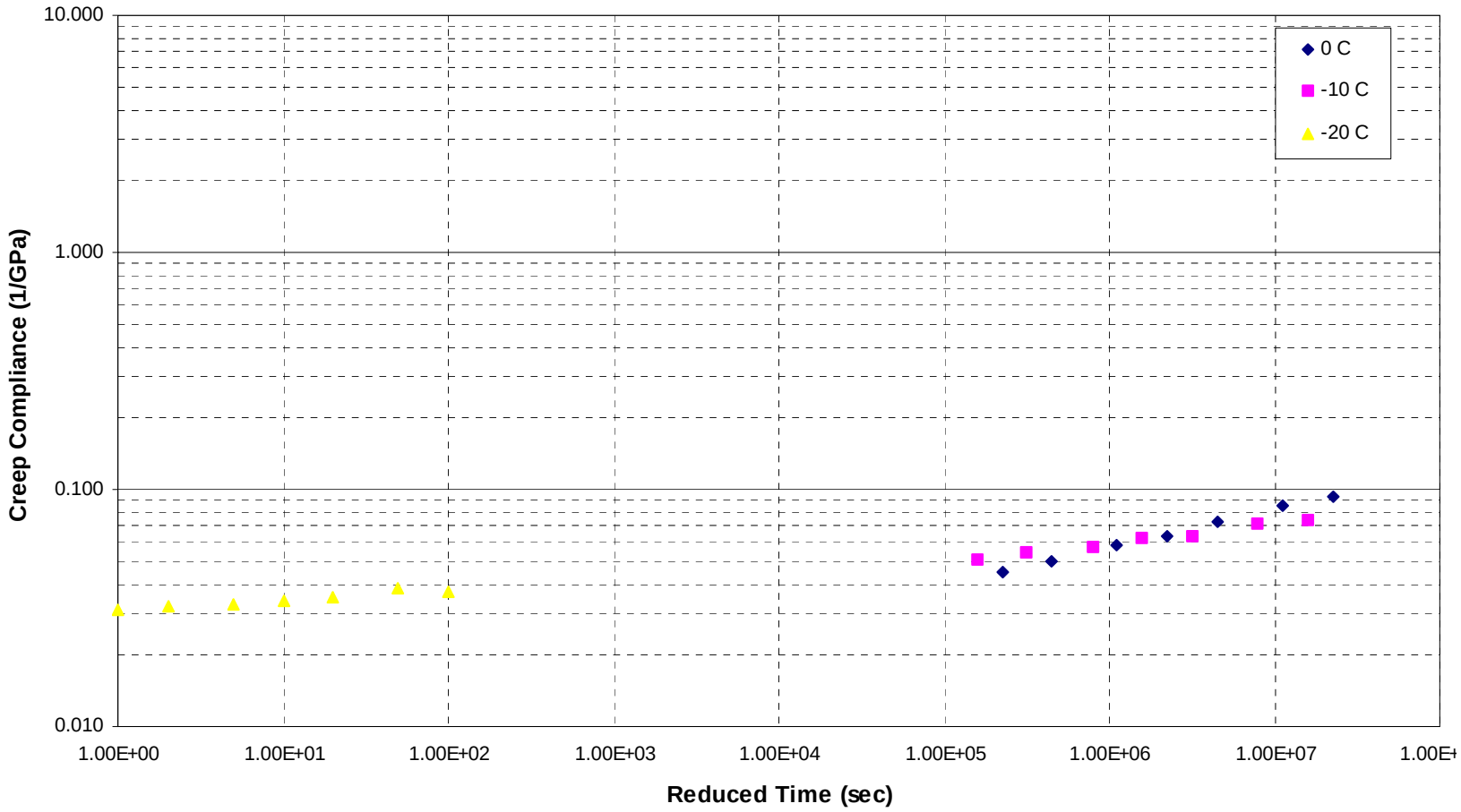

Figure C - 8. Creep Compliance Master Curve - SHRP 491008

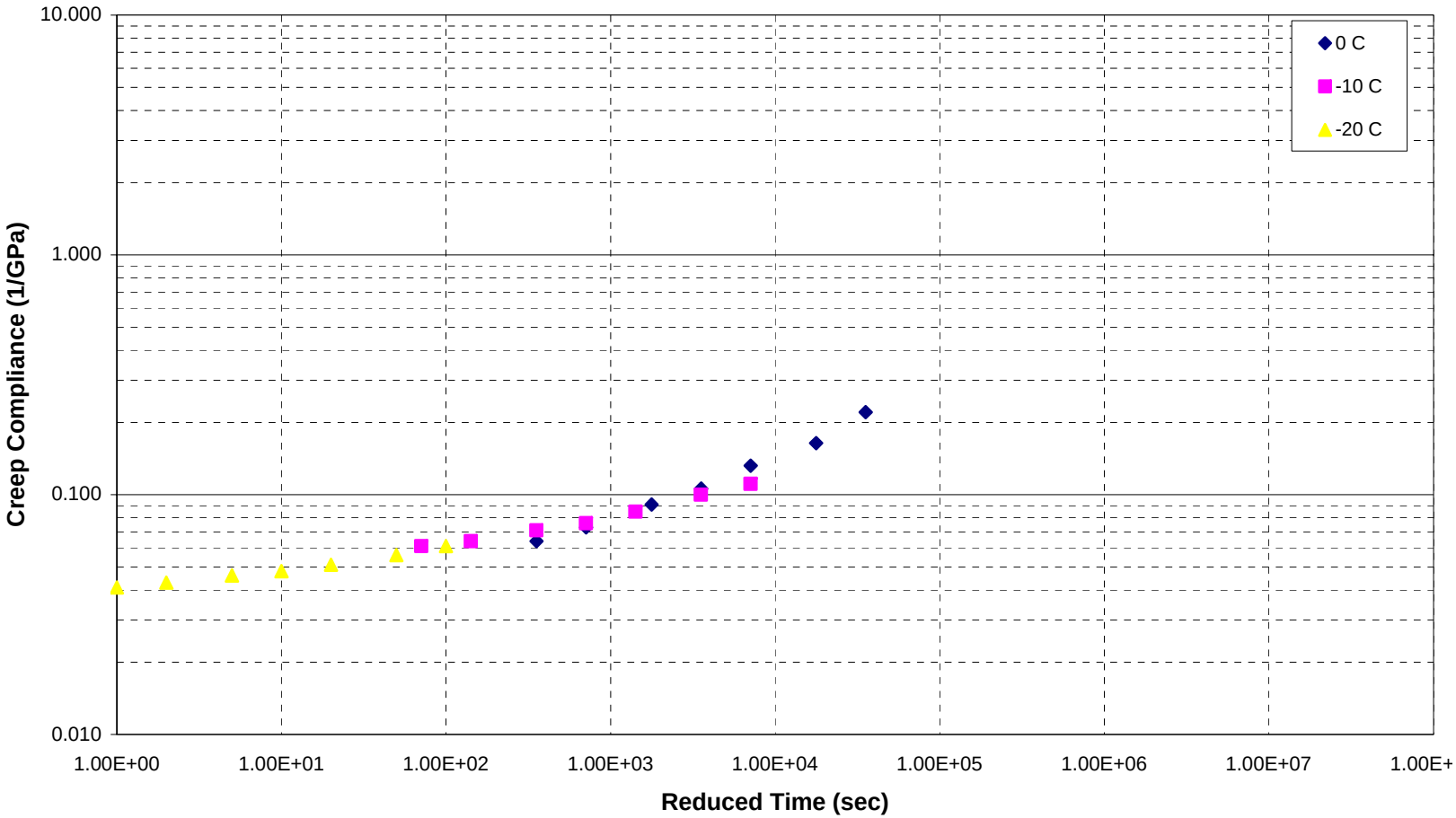

Figure C - 9. Creep Compliance Master Curve - SHRP 561007

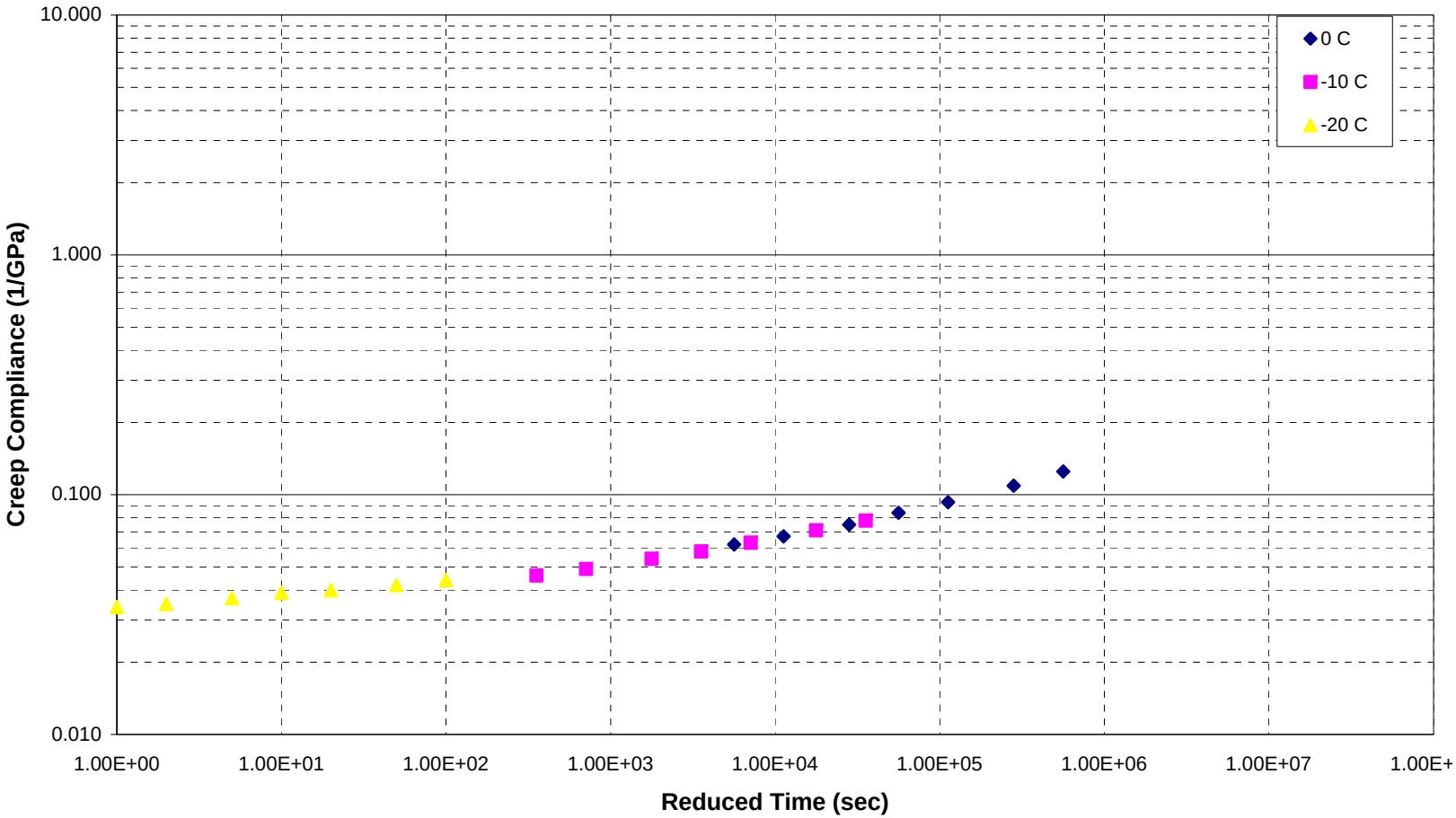

Figure C - 10. Creep Compliance Master Curve - SHRP 081047

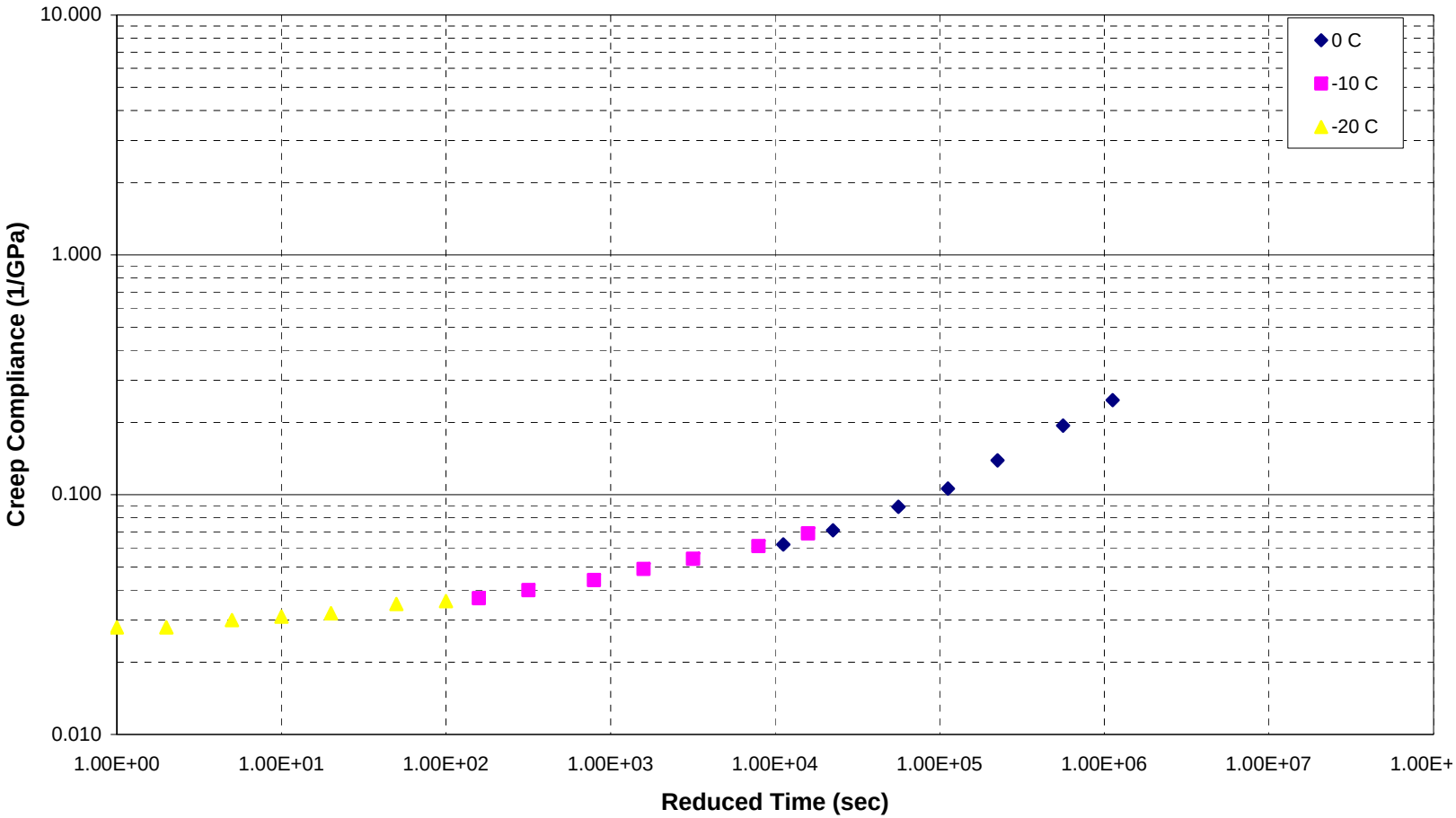

Figure C - 11. Creep Compliance Master Curve - SHRP 211034

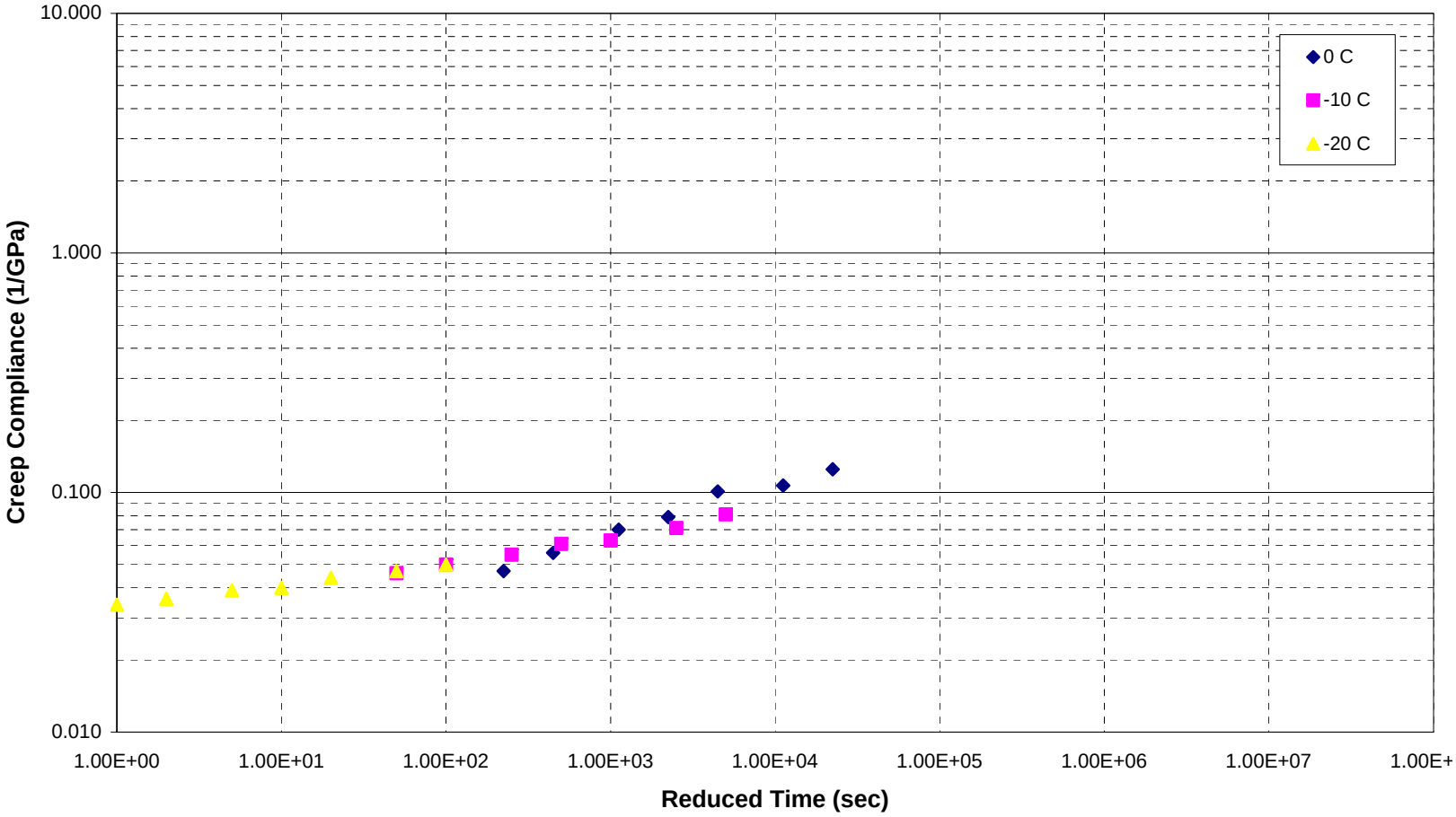

Figure C - 12. Creep Compliance Master Curve - SHRP 404088

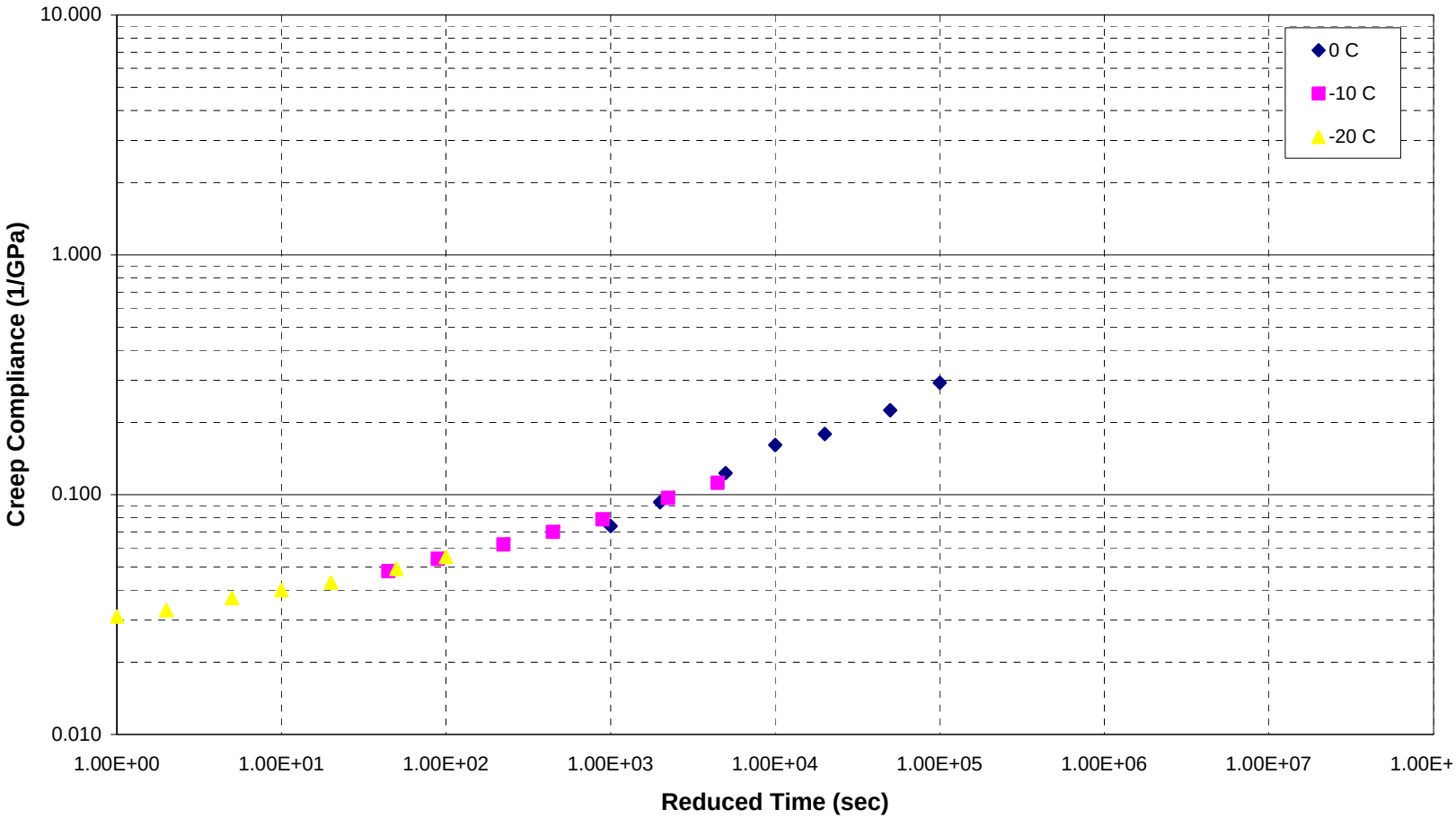

Figure C - 13. Creep Compliance Master Curve - SHRP 241634

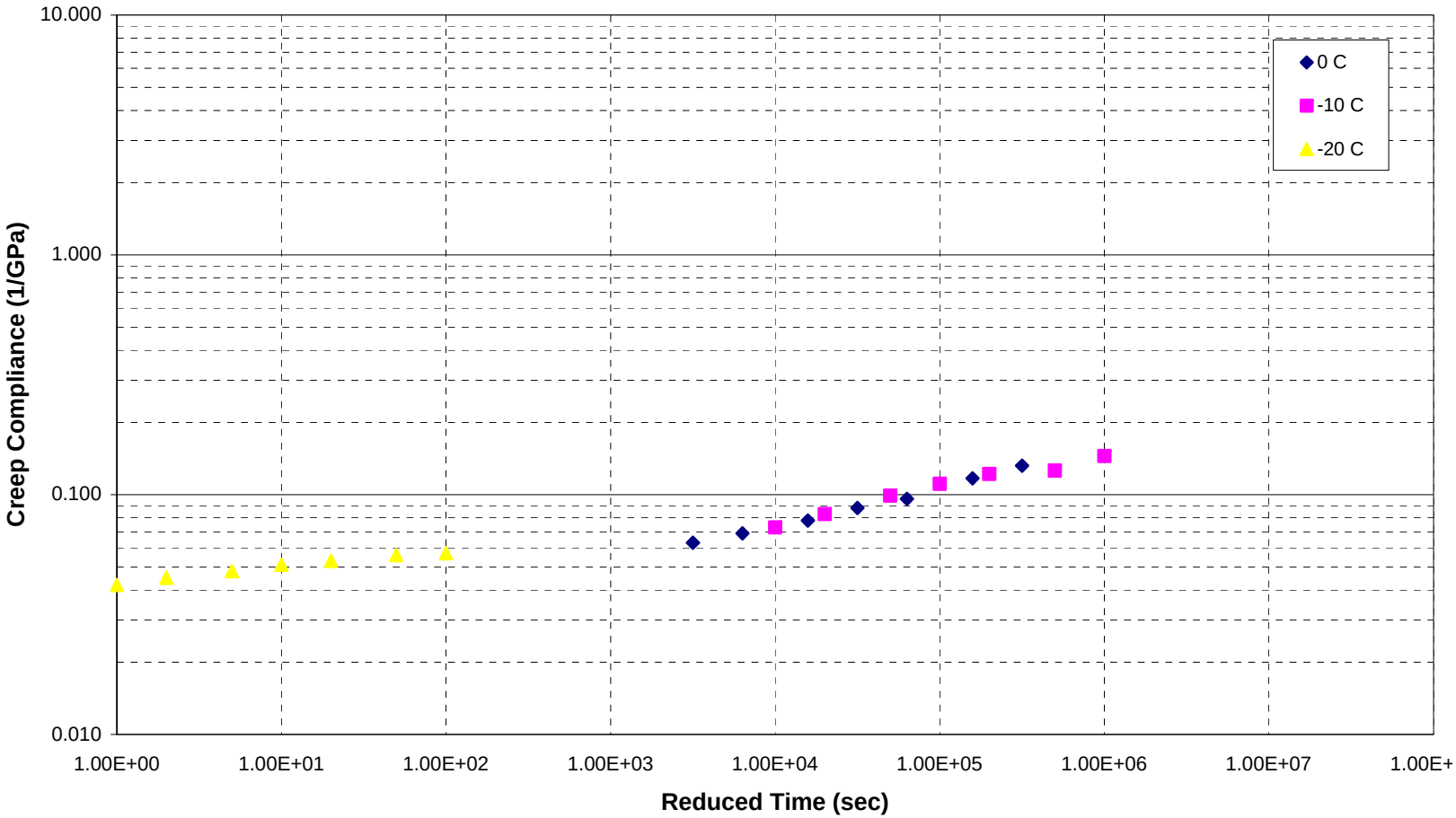

Figure C - 14. Creep Compliance Master Curve - SHRP 451008

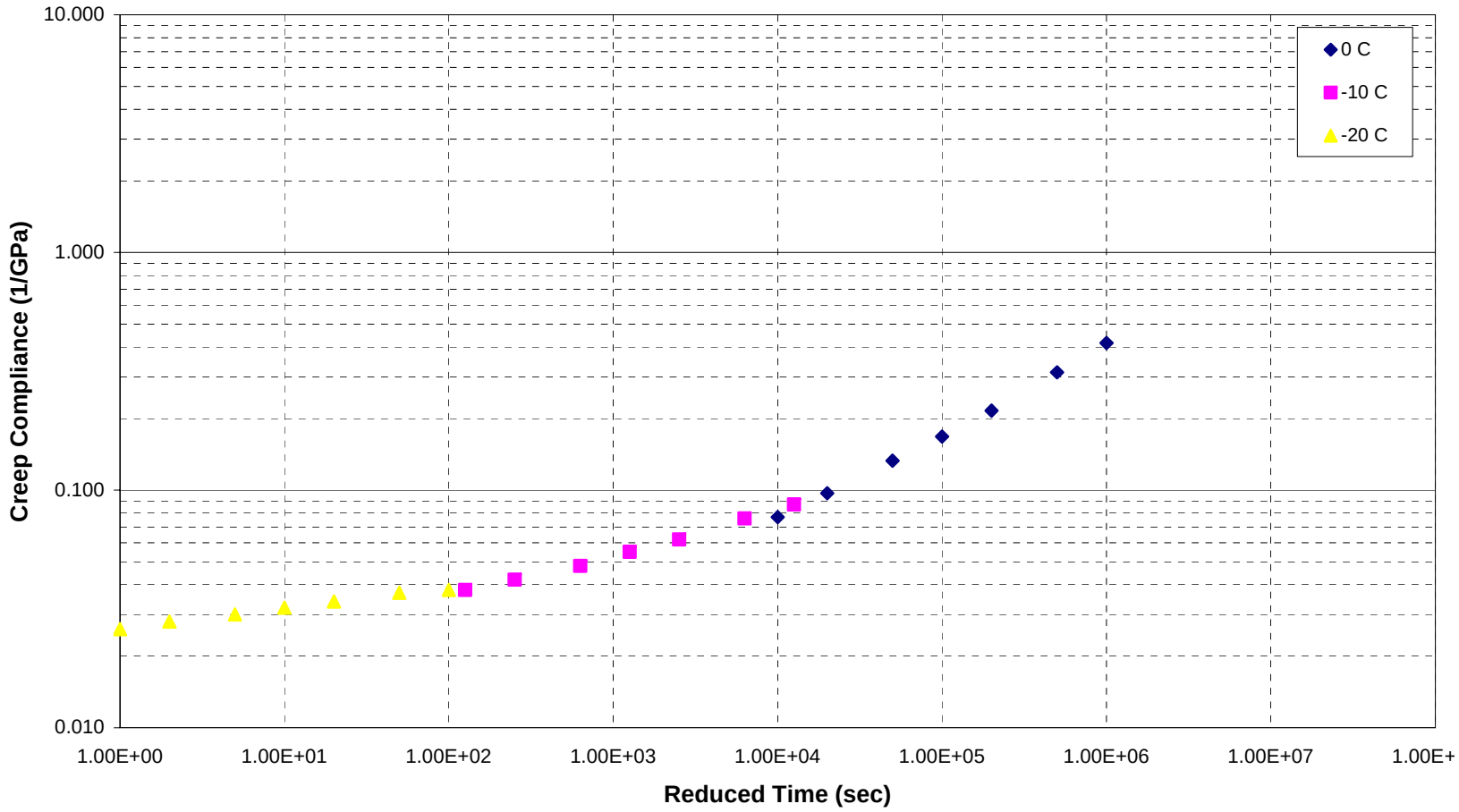

Figure C - 15. Creep Compliance Master Curve - SHRP 341011

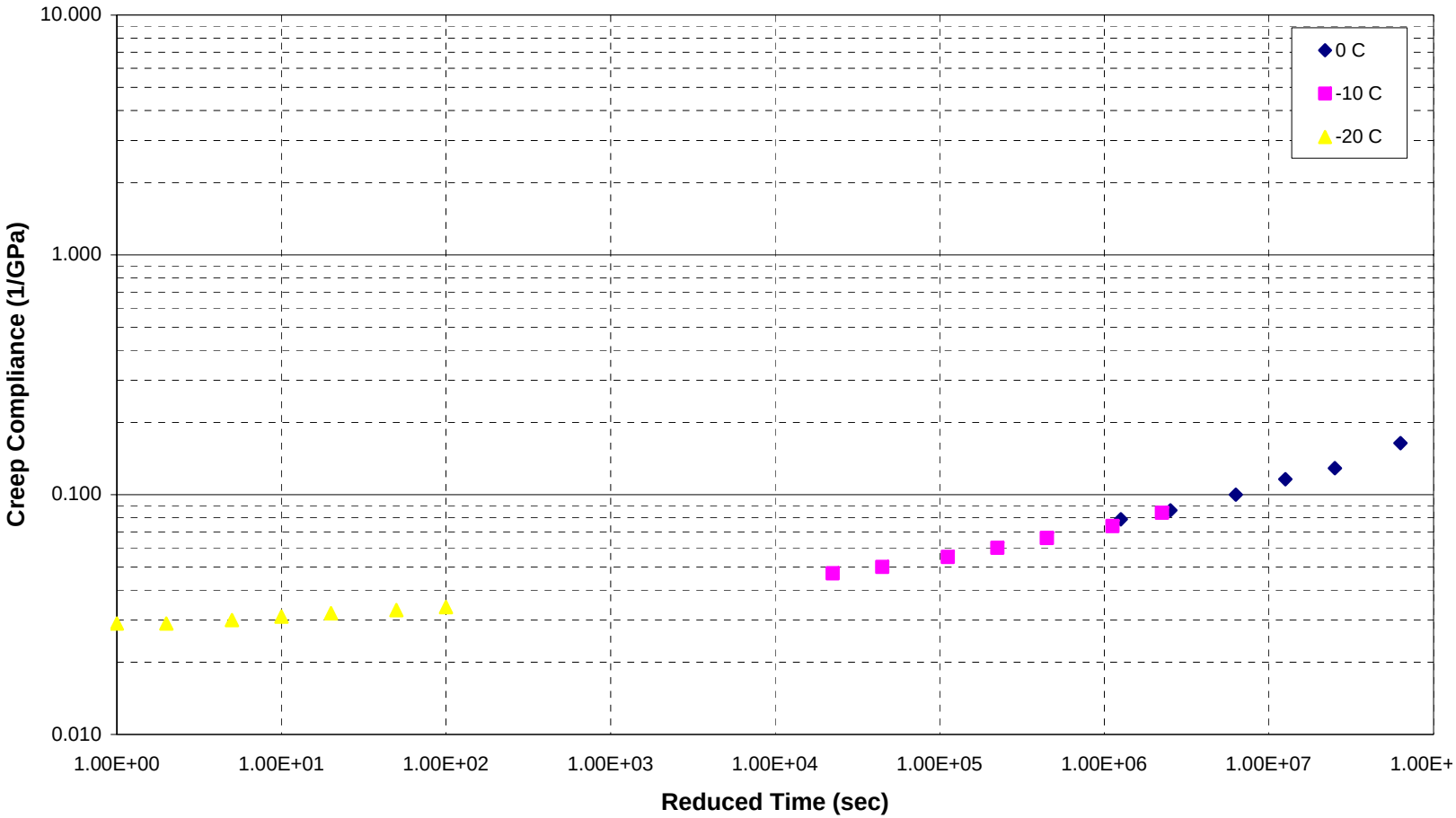

Figure C - 16. Creep Compliance Master Curve - SHRP 291010

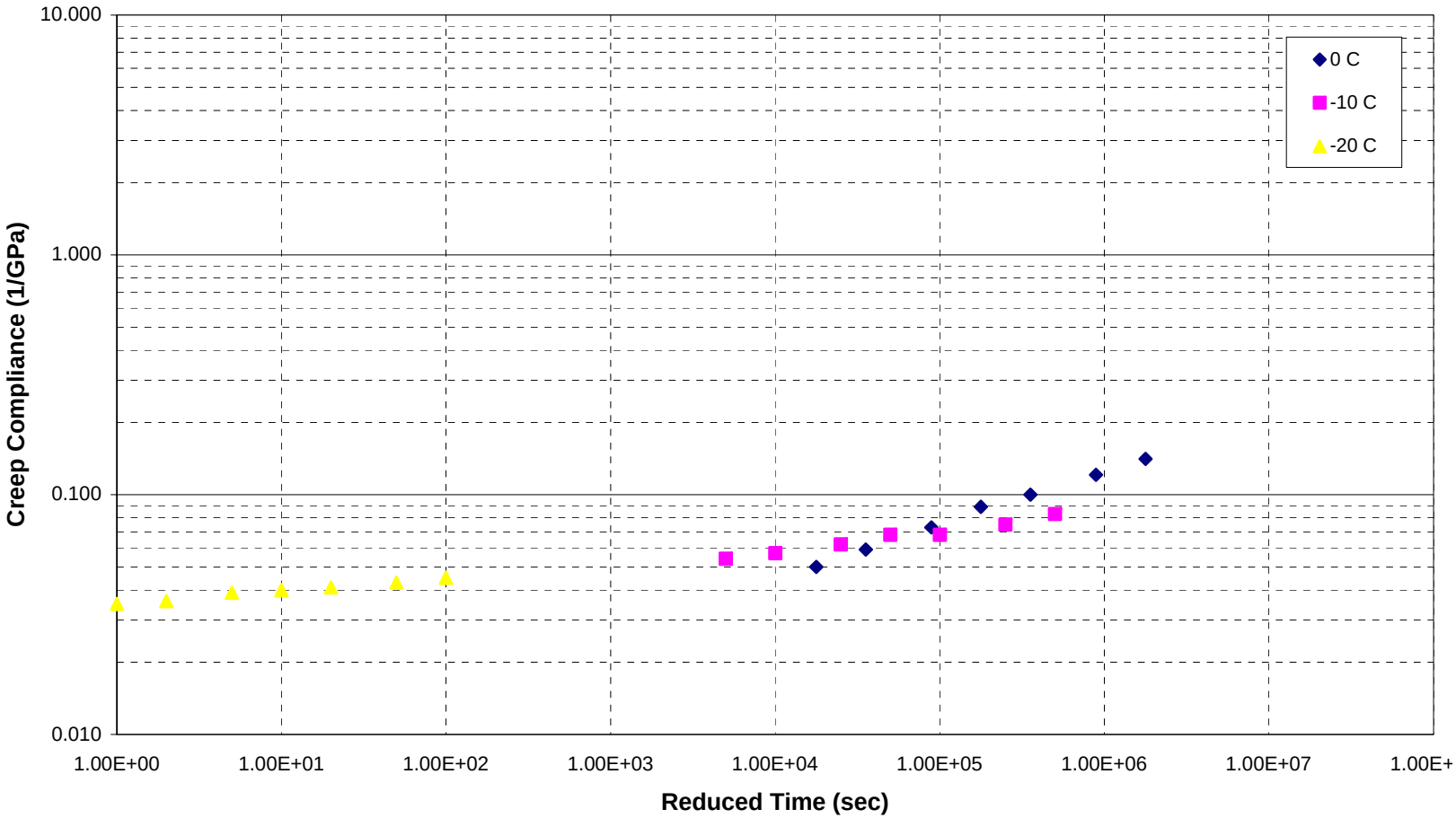

Figure C - 17. Creep Compliance Master Curve - SHRP 421597

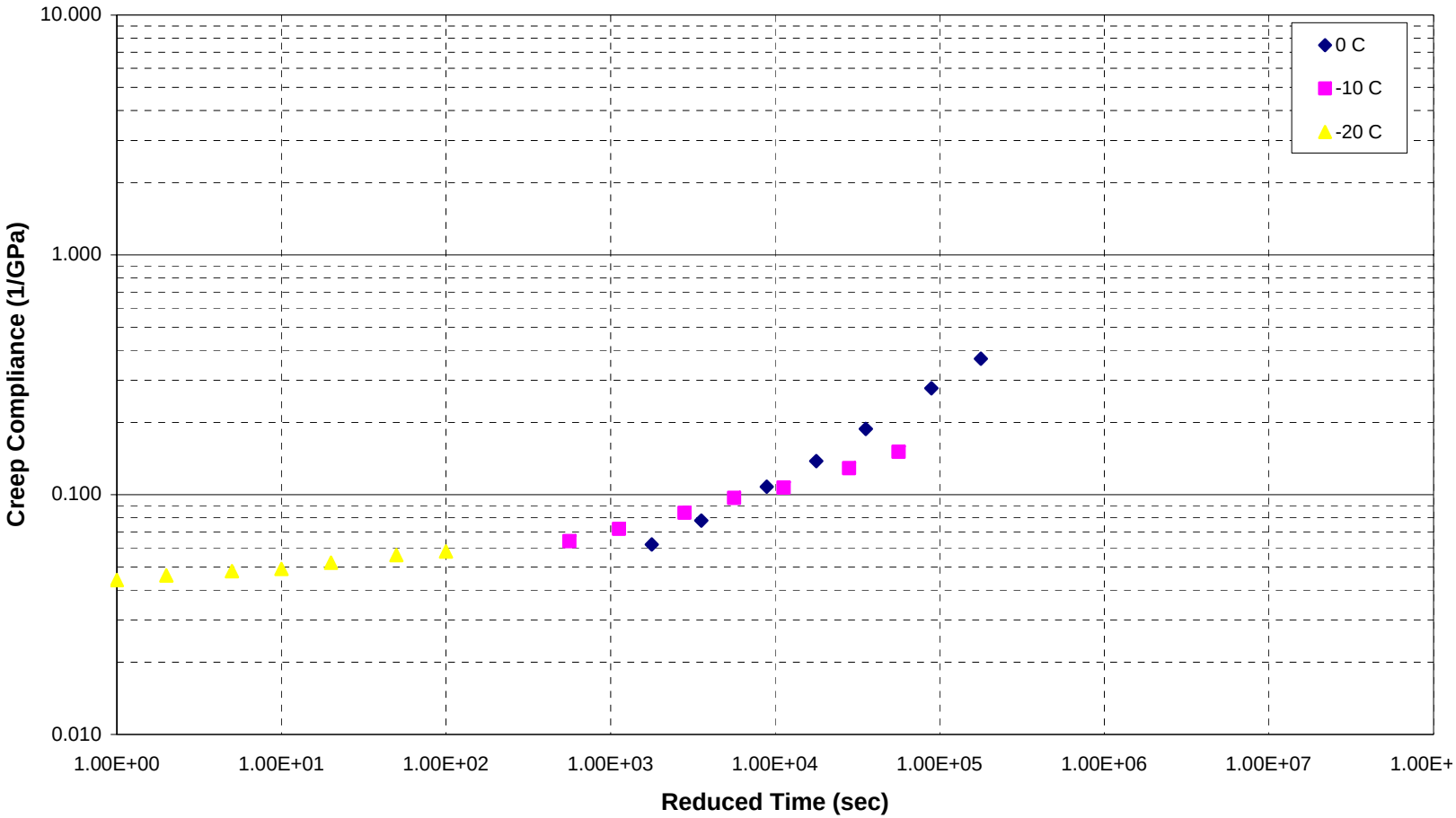

Figure C - 18. Creep Compliance Master Curve - SHRP 181028

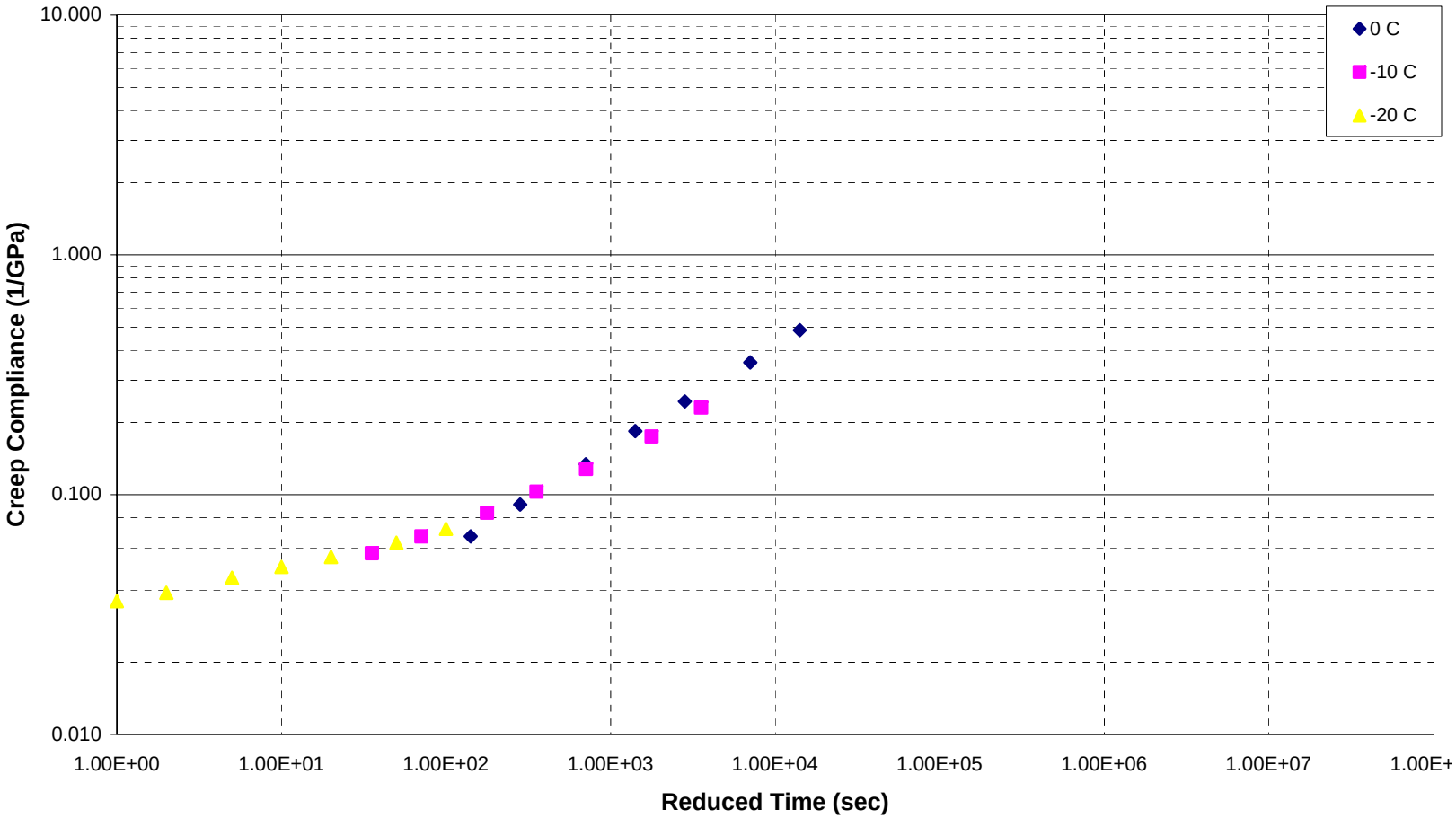

Figure C - 19. Creep Compliance Master Curve - SHRP 231026

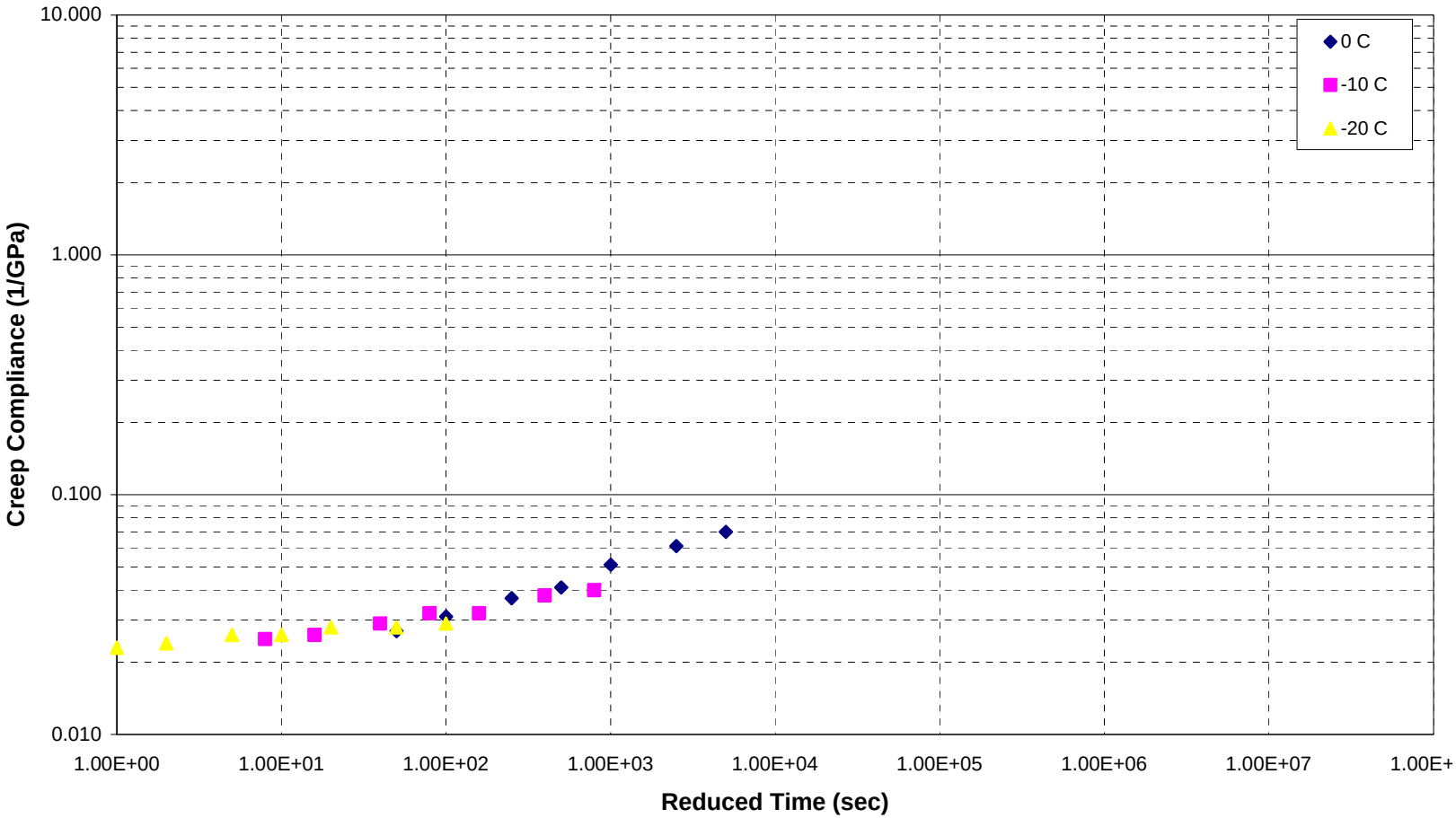

Figure C - 20. Creep Compliance Master Curve - SHRP 181037

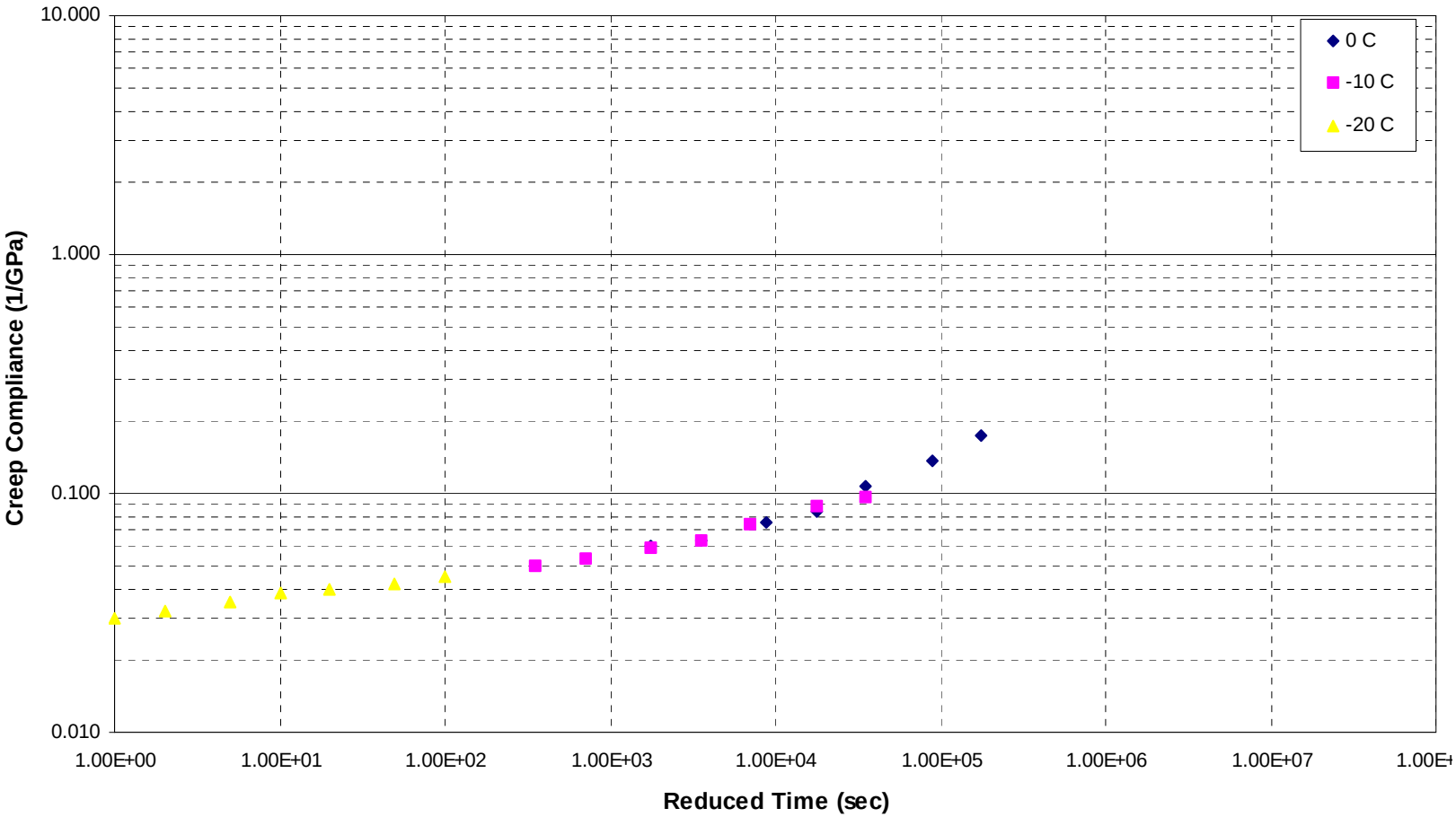

Figure C - 21. Creep Compliance Master Curve - SHRP 271087

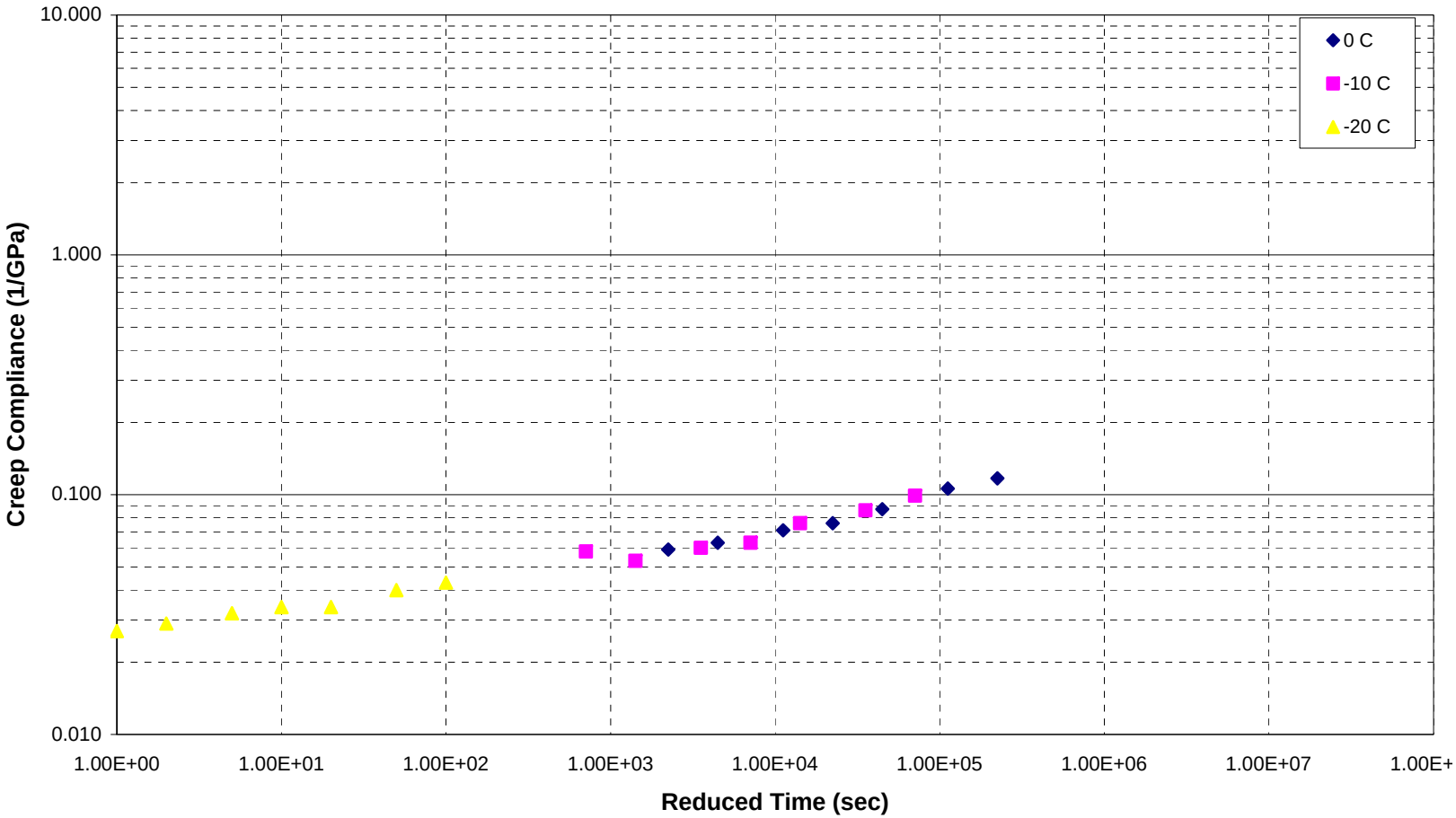

Figure C - 22. Creep Compliance Master Curve - SHRP 271028

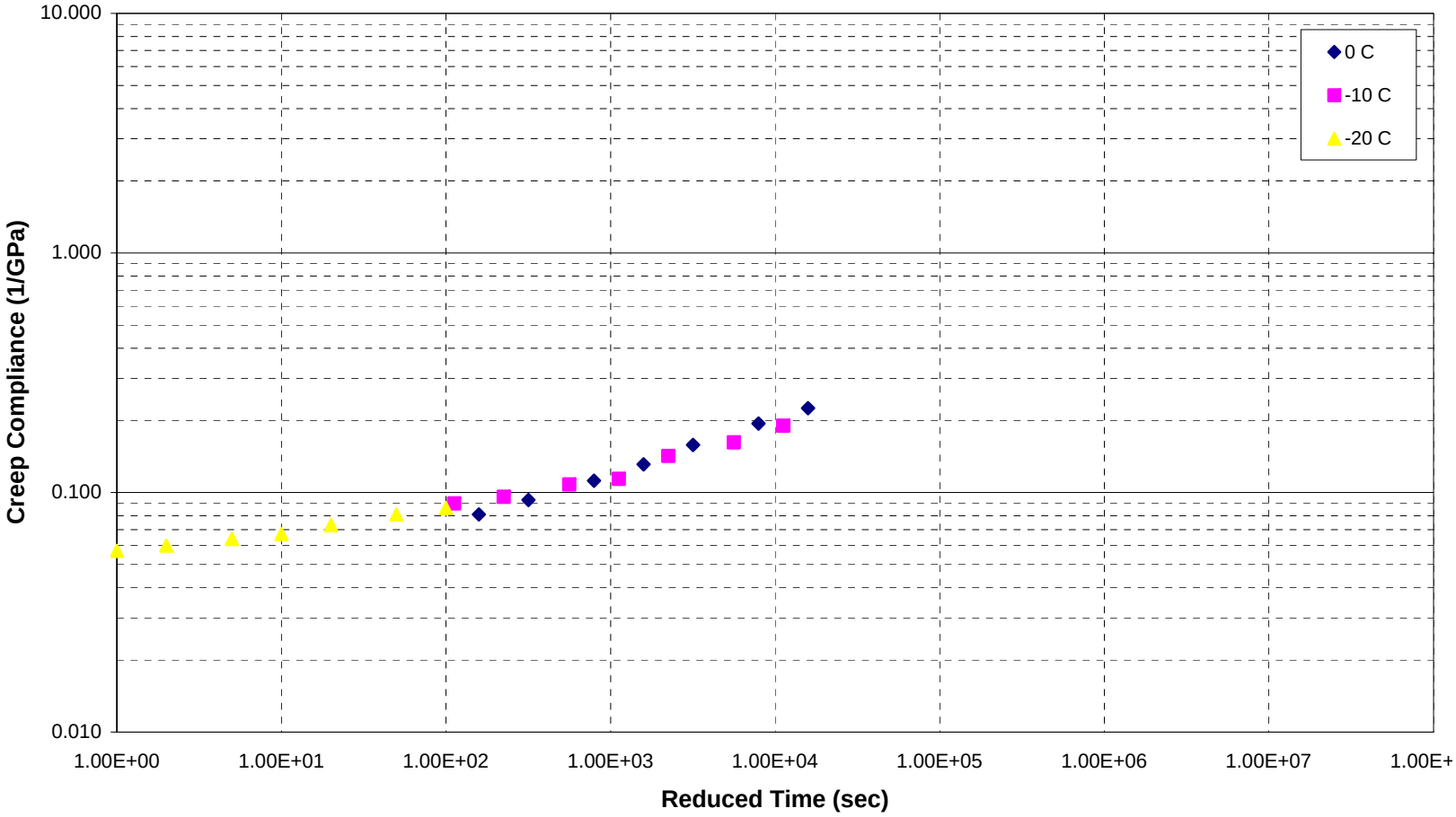

Figure C - 23. Creep Compliance Master Curve - CSHRP Lamont 1

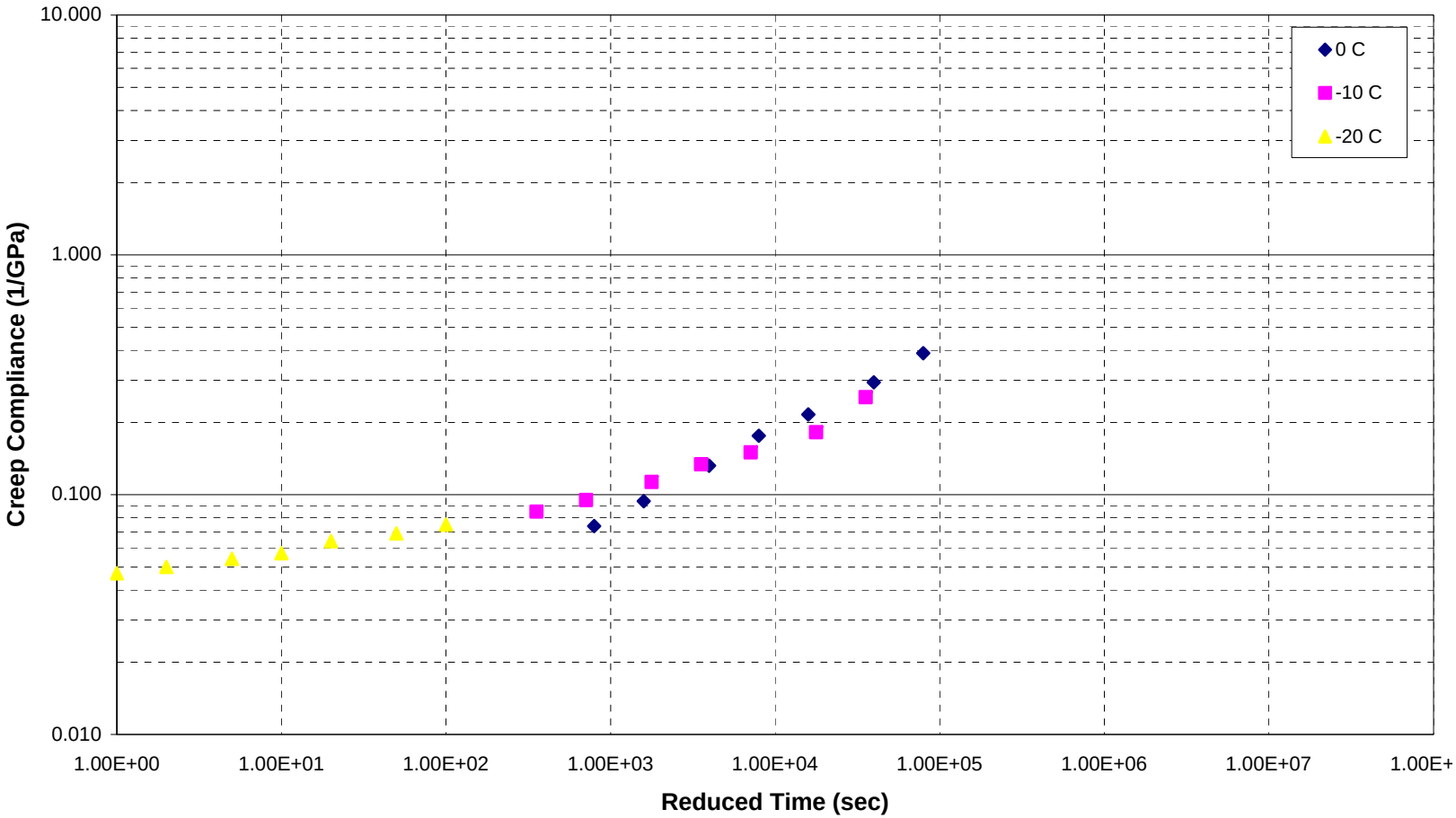

Figure C - 24. Creep Compliance Master Curve - CSHRP Lamont 2

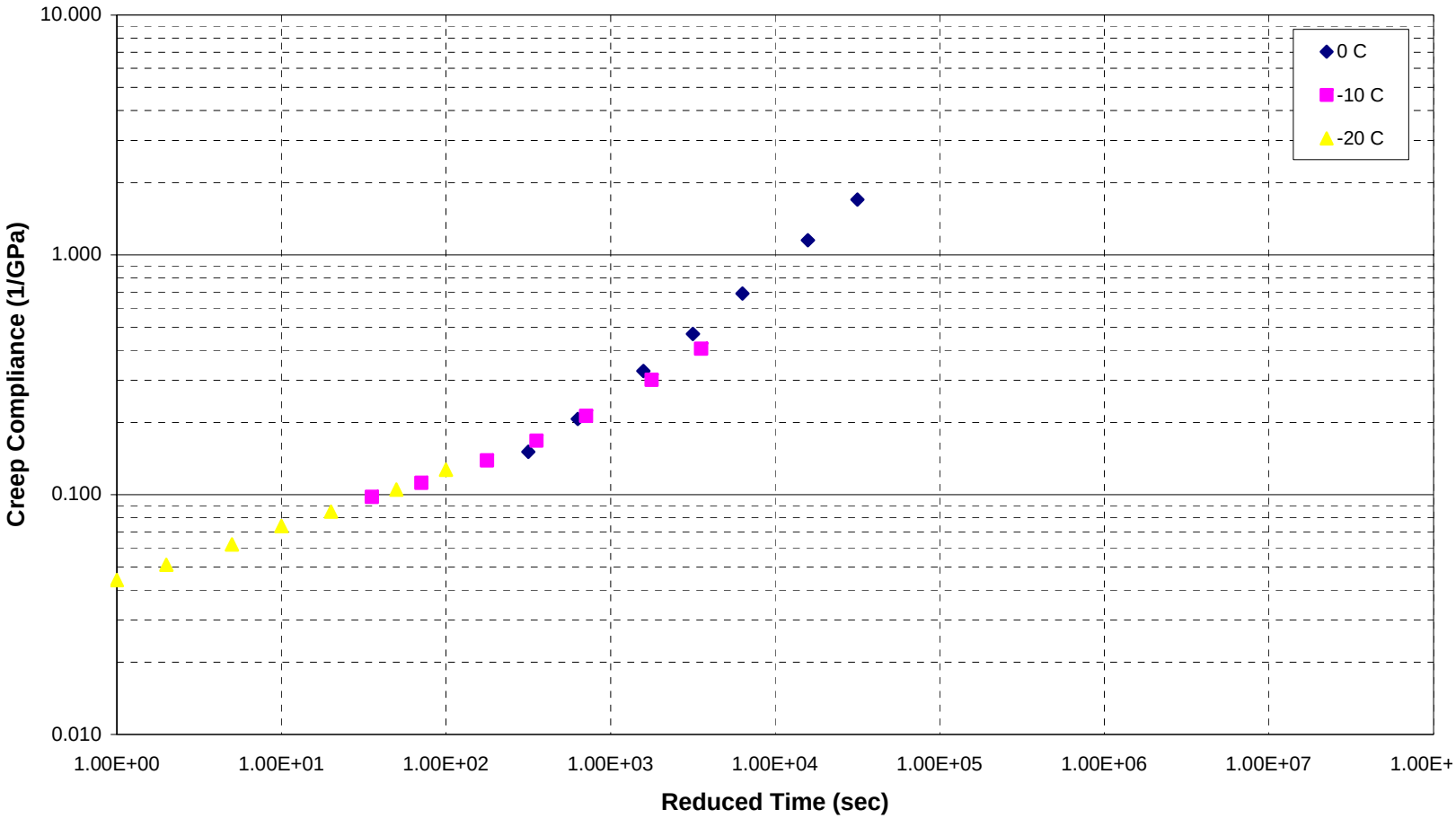

Figure C - 25. Creep Compliance Master Curve - CSHRP Lamont 3

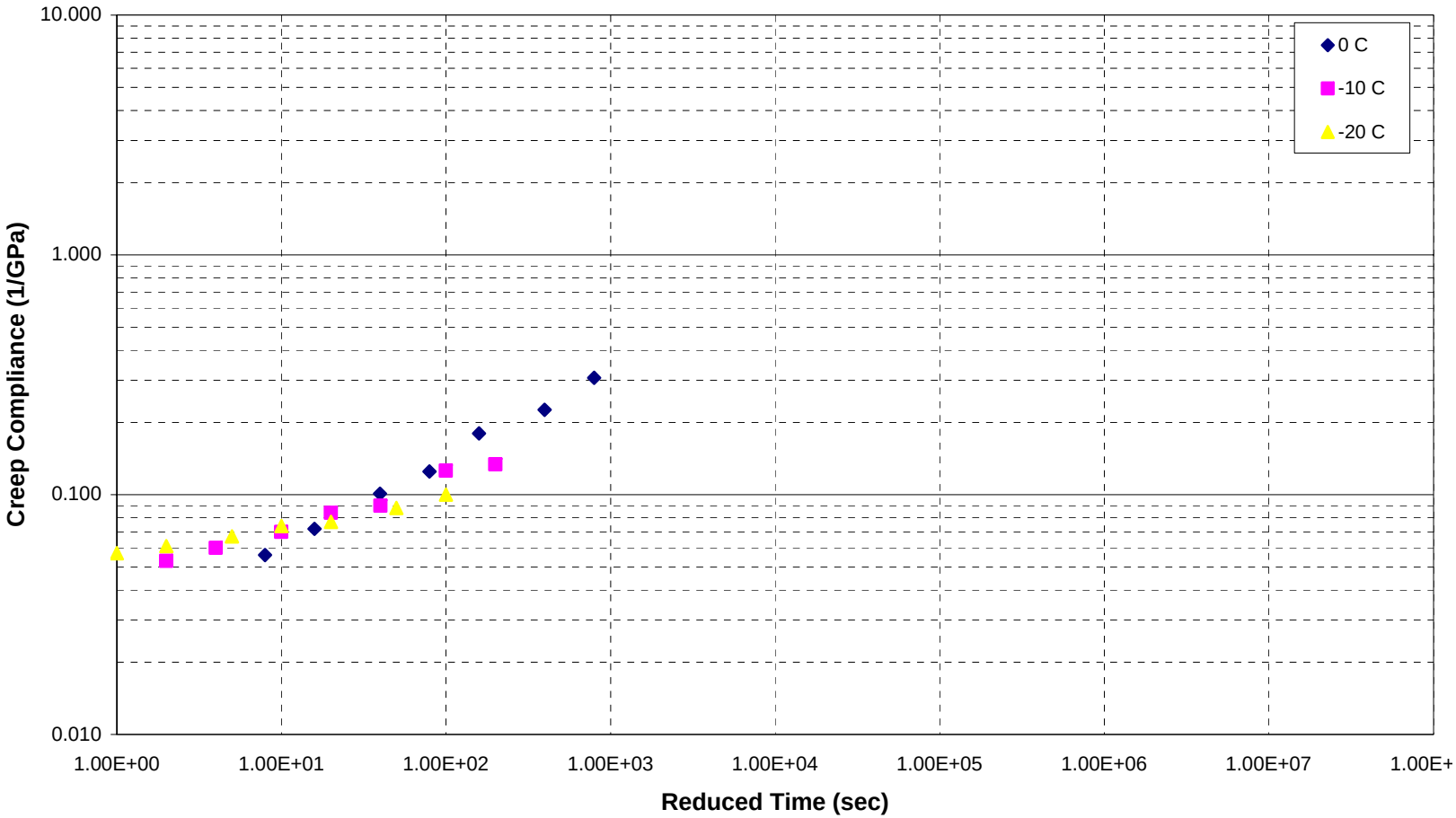

Figure C - 26. Creep Compliance Master Curve - CSHRP Lamont 4

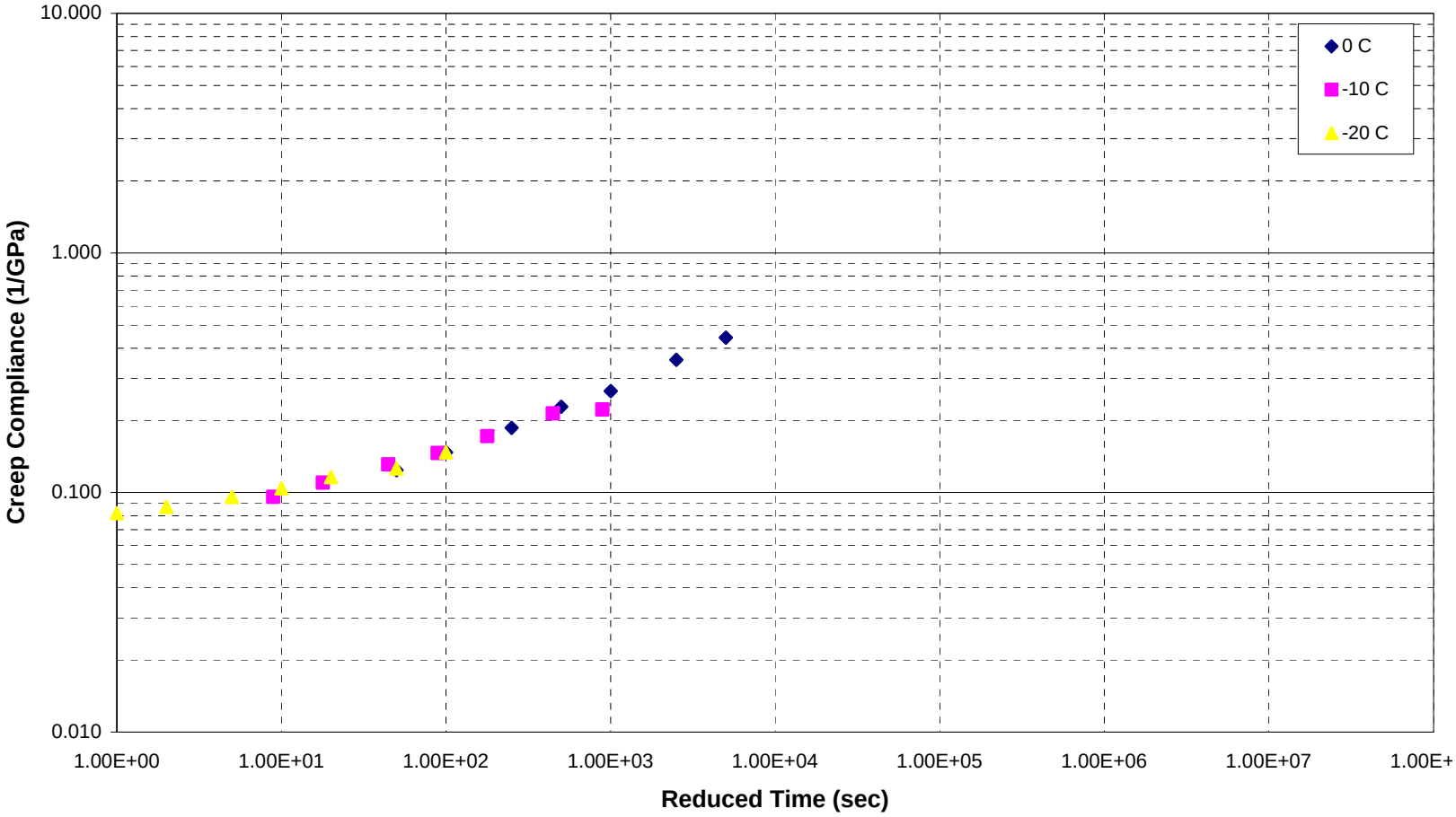

Figure C - 27. Creep Compliance Master Curve - CSHRP Lamont 5

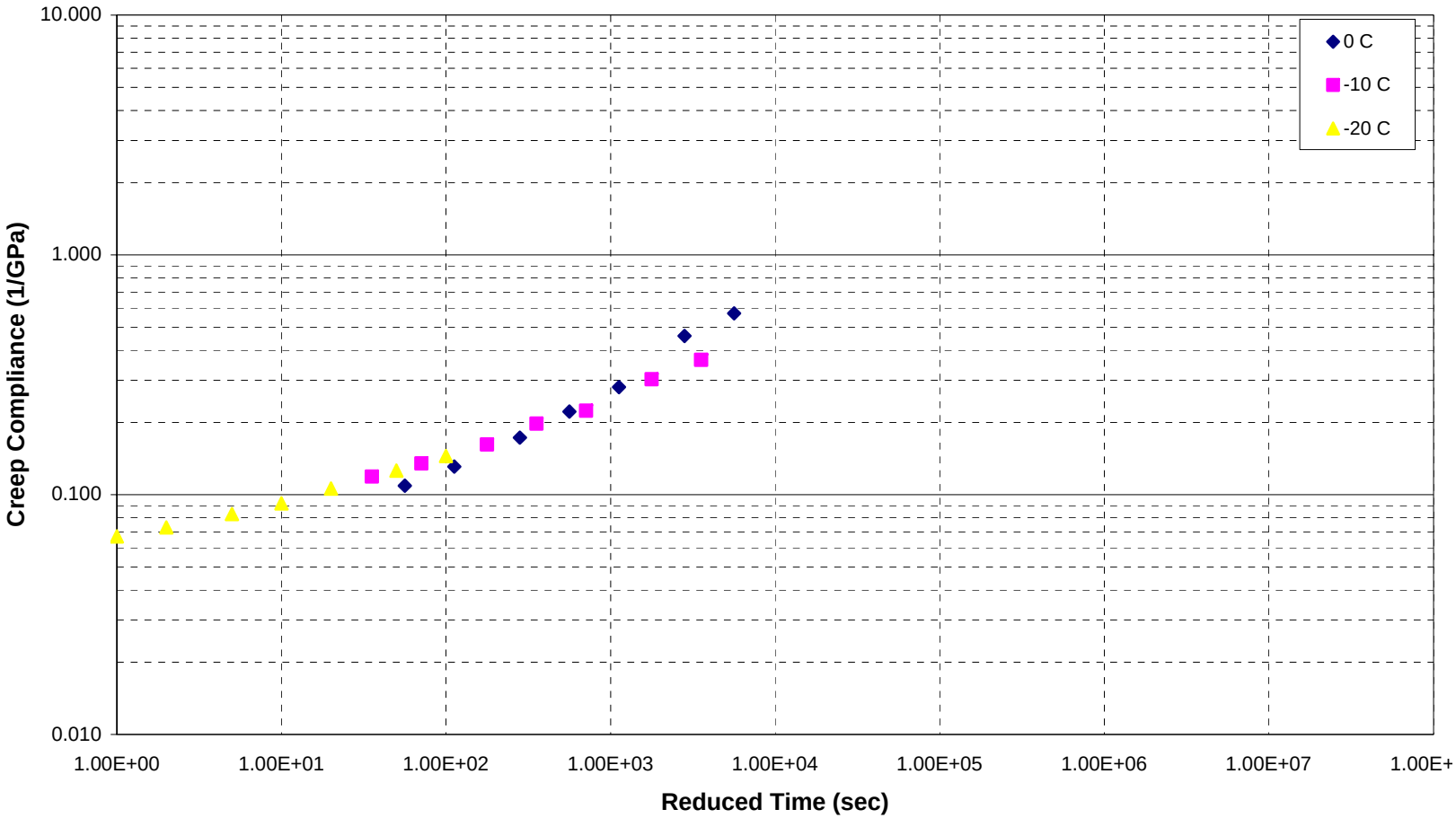

Figure C - 28. Creep Compliance Master Curve - CSHRP Lamont 6

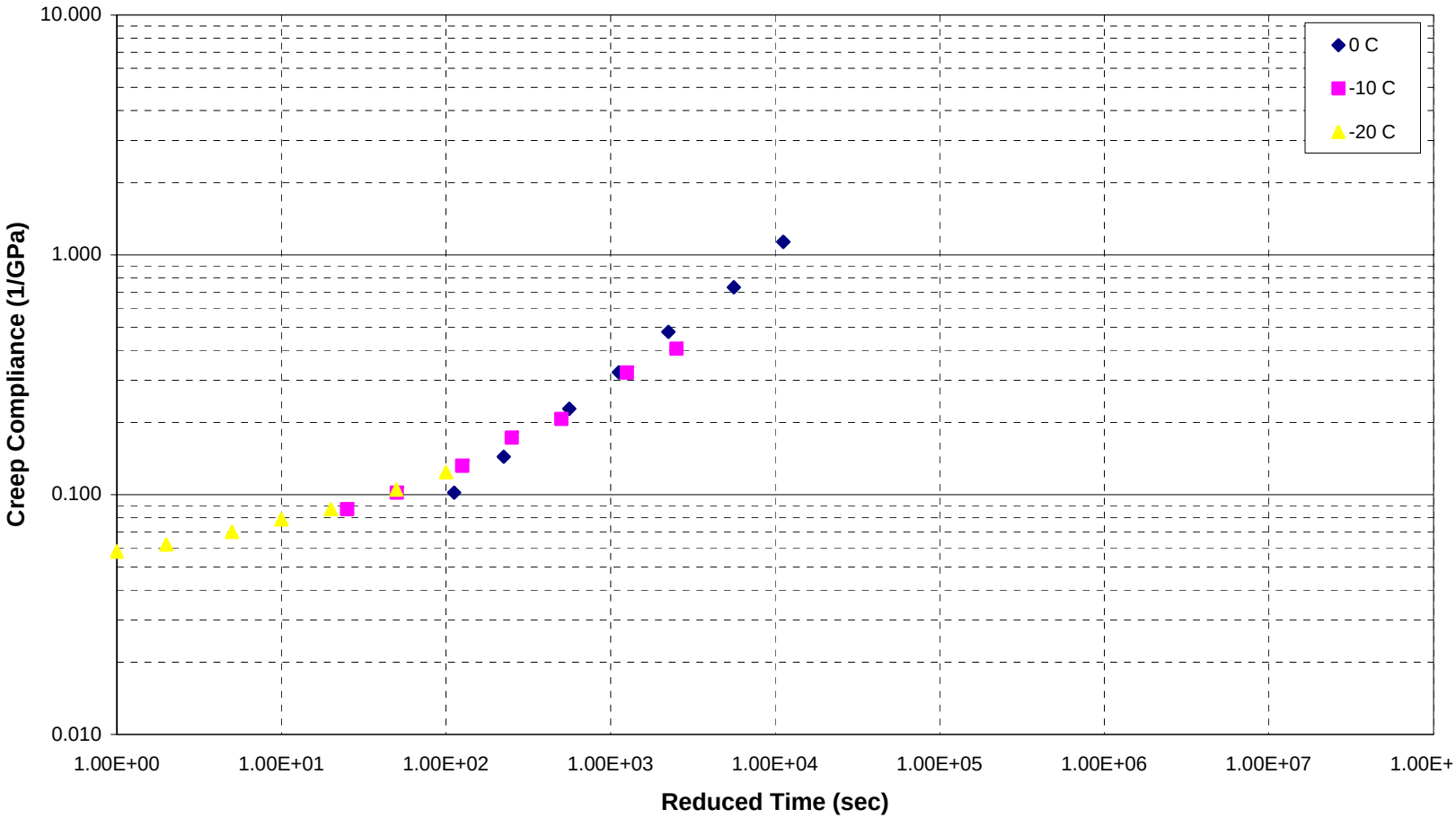

Figure C - 29. Creep Compliance Master Curve - CSHRP Lamont 7

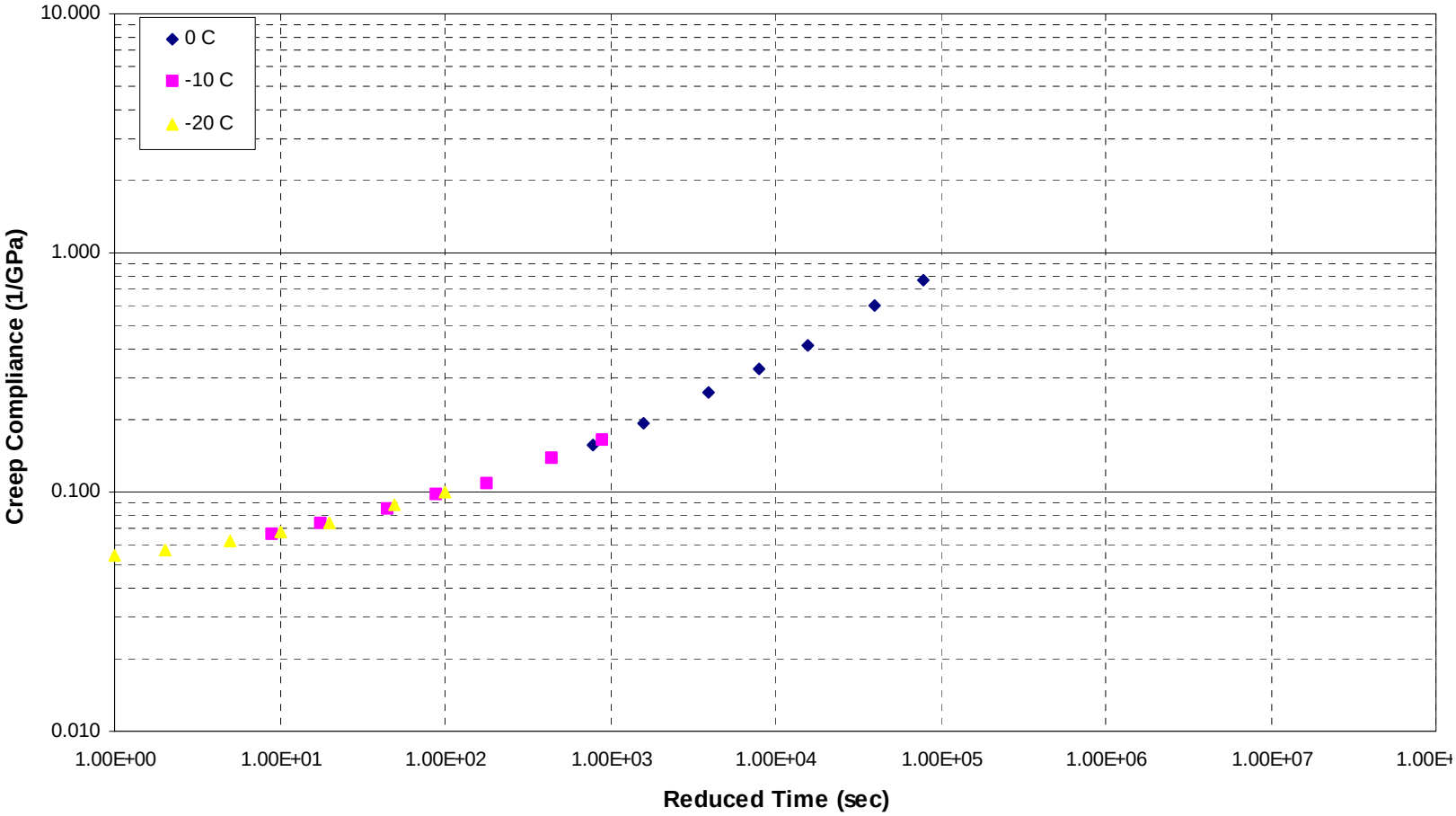

Figure C - 30. Creep Compliance Master Curve - CSHRP Sherbrooke A

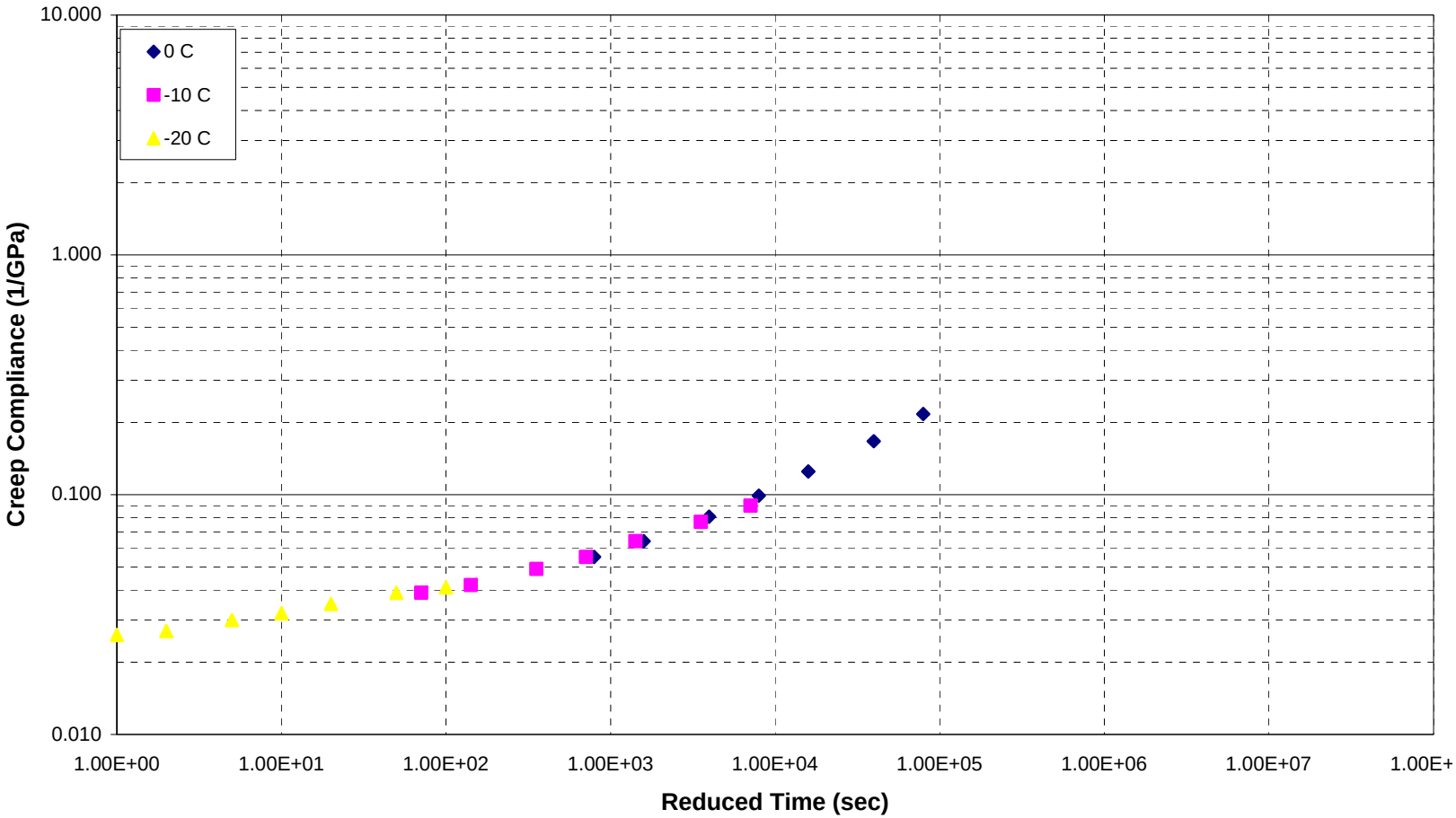

Figure C - 31. Creep Compliance Master Curve - CSHRP Sherbrooke B

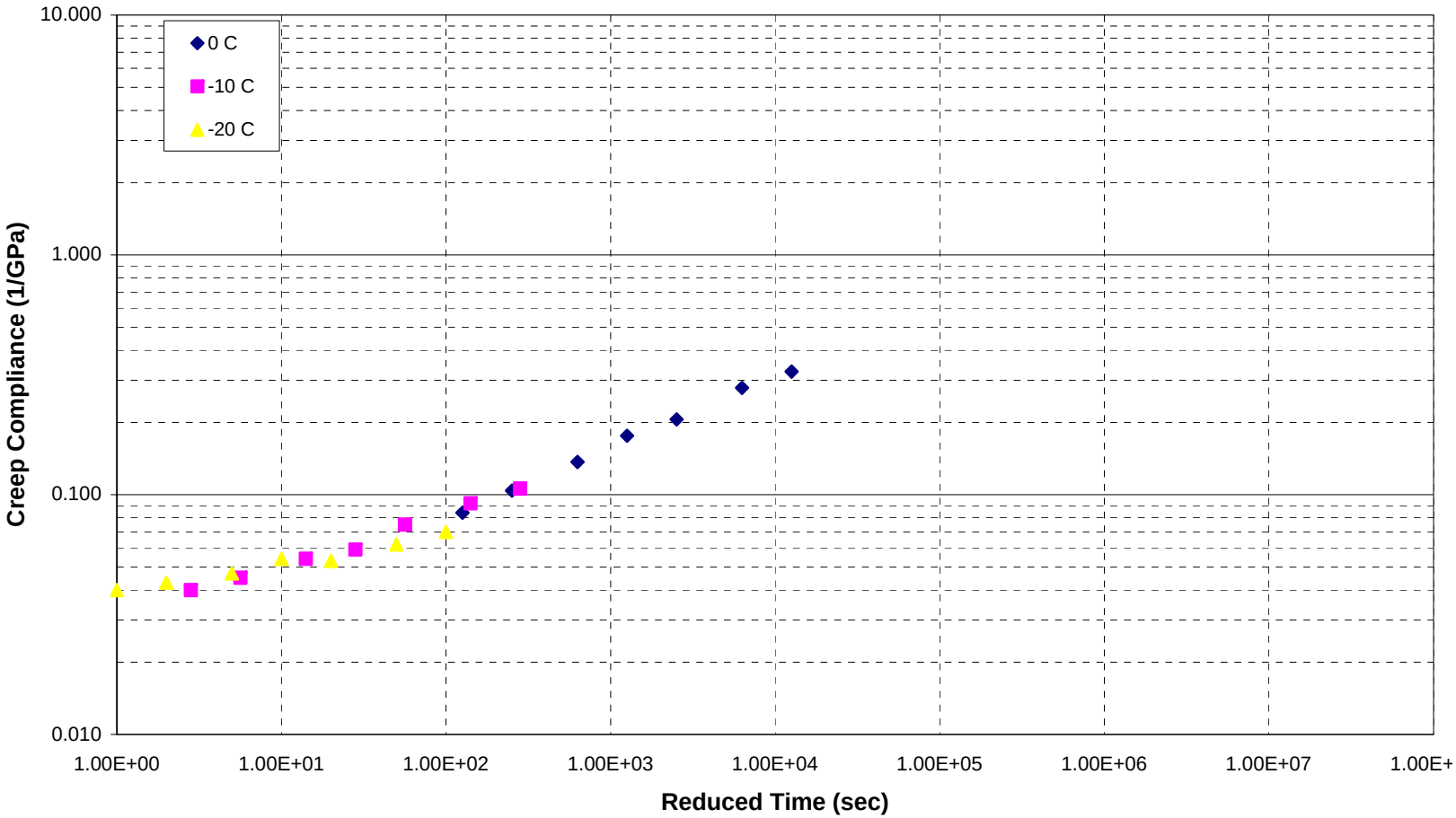

Figure C - 32. Creep Compliance Master Curve - CSHRP Sherbrooke C

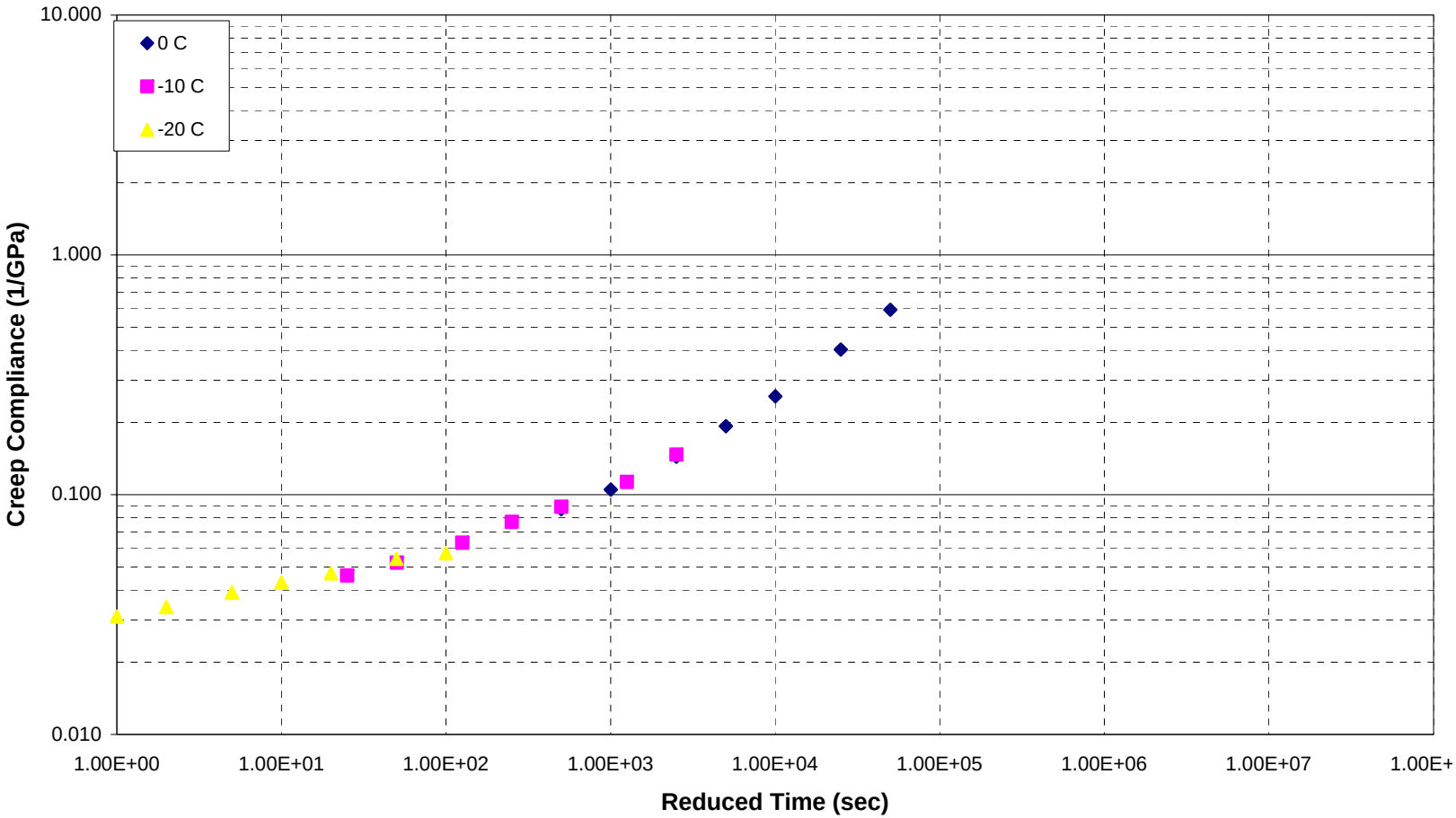

Figure C - 33. Creep Compliance Master Curve - CSHRP Sherbrooke D

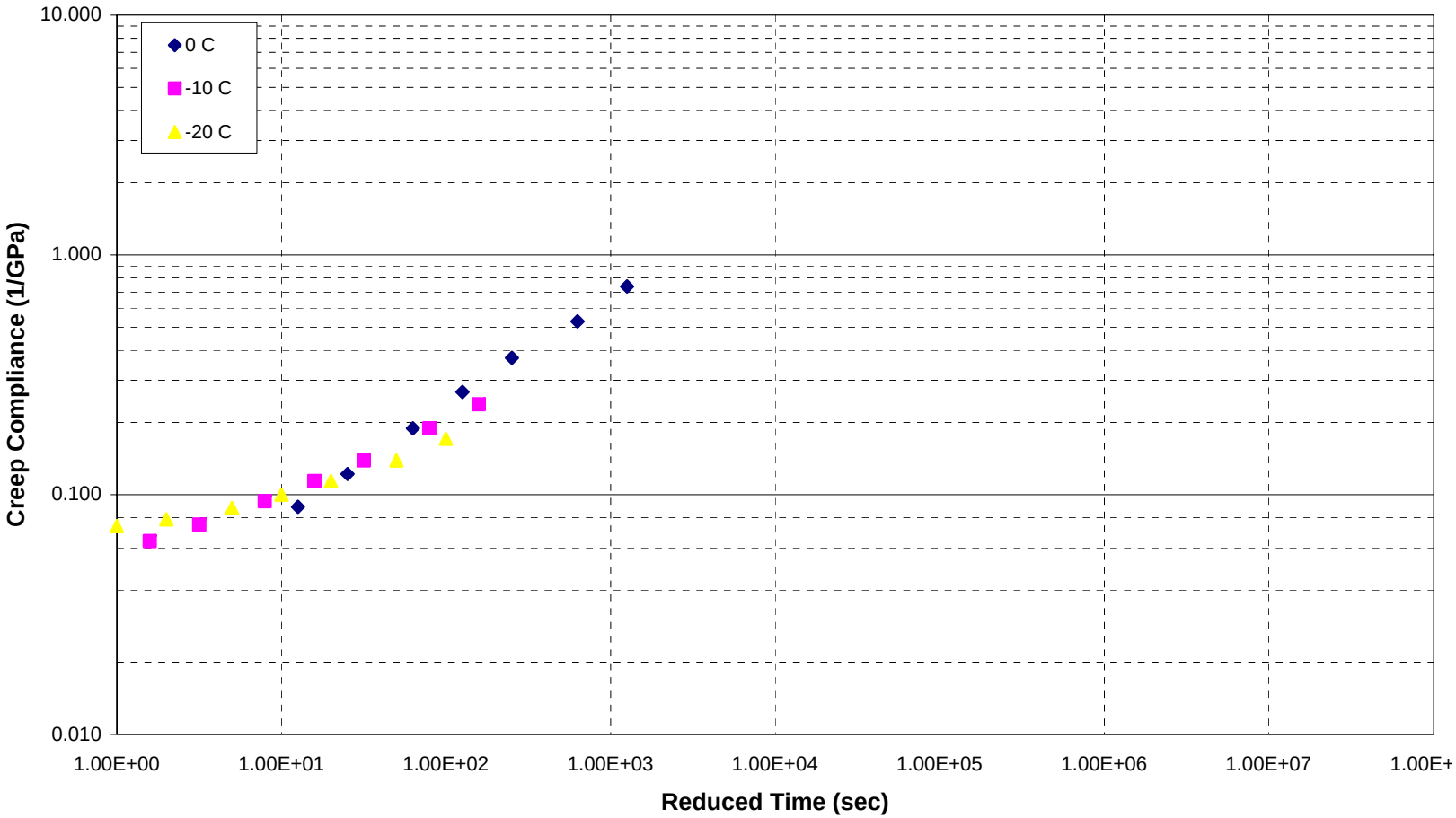

Figure C - 34. Creep Compliance Master Curve - CSRHP Hearst 1

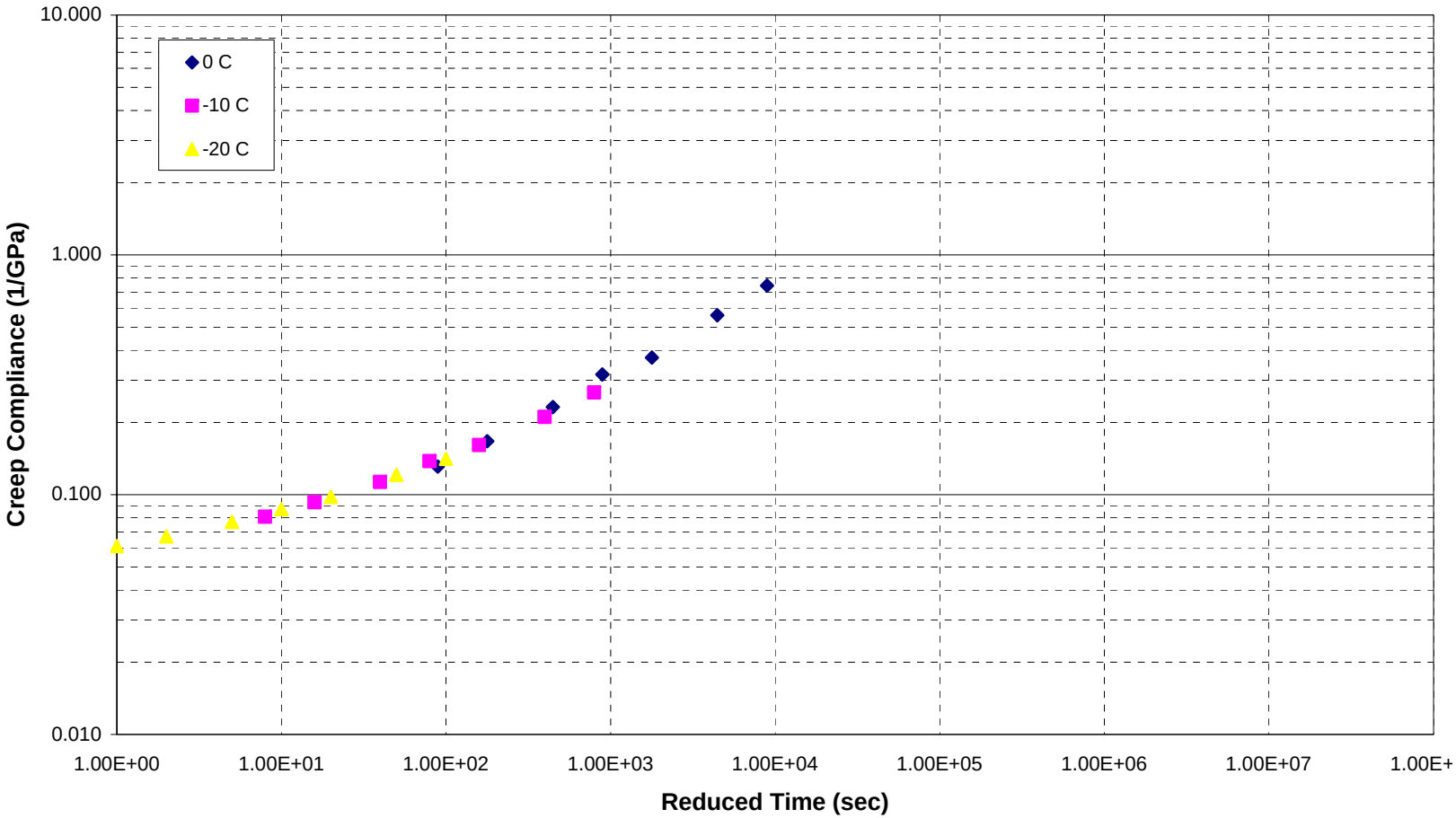

Figure C - 35. Creep Compliance Master Curve - CSRHP Hearst 2

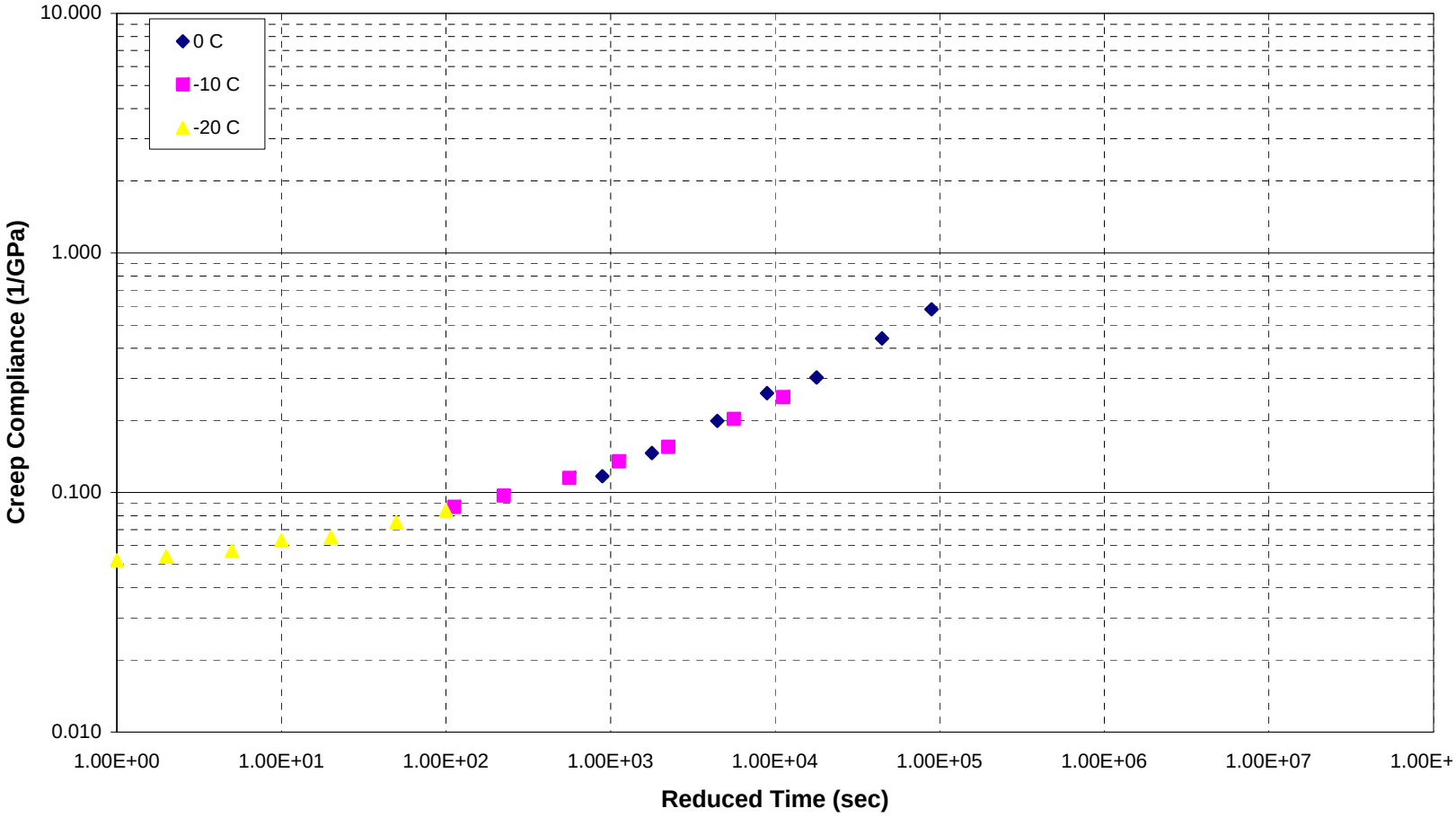

Figure C - 36. Creep Compliance Master Curve - CSRHP Hearst 3

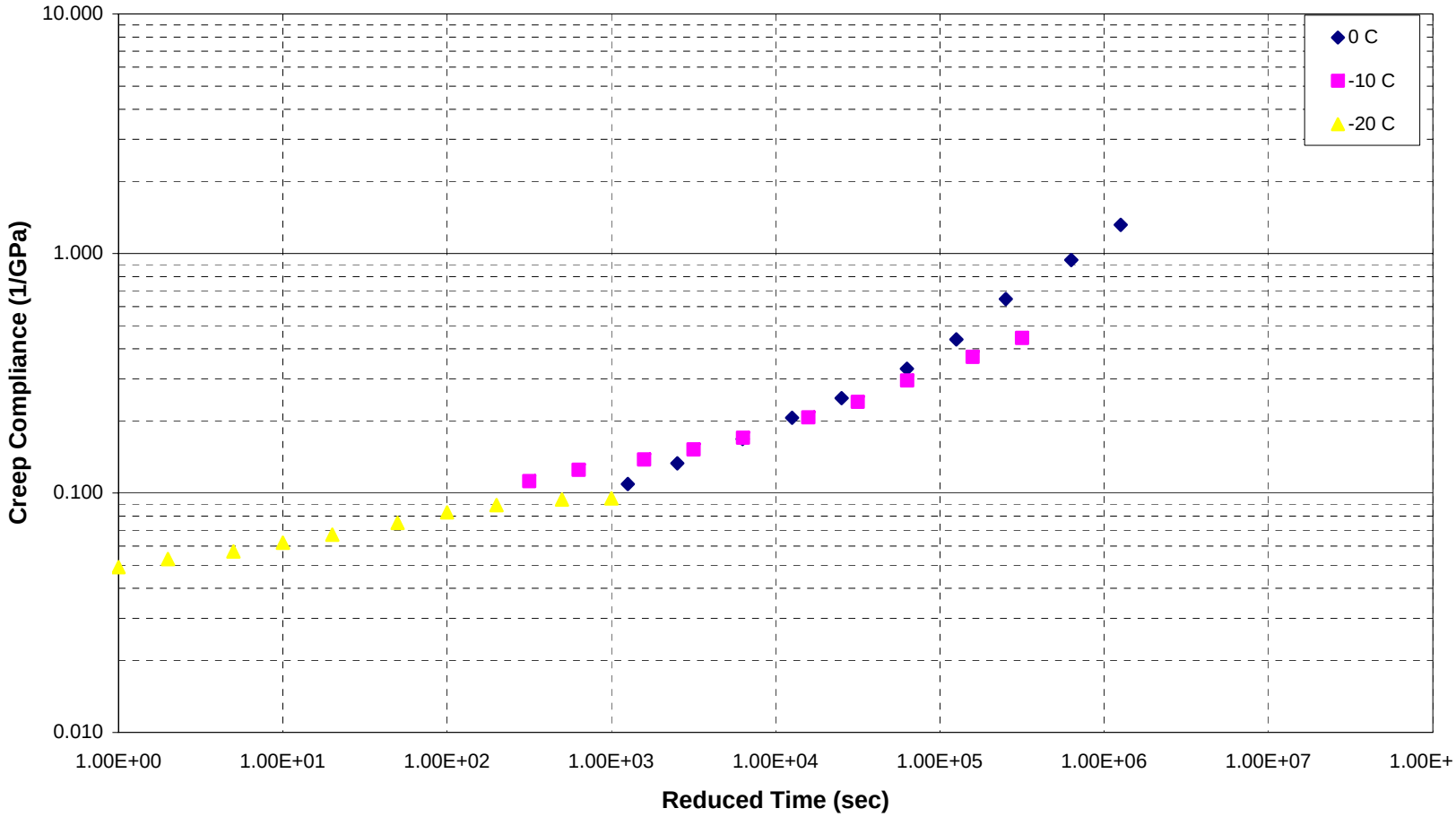

Figure C - 37. Creep Compliance Master Curve - Mn/Road Cell 16

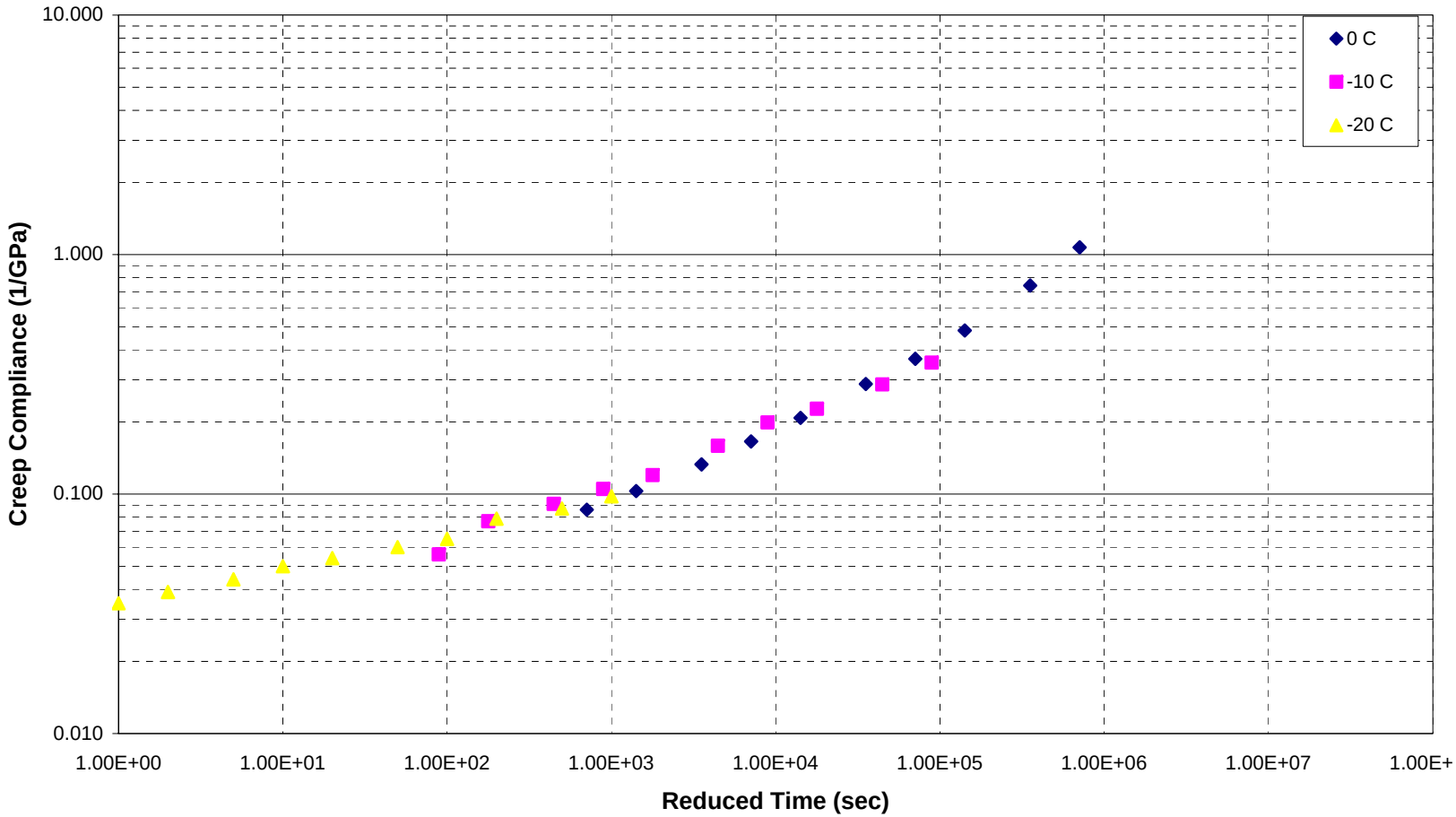

Figure C - 38. Creep Compliance Master Curve - Mn/Road Cell 17

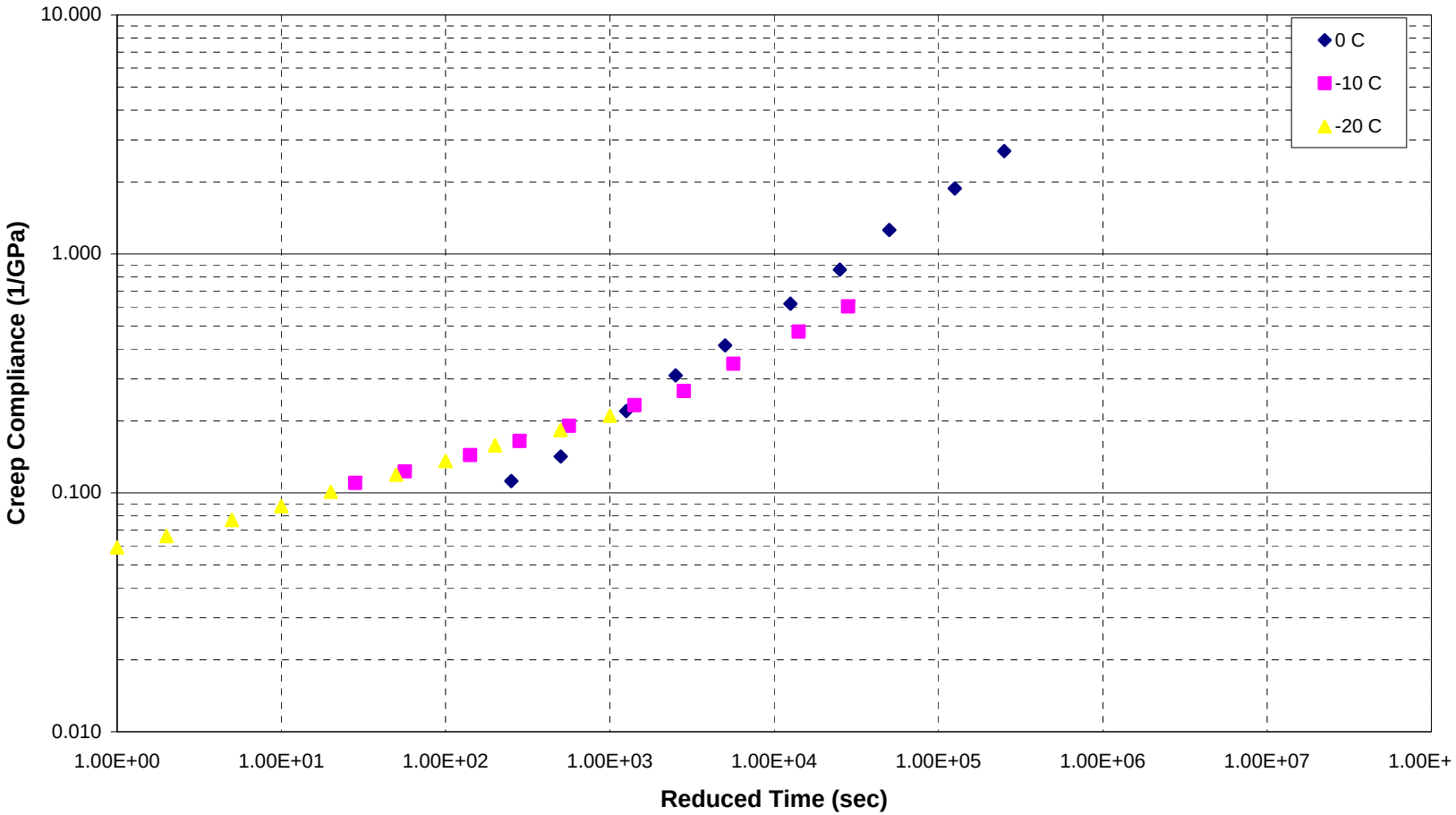

Figure C - 39. Creep Compliance Master Curve - Mn/Road Cell 26

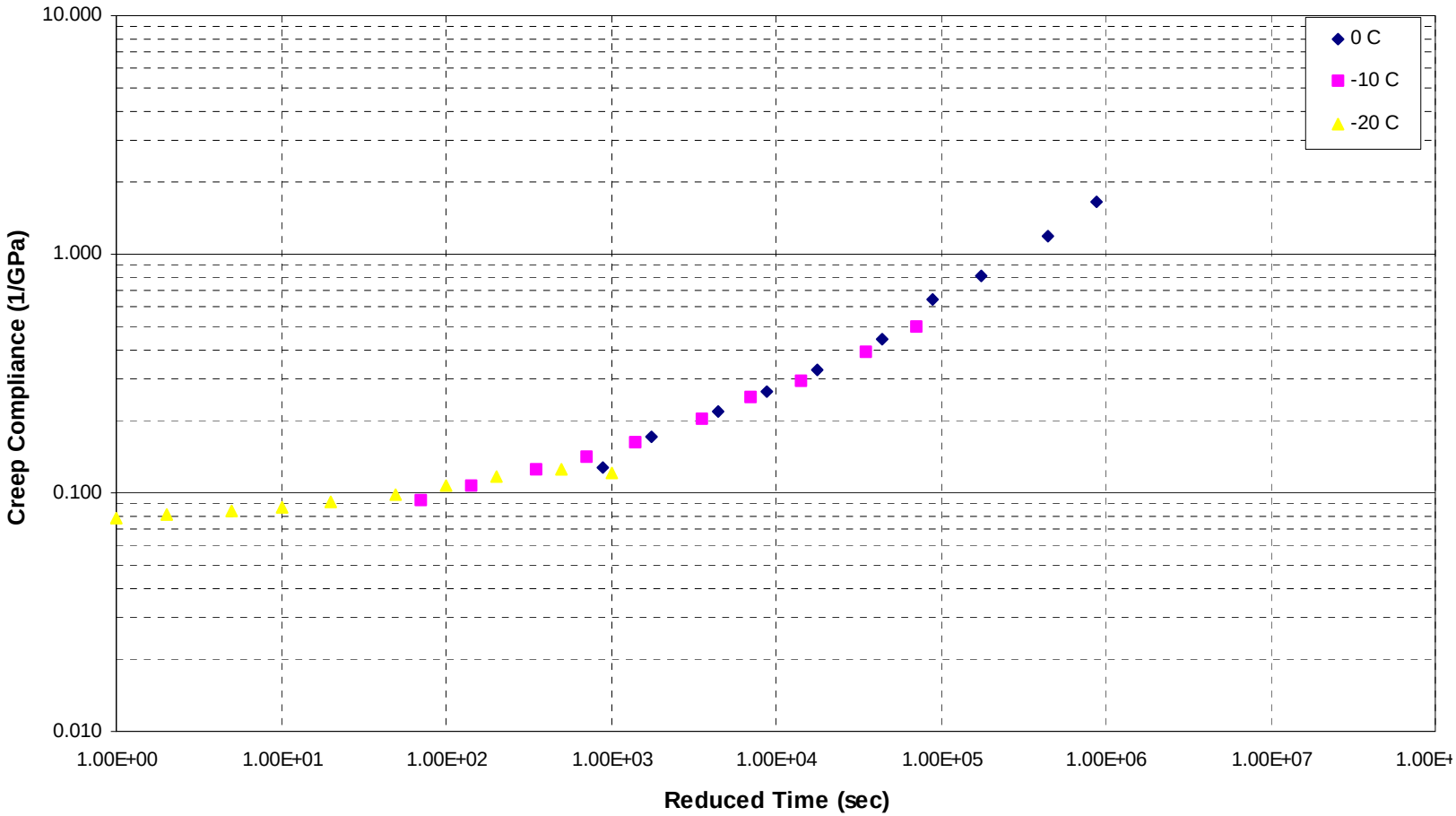

Figure C - 40. Creep Compliance Master Curve - Mn/Road Cell 27

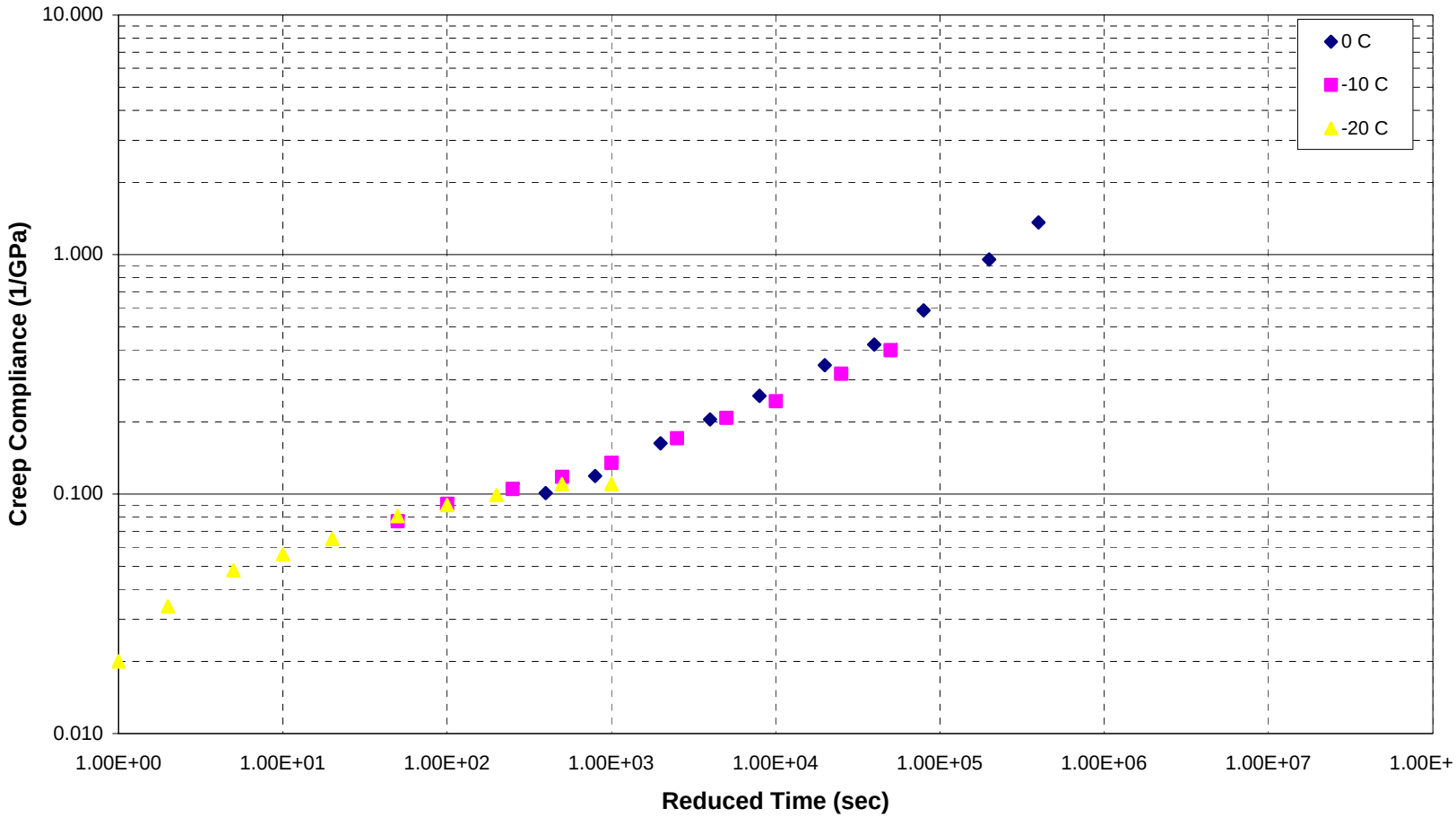

Figure C - 41. Creep Compliance Master Curve - Mn/Road Cell 30

Appendix D

Shift Factors and Fitted Model Parameters

Table D.2.a. Shift Factor and Power Law Parameter Results: SHRP General Pavement Study Mixtures

Parameter	404086	041022	322027	201005
Log (1/shift factor), -10°C[1]	2.70	1.90	5.85	1.55
Log (1/shift factor), 0°C[1]	3.90	3.95	5.75	3.35
D_o, (1/psi)	1.26E-07	1.58E-07	2.67E-07	2.63E-07
D_1, (1/psi)	2.15E-08	2.02E-08	9.21E-08	6.57E-08
D_2, (1/psi)	3.99E-08	5.22E-08	3.80E-08	7.79E-08
D_3, (1/psi)	3.71E-08	6.12E-08	1.53E-07	6.96E-08
D_4, (1/psi)	1.52E-07	2.23E-07	---[2]	1.70E-07
τ_1, (sec)	1.18	1.19	1.96	1.07
τ_2, (sec)	2.36	2.38	3.93	2.14
τ_3, (sec)	3.54	3.57	5.89	3.21
τ_4, (sec)	4.72	4.76	---[2]	4.28
Log η_v, (psi-sec)	12.53	12.03	14.36	11.91
Power Model Parameters				
D_o, (1/psi)	1.08E-07	1.39E-07	2.97E-07	8.69E-08
D_1, (1/psi)	2.07E-08	1.78E-08	1.28E-08	1.75E-07
m-value	0.2117	0.2632	0.1977	0.1072

Table D.1.b. Shift Factor and Power Law Parameter Results: SHRP General Pavement Study Mixtures

Parameter	161010	161001	311030	491008
Log (1/shift factor), -10°C[1]	1.00	2.25	2.50	5.20
Log (1/shift factor), 0°C[1]	3.20	3.65	2.70	5.35
D_o, (1/psi)	2.12E-07	1.88E-07	2.45E-07	2.18E-07
D_1, (1/psi)	4.35E-08	3.76E-08	1.21E-07	4.01E-08
D_2, (1/psi)	1.02E-07	8.54E-08	1.26E-07	5.10E-08
D_3, (1/psi)	5.30E-08	7.05E-08	1.76E-07	6.22E-09
D_4, (1/psi)	2.67E-07	3.57E-07	6.32E-07	1.11E-07
τ_1, (sec)	1.04	1.13	0.94	1.47
τ_2, (sec)	2.08	2.26	1.88	2.94
τ_3, (sec)	3.12	3.39	2.82	4.41
τ_4, (sec)	4.16	4.52	3.76	5.88
Log η_v, (psi-sec)	11.53	11.86	10.73	14.01
Power Model Parameters				
D_o, (1/psi)	1.42E-07	1.38E-07	2.10E-07	2.42E-07
D_1, (1/psi)	7.18E-08	4.76E-08	6.45E-08	6.71E-09
m-value	0.1898	0.2160	0.3103	0.2259

[1]Reference Temperature = -20°C

[2]Used three Voight-Kelvin Units (Spring-Dashpot Pairs)

Table D.1.c. Shift Factor and Power Law Parameter Results: SHRP General Pavement Study Mixtures

Parameter	561007	081047	211034	404088
Log (1/shift factor), -10°C[1]	1.85	2.55	2.20	1.70
Log (1/shift factor), 0°C[1]	2.55	3.75	4.05	2.35
D_o, (1/psi)	2.79E-07	2.35E-07	1.93E-07	2.29E-07
D_1, (1/psi)	5.43E-08	5.35E-08	2.96E-08	6.24E-08
D_2, (1/psi)	9.55E-08	2.39E-08	7.26E-08	3.34E-08
D_3, (1/psi)	4.17E-08	9.57E-08	7.38E-08	5.39E-08
D_4, (1/psi)	3.04E-07	1.95E-07	3.65E-07	2.08E-07
τ_1, (sec)	0.91	1.15	1.21	0.87
τ_2, (sec)	1.82	2.30	2.42	1.74
τ_3, (sec)	2.73	3.45	3.63	2.61
τ_4, (sec)	3.64	4.60	4.84	3.48
Log η_v, (psi-sec)	10.68	12.32	12.03	10.85
Power Model Parameters				
D_o, (1/psi)	2.25E-07	2.20E-07	1.71E-07	1.81E-07
D_1, (1/psi)	6.21E-08	2.36E-08	2.26E-08	5.93E-08
m-value	0.2440	0.2479	0.2670	0.2136

Table D.1.d. Shift Factor and Power Law Parameter Results: SHRP General Pavement Study Mixtures

Parameter	241634	451008	341011	291010
Log (1/shift factor), -10°C[1]	1.65	4.00	2.10	4.35
Log (1/shift factor), 0°C[1]	3.00	3.50	4.00	6.10
D_o, (1/psi)	2.13E-07	2.98E-07	1.88E-07	2.01E-07
D_1, (1/psi)	6.85E-08	8.20E-08	4.39E-08	3.76E-08
D_2, (1/psi)	1.26E-07	6.93E-08	8.61E-08	5.60E-08
D_3, (1/psi)	1.03E-07	1.96E-08	1.04E-07	9.79E-08
D_4, (1/psi)	6.81E-07	3.15E-07	7.42E-07	3.43E-07
τ_1, (sec)	1.00	1.20	1.20	1.62
τ_2, (sec)	2.00	2.40	2.40	3.24
τ_3, (sec)	3.00	3.60	3.60	4.86
τ_4, (sec)	4.00	4.80	4.80	6.48
Log η_v, (psi-sec)	11.08	12.61	11.75	14.27
Power Model Parameters				
D_o, (1/psi)	1.65E-07	2.96E-07	1.75E-07	2.14E-07
D_1, (1/psi)	5.65E-08	2.82E-08	1.80E-08	6.87E-09
m-value	0.2821	0.2351	0.3337	0.2710

[1]Reference Temperature = -20°C

Table D.1.e. Shift Factor and Power Law Parameter Results: SHRP General Pavement Study Mixtures

Parameter	421597	181028	231026	181037
Log (1/shift factor), -10°C[1]	3.70	2.75	1.55	0.90
Log (1/shift factor), 0°C[1]	4.25	3.25	2.15	1.70
D_o, (1/psi)	2.46E-07	3.02E-07	2.33E-07	1.60E-07
D_1, (1/psi)	4.72E-08	6.29E-08	1.25E-07	1.40E-08
D_2, (1/psi)	6.44E-08	4.70E-08	2.36E-08	1.21E-08
D_3, (1/psi)	7.88E-09	6.92E-08	1.69E-07	1.92E-08
D_4, (1/psi)	1.68E-07	3.17E-07	8.97E-07	1.45E-07
τ_1, (sec)	1.25	1.05	0.83	0.74
τ_2, (sec)	2.50	2.10	1.66	1.48
τ_3, (sec)	3.75	3.15	2.49	2.22
τ_4, (sec)	5.00	4.20	3.32	2.96
Log η_v, (psi-sec)	12.56	10.99	9.86	10.55
Power Model Parameters				
D_o, (1/psi)	2.23E-07	3.01E-07	2.43E-07	1.51E-07
D_1, (1/psi)	3.38E-08	1.67E-08	2.74E-08	1.19E-08
m-value	0.1754	0.3478	0.4764	0.3589

Table D.1.f. Shift Factor and Power Law Parameter Results: SHRP General Pavement Study Mixtures

Parameter	271087	271028
Log (1/shift factor), -10°C[1]	2.55	2.85
Log (1/shift factor), 0°C[1]	3.25	3.35
D_o, (1/psi)	2.09E-07	1.89E-07
D_1, (1/psi)	6.69E-08	5.65E-08
D_2, (1/psi)	5.55E-08	1.05E-07
D_3, (1/psi)	6.25E-08	3.24E-08
D_4, (1/psi)	2.14E-07	2.01E-07
τ_1, (sec)	1.05	1.07
τ_2, (sec)	2.10	2.14
τ_3, (sec)	3.15	3.21
τ_4, (sec)	4.20	4.28
Log η_v, (psi-sec)	11.46	11.96
Power Model Parameters		
D_o, (1/psi)	1.97E-07	1.82E-07
D_1, (1/psi)	3.05E-08	3.45E-08
m-value	0.2609	0.2370

[1]Reference Temperature = -20°C

Table D.2.a. Shift Factor and Power Law Parameter Results: Canadian SHRP Mixtures

Parameter	Lamont 1	Lamont 2	Lamont 3	Lamont 4
Log (1/shift factor), -10°C[1]	2.05	2.55	1.50	0.30
Log (1/shift factor), 0°C[1]	2.20	2.90	2.50	0.90
D_o, (1/psi)	3.80E-07	3.18E-07	3.87E-07	3.85E-07
D_1, (1/psi)	9.84E-08	1.06E-07	2.15E-07	3.44E-08
D_2, (1/psi)	6.30E-08	1.14E-07	1.65E-06	4.14E-07
D_3, (1/psi)	1.24E-07	5.09E-08	---[2]	---[2]
D_4, (1/psi)	3.43E-07	6.16E-07	---[2]	---[2]
τ_1, (sec)	0.84	0.98	1.50	0.97
τ_2, (sec)	1.68	1.96	3.00	1.93
τ_3, (sec)	2.52	2.94	---[2]	---[2]
τ_4, (sec)	3.36	3.92	---[2]	---[2]
Log η_v, (psi-sec)	10.47	10.73	9.50	8.77
Power Model Parameters				
D_o, (1/psi)	3.43E-07	3.39E-07	3.14E-07	3.33E-07
D_1, (1/psi)	6.22E-08	2.44E-08	6.30E-08	4.94E-08
m-value	0.2936	0.3809	0.4537	0.4736

Table D.2.b. Shift Factor and Power Law Parameter Results: Canadian SHRP Mixtures

Parameter	Lamont 5	Lamont 6	Lamont 7	Sherbrooke A
Log (1/shift factor), -10°C[1]	0.95	1.55	1.40	0.95
Log (1/shift factor), 0°C[1]	1.70	1.75	2.05	2.90
D_o, (1/psi)	5.56E-07	4.55E-07	3.80E-07	3.67E-07
D_1, (1/psi)	8.01E-08	1.79E-07	1.38E-07	1.01E-07
D_2, (1/psi)	2.05E-07	2.96E-07	1.26E-07	2.48E-07
D_3, (1/psi)	1.69E-07	5.41E-07	1.67E-07	3.48E-07
D_4, (1/psi)	8.66E-07	---[3]	1.68E-06	1.52E-06
τ_1, (sec)	0.74	0.94	0.81	0.98
τ_2, (sec)	1.48	1.88	1.62	1.96
τ_3, (sec)	2.22	2.81	2.43	2.94
τ_4, (sec)	2.96	---[3]	3.24	3.92
Log η_v, (psi-sec)	9.62	9.36	9.33	10.45
Power Model Parameters				
D_o, (1/psi)	4.08E-07	3.34E-07	3.74E-07	3.18E-07
D_1, (1/psi)	1.48E-07	1.36E-07	4.31E-08	6.24E-08
m-value	0.3091	0.3393	0.5187	0.3808

[1]Reference Temperature = -20°C
[2]Used two Voight-Kelvin Units (Spring-Dashpot Pairs)
[3]Used three Voight-Kelvin Units (Spring-Dashpot Pairs)

Table D.2.c. Shift Factor and Power Law Parameter Results: Canadian SHRP Mixtures

Parameter	Sherbrooke B	Sherbrooke C	Sherbrooke D	Hearst 1
Log (1/shift factor), -10°C[1]	1.85	0.45	1.40	0.20
Log (1/shift factor), 0°C[1]	2.90	2.10	2.70	1.10
D_o, (1/psi)	1.77E-07	2.66E-07	2.19E-07	5.12E-07
D_1, (1/psi)	5.38E-08	6.11E-08	6.69E-08	-2.54E-08
D_2, (1/psi)	6.11E-08	8.94E-08	1.20E-07	1.32E-06
D_3, (1/psi)	7.49E-08	3.10E-07	1.74E-07	---[2]
D_4, (1/psi)	3.96E-07	7.36E-07	8.18E-07	---[2]
τ_1, (sec)	0.98	0.82	0.94	1.03
τ_2, (sec)	1.96	1.64	1.88	2.07
τ_3, (sec)	2.94	2.46	2.82	---[2]
τ_4, (sec)	3.92	3.28	3.76	---[2]
Log η_v, (psi-sec)	11.03	10.16	10.27	8.55
Power Model Parameters				
D_o, (1/psi)	1.61E-07	2.26E-07	2.00E-07	4.15E-07
D_1, (1/psi)	2.71E-08	4.52E-08	3.20E-08	7.06E-08
m-value	0.3190	0.4234	0.4103	0.5559

Table D.2.d. Shift Factor and Power Law Parameter Results: Canadian SHRP Mixtures

Parameter	Hearst 2	Hearst 3
Log (1/shift factor), -10°C[1]	0.90	2.05
Log (1/shift factor), 0°C[1]	1.95	2.95
D_o, (1/psi)	4.03E-07	3.56E-07
D_1, (1/psi)	1.39E-07	5.78E-08
D_2, (1/psi)	2.28E-07	2.20E-07
D_3, (1/psi)	2.43E-07	1.50E-07
D_4, (1/psi)	1.72E-06	1.14E-06
τ_1, (sec)	0.79	0.99
τ_2, (sec)	1.58	1.98
τ_3, (sec)	2.37	2.97
τ_4, (sec)	3.16	3.96
Log η_v, (psi-sec)	9.57	10.63
Power Model Parameters		
D_o, (1/psi)	3.28E-07	3.19E-07
D_1, (1/psi)	1.03E-07	4.74E-08
m-value	0.4005	0.3622

[1]Reference Temperature = -20°C
[2]Used two Voight-Kelvin Units (Spring-Dashpot Pairs)

Table D.3. Shift Factor and Power Law Parameter Results: Mn/ROAD Mixtures

Parameter	Cell 16	Cell 17	Cell 26	Cell 27	Cell 30
Log (1/shift factor), -10°C[1]	2.50	1.95	1.45	1.85	1.70
Log (1/shift factor), 0°C[1]	3.10	2.85	2.40	2.95	2.60
D_o, (1/psi)	3.63E-07	2.52E-07	4.00E-07	5.45E-07	2.95E-07
D_1, (1/psi)	1.20E-06	1.20E-07	3.09E-07	8.80E-08	1.52E-06
D_2, (1/psi)	5.67E-07	1.84E-07	3.31E-07	1.83E-07	5.93E-07
D_3, (1/psi)	1.61E-07	3.76E-07	2.04E-07	5.21E-07	7.26E-08
D_4, (1/psi)	2.15E-07	1.47E-06	4.29E-06	2.78E-06	3.02E-07
τ_1, (sec)	5.10	1.17	1.08	1.19	4.60
τ_2, (sec)	3.83	2.34	2.16	2.38	3.45
τ_3, (sec)	2.96	3.51	3.24	3.57	2.67
τ_4, (sec)	1.68	4.68	4.32	4.76	1.52
Log η_v, (psi-sec)	11.27	11.16	10.27	11.08	10.77
Power Model Parameters					
D_o, (1/psi)	6.00E-07	3.81E-07	6.29E-07	5.78E-07	3.96E-07
D_1, (1/psi)	2.42E-09	8.89E-09	1.37E-08	1.47E-08	4.24E-09
m-value	0.5800	0.4922	0.5783	0.4819	0.5650

[1]Reference Temperature = -20°C

ANNEX- B

TCModel Recalibration

TCMODEL Recalibration: Spring 2003

Draft, June 3, 2003, by WG Buttlar

The final stage of TMODEL calibration involved checking the previous calibration against the more finalized design guide software package. In particular, it was anticipated that the difference between the pavement temperatures generated with the old TCMODEL procedures (which used version 2.0 of ICM, or earlier, I believe) and the latest ICM engine in DG2002, could be significant. The version of ICM used in the earlier calibration of TCMODEL (Spring, 2001) was over 10 years old, and a number of revisions, including bug fixes and more significant modeling changes have since taken place. Thus, it was deemed necessary to check, and if necessary, recalibrate levels 1 and 2 once again. In general, *thermal cracking was found to be under predicted when TCMODEL was combined with the most recent ICM version*. This can be observed in Tables 1 and 2.

The original calibration of TCMODEL involved three factors: β_1, σ, and E, which are selected parameters in the distress modeling system within TCMODEL, as follows:

$$AC = \beta_1 * N\left(\frac{\log C/D}{\sigma}\right) \qquad (5.24)$$

where:

AC	=	observed amount of thermal cracking
β_1	=	regression coefficient determined through field calibration
$N()$	=	standard normal distribution evaluated at ()
σ	=	standard deviation of the log of the depth of cracks in the pavement
C	=	crack depth
D	=	thickness of surface layer

The amount of crack propagation induced by a given thermal cooling cycle can be predicted using the Paris law of crack propagation:

$$\Delta C = A\Delta K^n \qquad \textbf{(2.8)}$$

where:

ΔC	=	change in the crack depth due to a cooling cycle
ΔK	=	change in the stress intensity factor due to a cooling cycle
A, n	=	fracture parameters

Where, experiments by Molenaar (1984) led to the following relationship:

$$\log A = 4.389 - 2.52 * \log(E * \sigma_m * n) \qquad \textbf{(2.9)}$$

where: E = mixture stiffness

σ_m = mixture tensile strength, undamaged

and:

$$n = 0.8 * (1 + \frac{1}{m}) \quad \textbf{(2.11)}$$

In the course of recalibrating TCMODEL in the winter of 2003, a new calibration parameter, β_2, was introduced as follows:

$$A = 10\text{^}(\beta_2 * (4.389 - 2.52 * \log(E * \sigma_m * n)) \quad \textbf{(2.9)}$$

In the course of recalibrating, the way in which TCMODEL reacted to various calibration parameters was reevaluated. In particular, the usefulness of parameter of β_1 (the multiplier placed on the probabilistic crack distribution model) was studied and found to be of marginal usefulness. This is because β_1 sets the upper limit for the amount of cracking that can be achieved in the model. In the past it was set at 353.47, which allowed a maximum number of cracks per 500 feet of 353.47/2 or about 176.7. However, the original model was intended to allow up to 200 feet/ 500 feet, or a crack spacing of 30 feet. Therefore, further calibrations of TCMODEL were made with a fixed value of 400 for β_1.

A more logical calibration approach appeared to involve the tuning of the fracture equations. This is because it was felt that the response model (far field thermal stress prediction) in TCMODEL was the most accurate portion of the model, while the LEFM fracture approach represented a more phenomenological aspect of the model, which needed a fair amount of calibration. Two methods of calibrating TCMODEL using fracture parameters was explored: 1) calibrating the 'E' parameter, and; 2) calibrating the delta-K parameter (β_2). Although similar model sensitivity was observed, the β_2 multiplier placed on the delta-K term of the Paris law crack growth model was the simpler of the two approaches and was therefore deemed the most appropriate.

As evident in Tables 1, the β_2 values were varied to create more conservative thermal cracking predictions. In particular, the new calibration parameters appeared to improve the underprediction of thermal cracking in GPS sections: 404086, 311030, and four of the five Mn/ROAD sections. More sections with low cracking predictions would undoubtedly have been noted, but only those listed in Table 1 were checked using the new ICM and 2001 calibration factors (at the present time). For the new calibration approaches, additional predictions were made to help fine-tune the parameters. Unfortunately, the available field data and site-specific information was insufficient to make all 41 predictions used in the original (2001) calibration. For example, the fourteen CSHRP sites could not be used, since the DG software does not currently include climatic data outside the United States. In addition, specific inputs to the climatic model, including depth to water table, thermal conductivity, heat capacity, etc., were not available and default values were used. Finally, not all locations of GPS sites could be matched up with a suitable weather station from currently available sites. Thus, a more rigorous approach

to recalibration of TCMODEL (such as the iterative, statistical press procedure used in earlier TCMODEL calibration efforts) does not seem to be justified at the present time, until more exact site specific information and age-appropriate fundamental material properties are available.

It may be noted that the predictive accuracy under the newest calibration is not as highly correlated as was found in 2001. This is not unexpected, because:

1) In 2001, the climatic data matched the service years of the pavements, while the current calibration uses the default weather data in the DG (in general, the past six years)

2) In 2001, the press procedure was used to fully optimize predictive accuracy.

Also as expected, the new level 1 predictive accuracy exceeds the level 2 accuracy. A more thorough comparison of level 2 and 3 thermal cracking predictions is recommended, as it is possible that level 3 predictions could eventually surpass those of level 2, depending upon the calibration rigor employed.

In summary, for national calibration, the following parameters are recommended based upon available data:

Level 1 analysis:

- k = 10,000
- β_1 = 400
- σ = 0.769
- β_2 = 5.0

Level 2 analysis:

- k = 10,000
- β_1 = 400
- σ = 0.769
- β_2 = 1.5

Local calibration is encouraged, which will have the added benefit of using mixtures from mix design, sampled at the hot-mix plant, or from field cores taken at the time of construction. Currently, the available data being used for calibration involves field-aged cores, taken at the time of the thermal cracking observation (greater than 10 years in service in some cases).

Table 1. Thermal Cracking Predictions, Chronological Summary, Level 1

SHRP ID	PTI Code	Location	Observed Cracking (ft/500 ft)	Predicted Cracking (ft/500 ft) 2001 Calibration (Spring 2001)	Predicted Cracking (ft/500 ft) After ICM Changes – Using 2001 Calibration.	Predicted Cracking (ft/500 ft) L1 Feb 03		
						E-1500, Beta1=400	E-10000, Beta1=400, Beta2=3	E-10000, Beta1=400, Beta2=5
404086	01-M	Chickasaw, OK	**96**	75		0	0	76.9
041022	02-M	Hackberry, AZ	**0**	11	0	0	0	0
322027	06-M	Oasis, NV	**≥200**	177		177	200	200
201005	07-M	Ottawa, KS	**≥200**	177	143	159.1	177.1	200
161010	11-M	Idaho Falls, ID-20	**≥200**	176		176	200	200
161001	12-M	Coeur D'Alene, ID-16	**0**	13	0	44.6		
311030	13-M	Edison, NE-8	**36**	8	0	7.1	0.3	38.2
491008	16-M	Marysvale, UT-17	**≥200**	174		157.5	200	200
561007	17-M	Cody, WY	**≥200**	177		200	200	200
081047	18-M	Rangley, CO	**≥200**	177		200	200	200
211034	21-M	Glasgow, KY	**0**	NA				
404088	22-M	Ponca City, OK	**96**	NA				
241634	23-M	Berlin, MD	**0**	0		0	0	0
451008	26-M	Salem, SC	**96**	177		200	200	200
341011	27-M	Trenton, NJ	**36**	0		200	200	200
291010	28-M	Waynesville, MO	**120**	177	100.6	149.9	142.4	159.9
421597	31-M	Lawrenceville, PA	**24**	NA				
181028	32-M	Huntington, IN	**12**	5		72.4	49.2	75.5
231026	33-M	Farmington, ME	**12**	0		0.7	0	0
181037	36-M	Boonville, IN	**≥200**	NA				
271087	37-M	Farmington, MN	**132**	177		145.7	144.2	151.8
271028	38-M	Frazee, MN	**≥200**	177		200	200	200
Cell 16	Mn/ROAD	≥200	177	0	0	170.6	200	200
Cell 17	Mn/ROAD	≥200	177		0	130.8	29.5	134
Cell 26	Mn/ROAD	0	14	0	0	0	0	0
Cell 27	Mn/ROAD	≥200	177	0	0	200	3.5	91.6
Cell 30	Mn/ROAD	108	130	0	0	0.3	0	2

Table 2. Thermal Cracking Predictions, Chronological Summary, Level 2

SHRP ID	PTI Code	Location	Observed Cracking (ft/500 ft)	Predicted Cracking (ft/500 ft) 2001 Calibration (Spring 2001)	Predicted Cracking (ft/500 ft) After ICM Changes – Using 2001 Calibration.	Predicted Cracking (ft/500 ft) L2 Feb 03		
						E-1500, Beta1=400	E-10000, Beta1=400, Beta2=2	E-10000, Beta1=400, Beta2=1.5
404086	01-M	Chickasaw, OK	**96**	75			185.7	
041022	02-M	Hackberry, AZ	**0**	11		0	0	0
322027	06-M	Oasis, NV	**≥200**	177				200
201005	07-M	Ottawa, KS	**≥200**	177		196.6		198.9
161010	11-M	Idaho Falls, ID-20	**≥200**	176				200
161001	12-M	Coeur D'Alene, ID-16	**0**	13		200		200
311030	13-M	Edison, NE-8	**36**	8		42.3	0	0
491008	16-M	Marysvale, UT-17	**≥200**	174				200
561007	17-M	Cody, WY	**≥200**	177				200
081047	18-M	Rangley, CO	**≥200**	177				200
211034	21-M	Glasgow, KY	**0**	NA				
404088	22-M	Ponca City, OK	**96**	NA				
241634	23-M	Berlin, MD	**0**	0				0
451008	26-M	Salem, SC	**96**	177				0
341011	27-M	Trenton, NJ	**36**	0				0
291010	28-M	Waynesville, MO	**120**	177		200	167.2	150.6
421597	31-M	Lawrenceville, PA	**24**	NA				
181028	32-M	Huntington, IN	**12**	5				151.9
231026	33-M	Farmington, ME	**12**	0				0
181037	36-M	Boonville, IN	**≥200**	NA				
271087	37-M	Farmington, MN	**132**	177			174.2	163.1
271028	38-M	Frazee, MN	**≥200**	177				200
Cell 16	Mn/ROAD	≥200	177	0		200	114.8	15.5
Cell 17	Mn/ROAD	≥200	177				89.5	6.5
Cell 26	Mn/ROAD	0	14	0		171	96.2	0.6
Cell 27	Mn/ROAD	≥200	177	0		200	10.6	1.1
Cell 30	Mn/ROAD	108	130	0		165.7	109.9	10.5

Some additional information regarding the thermal cracking sites:

SHRP ID	PTI[1] Code	Location	AC Thickness (in.)
404086	01-M	Chickasaw, OK	8.5
041022	02-M	Hackberry, AZ	--
322027	06-M	Oasis, NV	9.25
201005	07-M	Ottawa, KS	13.0
161010	11-M	Idaho Falls, ID	10.75
161001	12-M	Coeur D'Alene, ID	3.5
311030	13-M	Edison, NE	7.5
491008	16-M	Marysvale, UT	9.25
561007	17-M	Cody, WY	3.5
081047	18-M	Rangley, CO	4.0
211034	21-M	Glasgow, KY	14.25
404088	22-M	Ponca City, OK	12.5
241634	23-M	Berlin, MD	3.5
451008	26-M	Salem, SC	4.75
341011	27-M	Trenton, NJ	9.25
291010	28-M	Waynesville, MO	13.0
421597	31-M	Lawrenceville, PA	6.25
181028	32-M	Huntington, IN	15.0
231026	33-M	Farmington, ME	6.25
181037	36-M	Boonville, IN	14.0
271087	37-M	Farmington, MN	16.0
271028	38-M	Frazee, MN	9.5

[1]PTI = Pennsylvania Transportation Institute

Mn/ROAD Sections Utilized in the Recalibration of TCMODEL

Section ID	Traffic Volume	Location	AC Thickness (in.)
Cell 16	High/ I-94	Ostego, Minnesota	7.75
Cell 17	High/ I-94	Ostego, Minnesota	7.75
Cell 26	Low/ Closed Loop	Ostego, Minnesota	6.0
Cell 27	Low/ Closed Loop	Ostego, Minnesota	3.0
Cell 30	Low/ Closed Loop	Ostego, Minnesota	5.0

Future Research Areas (copied from earlier write-up, Chapter 4)

Although this report summarizes improvements to TCMODEL that should result in more accurate, more reliable thermal cracking predictions, there are still portions of TCMODEL that could be improved in the future that were not addressed in this work. One area worthy of study is the effect of mixture aging in the field on thermal cracking development. TCMODEL does not directly account for mixture aging with time; however, the model assumes that the very top of the pavement (the top 2.54 mm or 0.1") has numerous "starter crack" locations. The assumption that starter cracks are present allows the use of a single crack propagation law (Paris law for stable crack growth), which eliminates the need for a crack initiation model. The presence of starter cracks partially eliminates the importance of having a mixture aging model included as part of the thermal cracking model, since the pavement aging gradient is most severe at the very surface of the pavement. In addition, the fact that TCMODEL is calibrated to field performance also indirectly accounts for the effects of mixture aging in the field. In the future, TCMODEL can be improved once a better understanding of the effects of mixture aging on fracture behavior is obtained.

A second area where TCMODEL can be improved in the future which is also related to fracture, is in the utilization of tensile strength data. Currently, TCMODEL utilizes mixture tensile strength at a single test temperature of -10 C, and then develops fracture parameters by taking this value as an estimate of the undamaged tensile strength of the mixture, as described in chapter 2, along with a slope parameter from the master compliance curve (m-value). In the future, TCMODEL can be improved once a better understanding of mixture fracture behavior is obtained, and when improved fracture models are available. A third area where TCMODEL can be improved in the future is in the response model. Currently a pseudo two-dimensional pavement response model is used, which accounts only for temperature-induced stresses and strains. Recent work has indicated that traffic loads applied during critical cooling events can increase tensile stresses by more than fifty percent (Waldhoff, Buttlar and Kim [2000]). Although TCMODEL is calibrated to field performance and therefore indirectly accounts for average traffic effects, as three-dimensional finite element modeling becomes more computationally efficient, an improved response model should be incorporated into TCMODEL.

ANNEX- C

Sensitivity Analysis for the Level 3 Thermal Cracking Model

NCHRP 1-37 A

Development of the 2002 Guide for the Design of New and Rehabilitated Pavement Structures

Inter Team Technical Report

Sensitivity Analysis for the Level 3 Thermal Cracking Model

July 2003

TABLE OF CONTENTS

LIST OF TABLES

LIST OF FIGURES

1. OBJECTIVES

A sensitivity analysis was carried out to evaluate the validity of the Level 3 Thermal Cracking model (TCModel) built into the 2002 Design Guide. The parameters identified as key factors in the performance of the model were the climate, the binder type, and the asphalt thickness. The runs associated with these factors were run three times to assess the effect of the beta factor in the Paris Law and in the subsequent thermal cracking prediction. Values of $\beta = 1.0$, 3.0, and 5.0 were used.

To evaluate the impact of climate, a random city, located in a particular climatic region within the continental USA, was chosen to be representative of the area. Nine different regions were identified to cover the entire country. In addition, a site in Barrow, Alaska was added to the initial nine locations considered, to be representative of a very cold site.

Seven binders with PG grades varying from 82-10 to 46-46 were analyzed for each of the ten environmental locations. In addition, three different asphalt thickness levels, per site, were evaluated in this analysis to assess thermal fracture trends as a function of the asphalt layer thickness.

2. INPUT PARAMETERS

Design Life: 20 years
Initial IRI: 63 in/mi
Analysis Type: Deterministic

2.1 Traffic

Default and historical traffic values were used in the analysis. While this parameter is necessary to run the 2002 Design Guide program, it is not a factor in the Thermal Fracture analysis.

2.1.1 General Traffic Inputs

The general traffic inputs used in the analysis are the following:

- Two-way average annual daily truck traffic: 1000
- Number of lanes in design direction: 2
- Percent of trucks in design direction (%): 50
- Percent of trucks in design lane (%): 95
- Operational speed (mph): 60
- Mean wheel location (inches from the lane marking) 18
- Traffic wander standard deviation (in): 10
- Design lane width (ft): 12
- Mean wheel location (inches from the lane marking) 18
- Traffic wander standard deviation (in) 10
- Design lane width (ft) 12

2.1.2 Monthly Adjustment Factors

Table 1 shows the monthly adjustment factors:

Table 1 Monthly Adjustment Factors

Month	Vehicle Class									
	Class 4	Class 5	Class 6	Class 7	Class 8	Class 9	Class 10	Class 11	Class 12	Class 13
January	1.00	1.00	1.00	1.00	1.00	1.00	1.00	1.00	1.00	1.00
February	1.00	1.00	1.00	1.00	1.00	1.00	1.00	1.00	1.00	1.00
March	1.00	1.00	1.00	1.00	1.00	1.00	1.00	1.00	1.00	1.00
April	1.00	1.00	1.00	1.00	1.00	1.00	1.00	1.00	1.00	1.00
May	1.00	1.00	1.00	1.00	1.00	1.00	1.00	1.00	1.00	1.00
June	1.00	1.00	1.00	1.00	1.00	1.00	1.00	1.00	1.00	1.00
July	1.00	1.00	1.00	1.00	1.00	1.00	1.00	1.00	1.00	1.00
August	1.00	1.00	1.00	1.00	1.00	1.00	1.00	1.00	1.00	1.00
September	1.00	1.00	1.00	1.00	1.00	1.00	1.00	1.00	1.00	1.00
October	1.00	1.00	1.00	1.00	1.00	1.00	1.00	1.00	1.00	1.00
November	1.00	1.00	1.00	1.00	1.00	1.00	1.00	1.00	1.00	1.00
December	1.00	1.00	1.00	1.00	1.00	1.00	1.00	1.00	1.00	1.00

2.1.3 Vehicle Class Distribution

The default distribution for Level 3 analysis is depicted in Table 2.

Table 2 Vehicle Class Distribution

Class	Distribution
Class 4	1.8%
Class 5	24.6%
Class 6	7.6%
Class 7	0.5%
Class 8	5.0%
Class 9	31.3%
Class 10	9.8%
Class 11	0.8%
Class 12	3.3%
Class 13	15.3%

2.1.4 Hourly Truck Traffic Distribution

The default distribution for Level 3 analysis is depicted in Table 3.

Table 3 Hourly Truck Traffic Distribution

Time	Distribution	Time	Distribution
Midnight	2.3%	Noon	5.9%
1:00 am	2.3%	1:00 pm	5.9%
2:00 am	2.3%	2:00 pm	5.9%
3:00 am	2.3%	3:00 pm	5.9%
4:00 am	2.3%	4:00 pm	4.6%
5:00 am	2.3%	5:00 pm	4.6%
6:00 am	5.0%	6:00 pm	4.6%
7:00 am	5.0%	7:00 pm	4.6%
8:00 am	5.0%	8:00 pm	3.1%
9:00 am	5.0%	9:00 pm	3.1%
10:00 am	5.9%	10:00 pm	3.1%
11:00 am	5.9%	11:00 pm	3.1%

2.1.5 Traffic Growth Factor

The traffic growth factor for each Class is depicted in Table 4.

Table 4 Traffic Growth Factors

Vehicle Class	Growth Rate	Growth Function
Class 4	4.0%	Compound
Class 5	4.0%	Compound
Class 6	4.0%	Compound
Class 7	4.0%	Compound
Class 8	4.0%	Compound
Class 9	4.0%	Compound
Class 10	4.0%	Compound
Class 11	4.0%	Compound
Class 12	4.0%	Compound
Class 13	4.0%	Compound

2.1.6 Number of Axles per Truck

The number of axles per truck is shown in Table 5.

Table 5 Number of Axles per Truck

Vehicle Class	Single Axle	Tandem Axle	Tridem Axle	Quad Axle
Class 4	1.62	0.39	0.00	0.00
Class 5	2.00	0.00	0.00	0.00
Class 6	1.02	0.99	0.00	0.00
Class 7	1.00	0.26	0.83	0.00
Class 8	2.38	0.67	0.00	0.00
Class 9	1.13	1.93	0.00	0.00
Class 10	1.19	1.09	0.89	0.00
Class 11	4.29	0.26	0.06	0.00
Class 12	3.52	1.14	0.06	0.00
Class 13	2.15	2.13	0.35	0.00

2.1.7 Axle Configuration

The following information was used for axle configurations:

- Average axle width (edge to edge) outside dimensions, ft: 8.5
- Dual tire spacing (in): 12
- Tire pressure – Single tire (psi): 120
- Tire pressure – Dual tire (psi): 120
- Average axle spacing – Tandem axle (in): 51.6
- Average axle spacing – Tridem axle (in): 49.2
- Average axle spacing – Quad axle (in): 49.2

2.2 Environmental Conditions

Nine climatic regions within the continental United States were chosen for this analysis. From each climatic region, a representative location was chosen and the environmental conditions for that location were used to obtain the pavement temperature distribution with depth. The city chosen to be the representative location for each of the nine regions is shown in Table 6. In addition to the nine regions within the continuous US, a city in Alaska was chosen to be representative of a very cold climate. The ground water table depth was fixed at 15 ft from the top of the AC layer for all ten environmental sites.

It was expected that the Mean Annual Air Temperature gave a general indication of the lowest pavement temperature at the surface. To verify this assumption, the frequency distribution of the number of hours at which the pavement surface experienced temperatures lower than 15 ^{o}F is shown in Table 7. The results found correlates well and are in agreement with the MAAT.

Table 6 Cities Representing the Environmental Conditions for Ten Climatic Regions within the United States

Region	Location	Latitude (North)	Longitude (West)	Elevation (ft)	GWT Depth (ft)	MAAT (F)
Alaska	Barrow, AK	71° 17'	156° 46'	35	15	12.21
IA	Chicago, IL	41° 59'	87° 55'	655	15	52.77
IB	Washington, DC	38° 56'	77° 27'	306	15	55.16
IC	San Francisco, CA	37° 37'	122° 24'	86	15	56.76
IIA	Fargo, ND	46° 56'	96° 49'	908	15	42.68
IIB	Oklahoma City, OK	35° 23'	97° 36'	1281	15	60.63
IIC	Dallas, TX	32° 54'	97° 02'	559	15	66.65
IIIA	Billings, MT	45° 49'	108° 32'	3579	15	47.70
IIIB	Las Vegas, NV	36° 05'	115° 01'	2127	15	68.89
IIIC	San Antonio, TX	29° 32'	98° 28'	818	15	68.98

Table 7 Frequency of Hours with Pavement Surface Temperature less than 15 °F

Region	Site	Maat	Frequency of Hours with T < 15 °F				
		(F)	Year 1997	Year 1998	Year 1999	Year 2000	Average
Alaska	Barrow, AK	12.21	---	---	4308	4416	4362
IIA	Fargo, ND	42.68	928	625	612	1029	799
IIIA	Billings, MT	47.70	255	254	41	182	183
IA	Chicago, IL	52.77	180	38	157	186	140
IB	Washington, D.C.	55.16	5	0	0	0	1
IC	San Francisco, CA	56.76	---	0	0	0	0
IIB	Oklahoma City, OK	60.63	6	0	1	0	2
IIC	Dallas, TX	66.65	0	0	0	0	0
IIIB	Las Vegas, NV	68.89	0	0	0	0	0
IIIC	San Antonio, TX	68.98	0	0	0	0	0

2. 3 Pavement Cross Section

Three different asphalt layer thicknesses were evaluated in the sensitivity analysis: 1, 4, and 6 inches. This allowed for the evaluation verification that a greater level of thermal fracture (transverse) cracks should occur on the thinner asphalt sections.

A fixed unbound cross section was used, which included a granular base of 6 inches, a compacted subgrade of 12 inches and a natural subgrade. The bedrock was assumed to be deep enough to have no influence in the analysis. Table 8 shows the thicknesses and the description of each layer.

Table 8 Pavement Cross Section

Layer	Description	Material	Thickness (in)
1	Original surface	Hot mix asphalt	1, 4, 6
2	Granular base	A-1-a	6
3	Compacted subgrade	A-4	12
4	Natural subgrade	A-4	Infinite

2.4 Material Properties

2.4.1 Asphalt Material Properties

Seven different binders were used in the sensitivity analysis. Table 9 shows the binder and the corresponding mix characteristics.

Table 9 Binder and Mix Characteristics

Mix	Binder PG Grade	% Ret. ¾" Sieve	% Ret. 3/8" Sieve	% Ret. #4 Sieve	% Pass. #200 Sieve	Eff. Binder Content (%)	Air Voids at Construction (%)	VMA (%)	Total Unit Weight (pcf)
0	82-10	30	47	52.8	8.4	10.5	8.5	19	148
1	76-16	30	47	52.8	8.4	10	7	17	148
2	70-22	11.6	35.3	52.6	7.3	10	7	17	148
3	64-28	11.6	35.3	52.6	7.3	11	7	18	148
4	58-34	11.6	35.3	52.6	7.3	12	7	19	148
5	52-40	11.6	35.3	52.6	7.3	13	7	20	148
6	46-46	11.6	35.3	52.6	7.3	14	7	21	148

A and VTS parameters were estimated based on the regression of RTFO viscosity results found in the Design Guide program database. The default parameters used in this study are presented in Table 10.

Table 10 A and VTS Parameters (After RTFO)

Binder Type	A	VTS
82-10	9.514	-3.128
76-16	10.015	-3.315
70-22	10.299	-3.426
64-28	10.312	-3.440
58-34	10.035	-3.350
52-40	9.496	-3.164
46-46	8.755	-2.905

For Level 3 analysis of the thermal cracking model, a set of correlations were developed for the creep compliance and the tensile strength input parameters, based on volumetric and mixture properties. The creep compliance response at time *t*, can be written as:

$$D(\xi) = D_1 \xi^m$$

where D_1 and m are the fracture coefficients obtained from the creep compliance and strength of the mixture.

The creep compliance data used to obtain the fracture coefficients was the same gathered to calibrate the model: 22 GPS sections from the LTPP database, 14 sections from the Canadian C-SHRP program, one section from Peoria, IL, and 5 MnROAD cells from the Minnesota DOT.

The D_1 and m parameters were found at each temperature available: -20, -10, and 0 ^oC. Once the parameters D_1 and m for each selected mixture was found by nonlinear regression analyses, the team proceeded to correlate them against different volumetric and mixture properties, such as air voids, VFA, Penetration, and A_{RTFO} and VTS_{RTFO} values.

The best correlation found for the D_1 fracture parameters was:

$$\log(D_1) = -8.5241 + 0.01306T + 0.7957 \log(V_a) + 2.0103 \log(VFA) - 1.923 \log(A)$$

where: T = Test temperature (^oC)
V_a = Air voids (%)
VFA = Void filled with asphalt (%)
A = Intercept of binder Viscosity-Temperature relationship at RTFO condition.

For the m parameter, the best relationship found was:

$$m = 1.1628 - 0.00185T - 0.04596V_a - 0.01126VFA + 0.00247\,Pen_{77} + 0.001683 \times T \times Pen_{77}^{0.4605}$$

where: T = Test temperature (^oC)
V_a = Air voids (%)
VFA = Void filled with asphalt (%)
Pen_{77} = Penetration at 77 ^oF

A total of 714 data points were used to obtain the above correlations. With an R^2 of 0.80 and a S_e/S_y of 0.45, the relationship was considered to be acceptable.

The tensile strength at –10 ^oC was also correlated with mixture properties. The best indicators were the air voids, the void filled with asphalt content, the Penetration at 77 ^oF, and the A intercept of the binder temperature-viscosity relationship for RTFO conditions.

$$TS = 7416.712 - 114.016V_a - 0.304V_a^2 - 122.592VFA + 0.704VFA^2 + 405.71\log(Pen_{77}) - 2039.296\log A$$

A total of 31 data points were used to obtain the above correlation. With an R^2 of 0.62 and a S_e/S_y of 0.68, the correlation was considered to be acceptable.

Based on the above correlations, default values for creep compliance and tensile strength for the seven binders used in this analysis were calculated. A summary of the results is presented in Table 11.

Table11. Level 3 Creep Compliance and Tensile Strength Data

PG Grade	Time (sec)	Creep Compliance (1/psi)			Tensile Strength (psi)
		-20	-10	0	
82-10	1	3.7641E-07	5.08469E-07	6.86855E-07	354.77
	2	4.0378E-07	5.65524E-07	7.92068E-07	
	5	4.4302E-07	6.50888E-07	9.56284E-07	
	10	4.7523E-07	7.23924E-07	1.10277E-06	
	20	5.0977E-07	8.05155E-07	1.27169E-06	
	50	5.5932E-07	9.2669E-07	1.53535E-06	
	100	5.9998E-07	1.03067E-06	1.77053E-06	
76-16	1	3.313E-07	4.47529E-07	6.04535E-07	373.62
	2	3.6223E-07	5.09844E-07	7.17617E-07	
	5	4.0759E-07	6.05731E-07	9.00198E-07	
	10	4.4564E-07	6.90075E-07	1.06859E-06	
	20	4.8724E-07	7.86163E-07	1.26847E-06	
	50	5.4826E-07	9.34018E-07	1.5912E-06	
	100	5.9944E-07	1.06407E-06	1.88885E-06	
70-22	1	3.1396E-07	4.241E-07	5.72886E-07	420.28
	2	3.4383E-07	4.89337E-07	6.96419E-07	
	5	3.8773E-07	5.91225E-07	9.01514E-07	
	10	4.2463E-07	6.82171E-07	1.09591E-06	
	20	4.6504E-07	7.87106E-07	1.33222E-06	
	50	5.2442E-07	9.50994E-07	1.72456E-06	
	100	5.7432E-07	1.09728E-06	2.09644E-06	
64-28	1	3.3816E-07	4.56797E-07	6.17054E-07	422.02
	2	3.686E-07	5.33726E-07	7.72825E-07	
	5	4.1308E-07	6.55652E-07	1.04066E-06	
	10	4.5027E-07	7.66069E-07	1.30337E-06	
	20	4.908E-07	8.95082E-07	1.63239E-06	
	50	5.5003E-07	1.09956E-06	2.19812E-06	
	100	5.9954E-07	1.28473E-06	2.75302E-06	

Table 11. Level 3 Creep Compliance and Tensile Strength Data, Cont.

PG Grade	Time (sec)	Creep Compliance (1/psi)			Tensile Strength (psi)
58-34	1	3.8074E-07	5.14312E-07	6.94746E-07	479.31
	2	4.2726E-07	6.34948E-07	9.43599E-07	
	5	4.9759E-07	8.38901E-07	1.41433E-06	
	10	5.5838E-07	1.03567E-06	1.92094E-06	
	20	6.2661E-07	1.2786E-06	2.609E-06	
	50	7.2975E-07	1.6893E-06	3.91056E-06	
	100	8.1891E-07	2.08554E-06	5.31129E-06	
52-40	1	4.4857E-07	6.05945E-07	8.18528E-07	566.22
	2	5.4677E-07	8.38543E-07	1.286E-06	
	5	7.1033E-07	1.28836E-06	2.33677E-06	
	10	8.6583E-07	1.78291E-06	3.67134E-06	
	20	1.0554E-06	2.4673E-06	5.76811E-06	
	50	1.3711E-06	3.79083E-06	1.04811E-05	
	100	1.6712E-06	5.24598E-06	1.64671E-05	
46-46	1	5.518E-07	7.454E-07	1.007E-06	686.91
	2	8.108E-07	1.296E-06	2.070E-06	
	5	1.348E-06	2.690E-06	5.367E-06	
	10	1.981E-06	4.676E-06	1.103E-05	
	20	2.911E-06	8.126E-06	2.269E-05	
	50	4.841E-06	1.687E-05	5.882E-05	
	100	7.112E-06	2.933E-05	1.209E-04	

2.4.2 Unbound Materials

The unbound materials information used for this analysis is provided in Table 12.

Table 12 Unbound Materials Data

Layer	AASHTO Classification	Modulus (psi)	Plasticity Index	% Passing #200 Sieve	% Passing #4 Sieve	Diameter D_{60} (mm)
Granular Base	A-1-a	40000	0	5	30	3
Compacted Subgrade	A-4	25000	7	60	100	0.08
Natural Subgrade	A-4	25000	7	60	100	0.08

2.5 Beta (β) Factor in the Thermal Cracking Model

As defined in the main report, the amount of transverse cracking in the pavement system is predicted by relating the crack depth to an amount of cracking (crack frequency). In

turn, the amount of crack propagation induced by a given thermal cooling cycle is predicted using the Paris law of crack propagation:

$$\Delta C = A\Delta K^n$$

where:

ΔC = Change in the crack dpeth due to a cooling cycle.
ΔK = Change in the stress intensity factor due to a cooling cycle
A, n = Fracture parameters for the asphalt mixture

The β factor which varied from 1.0 to 5.0 was applied on the expression representing the A fracture parameters as follows:

$$A = 10^{(\beta*(4.389-2.52*\log(E*\sigma_m*n))}$$

where:

E = Mixture stiffness.
σ_m = Undamaged mixture tensile strength
β = Calibration parameter

The complete set of results using the three given values of β (1.0, 3.0, and 5.0) is provided in the following section.

3. RESULTS

To report in an organized manner the results obtained in this sensitivity analysis, they will be provided by the different β factors used.

3.1 β = 1.0

The predicted thermal cracking for the ten different climatic regions is tabulated in Table 13. The results show cracking predicted for sections with seven different binders, at three different asphalt thicknesses for a period of 20 years. It is emphasized that the results noted are consistent with only the last 4-5 years of environmental data (from the EICM) for a given site location. It is possible that much colder annual site conditions would greatly influence the results obtained.

Figures 1 through 4 show the thermal cracking in those regions were nonzero data was predicted. Same figures show the SHRP recommended Superpave performance grade in compliance with the lowest temperature to avoid thermal cracking for 50% and 98% reliability. This information was obtained from LTPPBIND, Version 2.1; July 1, 1999, LTPP software developed for the Federal Highway Administration. The data is shown in Figures 5 and 6. From the results using the TCModel with a β=1, the following can be concluded.

1. Thermal cracking was predicted for regions where the Mean Annual Air Temperature was lower than 53 ^{o}F. That includes Barrow, AK; Fargo, ND; Billings, MT; and Chicago, IL. No measureable cracking was predicted for Washington DC; San Francisco, CA; Oklahoma City, OK; Dallas, TX; Las Vegas,NV; and/or San Antonio, TX.

Table 13 Thermal Cracking after 20 years for Different Climatic Regions and Different Asphalt Thicknesses (β = 1.0)

Region	Site	TC at 20 years - Asphalt Thickness: 6"						
		82-10	76-16	70-22	64-28	58-34	52-40	46-46
Alaska	Barrow, AK	176.7	176.7	176.7	176.7	14.71	1.81E-06	0
IIA	Fargo, ND	170.4	96.9	6.7	0.54	1.58E-05	0	0
IIIA	Billings, MT	146.7	2.9	0.21	2.84E-02	7.12E-07	0	0
IA	Chicago, IL	1.25E-03	2.06E-07	1.87E-08	9.65E-10	0	0	0
IB	Washington, D.C.	0	0	0	0	0	0	0
IC	San Francisco, CA	0	0	0	0	0	0	0
IIB	Oklahoma City, OK	0	0	0	0	0	0	0
IIC	Dallas, TX	0	0	0	0	0	0	0
IIIB	Las Vegas, NV	0	0	0	0	0	0	0
IIIC	San Antonio, TX	0	0	0	0	0	0	0

Region	Site	TC at 20 years - Asphalt Thickness: 4"						
		82-10	76-16	70-22	64-28	58-34	52-40	46-46
Alaska	Barrow, AK	176.7	176.7	176.7	176.7	19.36	5.44E-06	0
IIA	Fargo, ND	176.7	99.1	6.6	0.71	3.39E-05	0	0
IIIA	Billings, MT	167.4	2.7	0.27	4.11E-02	1.83E-06	0	0
IA	Chicago, IL	1.39E-03	2.18E-07	2.48E-08	8.15E-10	0	0	0
IB	Washington, D.C.	0	0	0	0	0	0	0
IC	San Francisco, CA	0	0	0	0	0	0	0
IIB	Oklahoma City, OK	0	0	0	0	0	0	0
IIC	Dallas, TX	0	0	0	0	0	0	0
IIIB	Las Vegas, NV	0	0	0	0	0	0	0
IIIC	San Antonio, TX	0	0	0	0	0	0	0

Region	Site	TC at 20 years - Asphalt Thickness: 1"						
		82-10	76-16	70-22	64-28	58-34	52-40	46-46
Alaska	Barrow, AK	176.7	176.7	176.7	176.7	50.08	1.49E-04	0
IIA	Fargo, ND	176.7	176.7	54.8	10.2	2.65E-03	0	0
IIIA	Billings, MT	176.7	8.04	1.49	0.34	4.88E-05	0	0
IA	Chicago, IL	5.28E-03	1.03E-06	1.03E-07	4.96E-09	0	0	0
IB	Washington, D.C.	0	0	0	0	0	0	0
IC	San Francisco, CA	0	0	0	0	0	0	0
IIB	Oklahoma City, OK	0	0	0	0	0	0	0
IIC	Dallas, TX	0	0	0	0	0	0	0
IIIB	Las Vegas, NV	0	0	0	0	0	0	0
IIIC	San Antonio, TX	0	0	0	0	0	0	0

Figure 1 Predicted Thermal Cracking for Pavement Section in Barrow, Alaska as Function of Binder Grade and Pavement Thickness (β = 1.0)

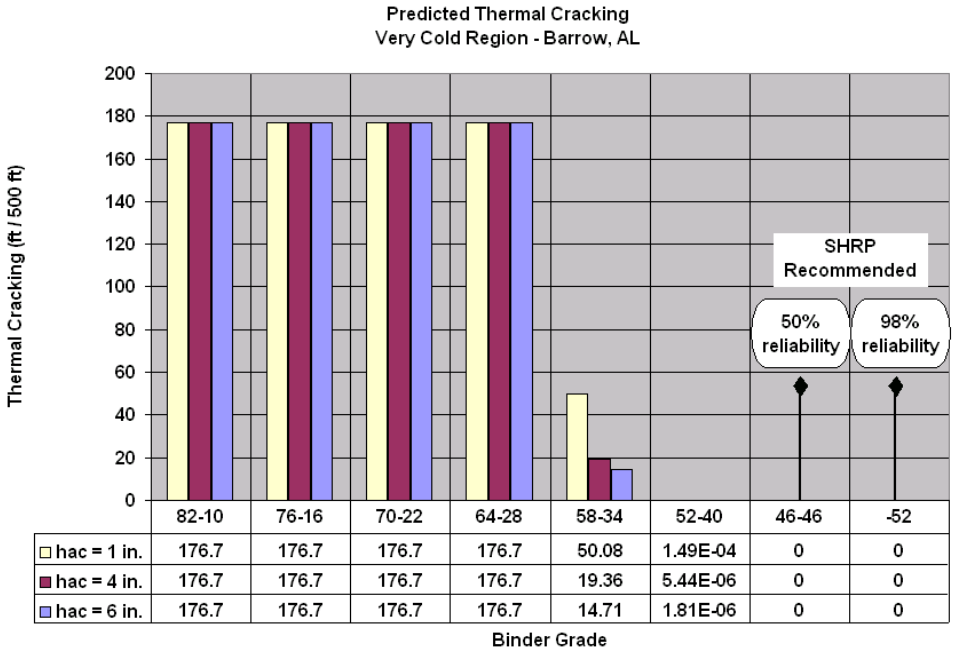

	82-10	76-16	70-22	64-28	58-34	52-40	46-46	-52
hac = 1 in.	176.7	176.7	176.7	176.7	50.08	1.49E-04	0	0
hac = 4 in.	176.7	176.7	176.7	176.7	19.36	5.44E-06	0	0
hac = 6 in.	176.7	176.7	176.7	176.7	14.71	1.81E-06	0	0

Figure 2 Predicted Thermal Cracking for Pavement Section in Fargo, ND as Function of Binder Grade and Pavement Thickness (β = 1.0)

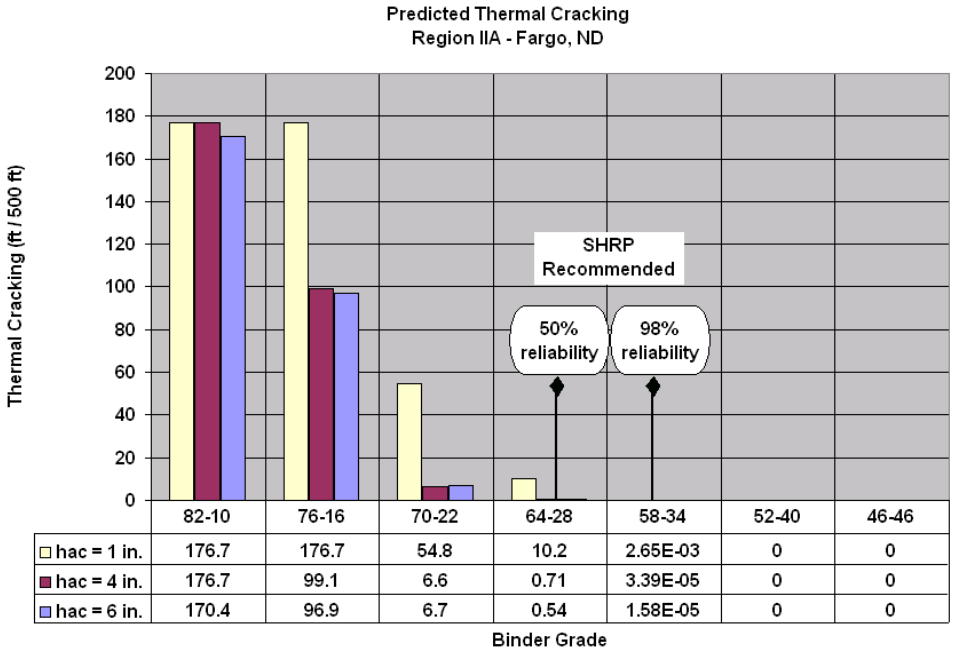

	82-10	76-16	70-22	64-28	58-34	52-40	46-46
hac = 1 in.	176.7	176.7	54.8	10.2	2.65E-03	0	0
hac = 4 in.	176.7	99.1	6.6	0.71	3.39E-05	0	0
hac = 6 in.	170.4	96.9	6.7	0.54	1.58E-05	0	0

Figure 3 Predicted Thermal Cracking for Pavement Section in Billings, MT as Function of Binder Grade and Pavement Thickness (β = 1.0)

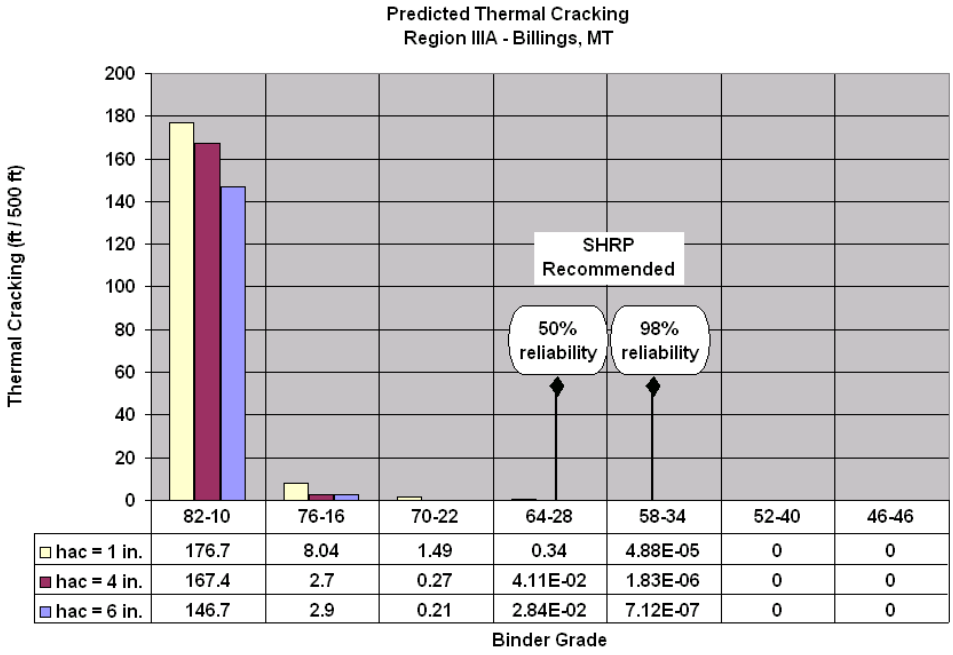

	82-10	76-16	70-22	64-28	58-34	52-40	46-46
hac = 1 in.	176.7	8.04	1.49	0.34	4.88E-05	0	0
hac = 4 in.	167.4	2.7	0.27	4.11E-02	1.83E-06	0	0
hac = 6 in.	146.7	2.9	0.21	2.84E-02	7.12E-07	0	0

Figure 4 Predicted Thermal Cracking for Pavement Section in Chicago, IL as Function of Binder Grade and Pavement Thickness (β = 1.0)

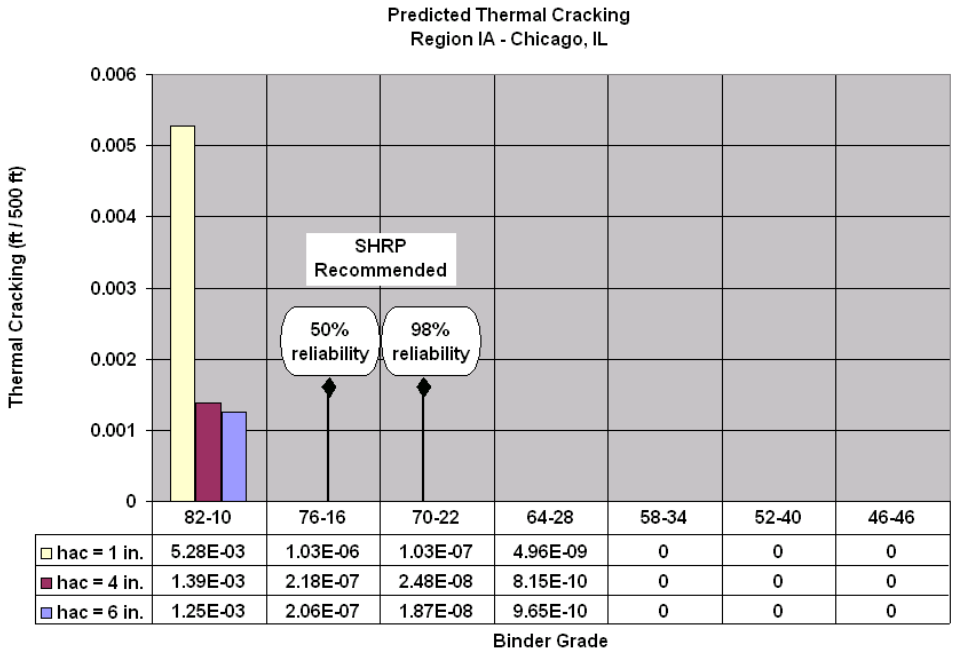

	82-10	76-16	70-22	64-28	58-34	52-40	46-46
hac = 1 in.	5.28E-03	1.03E-06	1.03E-07	4.96E-09	0	0	0
hac = 4 in.	1.39E-03	2.18E-07	2.48E-08	8.15E-10	0	0	0
hac = 6 in.	1.25E-03	2.06E-07	1.87E-08	9.65E-10	0	0	0

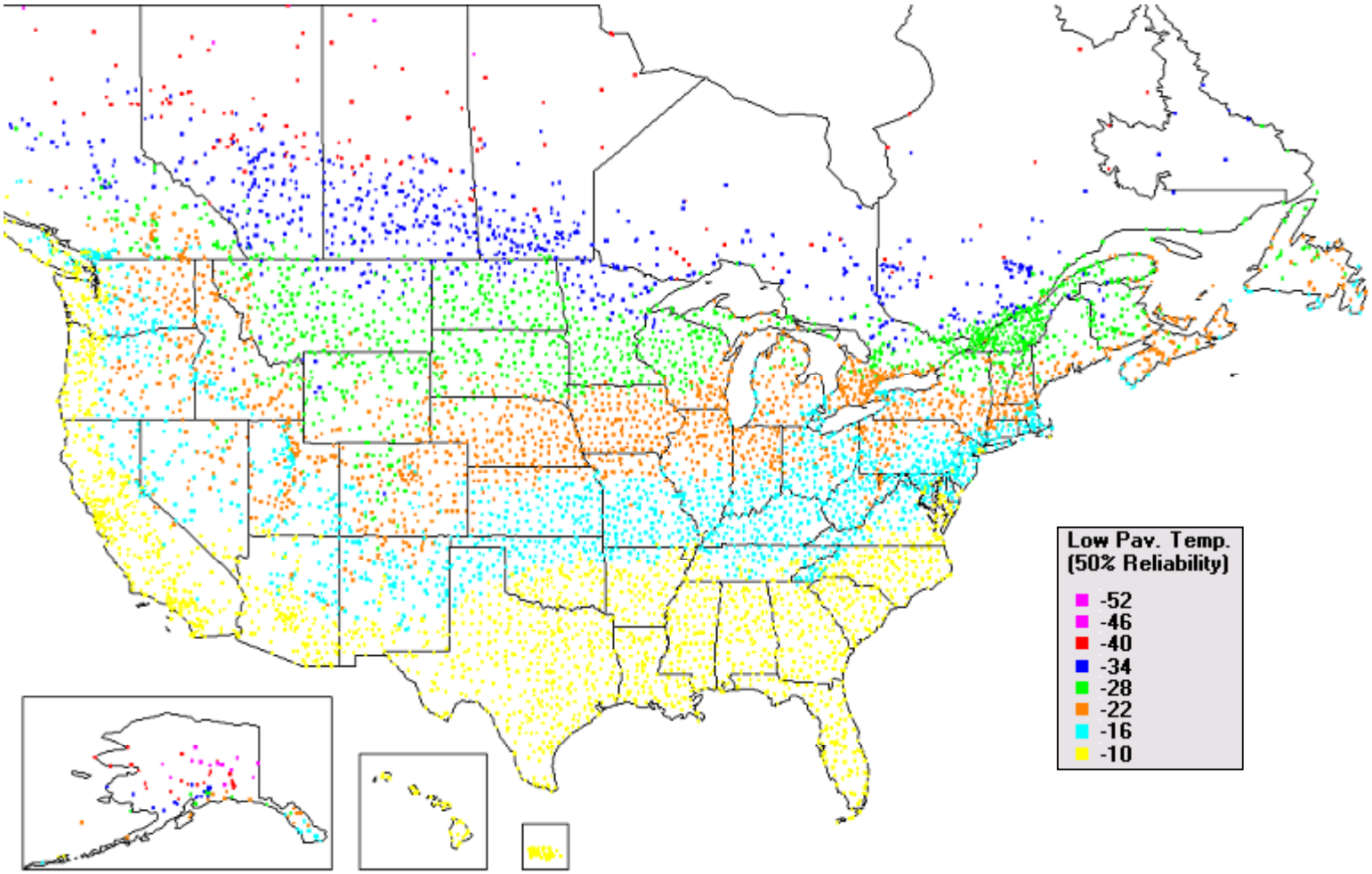

Figure 5 Low Pavement Temperatures- 50% Reliability (*LTTPBIND, Version 2.1, 1999, FHWA*).

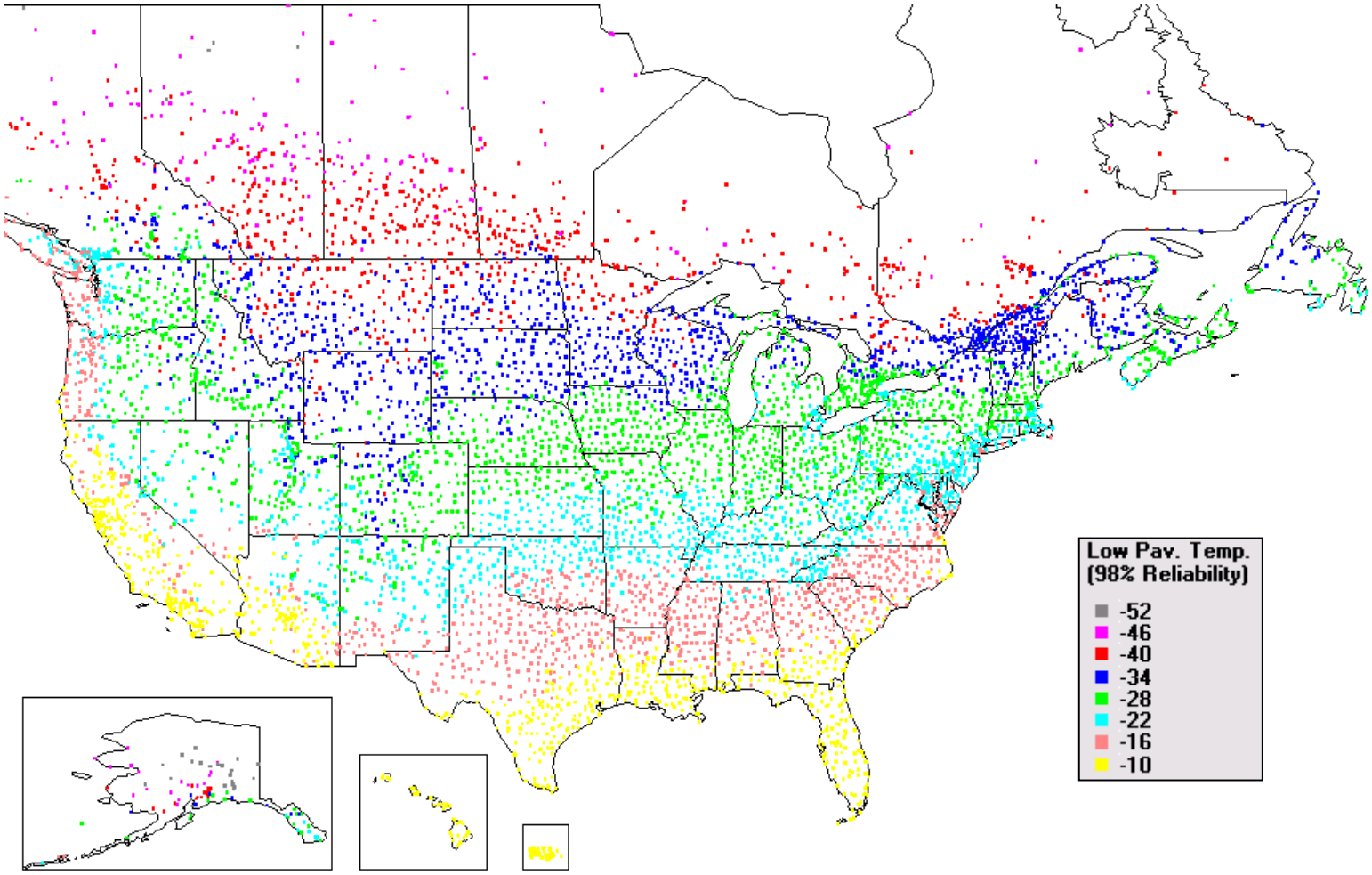

Figure 6 Low Pavement Temperatures- 98% Reliability (*LTTPBIND, Version 2.1, 1999, FHWA*).

2. For the same site, predicted cracking was higher for binders with higher performance grades. The program produced reasonable results for binders with PG grades ranging from 82-10 to 52-40.

3. As would be expected, the predicted thermal cracking increased as the Mean Annual Air Temperature decreased. In addition, the predicted thermal cracking was also found to be related to the average frequency of hours with pavement surface temperature less than 15 ^{o}F increased. As a consequence, predicted cracking of a section in Barrow, AK was higher than cracking predicted for Fargo, ND. Likewise, cracking predicted for Fargo was higher than the one predicted for Billings, MT.

4. Within any climate region, the predicted thermal cracking increased as the asphalt thickness decreased. This is in total agreement with the fundamental concepts and methodology of the general thermal fracture model used in the program.

3.2 β = 3.0

The predicted thermal cracking for the ten different climatic regions is tabulated in Table 14. The results show cracking predicted for sections with seven different binders, at three different asphalt thicknesses for a period of 20 years. It is again emphasized that the results noted are consistent with only the last 4-5 years of environmental data (from the EICM) for a given site location. It is possible that much colder annual site conditions would greatly influence the results obtained.

Figures 7 through 11 show the thermal cracking in those regions were nonzero data was predicted. Using Table 14, and the results from Figures 5 through 11, it was found similar conclusions to those obtained with a β = 1.0, with the exception that the maximum temperature were thermal cracking was predicted was 56°F instead of 53°F.

3.3 β = 5.0

The summary of results for this condition is presented in Table 15. They show cracking predicted for sections with seven different binders, at three different asphalt thicknesses for a period of 20 years. Again, it is emphasized that the results noted are consistent with only the last 4-5 years of environmental data (from the EICM) for a given site location. It is possible that much colder annual site conditions would greatly influence the results obtained.

Figures 12 through 16 show the thermal cracking in those regions were nonzero data was predicted. The conclusions were similar to those obtained with the previous β values.

Table 14 Thermal Cracking after 20 years for Different Climatic Regions and Different Asphalt Thicknesses (β = 3.0)

Region	Site	TC at 20 years - Asphalt Thickness: 6"						
		82-10	76-16	70-22	64-28	58-34	52-40	46-46
Alaska	Barrow, AL	200	200	200	200	200	0.54	0
IIA	Fargo, ND	200	200	200	187.9	6.8	3.06E-06	0
IIIA	Billings, MT	200	200	178.2	155.4	0.28	1.82E-07	0
IA	Chicago, IL	169.8	19.6	0.71	3.47E-02	1.27E-06	0	0
IB	Washington, D.C.	8.70E-04	1.71E-05	2.06E-06	1.11E-08	0	0	0
IC	San Francisco, CA	0	0	0	0	0	0	0
IIB	Oklahoma City, OK	5.14E-08	2.67E-10	0	0	0	0	0
IIC	Dallas, TX	0	0	0	0	0	0	0
IIIB	Las Vegas, NV	0	0	0	0	0	0	0
IIIC	San Antonio, TX	0	0	0	0	0	0	0

Region	Site	TC at 20 years - Asphalt Thickness: 4"						
		82-10	76-16	70-22	64-28	58-34	52-40	46-46
Alaska	Barrow, AL	200	200	200	200	200	1.0	0
IIA	Fargo, ND	200	200	200	200	8.3	8.76E-06	0
IIIA	Billings, MT	200	200	200	180.2	0.44	5.19E-07	0
IA	Chicago, IL	190.7	11.1	0.73	4.56E-02	2.92E-06	0	0
IB	Washington, D.C.	2.30E-03	5.23E-05	6.89E-06	4.43E-08	0	0	0
IC	San Francisco, CA	0	0	0	0	0	0	0
IIB	Oklahoma City, OK	1.93E-07	1.07E-09	0	0	0	0	0
IIC	Dallas, TX	0	0	0	0	0	0	0
IIIB	Las Vegas, NV	0	0	0	0	0	0	0
IIIC	San Antonio, TX	0	0	0	0	0	0	0

Region	Site	TC at 20 years - Asphalt Thickness: 1"						
		82-10	76-16	70-22	64-28	58-34	52-40	46-46
Alaska	Barrow, AL	200	200	200	200	200	4.9	0
IIA	Fargo, ND	200	200	200	200	49.1	2.51E-04	0
IIIA	Billings, MT	200	200	200	200	2.5	5.91E-06	0
IA	Chicago, IL	200	10.1	1.75	0.18	2.87E-05	0	0
IB	Washington, D.C.	2.09E-03	7.70E-05	8.50E-06	3.64E-08	0	0	0
IC	San Francisco, CA	0	0	0	0	0	0	0
IIB	Oklahoma City, OK	6.66E-07	4.29E-09	0	0	0	0	0
IIC	Dallas, TX	0	0	0	0	0	0	0
IIIB	Las Vegas, NV	0	0	0	0	0	0	0
IIIC	San Antonio, TX	0	0	0	0	0	0	0

Figure 7 Predicted Thermal Cracking for Pavement Section in Barrow, Alaska as Function of Binder Grade and Pavement Thickness (β = 3.0)

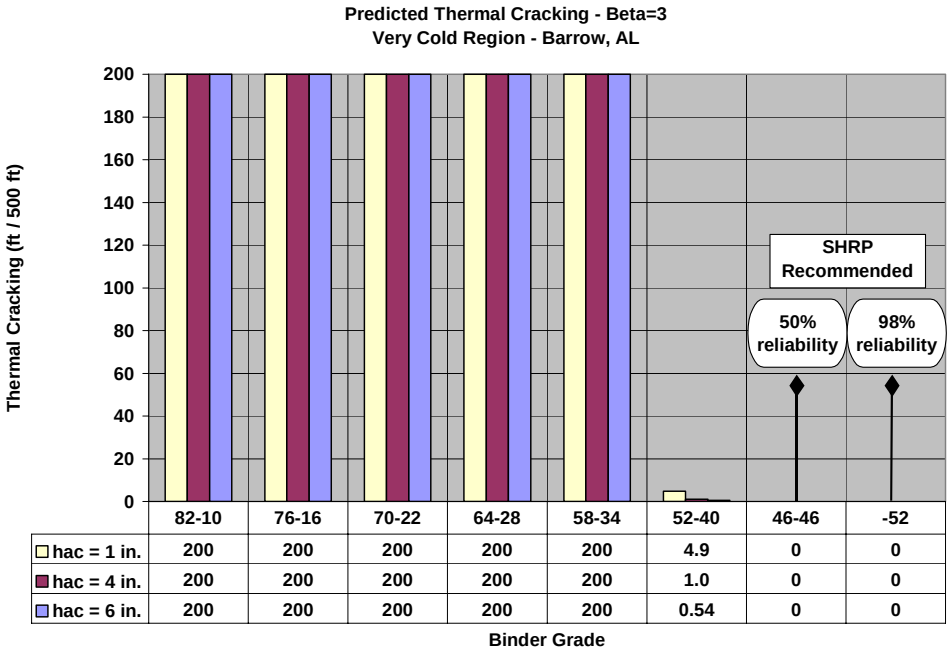

	82-10	76-16	70-22	64-28	58-34	52-40	46-46	-52
hac = 1 in.	200	200	200	200	200	4.9	0	0
hac = 4 in.	200	200	200	200	200	1.0	0	0
hac = 6 in.	200	200	200	200	200	0.54	0	0

Figure 8 Predicted Thermal Cracking for Pavement Section in Fargo, ND as Function of Binder Grade and Pavement Thickness (β = 3.0)

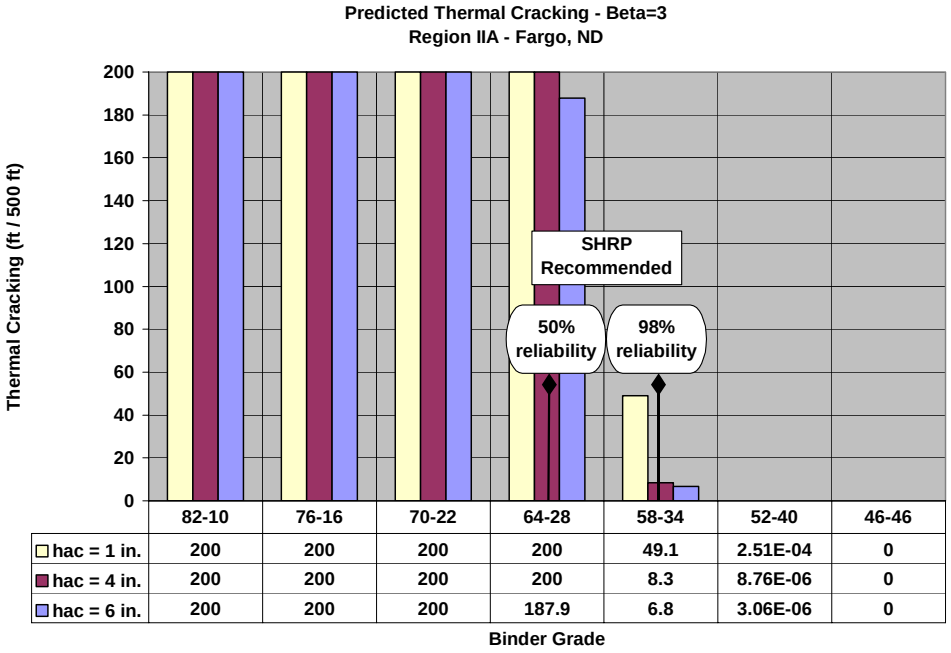

	82-10	76-16	70-22	64-28	58-34	52-40	46-46
hac = 1 in.	200	200	200	200	49.1	2.51E-04	0
hac = 4 in.	200	200	200	200	8.3	8.76E-06	0
hac = 6 in.	200	200	200	187.9	6.8	3.06E-06	0

Figure 9 Predicted Thermal Cracking for Pavement Section in Billings, MT as Function of Binder Grade and Pavement Thickness (β = 3.0)

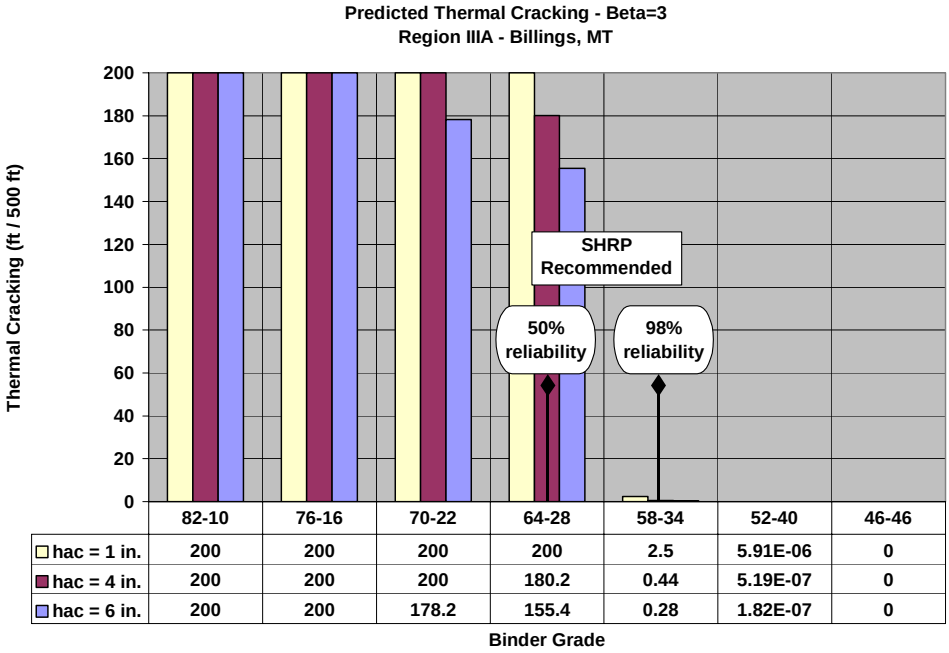

	82-10	76-16	70-22	64-28	58-34	52-40	46-46
hac = 1 in.	200	200	200	200	2.5	5.91E-06	0
hac = 4 in.	200	200	200	180.2	0.44	5.19E-07	0
hac = 6 in.	200	200	178.2	155.4	0.28	1.82E-07	0

Figure 10 Predicted Thermal Cracking for Pavement Section in Chicago, IL as Function of Binder Grade and Pavement Thickness (β = 3.0)

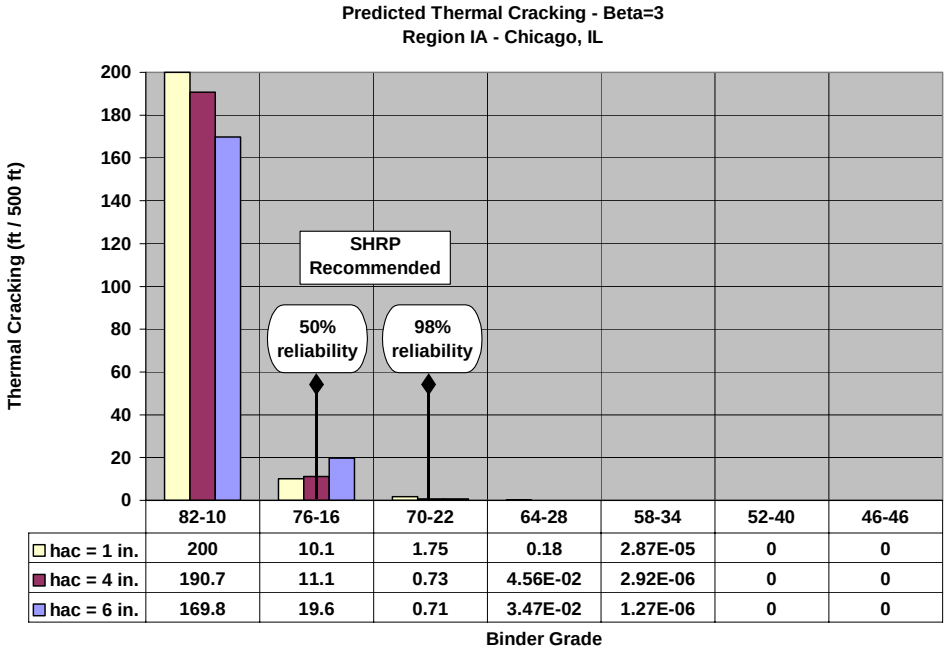

	82-10	76-16	70-22	64-28	58-34	52-40	46-46
hac = 1 in.	200	10.1	1.75	0.18	2.87E-05	0	0
hac = 4 in.	190.7	11.1	0.73	4.56E-02	2.92E-06	0	0
hac = 6 in.	169.8	19.6	0.71	3.47E-02	1.27E-06	0	0

Figure 11 Predicted Thermal Cracking for Pavement Section in Washington, D.C. as Function of Binder Grade and Pavement Thickness (β = 3.0)

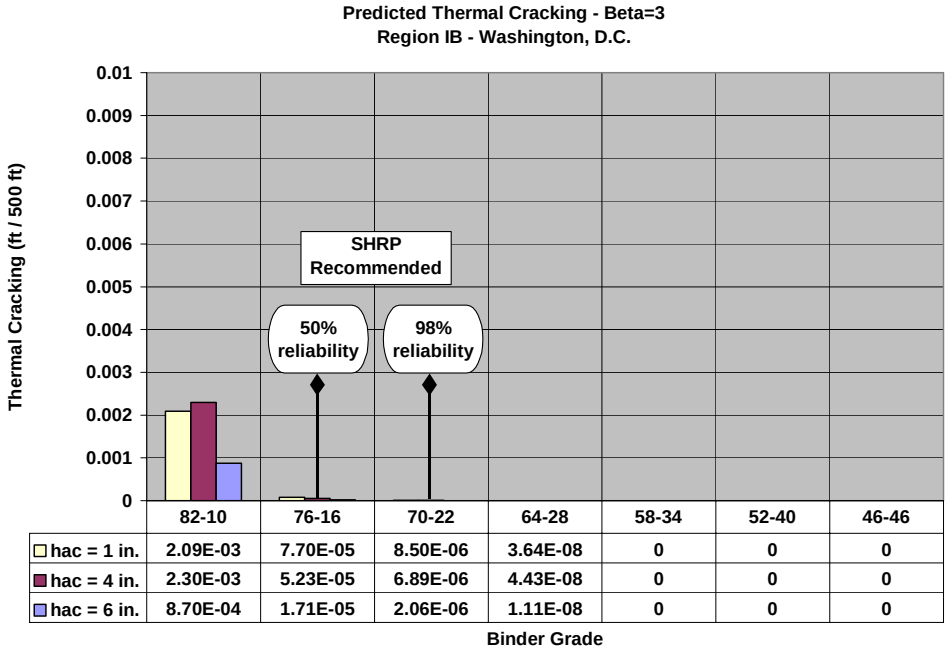

	82-10	76-16	70-22	64-28	58-34	52-40	46-46
hac = 1 in.	2.09E-03	7.70E-05	8.50E-06	3.64E-08	0	0	0
hac = 4 in.	2.30E-03	5.23E-05	6.89E-06	4.43E-08	0	0	0
hac = 6 in.	8.70E-04	1.71E-05	2.06E-06	1.11E-08	0	0	0

Table 15 Thermal Cracking after 20 years for Different Climatic Regions and Different Asphalt Thicknesses (β = 5.0)

Region	Site	TC at 20 years - Asphalt Thickness: 6"						
		82-10	76-16	70-22	64-28	58-34	52-40	46-46
Alaska	Barrow, AL	200	200	200	200	200	35.2	0
IIA	Fargo, ND	200.0	200.0	200.0	200.0	131.8	1.69E-03	0
IIIA	Billings, MT	200	200	200	184.8	50.1	6.87E-05	0
IA	Chicago, IL	200	166.1	134.9	26.9	1.20E-03	1.69E-11	0
IB	Washington, D.C.	6.3	4.34E-02	4.18E-03	5.56E-05	3.27E-09	0	0
IC	San Francisco, CA	0	0	0	0	0	0	0
IIB	Oklahoma City, OK	9.67E-04	3.95E-05	5.73E-06	4.38E-08	0	0	0
IIC	Dallas, TX	0	0	0	0	0	0	0
IIIB	Las Vegas, NV	0	0	0	0	0	0	0
IIIC	San Antonio, TX	0	0	0	0	0	0	0

Region	Site	TC at 20 years - Asphalt Thickness: 4"						
		82-10	76-16	70-22	64-28	58-34	52-40	46-46
Alaska	Barrow, AL	200	200	200	200	200	47.3	0
IIA	Fargo, ND	200.0	200.0	200.0	200.0	153.4	4.08E-03	0
IIIA	Billings, MT	200	200	200	200	55.87817	1.82E-04	0
IA	Chicago, IL	200	189.2	151.7	21.5	2.27E-03	5.49E-11	0
IB	Washington, D.C.	9.5	9.52E-02	1.03E-02	1.64E-04	1.45E-08	0	0
IC	San Francisco, CA	0	0	0	0	0	0	0
IIB	Oklahoma City, OK	2.31E-03	1.12E-04	1.79E-05	1.74E-07	0	0	0
IIC	Dallas, TX	0	0	0	0	0	0	0
IIIB	Las Vegas, NV	0	0	0	0	0	0	0
IIIC	San Antonio, TX	0	0	0	0	0	0	0

Region	Site	TC at 20 years - Asphalt Thickness: 1"						
		82-10	76-16	70-22	64-28	58-34	52-40	46-46
Alaska	Barrow, AL	200	200	200	200	200	93.1	0
IIA	Fargo, ND	200.0	200.0	200.0	200.0	200.0	6.36E-02	0
IIIA	Billings, MT	200	200	200	200	98.4	1.81E-03	0
IA	Chicago, IL	200	200	200	200	1.66E-02	1.07E-09	0
IB	Washington, D.C.	1.9	9.19E-02	1.67E-02	4.15E-04	1.10E-08	0	0
IC	San Francisco, CA	0	0	0	0	0	0	0
IIB	Oklahoma City, OK	1.02E-02	8.03E-04	1.38E-04	1.54E-06	0	0	0
IIC	Dallas, TX	0	0	0	0	0	0	0
IIIB	Las Vegas, NV	0	0	0	0	0	0	0
IIIC	San Antonio, TX	0	0	0	0	0	0	0

Figure 12 Predicted Thermal Cracking for Pavement Section in Barrow, Alaska as Function of Binder Grade and Pavement Thickness (β = 5.0)

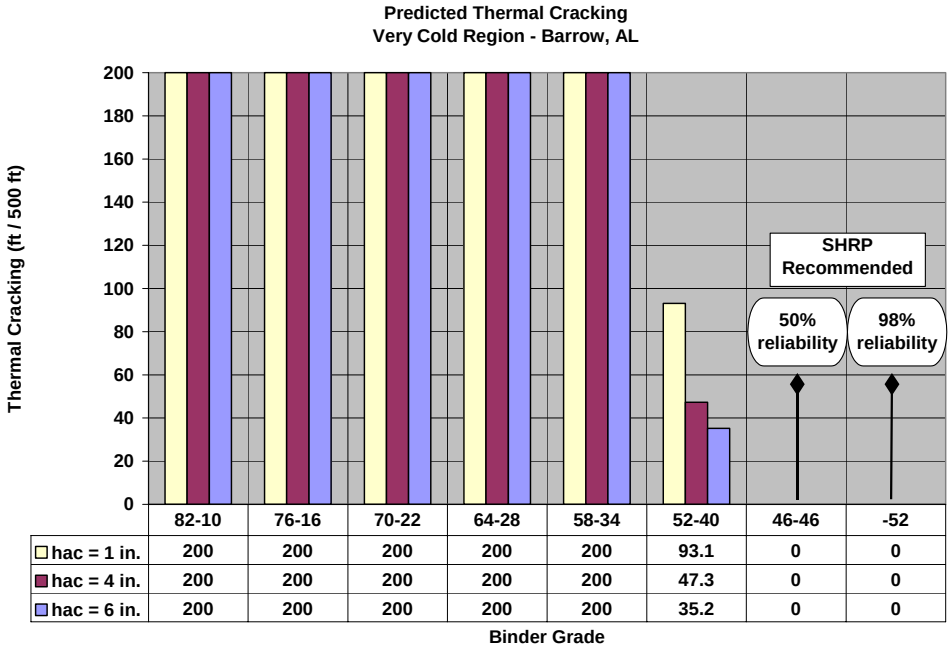

	82-10	76-16	70-22	64-28	58-34	52-40	46-46	-52
hac = 1 in.	200	200	200	200	200	93.1	0	0
hac = 4 in.	200	200	200	200	200	47.3	0	0
hac = 6 in.	200	200	200	200	200	35.2	0	0

Figure 13 Predicted Thermal Cracking for Pavement Section in Fargo, ND as Function of Binder Grade and Pavement Thickness (β = 5.0)

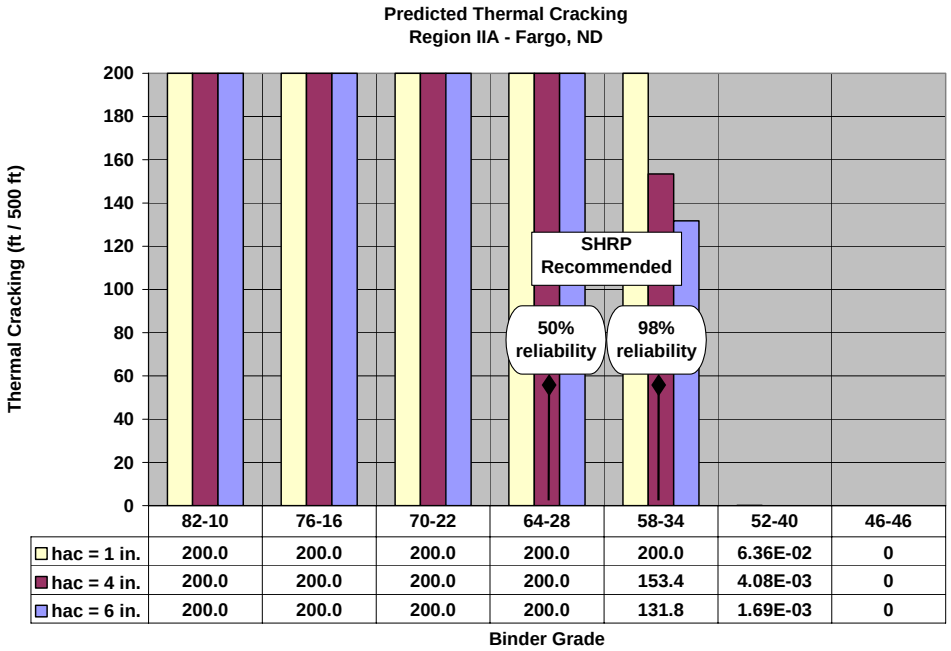

	82-10	76-16	70-22	64-28	58-34	52-40	46-46
hac = 1 in.	200.0	200.0	200.0	200.0	200.0	6.36E-02	0
hac = 4 in.	200.0	200.0	200.0	200.0	153.4	4.08E-03	0
hac = 6 in.	200.0	200.0	200.0	200.0	131.8	1.69E-03	0

Figure 14 Predicted Thermal Cracking for Pavement Section in Billings, MT as Function of Binder Grade and Pavement Thickness (β = 5.0)

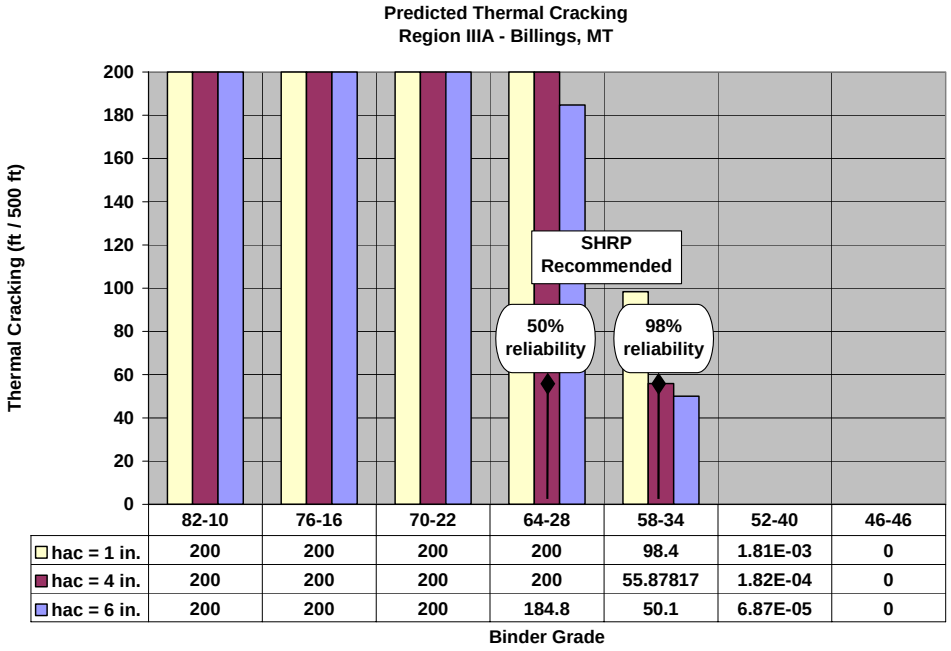

	82-10	76-16	70-22	64-28	58-34	52-40	46-46
hac = 1 in.	200	200	200	200	98.4	1.81E-03	0
hac = 4 in.	200	200	200	200	55.87817	1.82E-04	0
hac = 6 in.	200	200	200	184.8	50.1	6.87E-05	0

Figure 15 Predicted Thermal Cracking for Pavement Section in Chicago, IL as Function of Binder Grade and Pavement Thickness (β = 5.0)

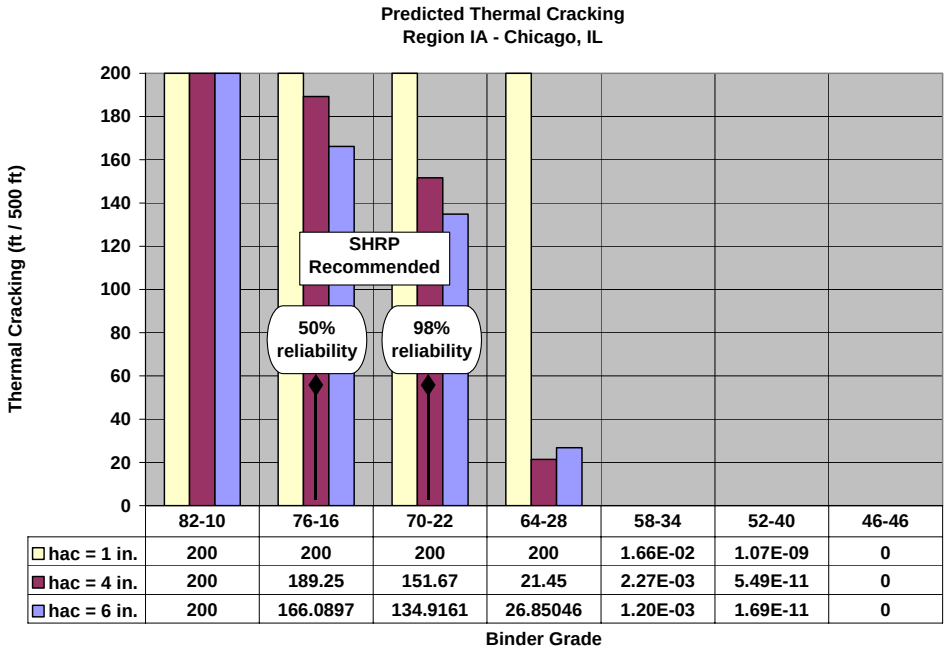

	82-10	76-16	70-22	64-28	58-34	52-40	46-46
hac = 1 in.	200	200	200	200	1.66E-02	1.07E-09	0
hac = 4 in.	200	189.25	151.67	21.45	2.27E-03	5.49E-11	0
hac = 6 in.	200	166.0897	134.9161	26.85046	1.20E-03	1.69E-11	0

Figure 16 Predicted Thermal Cracking for Pavement Section in Washington, D.C. as Function of Binder Grade and Pavement Thickness (β = 5.0)

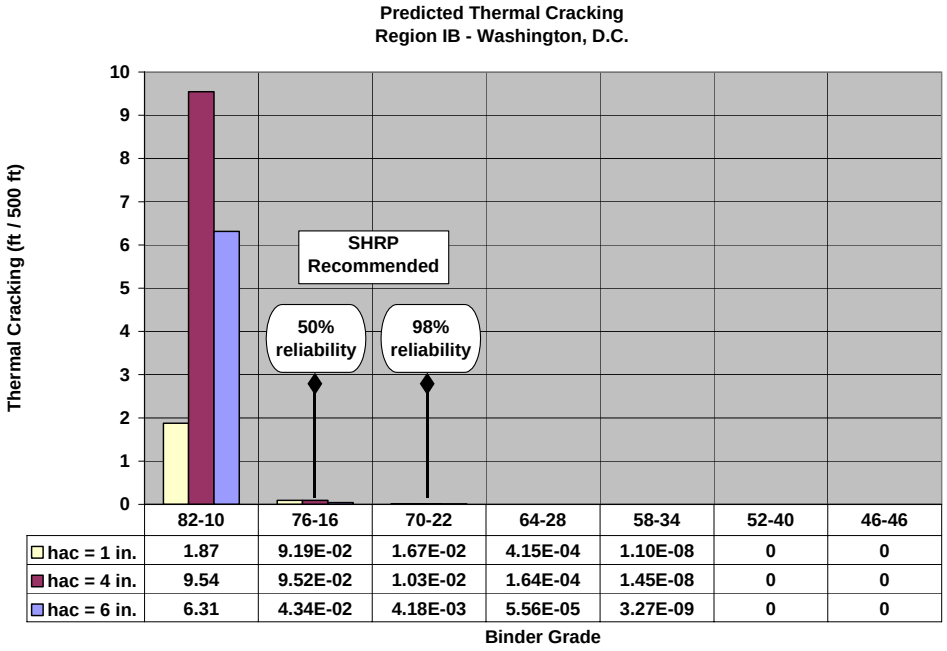

	82-10	76-16	70-22	64-28	58-34	52-40	46-46
hac = 1 in.	1.87	9.19E-02	1.67E-02	4.15E-04	1.10E-08	0	0
hac = 4 in.	9.54	9.52E-02	1.03E-02	1.64E-04	1.45E-08	0	0
hac = 6 in.	6.31	4.34E-02	4.18E-03	5.56E-05	3.27E-09	0	0

4. CONCLUSIONS

The results obtained from the sensitivity analysis of the Level 3 Thermal Cracking model for the 2002 Design Guide were found to be reasonable and as expected regardless of the β factor used. Thermal cracking was predicted to be higher for colder regions. The sensitivity of the asphalt thickness followed the trend expected; at higher thickness, less cracking was predicted. Furthermore, higher performance grade binders resulted in higher predicted cracking. However, the research team felt that using a value of $\beta = 3.0$ was more conservative, a because of this it will be used in the TCModel.